COATINGS FOR OUTDOOR HIGH VOLTAGE INSULATORS

BY

Shuaib Mohamed Braini

Thesis submitted to Cardiff University in
candidature for the degree of PhD

2013

School of Engineering
Cardiff University, Cardiff

ACKNOWLEDGEMENTS

I would like to express heartfelt gratitude to Prof. A. Haddad for giving me the opportunity to carry out this research. His invaluable support and encouragement gave me confidence in overcoming difficult times. His expert advice and continuous support combined with his deep knowledge in the field of High Voltage Engineering have been a permanent source of great help.

I would especially like to thank Dr. Noureddine Harid and Professor R. Waters for their support and advice.

Thanks to all members of the High Voltage Energy Systems Research Group for their friendship and unflagging support. I would like to thank members of the Research office, in particular Chris Lee and Aderyn Reid, and members of the academic and administrative staff who provided help in the course of my research and to the technicians who assisted me in maintaining the test facilities.

Special thanks go to my family for their patience, encouragement and their invaluable support.

SUMMARY

As the range of transmission voltage increases, the pollution severity of the site becomes the most important factor in determining the insulation level of the system. Flashover on polluted insulators poses a serious threat to the reliability of the system and leads to system outages.

There are many remedial measures to minimize the flashover of a porcelain insulator under pollution conditions. One such method is the application of hydrophobic coatings such as Room Temperature Vulcanizing Silicone Rubber (RTV- SiR) and Grease coatings on the surface of ceramic insulators. A recently proposed solution for contaminated outdoor insulators consists of the application of the Nanocoating "Voltshield" onto the surface of the insulator. This thesis reports a comparative assessment of the performance of these coating systems. Laboratory testing of coated porcelain insulators has been undertaken based on the solid layer method of IEC 60507 (artificial pollution- clean fog testing) and IEC 60587 (the inclined plane tests and constant voltage-liquid contaminants) to evaluate the coatings' resistance against tracking and erosion. The performance of these coatings was assessed by monitoring the leakage current on the insulator surfaces. The applied voltage and the leakage current signals were acquired throughout the tests and saved for further analysis. The effect of UV radiation on the coatings has also been investigated. In addition, hydrophobicity tests were performed on the coated insulators.

It was found that the Nanocoating reduces the leakage current by 90% whilst the energy absorbed on the insulator surface is reduced by 98% when compared to an uncoated insulator. The Nanocoating showed good resilience to sand blasting, but under long exposure to sand blasting, the surface began to degrade and showed pockmarks. The Nanocoated insulator showed good stability under UV exposure in terms of leakage current suppression. However, Nanocoated insulator lost its hydrophobicity on exposure to fog, and has lower flashover voltage than the uncoated insulator by 12.5%.

Similar observations were made for the RTV coatings, where the current magnitude reduced by 92%, the energy absorbed on the insulator surface is reduced by 99% when compared to uncoated insulator and the flashover voltage is increased by 50%. RTV coating materials showed good resistance against tracking and erosion even after UV exposure.

The electric field and voltage distribution along the leakage surface of coated and uncoated ceramic insulators under clean and polluted conditions were studied using finite element analysis COMSOL Multiphysics®.

The electric field peaked at both the HV electrode and the ground electrode, and the presence of pollution in the form of water droplets on the coated insulator increased the electric field at the HV electrode.

This study shows that the application of protective coatings to HV outdoor insulators significantly improves their performance. A reduction in surface current and power dissipation is observed, and a reduction in surface heating results in less dry-band arcing. A reduction in dissipated energy can make a contribution to reducing the total loss on the power system. In addition it showed the ability of coatings to resist tracking and erosion which leads to longer coating life under severe weather conditions. The coatings also increased the flashover voltage of the insulators which leads to more stable power system.

TABLE OF CONTENTS

LIST OF FIGURES

LIST OF ABBREVIATIONS

NaCl	Sodium chloride
ESDD	Equivalent salt deposit density
NSDD	Non-soluble deposit density
EPDM	Ethylene-propylene-diene-monomer
EPR	Ethylene-propylene-Rubber
RTV	Room Temperature Vulcanising
HTV	High Temperature Vulcanising
PDMS	Polydimethylsiloxane
ATH	Alumina trihydrate
IPT	Inclined plane test
LMW	Low molecular weight
TGA	Thermal Gravimetric Analysis
AC	Alternating current
DC	Direct current
UV	Ultra violet
HALS	Hindered amine light stabilizers
STRI	Swedish Transmission Research Institute
SiR	Silicone rubber
FRP	Fibre reinforced plastic
HV	High voltage
SEM	Scanning electron microscope
FTIR	Fourier Transformed Infra-red spectroscopy
FEM	Finite element method
DSO	Digital storage oscilloscope
HV	High voltage
2D/3D	Two/three dimensional

Chapter 1- Introduction

1.1. Background

The bulk of power delivery from generating plant to load centres is transported by overhead lines [1.1]. The energized high voltage line conductors not only have to be physically attached to the support structures but also electrically isolated from the support structures. The device used to perform the dual function of support and electrical isolation is the outdoor high voltage insulator.

The most important factor that determines the physical dimensions of outdoor insulators is their performance under pollution conditions. Depending on the pollution severity and the wetting conditions of the site, outdoor insulators need to have sufficient surface leakage length to ensure that dry band formation and surface arcing is minimised.

Decades of in-service performance have demonstrated that ceramic insulators, made of porcelain and glass, show good performance and resist environmental aging. In addition to high mechanical strength, they provide excellent resistance to material degradation caused by electrical stress and discharge activities [1.2]. However, they suffer from having hydrophilic surface properties, which means that water can easily form a continuous conductive film along the creepage path, thus allowing high surface leakage currents to flow on their wetted surfaces. Such currents cause dry bands at areas of high current density and lower wetting rates, which eventually cause surface arcing and frequently complete flashover of the insulator.

During recent decades, polymer insulators have been introduced and widely used at distribution voltage levels due to their better pollution performance. Currently, insulators made of polymeric materials are often called composite or non-ceramic insulators. Non-ceramic insulators, such as silicone rubber, offer several advantages over porcelain insulators. They have excellent hydrophobic (water-repellent) surface properties under wet conditions; this property helps to minimise the leakage current

and the probability of dry band formation. Moreover, they have high mechanical strength to weight ratio, resistance against vandalism, and reduced maintenance costs [1.3]. However, polymer materials have weaker silicone to oxygen (Si-O) bonds than porcelain materials so that they are more susceptible to chemical degradation under the multiple stresses likely to be encountered in service; including stresses due to high operating voltages, UV rays and pollution contamination.

Corona and electrical discharges can also result in secondary problems such as audible noise and electromagnetic interferences. Electrical discharges produce constant buzzing sounds, and the high-frequency electromagnetic wave from the discharge can cause disturbances in radio and television, as well as in other communication signals [1.4]. Under these stresses, the hydrophobicity on the surface of polymer weathersheds will be temporarily or permanently lost [1.5] after which the insulator will be vulnerable to flashover.

The pollution flashover performance of an insulator depends on the type of pollution deposit, properties of the insulator material and the wetting conditions of the site. Flashover of an insulator results in loss of power supply and may lead to damage to equipment and destruction of the insulator itself. Pollution type and its severity are dependent on the environment. In this context of pollution effects, rain can have a natural washing effect by removing the pollution layer before it has accumulated to a critical level.

In order to improve porcelain insulator performance under polluted conditions, coatings were used to mitigate surface leakage current, surface discharges and reduce flashover occurrence on existing and installed porcelain insulators. This practice is particularly suitable for insulators installed at substations with pollution severity.

Conventional coatings include greases and room temperature vulcanizing silicone rubber (RTV-SiR) coatings. In recent years, a novel Nanocoating: Voltshield has been proposed which is easier to apply, and it is claimed that it is highly performant with good hydrophobicity and low leakage current characteristics.

This thesis investigates the performance of this new coating and compares its leakage current suppression, its performance under UV radiations and its flashover voltage performance in comparison with existing coatings from various manufacturers.

1.1.1. The importance of high voltage insulator's coatings

Flashover of insulators due to the accumulation of contaminants poses a threat to the reliability of power systems. Insulator flashover results in undesirable power outages which are expensive. A combination of contaminants and moisture due to fog or rain on the surface of the insulator will give rise to a leakage current, and uncontrolled leakage currents in this manner leads eventually to complete insulator flashover.

The washing of insulators is a common method used to remove the accumulations of surface contaminants in polluted areas. This practice is labour intensive, and therefore expensive. The application of a suitable protective coating to these insulators eliminates the requirement for frequent washing, thus reducing maintenance costs.

The coating systems are able to suppress leakage currents. This enables an insulation system to attain increases in flashover voltage of up to 30% when compared with uncoated insulators [1.6]. Additionally, due to the reduced leakage current magnitudes on the surface of the coated insulators, power dissipation and hence energy losses are reduced, and the resulting reduction of surface heating lessens material degradation. This serves to increase the working life of the coating system.

Increasing the insulation level allows power systems engineers to utilise more compact transmission tower designs, which leads to reduced cost to the utilities [1.6].

1.1.2. Nature of contaminants

Depending on the environment, there is a mixture of contaminants that are deposited on the surface of the insulator. In the marine environment, the pollution consists mainly of soluble salt such as sodium chloride (NaCl). In the industrial environment, the pollution may contain a mixture of non-soluble materials and dissolved acids. These contaminants are classified into soluble and insoluble. The soluble contaminants are expressed in terms of Equivalent Salt Deposit Density (ESDD). ESDD is the weight of the NaCl in mg per unit of surface area and usually expressed in mg/cm^2. The Non-soluble contaminants are the weight of the kaolin in mg/cm^2 and expressed in terms of Non-Soluble Deposit Density (NSDD) [1.7]. However, as long as these contaminants are

soluble in presence of fog or rain and easily form a conducting film covering the surface of the insulator, flashover of the insulator becomes imminent.
Kaolin, also called china clay is a soft white inert material widely used in artificial pollution tests and recommended by IEC 60507standard.

1.1.3. Contamination flashover

Outdoor insulators work under different operating conditions. Under dry conditions, contaminants do not pose a threat as they are not conductive. However, under wet operating conditions, contaminants may dissolve to form a conducting layer. This layer can lead to leakage currents on the surface of the insulator. Under voltage stress, these currents result in heating and drying of the pollution layer. This process creates dry regions over the surface called dry bands. A concentrated electric field stress in the dry band region will lead to breakdown. When the voltage gradient across the dry band regions exceeds the dry bands' withstand capabilities, partial arcs over the surface starts to occur. If this arc propagates across the layer of contaminants which bridges the surface distance of the insulator, a flashover will occur [1.8]. Flashover may damage the insulator temporarily or permanently and may results in an interruption of the power supply depending on its severity [1.9]. Polymers, like silicone rubber and ethylene-propylene-diene monomer (EPDM), are hydrophobic materials and can suppress the leakage current much more efficiently than ceramic materials. This property makes the contamination flashover performance of the polymer much better than flashover performance of the porcelain [1.10].

1.1.4. Insulator contamination maintenance practices

Several practices have been used by utilities to reduce the occurrence of pollution flashover of the insulators to prevent disruption of the power system. One of these practices was to increase the leakage distance either by adding insulator sheds or by replacing the insulators with longer leakage path designs, thereby decreasing the voltage stress across the surface of the insulator [1.11]. This method cannot be implemented in every case as it is constrained by the dimensions of the towers. Another approach has been to apply a resistive glaze to porcelain insulators. This technique has been used to keep the insulator surface dry for extended periods of time

during natural wetting. Where difficulty is faced in wetting under the skirt area, fog bowls have also been used. The latter two practices have had limited success, and maintenance practices have also been variously successful.

High pressure cleaning techniques using either water or dry cleaning with an abrasive medium such as crushed corn cobs or walnut shells have been used regularly by most utility companies in severely polluted areas to wash insulators and prevent flashover. This method is labour intensive and therefore expensive. Although, it is hard to determine when washing is required, this method is constrained to heavily polluted areas. Due to their hydrophobic surfaces, silicone compounds for high voltage outdoor insulators offer advantages over other methods of protection. Experience with grease coating materials for porcelain insulators has shown that provided they retain their surface hydrophobic properties, they present total protection of the insulator [1.12]. In service, grease may decompose by the effect of dry band discharges and corona discharges. These decompositions will form filaments of the filler material in the grease coating. The concentration of fillers has the same effect on the grease as an atmospheric pollutant, and encourages the formation of dry band discharges within these paths, resulting in the formation of concentrated hot spots. If the temperature rise resulting from these discharges is large enough, the insulator may be subject to damage. Once fracturing of the insulator has occurred, flashover is expected soon afterwards. Formation of layers of fillers and dust, loss of hydrophobicity, and cracks are signs of grease degradations at this time the grease must be removed and new grease should be applied so that good protection performance of the insulators is maintained.

Non-ceramic insulators having silicone rubber weathersheds have been successfully used in maintenance of overhead lines for many years. The silicone rubber provides a water repellent surface, thereby preventing current leakage. When silicone rubber insulators are not available as direct replacements for porcelain and glass insulators, an alternative has been to coat the porcelain and glass surfaces with water repellent materials such as room temperature vulcanising (RTV) silicone rubber [1.13] and/or recently proposed coating systems such as Voltsheild or Nanocoating.

1.1.5. Nanotechnology

Nanotechnology refers to any technology that can be performed on a nanoscale and has applications in the real world. Much research has been carried out in this area, and potential applications are many and varied, including materials science, chemicals, textiles and semiconductors [1.14] Within the electrical/electronic area there have been many papers published on carbon nanotubes and nanofibres, nanowires, nano-diodes, and single-electron nano-transistors [1.15].

Lewis [1.16] pointed out the theoretical potential of "nanometric dielectrics" and to the role of nanometric interfacial processes in the initiation of electrical breakdown in insulating materials. Tanaka et al [1.17] reviews the types of nano-composite materials, their processing and manufacturing techniques, and their electrical properties, with a particular focus on improvements in insulation properties and dependability. The degradation of insulators' surfaces by partial discharges is shown to be greatly reduced by the incorporation of nano-fillers as reported by El-Hag [1.18]. Montanari et al [1.19] confirms that the electrical properties of nanocomposite insulating materials for outdoor high voltage applications, specifically, conductivity and breakdown voltage, can be improved with respect to the basic materials. Reference is made to two polymeric materials, polyethylene-co-vinylacetate (EVA) and polypropylene (PP) that are widely used as electrical insulation for cables and capacitors, the performance of which are improved when filled with synthetic nanofiller consisting of an organophilic silicate.

The aims of high voltage insulator research are to extend installed lifetime, to optimize life cycle costs, to reduce maintenance expense, to achieve reductions in size or weight and to increase the overall efficiency of the power systems into which they are installed. As an example of a recent practical application of nanotechnology in the field of outdoors insulators is the application of nano-coating for porcelain and glass insulators [1.20].

1.2. Aims, methods and results

1.2.1. Aims

The prime motivation of this work is to ensure safer and more secure distribution systems, to reduce maintenance expenses, to decrease the size or weight of the insulation system and to increase system efficiency. The aim of this research programme was to investigate and assess the performance of different coating materials used to minimise leakage current, reduce the heat and eliminate flashover in high voltage insulators that run in polluted environments.

The principal aims of this research work are as follows:

(a) To prove the effectiveness of protective coatings in reducing dry band formations and thermal damage of the coated surface due to surface discharges, and to reduce flashover incidence of insulators. A track is defined in IEC60587 [1.22] as a partially conducting path created by localized deterioration of the surface of an insulating material, and tracking is the process that produces tracks as a result of the action of electric discharges on the contaminated surface. Erosion is defined in the same standard as the wearing away of electrical insulating material by the action of electrical discharges.

(b) To identify the optimum coating system that exhibits the highest resistance to tracking and shows the maximum reduction in surface erosion .

(c) To set up test procedures for testing different coated insulators in clean-fog tests that include leakage current measurements.

(d) To test and assess the flashover performance of different coated insulators under artificial pollution conditions and clean-fog tests and to compare these results with those obtained with conventional ceramic insulators having the same geometry.

(e) To evaluate the effect of UV radiation on the performance of the coatings used under artificial pollution tests of IEC60507 [1.21] and under the inclined plane tests of IEC 60587 [1.22].

(f) To develop a data acquisition system for the fog chamber tests and for the inclined plane tests that would be used to acquire the test voltage and the leakage current waveforms and store these data into files for post-processing analysis.

The data acquisition system for the inclined-plane tests would be capable to control

the voltage application to the samples and terminate the test and any point of time.

In order to achieve these aims, it was required to use a computer techniques to analyse the voltage and the leakage current signals on tested insulators and to identify signs related to the insulator condition. In approaching these aims, the coating systems used in this investigation were:

- Two RTV coatings from different manufacturers.
- One Voltshield 'Nanocoating' system.
- Two different grease coatings.

1.2.2. Methods

The coating materials were tested under artificial pollution conditions according to the solid-layer clean-fog method of IEC60507 which is applicable for the determination of the power frequency withstand characteristics of ceramic insulators used in outdoor applications on AC systems and exposed to polluted atmospheres. The material's resistance to tracking and erosion was evaluated using a liquid contaminant and the inclined plane test under AC voltage according to IEC60587. Rectangular standard size samples are mounted at a 45° angle and subjected to high voltage stress. Contaminated solution is fed from the top of the sample and covers the test surface. This test is intended to promote the formation of partial arc discharges in order to evaluate the material's resistance to erosion and tracking. The performance of these coatings was evaluated by analysing the leakage current on their surfaces.

Data acquisition system programs were developed based on National Instruments' LabVIEW platform to interface with the test equipments used for both the clean-fog tests and the inclined-plane tests and allow extensive experimental data to be collected. The applied voltage and leakage current signals were acquired throughout the tests and saved for further analysis. In the case of the data acquisition system built for the inclined-plane tests, the software also performed the automated digital operation of the accelerated ageing unit to comply with the requirements and guidelines of the relevant international standard.

The effect of UV radiation on the coatings was investigated using an Atlas weathering machine. Hydrophobicity tests were also performed on the coating systems after

pollution tests by using a simple spray nozzle. The effect of UV on the hydrophobicity of the coatings was also investigated by placing a dye droplet on a surface of coated sample before and after UV exposure, and also by measuring the leakage current on the surfaces of the samples exposed to UV radiation under artificial pollution condition in the fog chamber tests, to evaluate the suppression capability of the coatings to current formation following UV exposure. Adhesion of the nanocoating to the surface of the insulator was investigated by exposing the nanocoated insulator to sandblast degradation, and testing under artificial pollution conditions in the fog chamber to examine the effect of sand storms on the adherence of the coating to the surface and its ability to suppress surface current.

Data analysis programs were developed to read and analyse the acquired data and to evaluate the performance of the coating systems. The programs produced descriptors characterising the leakage current, such as leakage current peak, RMS leakage current, energy dissipated on the surface of the insulators to identify trends related to the insulator performance.

The electric field and the voltage distribution along a defined surface distance of coated and uncoated insulators under clean and pollution conditions were studied using a finite element analysis and solver software package, COMSOL Multiphysics®. The insulators were modelled with a pollution layer having different forms of uniform and non-uniform pollution layers. The non-uniform pollution layer is applied in form of pollution patches and water droplets of different diameters having the pollution properties.

1.2.3. Contributions of this thesis

The results of this study show that:

- With a Nanocoating applied to the porcelain insulator, the surface becomes highly hydrophobic. A wetting agent was used in the pollution tests of all hydrophobic materials to help pollution adhere to the coated surface. Nanocoating suppressed leakage current and reduced the energy dissipated over the surface but the nanocoated insulator had a lower flashover voltage than an uncoated porcelain insulator having similar geometry. The nanocoated insulator lost its hydrophobicity showing a water film on its surface when exposed to fog application as seen through pollued wet tests. Nanocoating had good

performance after exposure to 8 hours of UV radiation in terms of minimizing leakage current on its surface, and showed good resilience to sand blasting. However, with long exposure to sand blast stress, the Nanocoated insulator began to deteriorate by exhibiting pockmarks on its surface.

- When applied to the porcelain insulator, RTV coating systems minimised the leakage current and reduced the dissipated energy over the surface. Most interesting was the finding that RTV coatings showed high resistance to tracking and erosion. Another important finding was that RTV coatings showed high stability under UV exposure, where the coatings were exposed initially to two hours of UV radiation equivalent to 87.5 hours or 3.64 days of continuous exposure to real sunlight. There was a significant positive correlation between the time of exposure to UV cycles and the performance of the RTV coatings in terms of leakage current suppression and retention of surface hydrophobicity when the coatings were exposed to 8 hours UV radiation equivalent to 350 hours or 15.60 days of continuous exposure to real sunlight. Also, associated with an increase of UV exposure time, there was an increase in the coating's resistance to tracking and erosion. RTV-coated insulators had higher flashover voltage than uncoated porcelain insulators under clean wet and polluted conditions.
- Grease coated insulators showed good performance for both suppressing leakage current and reducing energy dissipated over the surface of the insulator. Silicone grease coated insulators had the highest flashover voltages among the insulators tested under the artificial pollution test conditions.
- Uncoated insulators, when compared to coated insulators, had higher leakage currents (because of their hydrophilic surface property and the development of resistive surface currents), higher dissipated energy and resulting lower flashover voltage levels.
- The electric field peaked at the electrode regions for coated and uncoated insulators. However, it generally decreased along the insulator surface with distance from the high voltage (HV) electrode. The presence of a non-uniform pollution layer in the form of water droplets at the HV electrode increased the field magnitude on the surface drastically when compared to a uniformly polluted insulator.

1.3. Thesis outline

The structure of this thesis is as follows:

Chapter 2 provides an extensive review of published literature pertaining to the field of protective coatings used for HV insulators. An overview of protective coatings used to alleviate the problems arising from the use of ceramic insulators under pollution conditions, such as greases and RTV silicone rubber, is given. A review of the research work on pollution flashover and flashover mechanisms for ceramic insulators is presented. The discussion also includes key advantages, material properties, and factors contributing to the ageing process, including electrical and environmental stresses.

Chapter 3 describes the methods and the test facilities used for testing high voltage insulators with different surface coatings. The fog chamber test facility and the inclined plane test machine and their electrical circuits are explained and discussed. Preparation of the pollution contamination suspension and the method for applying the pollutant to an insulator surface are explained. Wetting rate tests to confirm the compatibility of the fog chamber to the international standard of IEC60507 are also presented and discussed. The developments of computerised data acquisition systems for the fog chamber and the inclined plane test facilities to acquire traces of voltage and current signals are discussed. Data analysis program was also developed and used to analyse the acquired leakage current and voltage traces. This data is used to characterise the pollution performance of the tested insulators. The effect of UV radiation on the coating materials was studied using an Atlas XXL+ artificial weathering test station which uses three air cooled Xenon arc lamps of 1700 W each capable of producing more than 90% of the natural sunlight spectrum.

Chapter 4 results of tests performed on insulators uncoated in comparison with insulators coated with Nanocoating, RTV1, RTV2 and grease coatings in a laboratory fog chamber using the solid layer method of IEC60507 are presented. In this method the insulators were polluted and wetted by exposure to a clean fog, and leakage current and test voltage were acquired and saved for further analysis. RMS current, Average power and accumulated dissipated energy were calculated using an analysis program

described in Chapter 3 and the results were presented and analysed with the aim of identifying trends related to insulator coating performance. The effect of different UV exposure dosage on the hydrophobicity of the coatings and on the performance of the coatings under artificial pollution tests are also presented and discussed. Flashover voltage results of all insulators, and sandblast test results for Nanocoated insulators are also presented.

Chapter 5 presents the results of the inclined plane tests performed on RTV1 and RTV2-coated samples. The tests were performed according to IEC60587, where the samples were tested using a liquid contaminant and fabricated insulator specimens in the inclined plane test facility. Leakage current and applied voltage were acquired and saved for further analysis. RMS current, Average power and accumulated dissipated energy were calculated using an analysis program described in Chapter 3 and the results presented and analysed with the aim of identifying trends related to coatings' resistance to tracking and erosion. The chapter also demonstrates the effect of different UV exposure dosages on the resistance of RTV1 and RTV2 coatings to tracking and erosion.

Chapter 6 presents results of electric stress simulations on coated and uncoated insulators. These simulations are intended to determine the electric field over the insulator surface to identify regions of high electric field stress. A commercial finite element package is employed for insulator modelling to determine electric potential and field distribution along the creepage path under dry-clean and wet-polluted surface conditions, with linear and non-linear pollution models characterised by field-dependent conductivity achieving a better and more realistic field simulation. The conductivity of the pollution layer was assigned a value based on laboratory measurements. The simulation results are discussed in this chapter.

Chapter 7 presents general conclusions based on the findings in this study, and outlines some recommendations for future investigation.

Chapter 2- Coatings for high voltage insulators - a review

2.1. Introduction

The failure of insulators in service primarily occurs during severe conditions of pollution and in the presence of fog, dew or heavy rain. This chapter presents a review of a number of remedies which were used by electricity companies in the past to improve the surface properties of high voltage insulators, including greasing and RTV coatings.

During the last four decades alternative materials, namely, polymers, have emerged. Recognition of the hydrophobic and adhesive properties of these materials led to the hypothesis that such materials might prevent surface discharges on insulators operating in humid contaminated atmospheres since water is dispersed of their surfaces [2.1]. Presently, they are being used in large numbers for a variety of outdoor HV applications. The main advantages of polymers when compared to ceramic insulators are: light weight, superior vandal resistance and better contamination performance [2.2]. However, corona discharges and dry band arcing due to the presence of electrolytic film on the surface of an energized insulator can contribute to degradation of the polymer material which will lead to material failure [2.3, 2.4]. In contrast, porcelain and glass insulators are inert materials and do not degrade due to corona and dry band arcing.

Many polymers have been tried as materials for outdoor insulators including: RTV silicone rubbers and high temperature vulcanized (HTV) ethylene propylene rubbers (EPR), epoxies and polyethylene. Initial service experience showed that some of these polymers were better than others. For example, although good electrical performance was obtained from silicone rubber insulators using the RTV weathersheds, the tear resistance of the RTV was inadequate [2.5]. Some of the earlier generation epoxy insulators were deficient in their resistance to moisture, tracking and UV radiation from sunlight. Polyethylene is flammable and insulators using this material have sometimes

resulted in pole fires. RTV silicone rubbers are also widely used as a thin coating on existing ceramic insulators in areas with contamination problems [2.6, 2.7].

This chapter provides a review of published literature related to the field of protective coatings used for outdoor HV insulators. Various types of protective coatings, such as greases and RTV silicone rubber, are used to alleviate the problems arising from the use of ceramic insulators under pollution conditions, and an overview of these coating materials is given. Pollution flashover and flashover mechanisms for ceramic insulators are presented. The electrical and environmental stresses that contribute to the ageing process of the protective material are also discussed.

2.1.1. Pollution flashover

CIGRE working group 33.04[2.8] describe the pollution flashover process for ceramic insulators as follows:

1. For insulators contaminated with a layer of pollution containing soluble salts or dilute acids or alkalis, there are two cases: if the pollution is wet in a form of a liquid electrolyte, steps 3 to 6 may proceed immediately whereas for the case of a dry non-conductive layer, a process of layer wetting described in step 2 is essential.
2. Under wet environmental conditions such as fog, mist light rain, sleet or melting snow or ice, the pollution layer becomes wet, either completely or partially, and thus conductive. Heavy rainfall may be beneficial by washing off the pollution from the insulator surface, or it could lead directly to flashover.
3. Under energisation, a surface leakage current starts to flow on the surface of the insulator which dries out parts of the wet layer due to the current heating effect.
4. A non-uniform drying of the wet layer results in the formation of dry areas, called dry-bands, which may be only a few centimetres in width. These areas interrupt the flow of current on the pollution layer.
5. The energisation voltage applied across the dry-bands creates the conditions for the air breakdown, and the dry-bands are bridged by surface discharges which are electrically in series with the resistance of the wet pollution layer. Fast current pulses are associated with the spanning of dry-bands by discharges.
6. If the resistance of the wet pollution layer is low enough, the dry-band

discharges remain active and gradually longer sections of the insulator are spanned. This in turn results in a further decrease in the wet layer resistance, increases the current and permits the arcs to bridge even more of the insulator surface, and finally in complete flashover of the insulator.

Figure 2.1(a) shows the main stages of pollution flashover for ceramic insulators.

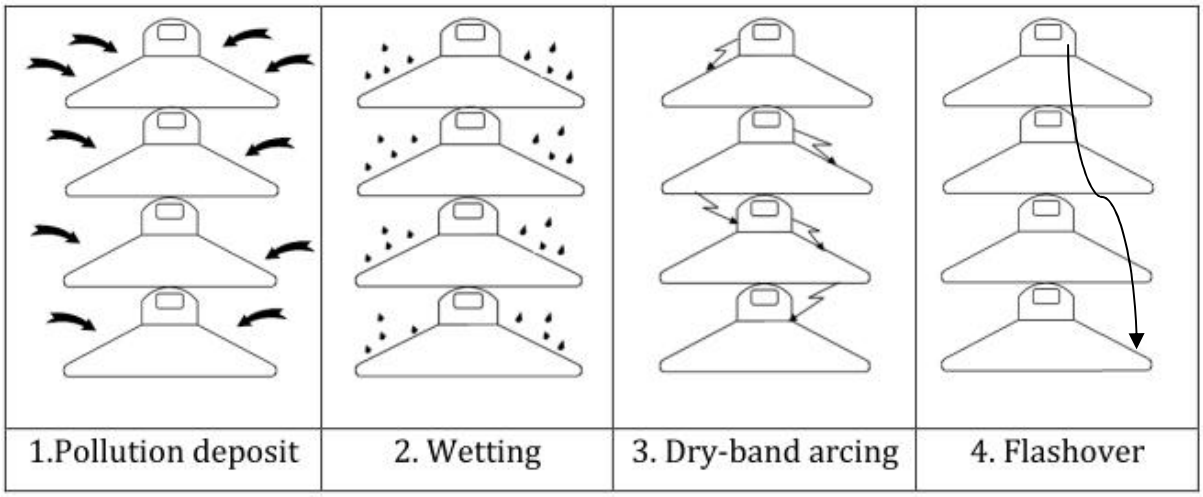

Figure 2.1(a). Pollution flashover process for the hydrophilic surface. Schematic representation recreated from [2.8].

Hampton [2.9] measured the voltage distribution along a polluted flat insulation strip and describes the process of dry-band formation. The processes governing flashover on polluted insulators have been the subject of many previous investigations. The simplest model that has been developed is a series arrangement of the dry zone partial arc and the resistance of the polluted wet zone [2.10]. The voltage across the insulator is determined from equation (2.1).

$$U = x\,A\,I^{-n} + (L-x)\,R_p\,I \qquad (2.1)$$

Where $x\,A\,I^{-n}$ is the arc stress and $(L\text{-}X)\,R_p\,I$ is the field stress in the pollutant layer. x is the arc length, L is the length of the insulator leakage path, R_p is the resistance per unit length of the pollution layer, I the leakage current and A and n are experimentally derived arc constants.

Measurement of R_p for a wet zone is not straightforward, and it may therefore be replaced by an expression including the conductivity σ_p of the pollution layer:

$$\sigma_p = \frac{1}{Rp} \quad F_i \qquad (2.2)$$

where F_i is a form factor for the insulator, defined as follows:

$$F_i = \int_0^L \frac{1}{\pi D(l)} dl \qquad (2.3)$$

where $D(l)$ is the insulator diameter which varies along the leakage path.

Equation (2.4) defines the critical condition for propagation of the discharge along the surface of the insulator to lead to flashover.

$$\frac{dI}{dX} > 0 \qquad (2.4)$$

The voltage under this critical condition yields

$$U_c = x_c A I_c^{-n} + (L - x_c) K R_p I_c \qquad (2.5)$$

The coefficient K is added to validate Equation (2.1) at the instant of flashover and to modify R_p in the presence of current concentration at the arc foot point.

At the critical flashover condition, the arc length is given by:

$$x_c = \frac{1}{n+1} L \qquad (2.6)$$

Solution of the moment of flashover yields for the critical current:

$$I_c = (\pi D_r \sigma_p A)^{1/(n+1)} \qquad (2.7)$$

and for the critical voltage:

$$U_c = \frac{A}{n+1} (L + \pi D_r F_i k_n) (\pi D_r \sigma_p A)^{-n/(n+1)} \qquad (2.8)$$

where D_r is the diameter of the insulator.

Eqn (2.8) allows one to calculate a critical value of the voltage occurring at the instant of flashover, as a function of the dimensions of the insulator (D_r and L), the arc constants A , n and the pollution σ_p (F_i, and K are themselves functions of the insulator dimensions). Once the arc constants A and n have been determined, it is possible calculate a value for the critical voltage. A genetic algorithm has been explained and used by Gonos [2.10] to determine the arc constants.

2.2. Types of protective coatings

Protective coatings are applied to ceramic insulators to improve their hydrophobic surface properties. An effective protective coating for inhibiting the formation of surface water films must be water-repellent, such that a contaminated insulator presents a high resistance with low leakage current and dry band arcing [2.11, 2.12, 2.13,2.14].

Many coatings have been used on ceramic insulators such as waxes, paints, lacquers and varnishes. However, their use is limited because of concerns about their long term performance. These coatings tend to wet-out as easily as normal porcelain insulators, and may also damaged by corona discharges. These coatings are easily loss their hydrophobicity when exposed to environmental stresses such as corona discharges and UV. When hydrophobicity is lost they wet-out as normal porcelain insulator and exposed to flashovers. Furthermore, paints and lacquers do not necessarily show good hydrophobic surface properties as they wet as easily as ceramic insulators and are, therefore, subject to weathering stresses and easily damaged by corona discharges [2.15].

2.2.1. Oil-bath insulators

Satisfactory insulators to combat pollution flashover have been used with oil baths. An oil surface is practically un-pollutable, as all solid particles are mixed with the oil. It is manufactured using pedestal-post and weathershield and also cap-and-pin and pin-type constructions. Figure 2.1 (b) shows a single string of an oil path type insulator of multi-units cylindrical post insulator with a closed oil reservoir at the top from which there is a controlled slow leak. By the effect of the wind and owing to the tendency of oil to creep and deposit on the surface of the lowest insulator in the string. The entire

surface of the insulator becomes covered with oil and presents a very high resistance to the flow of leakage current. As oil creeps over the rest of the surface, impregnating any solid pollution and rendering it water-repellent. Consequently, the pollution performance of this type of insulator has been very satisfactory. When the oil becomes polluted with water and dirt, it should be replaced with new oil. Wind is a prime cause of oil loss and insulators, with small baths or when the oil baths are improperly protected from rain and wind, need frequent checking and refilling [2.16]. Service experience with oil-bath post insulators at extremely polluted sites has been quite good, but there have been some flashovers. Complexity of profile makes their manufacturing extremely difficult and this is considered as their main drawback as the oil was blown out of the reservoir and was hard to adequately protect the oil paths from rain and wind [2.17].

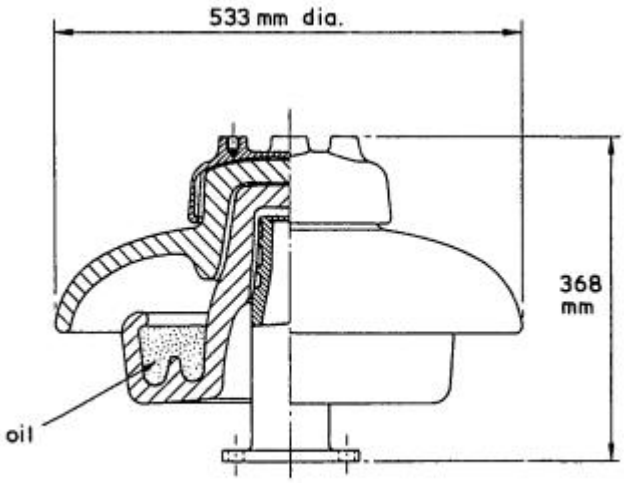

Figure 2.1(b): Oil path insulator [2.16]

2.2.2. Control of voltage distribution

If a fairly uniform voltage distribution could be maintained over an insulator surface under all conditions, flashover would be avoided. However, under wet operating conditions the voltage distribution on a porcelain insulator becomes non-uniform due to the wetted pollution layer on its surface, as a result surface discharges and perhaps complete surface flashover may occur [2.18]. This difficulty can be overcome if the insulator is subdivided into a number of sections and each section paralleled with a suitable fixed resistance. There are various ways in which the fixed resistances can be incorporated in the insulator, but one of the most attractive methods is to coat the porcelain with a glaze having the required resistance. Glazes consist mainly of glass containing a small proportion of tin oxide particles. The thickness of the glassy layer was estimated to be about 4 μm, while its resistivity was found to be in the order of 10^8-10^9 Ωm. The glaze permits a small current to flow which results in a continual resistive heating. This has a tendency to keep large areas of the insulator surface dry, thus minimizing leakage current and reducing the arcing activity that leads to flashover [2.7]. Unfortunately, field tests showed that the glaze deteriorated in less than a year, particularly near metal fittings where contact was made between the cement and the glaze. Experience has shown that, for a heavily contaminated glazed insulator, the instant of HV line energization is when this insulator is most likely to flashover [2.19].
Accordingly, alternative methods were pursued. One of the most attractive methods of obtaining the required resistance is to coat the porcelain with a semiconducting ceramic glaze having the desired surface resistivity. Semiconducting glaze contains conductive oxides and a small amount of antimony in addition to niobium-oxide, all in an ordinary glaze base. These additives were found effective to improve performance of the glaze against corrosion. Tests confirmed that the voltage distribution is effectively controlled and performance is greatly improved in comparison with that of similar insulators with normal glaze. Tests also showed that the leakage current of the insulator with semiconducting glaze remained relatively low, and showed no current spikes [2.21, 2.21]. An intensive investigation of the electrical properties of semiconducting glazes under polluted conditions has shown that the deterioration of the glaze was caused by a kind of electrolytic corrosion, and also because most of the semiconducting ceramic glazes are thermally unstable. These difficulties limited the adoption of insulators with

semiconducting ceramic glaze. However, it should be noted that a limited amount of success has been achieved in reducing the number of flashovers compared with the performance of untreated porcelain insulators [2.22].

2.2.3. Greases

Greases, like oils, are water-repellent, and since some oil-bath insulators had proved successful in service operation, it was worthwhile to investigate the behaviour of grease-coated insulators.

Greases have been a popular method and are still being used by many utilities for insulator maintenance for minimizing contamination flashover. Grease mainly is a combination of fumed silica and oil (fluid). The presence of grease on the surface of the insulator makes it hydrophobic and so the moisture tends to remain in discrete droplets. The contaminants are encapsulated by oil from the greasy surface, thus retaining water repellency to the surface. Furthermore, the solid salts in the pollutant are engulfed by oil from the greasy surface and cannot easily be dissolved by water. For these two reasons, grease has been found to give a high flashover voltage to insulators in areas of heavy pollution [2.17].

Petroleum jellies and silicone greases are the most known types of greases.

2.2.3.1. Petroleum jellies

Petroleum jellies or petrolatum are obtained from a wide range of petroleum fractions, but are mostly synthesised from hydrocarbon oils, slack and microcrystalline waxes. Due to their composition, petroleum jellies are stable under severe environmental and service conditions. Softening of the jellies occurs with an increase in temperature, and melting is typically observed at the sites of current discharges. On cooling these coatings then resume their former properties. The temperature at which this happens, the 'sliding temperature', is an important characteristic of the material. This limits their application to relatively moderate climate conditions [2.7]. In the UK, insulator surface temperatures of 50° C have been recorded [2.17] and earlier petrolatum slid below this temperature, but petrolatum with very high sliding temperatures of up to 115° C are now available.

2.2.3.2. Silicone greases

Originally, silicone greases were composed of inert filler, usually silica flour, fumed silica filler, or silicone fluid and a coupling agent. Since 1975, however, a new range of silicone greases have been available with the addition of alumina trihydrate; the concentration of which significantly changes the characteristics. Silicone greases maintain practically the same viscosity over a temperature range of -50° C to +200° C and do not melt so they can be used in all climates, but they decompose at temperatures above about 200°C. Apart from their high cost, their main disadvantage is that electrical sparking causes decomposition, leaving the silica filler and some solid carbon which then act as pollutants. The inorganic backbone of the silicone polymer is composed of silicone and oxygen atoms, exhibiting an increased resistance to UV degradation in comparison with petroleum greases having an organic backbone [2.1, 2.7].

2.2.3.3. Application of grease coating

Petrolatums are relatively cheap and are applied at least 3 mm thick. When melted, they can be sprayed using an airless-spray, or insulators may be dipped to produce a more uniform coating. The newer soft compounds with high sliding temperatures can be applied by hand. When grease loses its efficacy due to the dirt which is accumulated in it, it may be removed by scraping (if hard) or wiping (if soft enough). A major problem with petrolatums is the relatively long time it takes to remove the grease layer. However, only the dirt accumulated on the top layer needs to be removed if the insulator is to be regreased.

Silicone greases are normally applied to clean insulators by hand, brush or spray application. The sprayable compounds can be dispersed in a solvent such as 1,1,1, trichloroethane to produce a consistent coating [2.7]. The properties of silicone grease spray coatings vary considerably due to different quantities of alumina trihydrate filler and varying quantities of the different solvents which when evaporated leaves a very thin coating [2.1] so that this method is not recommended.

2.2.3.4. Service experience with grease

When compared with bare ceramic insulators, grease coated insulators typically provide a better protection, provided surface hydrophobicity is maintained. The effectiveness of coating with grease is dependent on a number of factors, principally the coating thickness and uniformity, and the severity of contamination. However, during extended exposure to corona, ultraviolet light, water erosion or contaminant encapsulation, ceramic insulators with grease coatings behave no better than their uncoated equivalents. Silicone compounds exude oil around dirt deposits on the surface within minutes, thus keeping a water-repellent surface, but, if sufficient pollution has accumulated and absorbs all the oil, the surface will become non-oily and in this case hydrophobicity is lost. This exposes the grease to increasing leakage current and dry band discharges [2.17]. The heat generated from dry band discharges will cause the grease to decompose over time. Signs of degradation include the appearance of cracks, loss of hydrophobicity, the formation of channels with thick layers of dirt, and tracking. In this case, the grease must be removed and new grease applied. Because the petrolatum layer used is so much thicker than a silicone-compound layer, the effective life of a petrolatum layer is 2-3 times that of a silicone-compound layer [2.23].
Field experience with grease coated cap and pin insulators within a cement plant showed that it was essential maintenance to re-grease these units with silicone grease every three months to avoid contamination flashover as the contamination rate was extremely high. The useful life of grease ranges from less than a year to 10 years depending on the pollution level of the site. In most cases, the insulators need to be re-greased every two years. Hot-line re-greasing is labour intensive and expensive, while off-line re-greasing results in service interruption [2.7].

2.2.4. Room temperature vulcanizing (RTV) silicone rubber coatings

Grease coatings fail to provide protection to porcelain insulators from flashover under severe pollution conditions, thus it needs to be replaced regularly, which requires maintenance shutdowns of the electrical power system. This triggers the need for longer-lasting coatings with good electrical performance that resist UV radiation, minimise dry band arcing and require less maintenance. This has led to the development and application of a protective elastomeric coating for porcelain insulators

that can be used in severe contamination areas that require frequent cleaning [2.24,2.25,2.26].

RTV coating is a liquid polymer that vulcanizes when exposed to moisture in air. Vulcanization is a chemical process for converting the rubber or other polymers into more durable materials via the addition of curative components. These additives modify the polymer by forming crosslinks between individual polymer chains. Vulcanized materials are less sticky, and have superior electrical and mechanical properties. RTV silicone rubber insulator coating systems consist of a polydimethylsiloxane (PDMS) polymer with an alumina trihydrate (ATH) or alternative filler. Several systems also contain an adhesion promoter, reinforcing filler and pigment. These systems are dispersed in a carrier medium such as naphtha or 1,1,1 trichloroethane, such that the RTV rubber may be applied to the insulator surface. Curing occurs when the RTV coating is exposed to atmospheric moisture. Basically, RTV coating materials are solvent based. After application of RTV on the surface of the insulator, the solvent evaporates, and the RTV vulcanizes in the air and forms a solid rubber coating. The type of solvent, the curing chemistry and the relative humidity of the air all determine the reaction rateby which this process is accomplished [2.27]. An RTV coating can be applied to a ceramic insulator by a process of dipping, painting or spraying. Coatings dispersed in 1,1,1 trichloroethane can be applied to energised insulators with safety precautions, while those dispersed in naphtha must not be applied to energized insulators due to the inflammability of the carrier medium. The ATH filler is added to polymeric materials to impart the coating resistance to tracking and erosion [2.28, 2.29]. There is considerable variation in the electrical and physical properties of the available formulations of RTV coating systems. Such variation is the result of the relative amounts of ATH and reinforcing fillers in the coating, the degree of cross-linkage in the polymer, and the adhesion of the coating to the insulator surface. The properties of adhesion, water repellency and electrical tracking and/or erosion resistance are of paramount importance to ceramic insulator performance [2.30].

2.2.4.1. Effect of coating thickness on leakage current

Deng et al. [2.31, 2.32, 2.33] investigated the dependence of leakage current on coating thickness by coating fibre glass reinforced plastic fibreglass (FRP) (polyester resin) rods

with RTV silicone rubber coatings with thicknesses ranging from 0.15 to 1.40 mm. Figure 2.2 shows the current pulse rates over time for coated specimens. At the start of salt-fog test the hydrophobic properties and the roughness of the surface of all coatings were independent of the coating thickness. But as the test progressed, the surface gradually lost its hydrophobicity allowing dry band arcing activities on the surface. This resulted in a higher surface temperature and more damage to the RTV-SiR coating. The thicker coating conducts the heat away from the surface more slowly and, therefore, experiences higher temperature which leads to greater damage to the surface and causes higher leakage current. The current increased with increasing coating thickness and also developed earlier for the thickest coatings. This, in turn, increased the surface roughness and reduced water repellency, leading to further growth in the occurrence of dry band discharges on the surface of the thicker coatings. As a result, the heat transfer from the surface to the substrate rods depends on the thickness of the polymeric coating.

The dry band discharges in the coating layer of thickness of 0.15 mm developed earlier than for thicknesses 0.38 and 0.57 mm, and the resulting heat is conducted to the substrate far more effectively, and thereby reducing surface temperature and associated damage. Conversely, the thin coating has less material available to be eroded, and this has the potential to expose the substrate to damage far earlier than would be the case with a thicker coating. Specimens with thin coatings had a tendency to fail sooner as a result.

Deng et al. [2.34] showed that the development of leakage current pulse over time by performing experiments on porcelain substrates coated with RTV-SiR of different thicknesses, the leakage current pulses were dependent on the coating thickness and the results can be seen in Figure 2.3. Deng used analogue to digital converter to measure the current peaks across a high voltage resistor which is connected to desktop computer through protection elements.

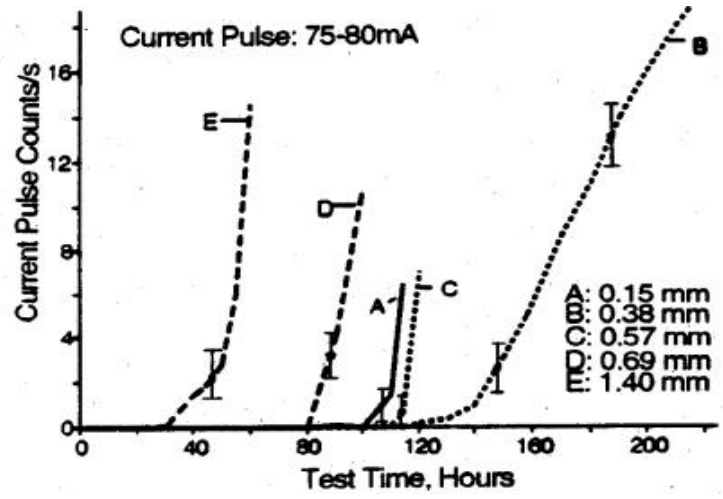

Figure 2.2: Time-variation of leakage current pulse rate in RTV exposed to salt-fog for different coating thicknesses [2.31]

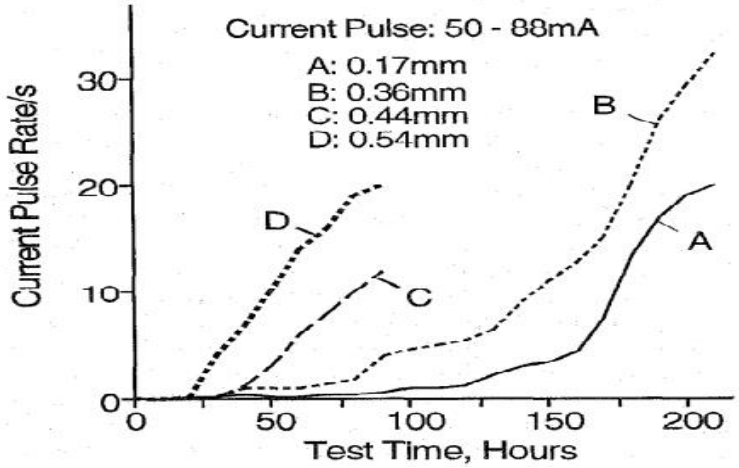

Figure 2.3: Current pulse rate as a function of time in salt-fog for different RTV coating thicknesses [2.34]

Abd-Elhady et al. [2.35] have studied the effect of RTV coating thickness on leakage current development on coated glass samples under solid layer and clean fog conditions for both DC and AC applied voltages. The study showed that the leakage current is dependent on the coating thickness for both AC and DC voltages under clean fog conditions. In contrast, the current developed earlier in the un-coated samples. On the other hand, the coatings suppressed the leakage current formation for a time which depended on the type of the applied voltage;AC or DC. The reason for this is attributed to that the melted salt on the surface of the coating, which because of fog condensation, form droplets due to the hydrophobic property of the surface. However, as the test continued, the melted salt, created dry band arcing which led to loss in hydrophobicity, and as a result, leakage currents started to develop for the coated samples at different

test times, as shown in Figure 2.4. Under DC voltage test, the coatings had suppressed the leakage current for time almost double the time under that of AC test.

The heat generated from the dry band discharges damaged the RTV coating by erosion which exposes the substrate to the heat which in turn determine the lifetime of the coating. There is an optimum coating thickness that gives the longest lifetime, see Figure 2.5. Typically, from 0.3 to 0.6 mm thickness is used on FRP rods in outdoor insulators [2.31]. However, the optimum coating thickness is dependent upon the formulation of the materials used in the polymer and on the type of substrate as these have different thermal conductivities which determine the rate of erosion of the RTV materials and its lifetime under dry band arcing conditions [2.33].

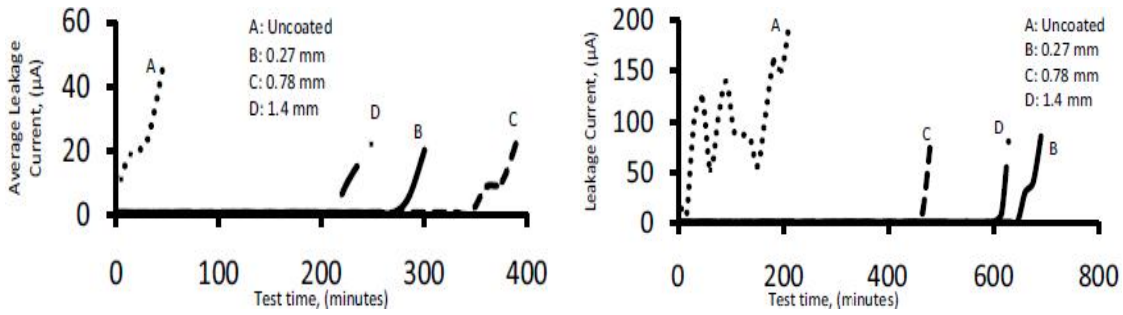

Under AC voltage Under DC voltage

Figure 2.4: Leakage current on glass slab sample coated with RTV as a function of test time in clean fog under AC and DC voltage with different coating thicknesses. Conditions: 0.6 mg/cm², of ESDD [2.35]

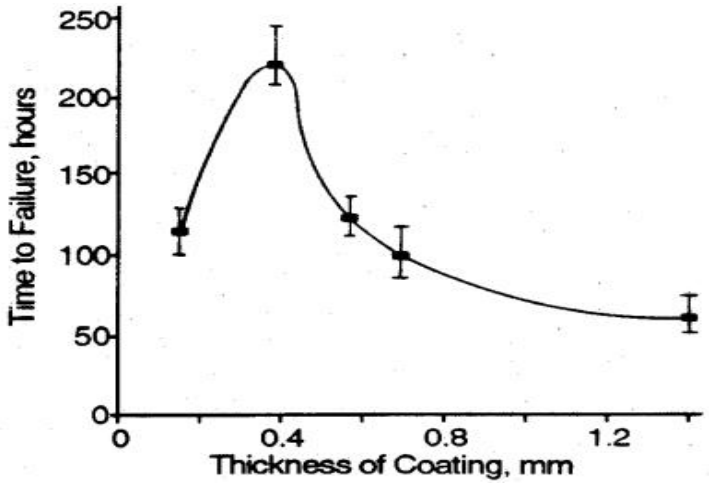

Figure 2.5: Time to failure of RTV-SiR as a function of coating thickness [2.31]

2.2.4.2. Dependence of leakage current and time to failure on substrate type

In the same investigations, Deng et al. [2.31, 2.33] studied the dependence of leakage current and time to failure on substrate type. The current pulse rate as a function of test time for RTV coatings applied to epoxy FRP, polyester FRP and glass substrates is depicted in Figure 2.6. The RTV coating thickness of 0.37 mm is about the same for the three substrates. It was observed that at the start of the test, the RTV coating transferred the heat generated from the dry band arcing from the surface to the substrate equally. As the test progressed, the current pulse rate developed earlier with the epoxy FRP compared with the other samples and the current discharges partly eroded the RTV-SiR and exposed the epoxy FPR to the salt fog which resulted in more discharge current on the substrate leading to substrate failure by tracking at an earlier time than with the other two samples. The time to failure of the RTV-SiR coated substrates is given in Table 2.1. Glass can withstand a large amount of heat without serious damage because of its high melting temperature (1252 °C), and specific heat capacity of (0.837 kJ/kg K) [2.6]. On the other hand, because of its lower thermal stability, epoxy FRP was more easily damaged by the heat generated during dry band arcing on the surface which resulted in a shorter life time of the coatings as shown by Table 2.1.

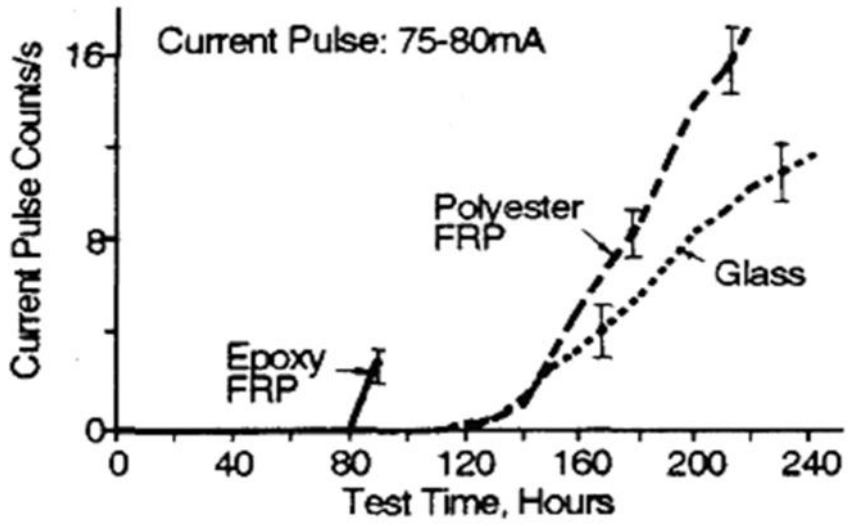

Figure 2.6: Dependence of current pulse count rates on test time for coated substrates exposed to salt-fog [2.31]

Table 2.1: Time to failure of RTV coatings on different substrates [2.31]

Substrates	Epoxy FRP	Polyester FRP	Glass
Coating Thickness, mm	0.38 ± 0.05	0.36 ± 0.04	0.30 ± 0.03
Time to Failure, hours	90 ± 39	220 ± 36	244 ± 22

2.2.4.3. Dependence of leakage current on the amount and type of filler

I. Amount of filler

Silicone elastomers have long been known to maintain their hydrophobicity and water repellency characteristics when exposed to adverse weather conditions [2.3,2.6,2.10,2.29]. However, under prolonged wetting conditions, the surface hydrophobicity can be lost temporarily and leakage current can develop. Localized drying of the surface results, which leads to the initiation of dry band arcing. The presence of ATH filler in the formula of Silicone Rubber insulators plays an important role in combating against material degradation in the form of tracking and erosion. The ATH filler decomposes into anhydrous alumina and water if a temperature of above 220°C is attained [2.36]. Kim et al. [2.37] studied the effect of different filler levels on the coating performance and found that, in one hour tests coatings with increased filler levels develop higher leakage current earlier than coatings with lower filler levels. In long duration tests of 10 hours, however, coatings with increased filler levels suppress leakage current even after loss of surface hydrophobicity. Measurements of the IR spectra using fourier transform infrared (FTIR) spectroscopy which is a powerful technique that can provide information on molecular structure. FTIR spectroscopy is a technique based on the use of infrared radiation which changes the vibrational behavior of molecules by delivering energy quanta and changing their vibrational and rotational modes. This technique showed that increased filler in the coating formula is seen as impeding the diffusion of the fluid from the bulk of the coating to the surface and, therefore, resulting in longer recovery time. Very large levels of filler are not easily compounded, while small amounts do not provide sufficient protection against damage. Typically, 40 to 60% of ATH in SiR formulations is used by the industry [2.27]. Contact angle measurement is a technique used to measure the surface hydrophobicity by

measuring the contact angle of water droplets on the surface [2.38]. Figure 2.7 shows that the contact angle on the surface of a virgin RTV- SiR coating at filler levels ranging from 50 to 150 pph is constant at (98 ± 2°). The reason for this is that filler particles on the surface of the coatings were encased in the silicone rubber for all concentrations of ATH filler [2.38].

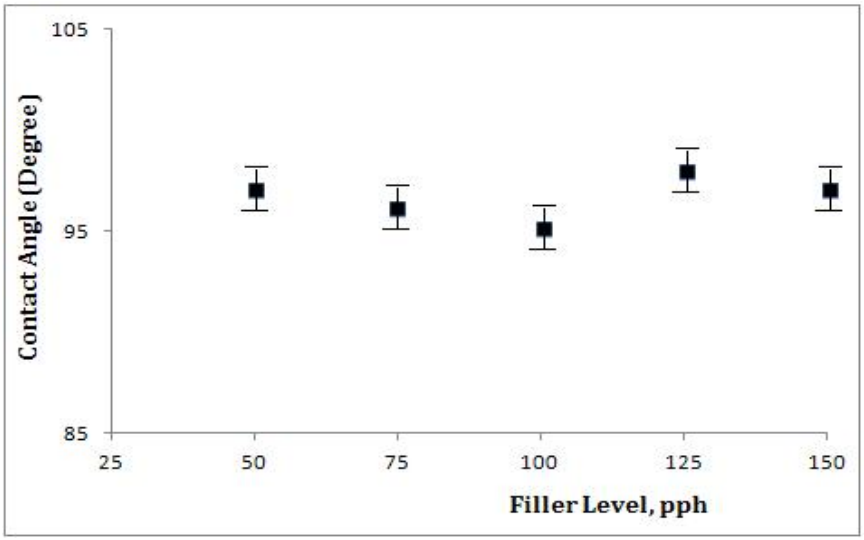

Figure 2.7: Variation of contact angle on the surface of RTV- SiR with ATH filler level. Particle size 13 µm; thickness 0.39 mm [2.38]

Figure 2.8 shows the contact angle of a droplet of water on RTV- SiR coating during the recovery period, which is the time period required for the silicone rubber to retain its hydrophobic surface properties, after removal of the specimens from an energized salt-fog test. It is observed that the contact angle recovered much faster for coatings having 100 and 200 pph of ATH concentration. The 0 pph ATH (unfilled) RTV-SiR did not fully recover even after 10 days [2.28].

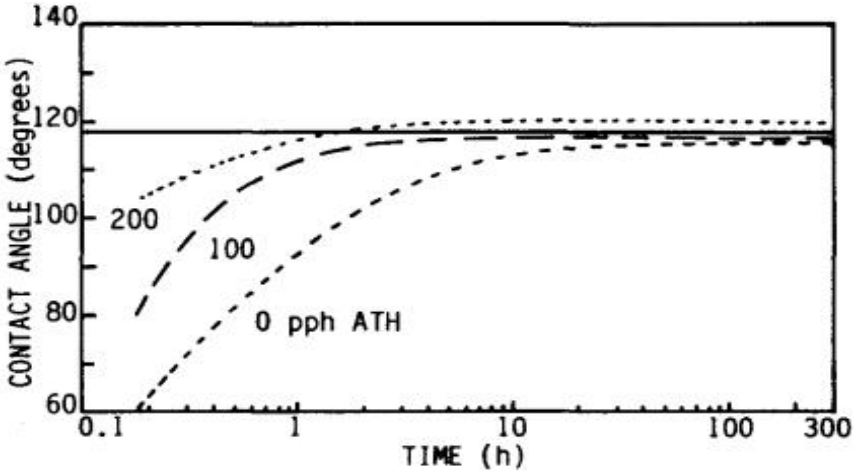

Figure 2.8: Contact angle of a droplet of water on RTV- SiR during recovery as a function of time after removal from energized salt-fog [2.28]

II. Type of filler

Pasand et al. [2.39] studied the influence of the filler type on the resistance of the RTV SiR coating against tracking and erosion using the inclined plane test (IPT). The results showed that the ATH-filled coatings performed better than that of the silica-filled coatings. Three samples out of six samples of silica-filled coatings failed during the test. The length of erosion and erosion area are shown in Table 2.2.

Table 2.2: IPT result of different coatings [2.39]

Coating	ATH filled	Silica filled
Failed samples	0	3
Length of erosion (mm)	6.8	22.5
Erosion area (mm^2)	65	150

However, Omranipour et al. [2.40] studied the effect of filler type on the tracking and erosion resistance of RTV SiR samples and found that ATH and silica perform very similarly at 50% of filler concentration by weight. However, at 10% concentration, ATH showed better resistance to tracking and erosion than silica filled samples.

On the other hand, the thermal conductivity of the composite material is dependent on the thermal conductivity, concentration, particle size, and bonding of the filler particles to the silicone matrix. In this regard, depending on formulation, either filler can perform better than the other. Therefore, "the perception that ATH filler imparts better erosion resistance than silica in silicone rubber can be misleading" [2.30]. However, in silicone

compositions having low filler concentration, hydrated water released from the ATH filler appears to have a less important effect on the performance of the coatings.

III. Particle size of ATH filler

The role of the size of the ATH filler particle and its influence on the electrical performance of the RTV-SiR has been examined by Deng et al. [2.36] by testing polyester fibre glass rods coated with RTV coating in energized salt-fog. Figure 2.9 shows the effect of different particle size, on the current pulse rate. After 150 hours of the test, the current pulses started to develop rapidly for all sizes of filler particle apart from 4.5 μm and 13 μm. A water film developed on the surface for all compounds which indicates a loss of hydrophobicity of the surfaces compared to that with particle size 4.5 μm. This resulted in earlier initiation of dry band discharges, resulting in a faster rate of erosion, and ultimately failure of the samples.

Meyer et al. [2.41] tested RTV coated samples with ATH and silica as fillers using inclined plane tracking and erosion tests. They found that the samples with 5.0 μm particle size and 50% filler by weight had higher thermal conductivity and showed less tracking and erosion than other samples with different particle sizes and different filler percentages.

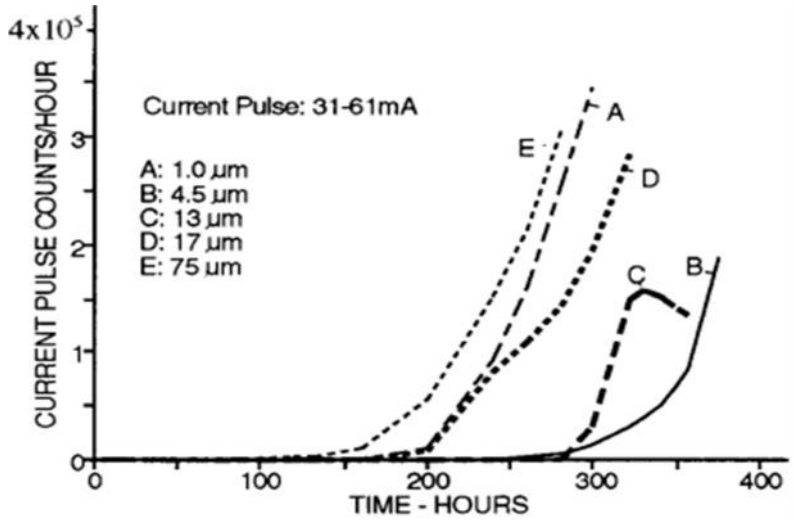

Figure 2.9: Current pulse count per hour in RTV- SiR as a function of time in energized salt-fog showing the effect of ATH particle size [2.37]

The heat generated from dry band arcing is considered as the main factor in determining the lifetime of a compound. The time to failure of ATH filled RTV-SiR with varying particle size can be seen in Figure 2.10. The 4.5 μm particle gives the longest time to failure. This demonstrates that the size of the particles play an important factor in determining the material's time to failure. The surface of the RTV- SiR is rougher, with larger ATH particles. This leads to increased leakage current, rapid loss of surface hydrophobicity and considerable surface damage due to the resulting intense discharges. These discharges result in shorter lifetime of the material. RTV coatings with an average ATH filler particle size of 1.0 μm failed in a short time due to aggregation of particles come at discrete points on the surface. The finer particles can produce greater surface roughness which can lead to localized hot spots. The corresponding non-uniform surface was investigated using a surface roughness detector, giving a value of 9.2 μm in certain locations of the virgin specimen. The coating with 4.5 μm average particle size gave a surface roughness of 1.2 μm [2.33]. However, the diffusion of silicone fluid for coatings with 4.5 and 13 μm particles resulted in a quicker recovery of surface water repellency, and resulted in longer life time. The influence of fillers type, particle size, and concentration on the erosion resistance of SiR materials has been reported in [2.42, 2.43].

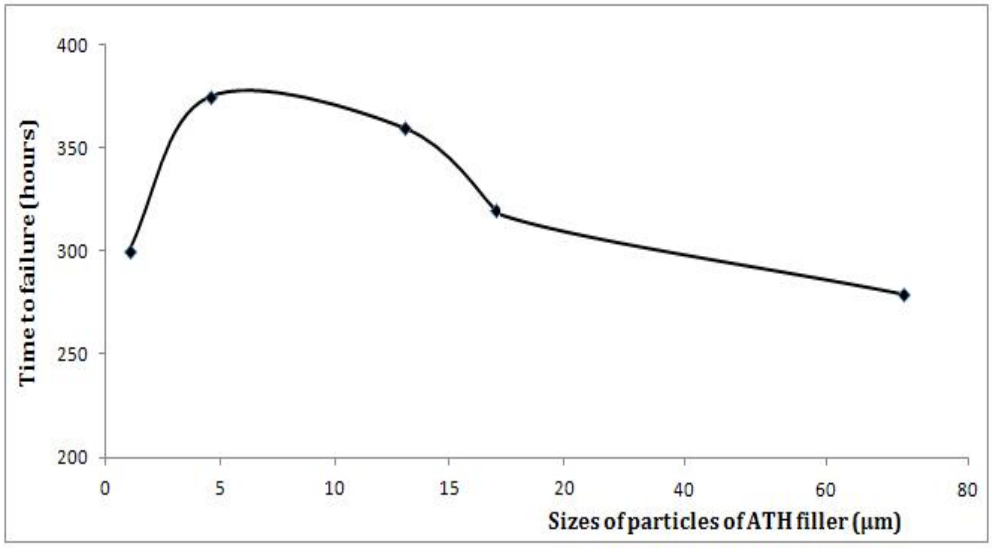

Figure 2.10: Time to failure of RTV coatings as a function of ATH particle size (reproduced from[2.36])

As much of the work reported for SiR materials was with micro-fillers, El-Hag et al. [2.44] performed a comparison study between micro-filled and nano-filled SiR samples at different concentrations of fumed silica filler by weight using the inclined plane tracking and erosion test. It was concluded that the erosion resistance of the SiR materials increased with increasing percentage of the fillers. 10% of nano-filled SiR by weight performed similar to that with 50% of micro-filled SiR by weight as can be seen in Figure 2.11.A silicone rubber sample filled with 10% micron-size ATH or silica has an average thermal conductivity of 0.31 W/m°C, whereas a sample filled with 50% micron-size of ATH or silica has an average thermal conductivity of about 0.56 W/m°C. As a result the coating filled with higher thermal conductivity filler showed less erosion and less damage to the surface of the coatings [2.30].

Venkatesulul et al. [2.45] studied the effect of nano-sized magnesium dihydroxide (MDH) and micro-sized ATH fillers as flame retardants in RTV silicone rubber. The studies were also carried out using an inclined plane tracking and erosion test. At lower filler concentrations of 5% by weight, the MDH performed better than the ATH in terms of eroded mass. This is attributed to the higher thermal stability of the nano-sized MDH filler. Thermal Gravimetric Analysis (TGA) results also showed that MDH system was more thermally stable against decomposition. TGA is a method of thermal analysis in which changes in physical and chemical properties of materials are measured as a function of temperature. TGA is commonly used to determine selected characteristics of materials that exhibit either mass loss or gain due to decomposition and oxidation [2.45].

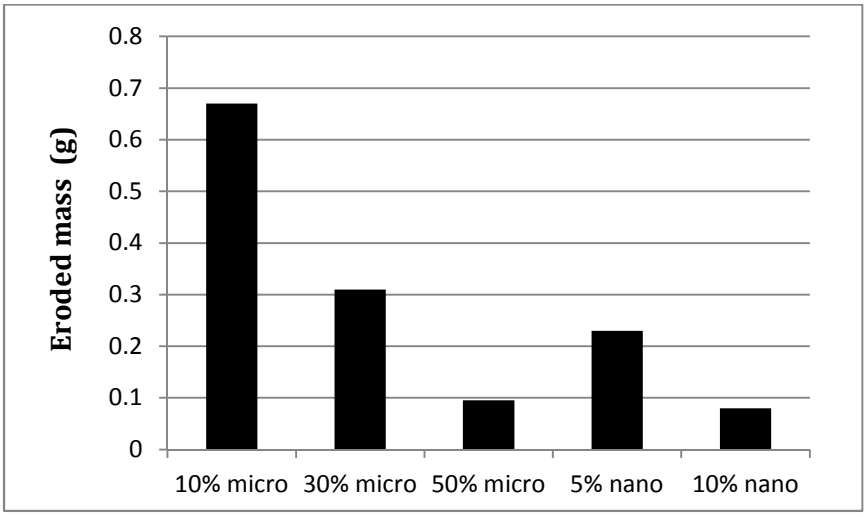

Figure 2.11: Comparison between micro and nano-filled silica composites in terms of eroded mass after IPT test [2.44]

2.2.4.4. Dependence of low molecular weight (LMW) silicone fluid on the coating thickness

Deng et al. [2.31] correlated the dependence of low molecular weight (LMW) silicone fluid content and its diffusion to the coating surface to the coating thickness. Figure 2.12 shows the percentage content of LMW silicone fluid by weight as a function of the thickness of the RTV-SiR specimen. For virgin specimen, the amount of LMW fluid decreased with increasing coating thickness as in Figure 2.13(curve A). Further, the percentage of LMW content decreased after 570 h exposure to salt-fog and depended on the location of the coating on the porcelain rods as in Figure 2.13(curves B and C) and was largely independent of thicknesses in the range from 0.17 to 0.99 mm. Near the HV electrode of the vertically placed rod, the loss of the LMW fluid was larger (curve C) where there were more intense discharges compared to the bottom electrode (curve B) where there are less discharge.

The heat energy generated from dry band arcing penetrates into the bulk of the coating thereby breaking the side groups of the main chain of the PDMS molecules which are responsible for the formation of LMW silicone fluid [2.47].

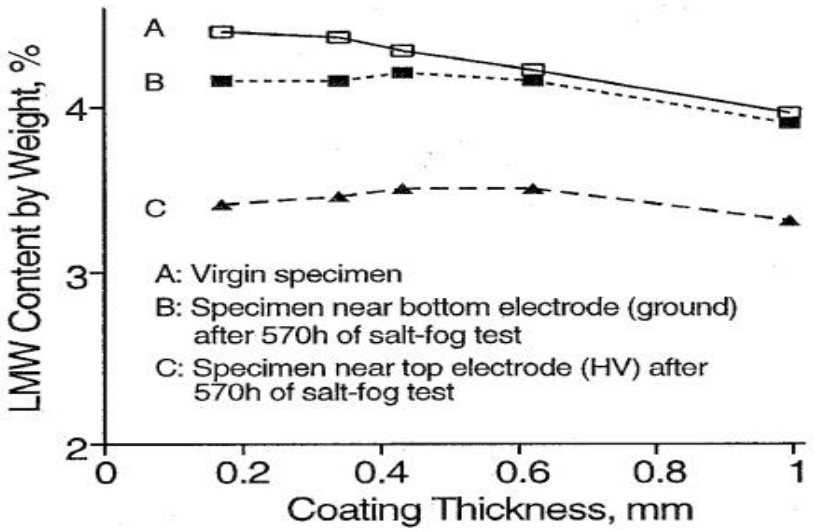

Figure 2.12: Percentage content of LMW silicone fluid by weight as a function of the thickness of RTV- SiR specimens [2.34]

The silicone fluid increased on the surface of the RTV specimen after it was exposed to a high temperature of 240°C. RTV coated specimens were heated for 3 hours in air and the silicone fluid was extracted. Figure 2.13 shows the production of silicone fluid by

percentage of weight of the specimen increased from 0.13 % at 150°C to 0.75 % at 240°C and then to 5.12% at 370°C.

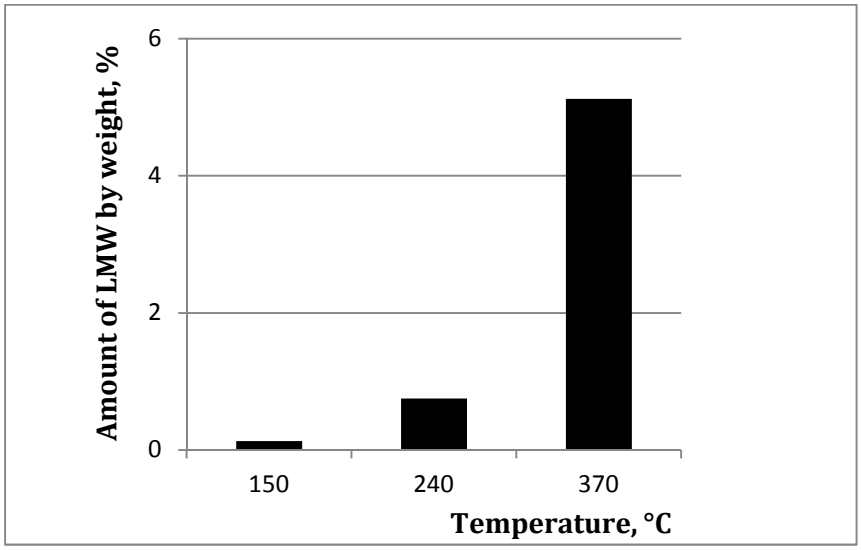

Figure 2.13: Production of LMW silicone fluid in RTV [2.31]

Similar results on silicone fluid regenerated by heating were observed in an alloy of ethylene propylene diene monomer (EPDM) and SiR, see Figure 2.14 [2.46, 2.47]. The contact angle increased with increasing temperature which is an indication of re-generation of new silicone fluid, or release of trapped silicone fluid in the bulk which then diffused from the bulk to the surface.

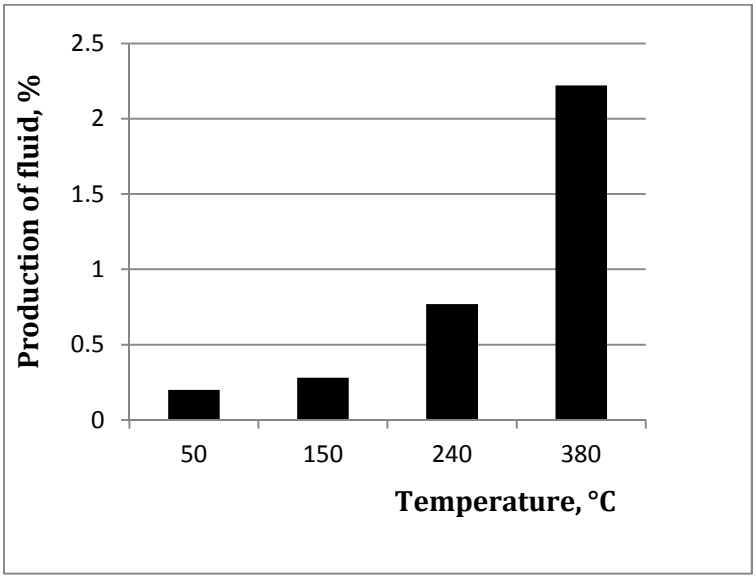

Figure 2.14: Percentage weight of LMW fluid regenerated in EPDM alloyed with SiR. Duration of heating 1 hour [2.46]

As the silicone fluid is formed during heat treatment. Dry band arcings on the surface of RTV coatings could also produce silicone fluid on HV insulators. Thus, the heat from the

arcs could provide a hydrophobic surface on the RTV coated insulator via the production of silicone fluid. However, continued exposure to intense dry band arcing could cause damage to the surface as it results in higher temperatures than those produced by the oven [2.48].

2.2.4.5. Effect of adding silicone fluid

The LMW silicone fluid (PDMS), inherently present in SiR, is often added to EPDM during compounding and/or processing. The diffusion of LMW silicone fluid from the bulk to the surface of the silicone rubber is one of the factors responsible for the maintenance of hydrophobicity as shown by the water repellency of the surface [2.49].
In [2.31, 2.33] silicone fluid was added to a formulation of RTV-SiR to explore the possibility of extending the life time of the RTV-SiR. Specimens of RTV-SiR formulation with no added silicone fluid, with additions of 1% and 10% by weight of silicone fluid were tested in an energized salt-fog. Figure 2.15 shows the current pulse count rate in RTV-SiR coating on polyester FRP rods as a function of test time. Currents developed on the specimens with added fluid sooner than on the specimens with no added fluid, as the specimen with added silicone fluid was visibly covered with a thin layer of the fluid. The silicone fluid on the surface was found to impede the conduction of the heat generated by the discharges from the surface, through the bulk material to the substrate. The temperature decomposes the silicone fluid into hydrophilic products which resulted in larger current developed as the test continued. The time to failure was also found to reduce for specimens with added silicone fluid, as can be seen from Figure 2.16.

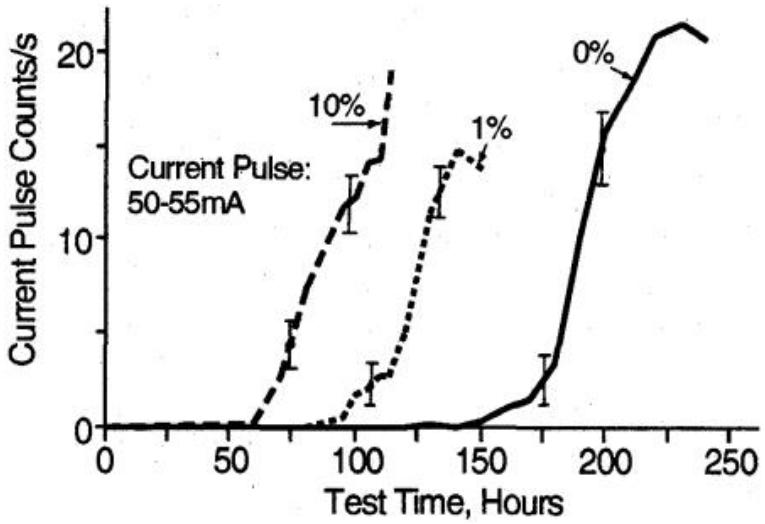

Figure 2.15: Dependence of current pulse count rates on test time in salt-fog for RTV coated rods without and with additions of 1% and 10% silicone fluid [2.31]

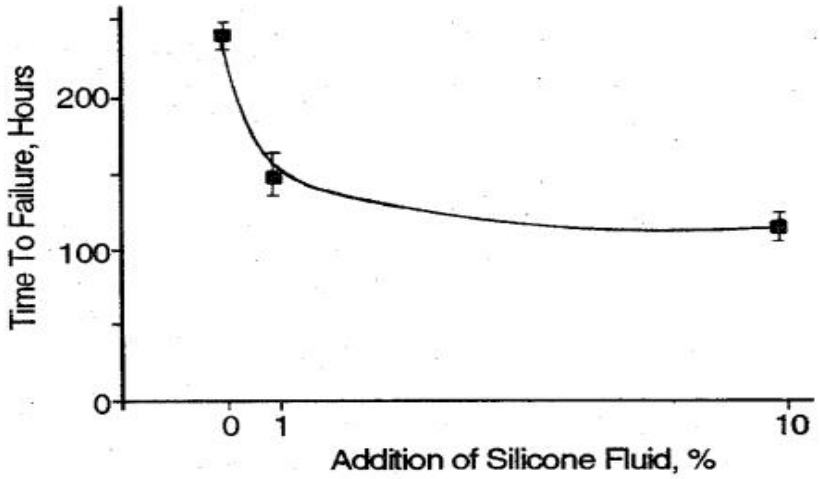

Figure 2.16: Time to failure of RTV- SiR coating with no added silicone fluid and with additions of 1% and 10% silicone fluid by weight [2.31]

2.2.4.6. Effects of different solvents

RTV coatings are dispersed in carrier solvents such as Naphtha and 1,1,1, trichloroethane so as the RTV coatings can be easily applied to ceramic insulators. Deng et al. [2.31] investigated the effect of these two solvents on the performance of RTV coating. In their investigations, polyester rods were coated with RTV coatings having Naphtha and 1,1,1, trichloroethane as solvents and tested in a salt-fog chamber. Figure 2.17 shows that with 1,1,1 trichloroethane the number of current pulses was initiated

earlier than that for the coating dispersed in naphtha. This led to a large erosion of the RTV coating and a shorter time to failure by tracking on the polyester FRP substrate as can be seen in Table 2.3. However, it was reported that the type of carrier solvent (1,1,1 trichloroethane and naphtha) does not influence the proportion of LMW silicone fluid in the RTV-SiR; it also has no effect on diffusion of the LMW fluid from the bulk material to the coating surface [2.50]. Measured contact angles on the surfaces of the virgin specimens were found to be identical for both solvents.

Table 2.3: Time to failure (hours) of RTV coating with different solvents [2.31]

Solvents in RTV Liquid	Naphtha	1,1,1, trichloroethane
Coating Thickness, mm	0.79±0.10	0.50±0.06
Time to Failure, hours	218±10	158±20

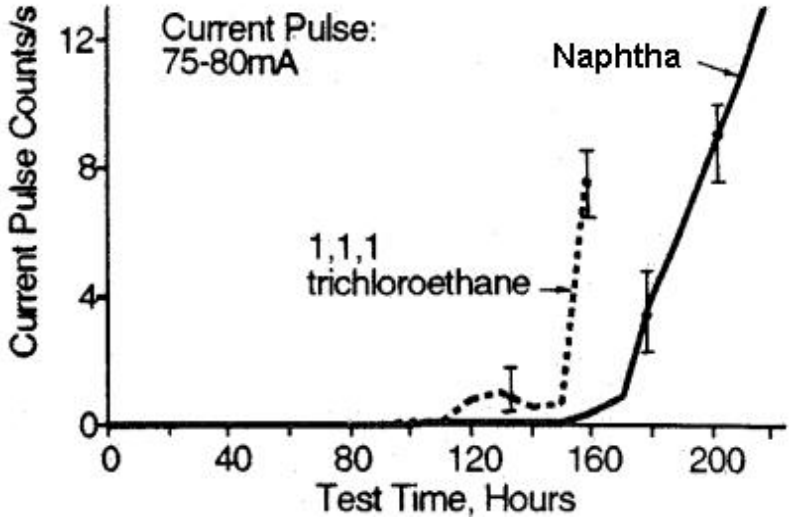

Figure 2.17: Dependence of current pulse for RTV coating on type of solvent [2.31]

2.2.4.7. Coatings under direct voltage stresses

In general, the performance of polymeric insulating materials stressed with AC voltage has been investigated more than their performance under DC voltage. In fact, evaluating the resistance of polymeric materials under DC voltage has not yet been standardized. Moreno and Gorur [2.51] have performed inclined plane tests on different types of polymeric materials, using both AC and DC voltage. They concluded that polymeric materials under the DC voltage test had lower resistance to tracking and erosion than

that under AC voltage tests. This inferior performance was found to be due to the higher magnitudes and longer duration of the discharge current pulses. Gorur et al. [2.52] performed AC and DC tests on cylindrical rod samples coated with HTV silicone rubber and EPDM rubber in a fog chamber. It was found that the time to failure was similar for AC and positive DC but much shorter for negative DC due to increased pollution collection. Gustavson et al. [2.50] tested cylindrical silicone rubber samples in a coastal environment under AC and DC voltages. The DC stressed samples showed higher leakage currents and more severe surface degradation compared with the samples stressed with AC voltage. Their investigations pointed to thermal depolymerization activated by the electrical discharge as the main degradation factor.

Heger et al. [2.54] conducted an experimental study using the inclined plane test method to evaluate the performance of porcelain samples coated with RTV silicone rubber, HTV silicone rubber and EPDM rubber using the constant voltage method of IEC60587 under AC and DC (both polarities) voltages. The RTV silicone rubber coating showed the least erosion under AC voltage but showed most erosion under negative DC voltage. The HTV silicone rubbers exhibit only minimal erosion when exposed to the AC test voltage but showed strong erosion under positive DC voltage which resulted in failure of the sample. EPDM experienced the least erosion for a negative DC voltage but showed maximum erosion severity for the AC voltage.

2.3. Material degradations

Due to their weak organic bonds, polymeric materials are susceptible to aging and degradation when used in high voltage outdoor applications. These chemical changes are a result of exposure to the combined effects of electrical stresses and environmental stresses [2.55]. The degradation is an electrochemical process of de-polymerization that is more severe in the presence of electrical stress. It has been reported that acid rain produces greater degradation of RTV silicone rubber coatings containing ATH than those containing silica [2.56]. The effects of acid rain on RTV silicone rubber have been reported in [2.57, 2.58].

2.3.1. Electrical stress

One of the most important factors that determine the electrical performance of HV insulators is maintenance of a uniform electric field distribution along the surface of the

insulator. Pollution under wet conditions causes electric field distortion and contributes to localised non-uniform enhancement of the electric field. This could lead to electric discharges in the form of dry band arcing and to complete insulator flashover [2.59].

The magnitude of the electric field near the electrodes can be several times higher than the field along the surface distance of the insulator. Ceramic insulators formed by a string of discs under dry conditions have a large capacitance. This, in addition to the effect of intermediate metal parts along the string, leads to a naturally graded voltage distribution along the string. This phenomenon helps to reduce the high electric stress at or near the ends of the string. However, pollution accumulation on the surface of these HV insulators will result in a non-uniform field distribution and a high field in areas near metal electrodes. This field triggers faint discharges as a streamer anchored at the metal electrodes as the field exceeds the air ionisation threshold [2.60].

Loss of hydrophobicity in the vicinity of the HV electrode of RTV coated insulators has been mentioned as a possible cause of flashovers that occurred under severe weather conditions. However, flashover of RTV coated insulators has been rarely reported [2.61]. The presence of these water droplets closest to the HV electrode causes substantial increase in the electric field that could lead to discharges. However, the maximum electric field is reduced as the droplets join together to form bigger droplets. This is to be expected due to the inverse relationship of the electric field with the radius of curvature of the water droplet. Induced charges within the droplet experience a strong electromagnetic force that causes the hemispherical shaped droplet to flatten and extend in the direction of the electric field, thus covering a wider surface area. Katada et al. [2.62] showed that water droplets deform when stressed with AC electric field where the droplets are subjected to vibration due to the change of voltage polarity.

As the RTV silicone rubber coating loses its hydrophobicity due to electric field intensification, its surface will be covered with a conductive layer which permits the initiation of leakage current along the conductive path. The flow of leakage current results in resistive heating and leads to drying of the wet layer on the insulator surface. Dry bands are likely to become visible on the smallest circumferential region where the current density is highest [2.63]. Electric discharges gradually elongate as the dry regions widen and may extend over multiple dry bands and join with other electric discharges to form intense electric discharges which eventually bridge the whole insulator. The mechanisms leading to flashover of polluted and wetted polymeric

insulators have not been quantitatively modelled. However, descriptions of the developments process leading to flashover have been given [2.64]. The development of flashover on the polymeric surface is depicted in Figure 2.18.

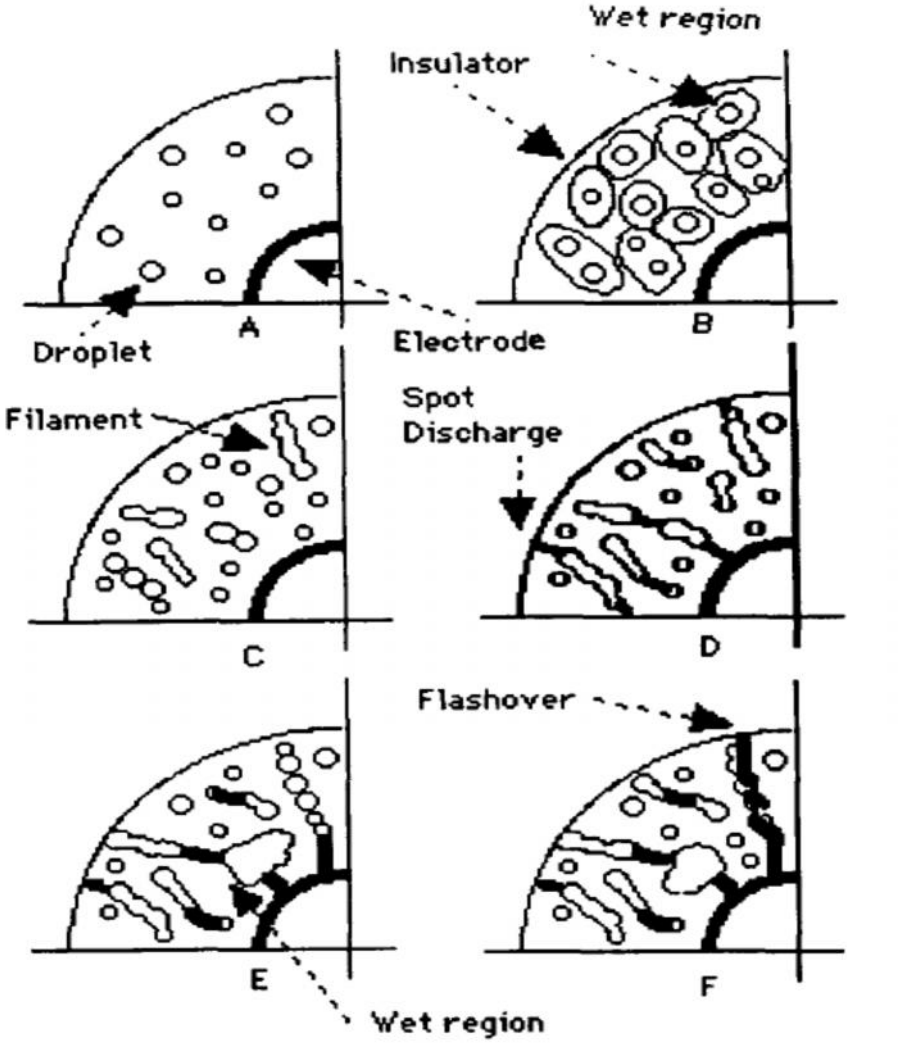

Figure 2.18: Development of flashover mechanism on polymeric insulator [2.67]

Due to the high surface hydrophobicity of polymeric materials, wet layers tend to form as discrete water droplets on their surface. However, under prolonged wetting, the droplet regions join to form a wet region resulting in a resistive layer. The resistive layer allows leakage current to flow and resistive heating and drying occur. Intensification of the electric field around the droplets and filaments causes discharges to occur between them which results in hydrophobicity loss. As hydrophobicity is lost, large conductive regions cover the insulator surface, and arcs propagate and may expand to complete flashover.

2.3.2. Photo-degradation

Polymeric coatings used for outdoor high voltage insulators are exposed to sunlight. Sunlight and some artificial lights can have adverse effects on the useful life of the coatings. Sunlight generally results in photo-degradation which leads to photo-oxidation. Photo-oxidation is a chemical change that reduces the polymer's molecular weight. As a consequence of this change the material becomes more brittle, with a reduction in its tensile strength. Discoloration and loss of surface smoothness accompany photo-oxidation [2.65].

UV radiation can break down the chemical bonds in a polymer. In addition to using antioxidants during processing of the polymer materials, many manufacturers started to use UV stabilizers. Various UV stabilizers and UV absorbers have been widely incorporated into the coating systems to enhance their UV stability while maintaining its superhydrophobicity. The mechanism of stabilization of UV stabilizers is attributed to one or more of the following (a) absorption/screening of UV radiation, (b) deactivation (quenching) of chromophoric excited states.

The incorporation of opaque pigments in the polymer work as UV screens which can stabilize the polymer by screening the incident UV high energy.

UV absorbers protect the polymer against UV by reducing the amount of light absorbed by chromophores. The chromophore is a region in the molecule where the energy difference between two different molecular orbitals falls within the range of the visible spectrum. The sun light rays that hits the chromophore can be absorbed by exciting an electron from its ground state into an excited state.

Excited-state quenchers interact with an excited polymer atom by indirect energy absorption. The quenchers bring the high-energy chromophore back to ground state by absorbing the energy and then dissipating the energy harmlessly before the energy can degrade the material.

Hindered amine light stabilizers are the most common category of light stabilizers, and consist of what are known as hindered amine light stabilizers (HALS). They are extremely efficient stabilizers against light-induced degradation of most polymers. HALS does not absorb UV radiation, but acts to prevent degradation of the polymer as they slow down the photo-chemically initiated degradation reactions [2.66].

2.4. Measurement of hydrophobicity

Hydrophobicity is the ability of a surface to repel water, so that water on the surface forms individual droplets rather than a film. Hydrophobicity is the most important property of silicone rubber insulators and its measurement has been investigated and widely used as an indication to the insulator's performance [2.68].

2.4.1. Contact angle

The contact angle depends on the interfacial tension at three boundaries; solid and water, water and air, and air and solid. A surface is said to be hydrophobic when the contact angle is greater than 90°, and hydrophilic is when the contact angle is less than 90°, see Figure 2.19.

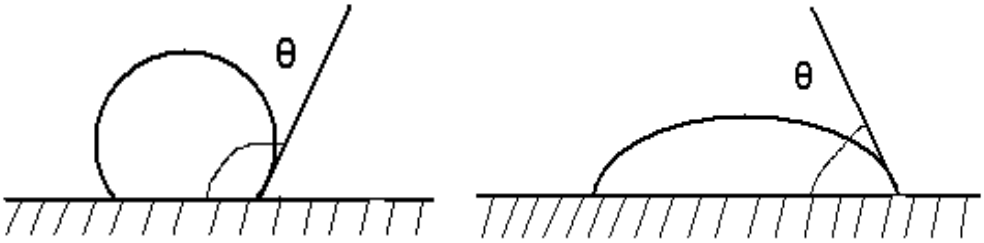

a) hydrophobic surface b) hydrophilic surface

Figure 2.19: Contact angle of a water droplet [2.68]

The Swedish Transmission Research Institute (STRI) Index [2.69] classifies the hydrophobicity of the surface into 6 classes from hydrophobic to hydrophilic, based on the appearance of the wetted surface. HC1 corresponds to the most hydrophobic surface and HC6 corresponds to a completely hydrophilic surface. This method only needs a spray bottle and is not affected by roughness and hardness of the surface. It is, however, not a precise method as it depends on the judgement of the individual performing the test. The criteria for determination of hydrophobicity class are given in Table 2.4. While photos of surfaces with different wetting properties are also depicted in Figure 2.20.

Table 2.4: Criteria for the hydrophobicity classification (HC) [2.69]

HC	Description
1	Only discrete droplets are formed. $\theta_r \approx 80°$ or larger for the majority of droplets.
2	Only discrete droplets are formed. $50° < \theta_r < 80°$ for the majority of droplets.
3	Only discrete droplets are formed. $20° < \theta_r < 50°$ for the majority of droplets. Usually they are no longer circular.
4	Both discrete droplets and wetted traces from the water runnels are observed (i.e. $\theta_r = 0°$). Completely wetted areas < 2 cm^2 . Together they cover < 90% of the tested area.
5	Some completely wetted areas > 2 cm^2, which cover < 90% of the tested area.
6	Wetted areas cover > 90%, i.e. small unwetted areas are still observed.
7	Continuous water film is formed over the whole observed area.

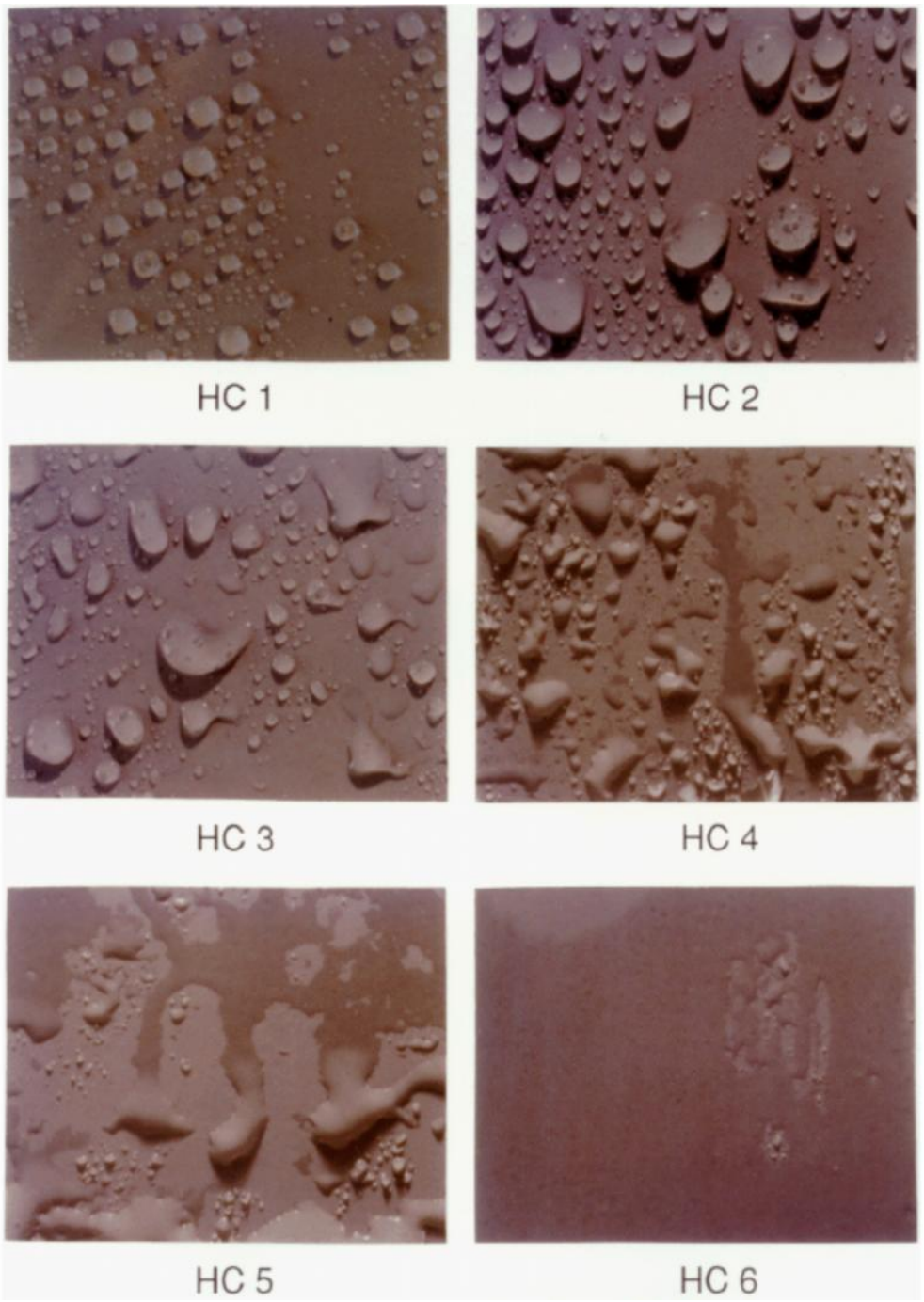

Figure 2.20: The STRI hydrophobicity classification, from HC1 to HC6 [2.67]

2.5. Conclusions

Ceramics are inert materials that can withstand dry band discharges without serious surface degradations. Because of their high surface energy, however, these materials wet easily when exposed to fog or rain and form water channels on their surfaces. During severe weather conditions of pollution, wetted and polluted insulators becomes susceptible to the formation of high currents that lead to complete flashover of the insulators followed by power outages.

These insulators are coated with low surface energy coatings such as silicon rubber to improve their surface properties and contamination performance. Silicone elastomers exhibit high hydrophobic surface properties and prevent the formation of leakage current during prolonged wetting conditions. However, when the hydrophobicity is lost leakage current starts to flow causing a localized drying of the surface which leads to the initiation of dry band arcing. The heat from the dry band discharges result in premature aging of the protective coating.

Different formulations of the RTV coatings differ in their ability to provide resistance to dry band arcing even though the same base material (PDMS) was used with all the formulations. The type, concentration and the size of the filler particles used in the RTV formulations affect the life of the RTV coating. A coating with properly selected formulation can maintain a high resistance to damage from dry band arcing and have a longer life. When the RTV coating is covered with wet contamination layer, the surface hydrophobicity is reduced. The LMW silicone fluid, which is inherently present in the coating, diffuses from the bulk to the surface of the RTV coating and then envelops the contamination layer. The presence of a sufficient quantity of LMW silicone fluid in the bulk of the RTV coating and its ability to diffuse to the surface are of paramount importance in maintaining the hydrophobic properties of the coating. This process modifies the physical properties of the pollution layer giving it a hydrophobic surface property. This prevents the occurrence of flashover, provides better reliability and integrity to the power system.

The following chapter explains the test facilities that used to evaluate the performance of different coatings used in this study and also discussed the computer programs and the techniques used to acquire and analyse the leakage current waveforms developed on the surface of different coating materials.

Chapter 3 – Test facilities and data acquisition systems

3.1. Introduction

High voltage insulators achieve their highest performance under dry conditions. Under wet conditions, however, polluted insulators are susceptible to dry band arcing and flashover. In this regard, coated insulators were tested in the laboratory under artificial pollution conditions and the coating's resistance to tracking and erosion was also investigated. This chapter describes the methods and test facilities used for testing high voltage insulator coatings. The fog chamber test facility and inclined plane test machine, with their associated electrical circuits, are explained and discussed. Preparation of the contaminant suspensions and the process of polluting insulators detailed.

Wetting rate tests to confirm the compatibility of the fog chamber to the international standard of IEC60507 are also presented and discussed. The development of computerised data acquisition systems for the fog chamber and inclined plane test facilities, to acquire waveforms of applied voltage and leakage current, is discussed. A data analysis program was also developed and used to analyse the leakage current and voltage waveforms. These data were used to characterise the pollution performance of the tested insulators. The effect of UV radiation on the coating materials was studied using an Atlas XXL+ artificial weathering test station which uses three air cooled Xenon arc lamps, capable of reproducing more than 90% of the natural sunlight.

3.2. Fog chamber and data acquisition system

3.2.1. Fog chamber

Figure 3.1 shows the schematic layout of the fog chamber. The chamber is constructed from polypropylene with a volume of 12 m^3, 3 m height, and 2 m × 2 m base area in an earthed compartment. The voltage was applied to the insulators by means of a tubular aluminium conductor passing through the roof of the fog chamber. Stress control rings

were installed at locations of sharp edges along the conductor to reduce corona discharges. The chamber was equipped with three pairs of spray nozzles, two pairs were mounted vertically on opposing corners and the third pair mounted on the base of the chamber. The base jets are intended to increase the flexibility of operation and could be used if required for testing the insulator in different orientations. Each spray nozzle conformed to IEC60507. Each nozzle comprised two ducts, one for supplying water and the other supplying the atomizing air, which breaks the water flow to form a fine fog. The fog chamber was supplied by swalec company.

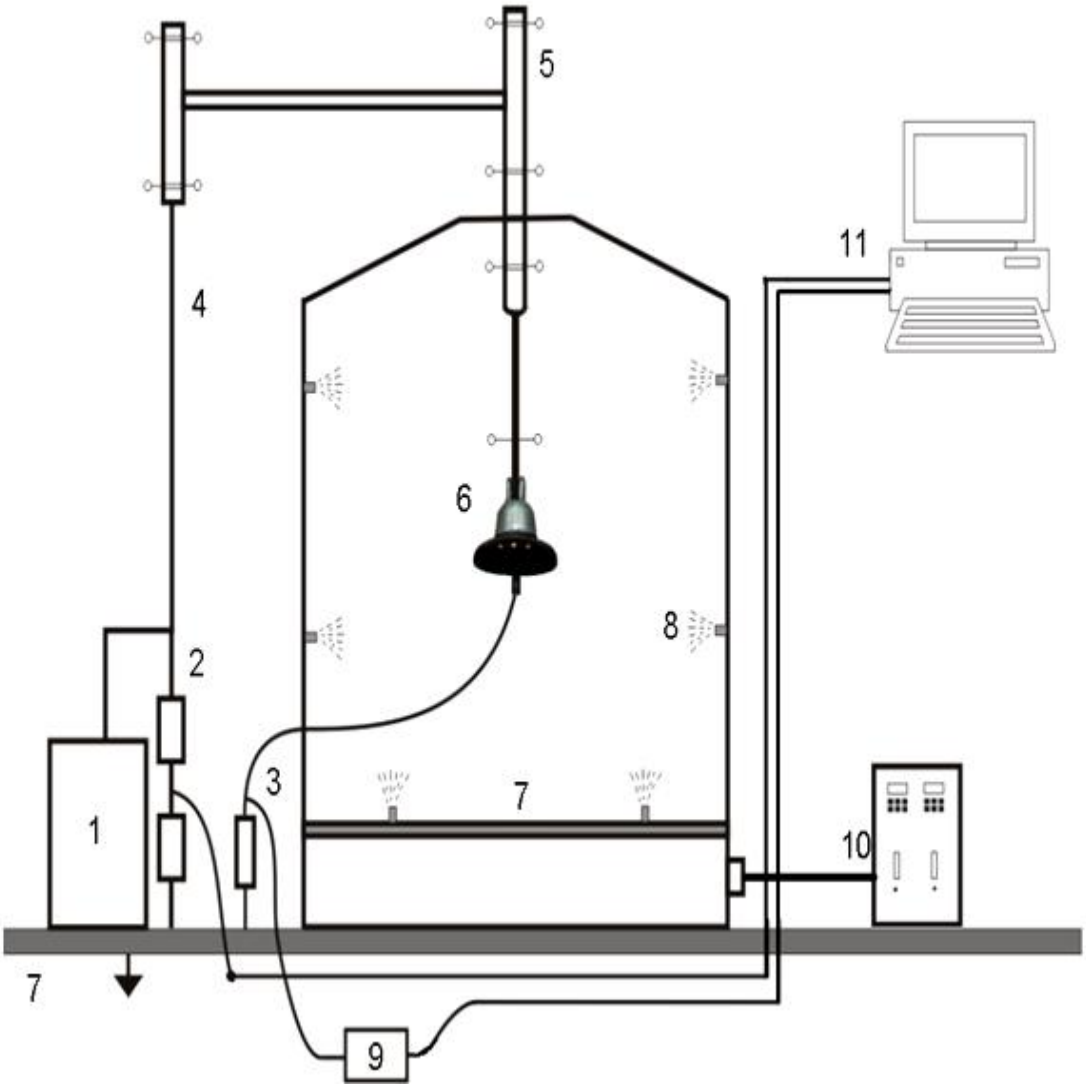

(1) High voltage source; (2) capacitive HV divider; (3) Leakage current: to variable shunt resistor; (4) High-voltage conductor; (5) Corona shield; (6) Test insulator; (7) Earthing mesh; (8) Spray nozzles; (9) Protection box; (10) Air, and fog/rain control unit; (11) Computer containing Data Acquisition (DAQ) card [3.1]

(a) Schematic layout of the fog chamber

(b) Fog chamber in the high voltage laboratory (Cardiff University)

Figure 3.1: Schematic layout and picture of fog chamber

The particle size produced by any spray nozzle is dependent on the water flow rate, air pressure and the properties of fluid used. The median volume diameter of the fog particles is 15 μm at a water flow rate of 4.14 l/hr and 4.2 bars, as quoted by the supplier. The test insulator is positioned axi-symetrically in the middle of the chamber and isolated from the earth. The HV is applied to the cap of the test insulator, while the leakage current is taken from the pin of the insulator and passes through a protection circuit, which provides protection to the data acquisition (DAQ) system and PC against surges and possible flashover of the test object; this is in parallel with a shunt resistor to earth. The measurement of leakage current across the surface of the insulator was measured across the shunt resister and was connected to the DAQ card. The value of the resistance was selected so that the maximum expected leakage current through the insulator caused a voltage drop across the resistor within the rated values of the DAQ card. An earthed mesh is set on the floor of the chamber and on the HV compartment. Water formed by fog condensing on the chamber walls is collected in a sump at the base under the chamber and is later removed using a water pump. The

door of the chamber was made from transparent polycarbonate so the tested insulator could be observed throughout the test. The water flow rate and the atomizing air pressure through the nozzles are controlled by a control unit placed adjacent to the fog chamber outside the HV compartment.

3.2.2. Electrical test circuit

A Hipotronics AC Dielectric test set was used for the fog chamber tests and consisted of: A control unit for voltage and circuit breaker control. The control unit was connected to the HV transformer through a Peschel variable transformer.

a) The control unit featured HV ON/OFF, RAISE/LOWER, and AUTO/MAN pushbuttons.

b) The Peschel variable transformer unit (PVT) had a rated voltage of 0-960V, 230 kVA with a protection system which provided isolation in the event of transient overvoltage.

c) The HV test transformer had a 400 Vac input voltage and three tap settings:

- Tap 1: 75 kV ac @ 112.5 kVA continuous.
- Tap 2: 50 kV ac @ 75 kVA continuous.
- Tap 3: 25 kV ac @ 37.5 kVA continuous.

A North Star capacitive divider with a ratio of 10,000:1 was used to measure the voltage across the test insulator. The leakage current was obtained from the voltage drop across a variable shunt resistor connected in series with the test insulator.

Both voltage and leakage current measurements are simultaneously displayed and stored using a DAQ system installed on the PC, Figure 3.2 shows the test set-up.

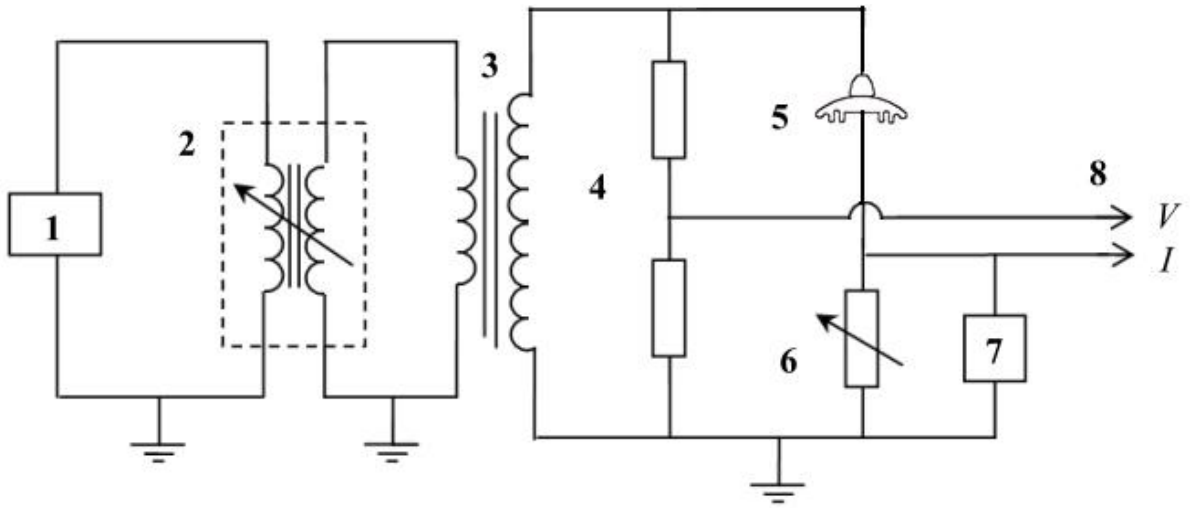

(1) Power supply and Control unit; (2) Peschel variable transformer, (3) High voltage transformer, (4) Capacitive divider, (5) Test insulator, (6) Variable shunt resistor, (7) Over voltage Protection box, (8) Voltage and Current signals

Figure 3.2: Circuit diagram of the test set-up

3.2.3. Standard test method

IEC60507 [3.2] is a standard test method for testing ceramic insulators regardless of their profiles using ac voltages between 1 and 765 kV and 48 to 62 Hz. Although, the standard is not used for ceramic insulators treated with polymeric coatings, however, it has been adopted for testing insulators coated with highly hydrophobic materials.

3.2.3.1. Preparing the test insulator

The insulators to be tested are prepared according to the IEC 60507 standard (Clause 5.2); the insulators are first cleaned with hot water contains tri-sodium orthophosphate to get rid of all the dirt and grease from the surface and then rinsed with tap water. Insulators coated with hydrophobic coatings were not cleaned because the coating processes were done in the Laboratory. However, they are cleaned after each pollution test with tap water but no detergents.

3.2.3.2. Preparing the pollution

The standard solid layer method as described in the IEC 60507 standard has two different pollutants: kieselguhr and kaolin compounds. The kaolin compound was used in this work. When mixed with water, the kaolin suspension has non-conductive properties. The pollution suspension consists of:

- 40 g kaolin compound.
- 1000 g tap water.
- Suitable amount of sodium chloride.
- Wetting agent, this was introduced when testing insulators having highly hydrophobic surfaces.

In terms of a salt deposit density (*SDD*), the contamination level was chosen according to Table 3 of IEC60507, which gives specific details of the *SDD* and their corresponding volume conductivities at 20°C. Using Equation (3.1) the volume conductivity corresponding to the selected *SDD* is corrected to the temperature of the kaolin-water suspension as follows:

$$\sigma_\theta = \frac{\sigma 20}{1-b(\theta-20)} \quad (3.1)$$

$$S_a = (5.7\ \sigma_{20})^{1.03} \quad (3.2)$$

$$SDD = \frac{Sa.V}{A} \quad (3.3)$$

where:

θ : the solution temperature (°C).

σ_θ : the volume conductivity at temperature of θ °C (S/m).

σ_{20} : the volume conductivity at temperature of 20 °C (S/m).

b : factor depending on the temperature θ, as shown in Figure 3.3.

S_a : the salinity of the suspension (kg/m^3).

SDD: the salt deposit density (mg/cm^2).

V : the volume of the suspension (cm^3).

A : the area of the cleaned surface (cm^2).

A polluted insulator was chosen for the *SDD* measurement (Clause 16.2). The *SDD* is determined by removing the deposit from the insulator surface and dissolving it in a known quantity of demineralised water (2-4 litres per m^2 of the sample) the volume conductivity σ_θ of the volume was then recorded using a commercially conductivity meter. The volume conductivity σ_{20} , salinity S_a and *SDD* can be calculated using the above equations. A pollution suspension containing the above compostions was prepared in a container and the conductivity was adjusted to 2.8 S/m which is equivalent to an *SDD* of 0.07 mg/cm^2. The insulators are then dipped into the suspension and then hung on a drying shelf for 8 hours drying period. The insulators should be uniformly polluted and the pollution layer on the surface of the insulator should cover the surface of the insulator without leaving any unpolluted areas. Non-uniformly polluted insulator has to be cleaned and re-polluted again until a uniform pollution layer is achieved. Uniformity test was normally performed by eye inspection as the uniformly polluted insulator should be completely covered by a pollution layer. Figure 3.3 shows change in values of b factor with increasing pollution temperature. Figure 3.4 shows an overview chart of the solid layer method.

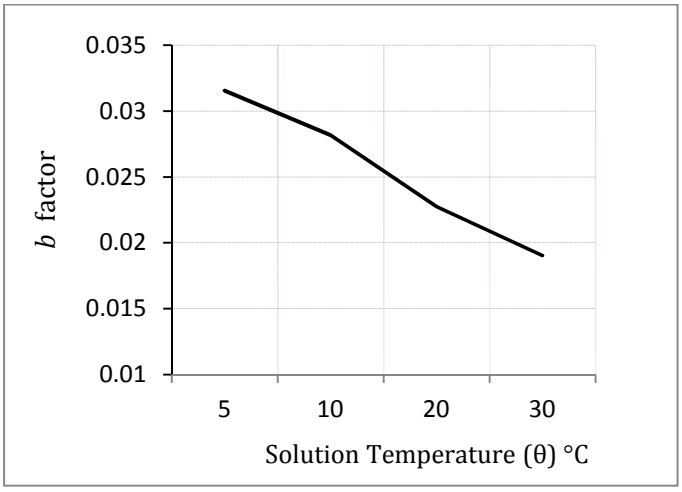

Figure 3.3: Variation with temperature of b factor appearing in Equation (3.1) (reproduced from IEC60507)

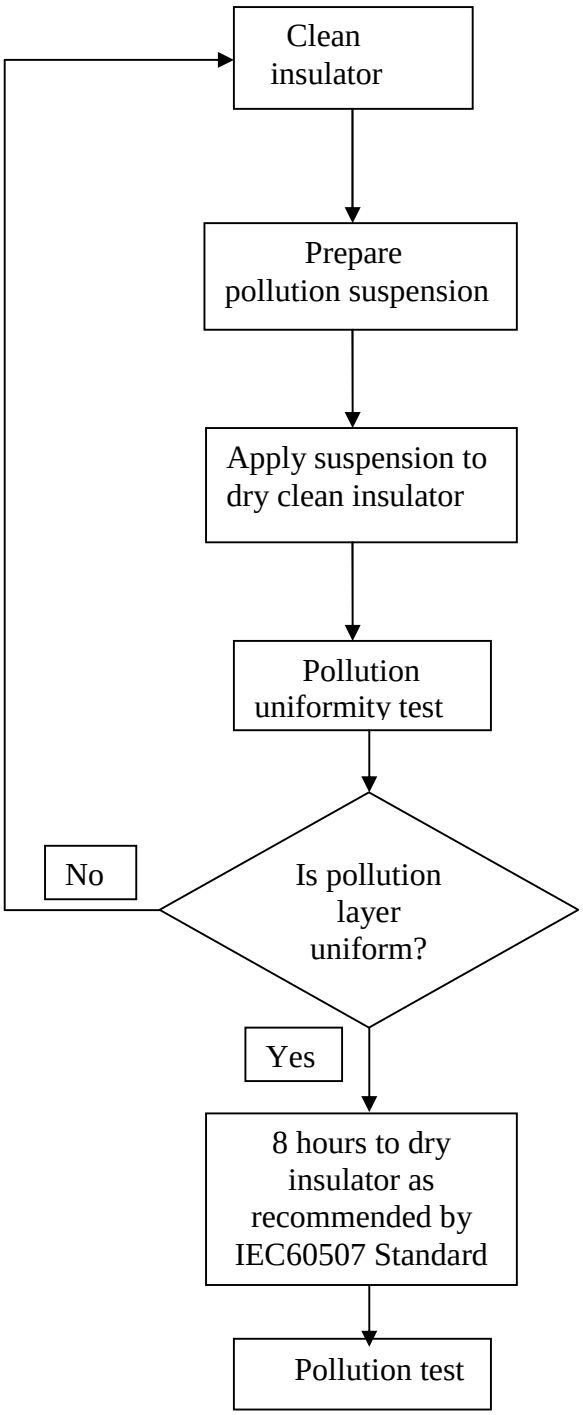

Figure 3.4: Overview of the solid layer method

3.2.4. Wetting rate test

Wetting rate test is a calibration test performed to check the ability of the fog chamber itself to satisfy the standard's criterion. According to the IEC 60507 the rate at which the fog is input into the chamber should produce the most conductive state of the tested insulators between 20 to 40 minutes from the start of the fog generation at this time the test voltage is applied to the test samples. However, the rate by which the conductance of the pollution layer reaches its maximum conductance is totally dependent on the fog density which is dependent on the water flow rate and the air pressure input to the nozzles. In these tests, the water flow rate and air pressure for fog generation were varied from one insulator type to another so that each insulator reaches its maximum conductivity in the given time span and in order to satisfy the reference curve of Figure 3.5.

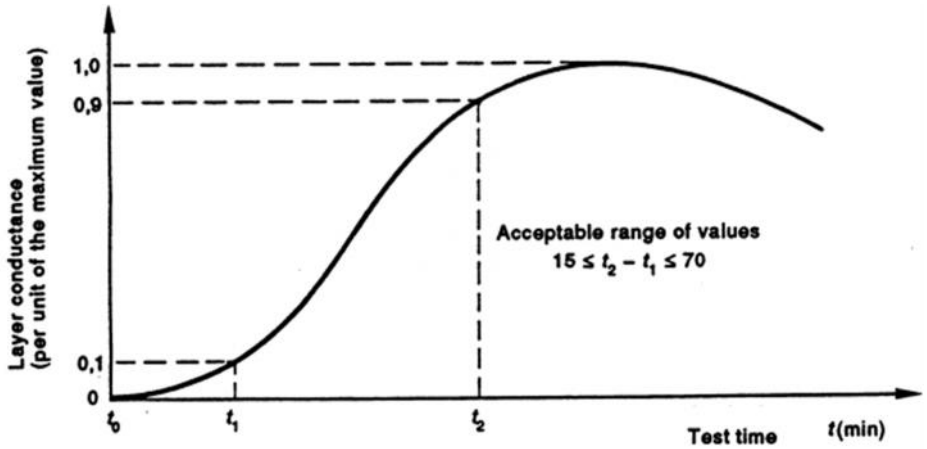

Figure 3.5: Control of wetting action (Appendix D of IEC60507)

The conductivity of the pollution layer deposited on the insulator is determined by measuring the current on its surface when momentary voltage is applied across the insulator. The test voltage is momentary applied to avoid drying of the pollution layer which affects the current readings. The current measurements are repeated many times throughout the wetting test and the value of the maximum conductance is determined. In each measurement, a reasonably low voltage (700 V_{rms} per meter of overall creepage distance) is applied to the insulator.

A cap and pin porcelain insulator of creepage distance 300 mm polluted to a salt deposit density *SDD* of 0.07 mg/cm^2 was used for this test as recommended by IEC60507.

Nanocoated insulator, two RTV coated insulators and standard uncoated porcelain insulators were used in this test to determine their maximum layer conductivity. At the start of the fog application, a low voltage of 250 V_{rms} was applied to the insulator every 5 minutes for a time period long enough to measure and record the leakage current. The wetting rate tests were performed on four different types of insulators: porcelain, porcelain coated with RTV1, porcelain coated with RTV2 and Nanocoated insulator. Figure 3.6 (a) to (d) shows the results of the wetting rates for the various insulators. The specified flow rate relates to the amount of water being supplied by the two pumps, where each pump supplies two nozzles.

Table 3.1 shows the water flow rate and the air pressure used in the wetting rate tests for determining the maximum layer conductivity. These values will be used in the artificial pollution tests in chapter 4.

The applied voltage across the insulator and the resulting leakage current were measured simultaneously and recorded using a LabVIEW (Laboratory Virtual Instrumentation Engineering Workbench) program. The layer conductance of the pollution layer, G, along the insulator surface was calculated using the expression:

$$G = I_l / V \qquad (3.4)$$

where V is the energisation voltage and I_l is the resulting leakage current flowing through the pollution layer at the moment of voltage application.

Table 3.1: Water flow rate and nozzle air pressure

	Water flow rate (litres/hour)	Nozzle air pressure (bar)
Uncoated insulator	2.5	2.75
RTV1	3.0	3.0
RTV2	3.0	3.0
Nanocoating	2.75	2.75

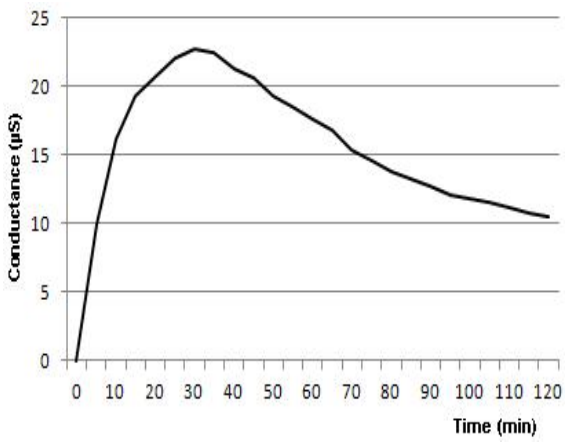

(a) Standard uncoated porcelain insulator

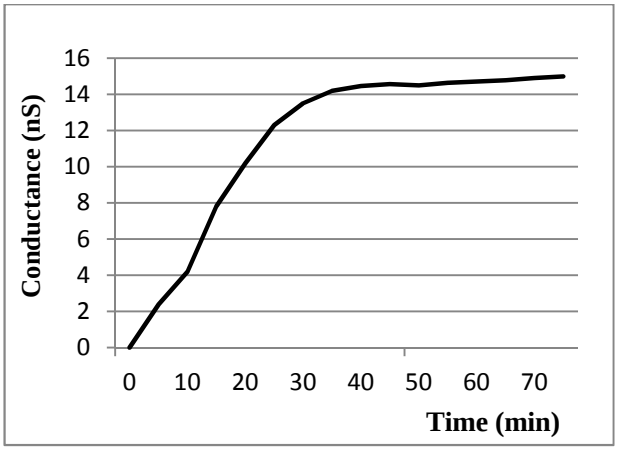

(b) Porcelain insulator coated with RTV1 Coating

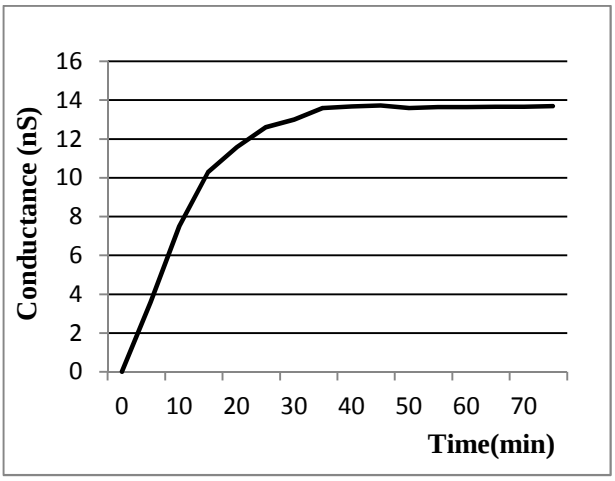

(c) Porcelain insulator coated with RTV2 Coating

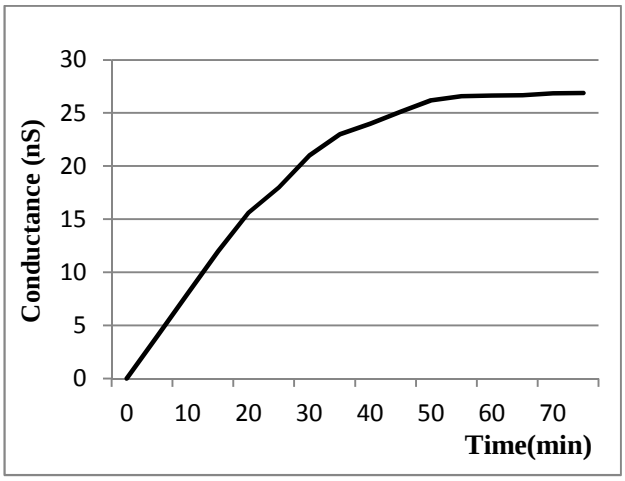

(d) Nanocoated insulator

Figure 3.6: Fog chamber wetting rates

The inputs to the data acquisition system (DAQ) system are voltages signals. However, the leakage current signals across the test insulators were measured as a voltage drop across suitable known resistor connected across the DAQ between the insulator and the earth. To protect the DAQ card and the oscilloscope the value of the shunt resistance was selected so that the leakage current on the tested insulator resulted in a voltage drop across the resistor within their permissible rated values. In these tests the conductance values of the pollution layer are very low. However, these tests were performed to confirm the compatibility of the fog chamber with the IEC60507 standard,

and to determine the maximum wetting rate for the tested insulators, and thus the signal to noise ratio of the measurements was not considered.
Following IEC60507, a specific creepage distance of 20 mm/kV and maximum withstand layer conductivity of 2.8 S/m (corresponding to a *SDD* of 0.07 mg/cm^2) were used to determine the test voltage to be applied to the insulators in the pollution tests.

3.2.5. Measured quantities

Evaluating the performance of the coated insulators and material degradation requires the need to study the leakage current behaviour on the surface of the insulators during the artificial pollution and in IPT tests in the laboratory. These require the capture and analysis of leakage current and voltage waveforms.
The RMS current was used as a measure to the ability of the coating system to suppress the leakage current on the surface of the insulator. While, the average power was used to measure the rate by which the energy is changing on the surface, and was also used as an indicator of the heat dissipated on the surface of the insulator which is principal cause of material degradation. The accumulated energy indicates the total energy loss on the surface of the insulator. The power factor index shows the phase shift between the voltage and the current which can be used to determine whether the current flowing on the surface of the insulator is capacitive or resistive. Capacitive current indicates a less conductive surface, with lower current and reduced power dissipation, while resistive current indicates a more conductive surface, and thus both higher current and power loss. These quantities are evaluated as follows:

(*i*) Leakage current root mean square (RMS)

The RMS is the square root of the mean of the integral of the square of a signal *i(t)*.

$$i_{rms} = \sqrt{\frac{1}{T} \cdot \int_{t=0}^{T} i(t)^2 \, dt} \qquad (3.5)$$

where T is the period of one cycle at 50 Hz = 0.02 seconds.
and *i(t)* is the instantaneous of current signal.

In this application, the RMS value of one cycle is calculated according to Equations (3.6) and(3.7).

$$i_{rms} = \frac{1}{N} \sum_{n=1}^{N} i_n^2 \qquad (3.6)$$

$$v_{rms} = \frac{1}{N} \sum_{n=1}^{N} v_n^2 \qquad (3.7)$$

Here *n* equals 200 samples and represents the number of samples per cycle.

***(ii)* Average power and accumulated energy**

The instantenous power $p(t)$ is the power at any instant of time of the measured signals.

$$p(t) = v(t) \, . i(t) \qquad (3.8)$$

Where *v(t)* and *i(t)* are the instantaneous values of voltage and current respectively.
The average power p_{av} is the average of the instantaneous power over one period .

$$p_{av} = \frac{1}{T} \int_{t=0}^{T} p(t)dt \qquad (3.9)$$

where T for at 50 Hz, = 0.02 seconds.

In the analysis program, the instantaneous power of one cycle is calculated numerically by multiplying each sampled voltage point by its corresponding current point at the same moment of time. The average power is then calculated by summing the values of the instantaneous power of one cycle and dividing the sum by the number of the data samples in that cycle, thus;

$$p_{av} = \frac{1}{N} \sum_{n=1}^{N} v_n \, . i_n \qquad (3.10)$$

The energy in one cycle is calculated by integrating the average power over one cycle (T).

$$E(t) = \int_{t=0}^{T} v(t)\,.i(t).dt \qquad (3.11)$$

The accumulated dissipated energy during the test time is calculated by adding the energy of each cycle to a running accumulated total. Where the energy per cycle may vary, the total dissipated energy is calculated from Equation (3.12).

$$E(t) = \sum_{t=0}^{t} p_{av}\,.T \qquad (3.12)$$

where T is the time for one cycle.

3.2.6. Data acquisition system and analysis program

A 16-bit, 16 analog input National Instruments NI PCI-6221, M Series data acquisition (DAQ) card was used to acquire the test signals. The DAQ card is an analogue to digital converter interfaced with and controlled by a PC. The DAQ card was physically connected to the PCI bus of a desktop computer through a 68 pin I/O connector.
The maximum sampling rate of the card was 250 kSample/s with programmable input ranges of up to ±10 V per channel. Two channels were used, for voltage and leakage current signal acquisition with a sampling frequency of 10 kSample/s in a continuous acquisition mode and 200 samples per cycle at (50 Hz).
On starting, the programme prompts the user to select the directories in which the acquired voltage and leakage current data are to be stored. The applied r.m.s voltage as displayed on the computer screen was the same as that indicated by the power supply and control unit displayes. A digital oscilloscope was also connected in parallel to the DAQ card to verify the accuracy and reliability of the measured quantities.
The voltage and leakage current traces were saved in a TDMS file format [3.3] with 10,000 samples of each channel saved into one file. A new file is automatically created

to save the next segment of the acquired data. A data flow diagram for the developed program for the pollution tests for this work is shown in Figure 3.7.

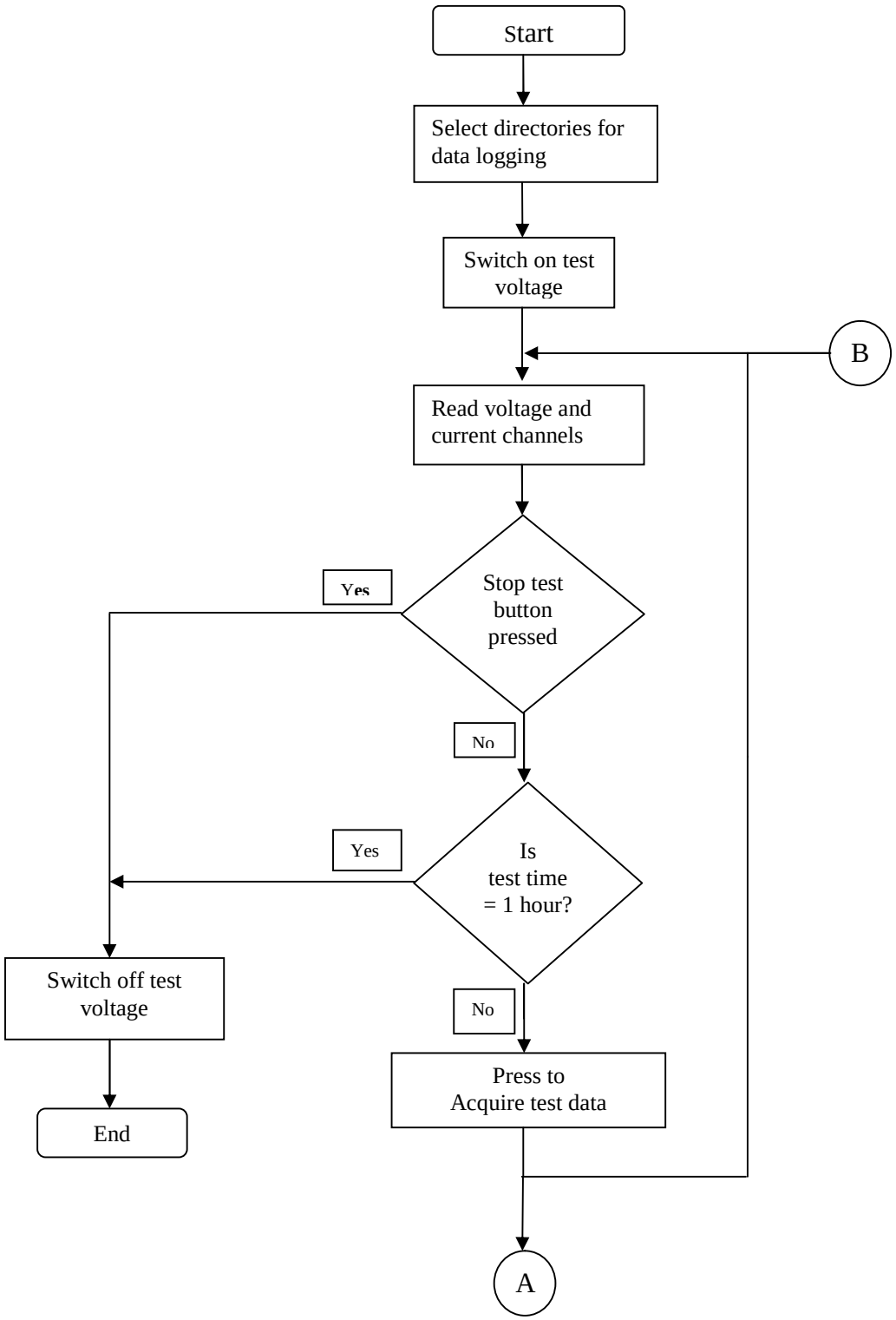

Figure 3.7: (a) Flow chart for the data acquisition program

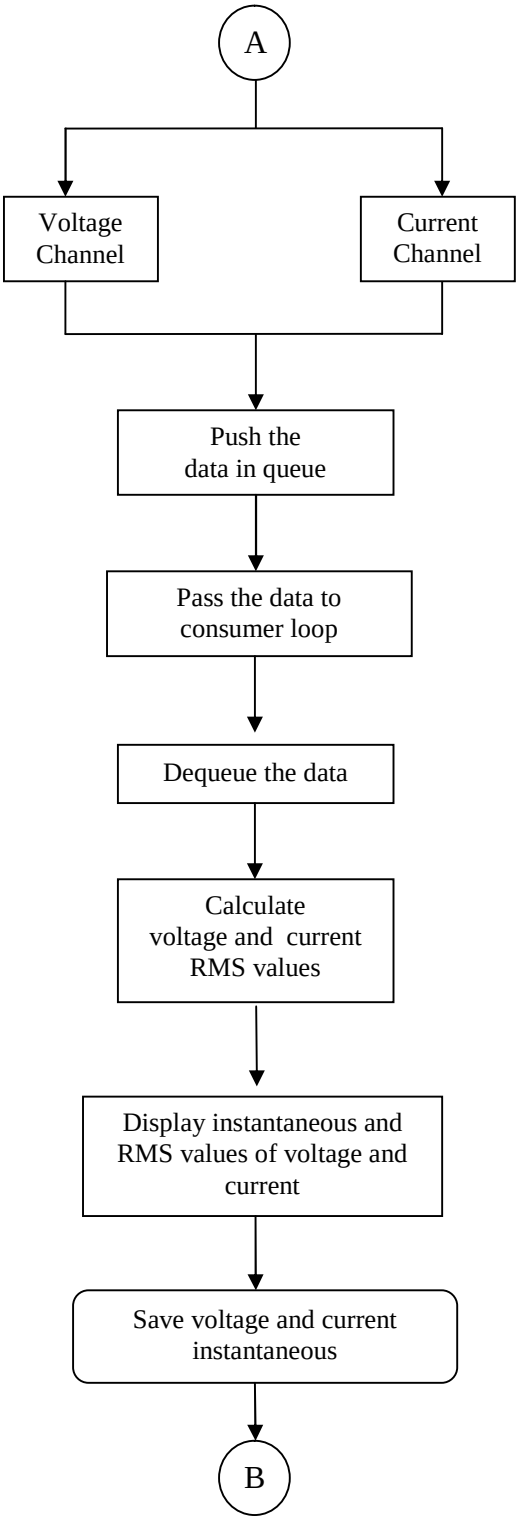

Figure 3.7: (b) Flow chart for the data acquisition program (continued)

3.2.6.1. Description of the programming language

The software that controls the DAQ was written using the LabVIEW platform, which is a system design platform and development environment for a visual programming language from National Instruments. LabVIEW is commonly used for data acquisition, instrument control and industrial automation. The programming language used by LabVIEW is a dataflow programming language capable of parallel execution. The program execution is determined by the structure of a graphical block diagram on which the programmer connects different function-nodes by drawing wires [3.4].

3.2.6.2. Data acquisition system

The DAQ hardware consisted of the DAQ card and its accessories. The DAQ software is a custom computer program designed to control the application of the test voltage to the samples, to acquire waveforms of the applied test voltage and the leakage current for each sample throughout the test and to manage the storage of the acquired data in series of files for later analysis. In order not to lose any data due to acquiring and processing the data at the same time, a Producer/Consumer architecture was implemented [3.5]. This architecture was used to decouple the processes that produce and consume data at different rates. The Producer/ Consumer patterns are broken down into three categories; those that produce data, those that consume the produced data and the data queues which are used to communicate data between the producer and the consumer loops. The Producer/Consumer configuration is shown in Figure 3.8. The Producer/Consumer pattern approach to this application was to acquire the voltage and current signals, and to queue the data in the producer loop based on the first-in/first-out technique. The consumer loop performed the calculation of the RMS values of the voltage and the leakage current, and saved the data while being displayed on the computer screen. This allows the consumer loop to process the data at its own pace, while allowing the producer loop to queue additional data at the same time.

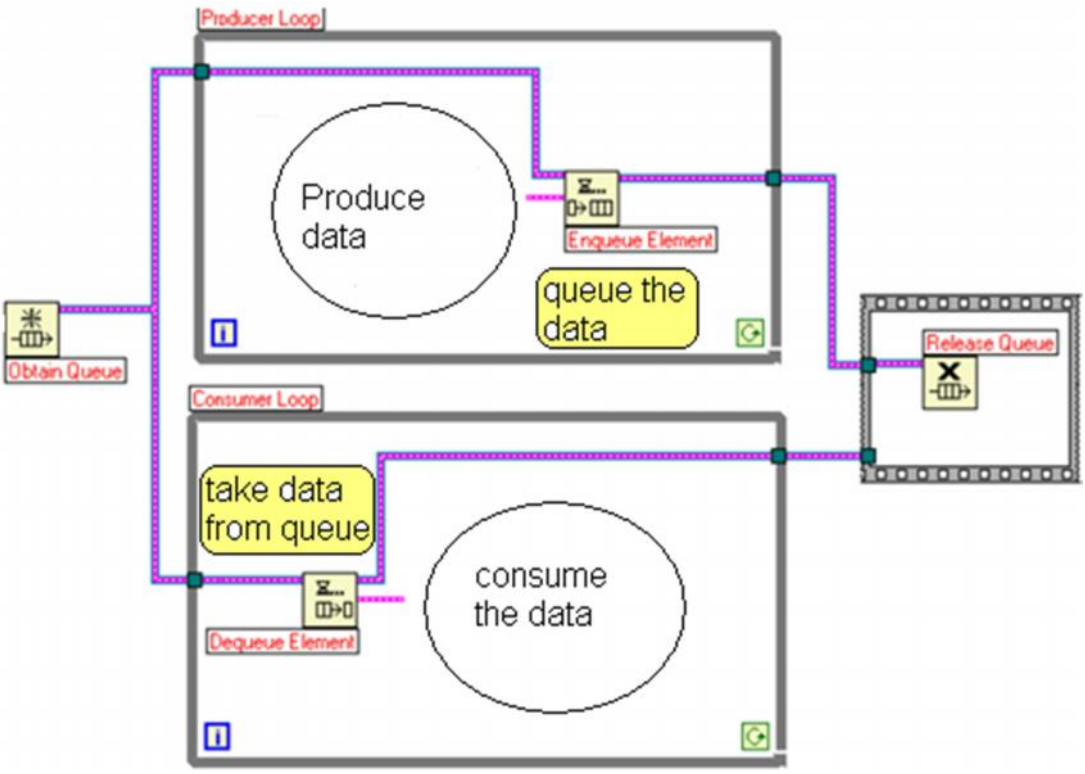

Figure 3.8: Producer/Consumer Design Model

The front panel screen of the data acquisition program used for the artificial pollution tests is shown in Figure 3.9. The instantaneous waveforms of the voltage and the leakage current are displayed and logged in series of files. The program calculates and displays the current RMS values for each voltage and leakage current cycle against time. The program is designed to stop automatically after the test duration. Two physical channels were used, one for voltage and the other for current. At the start of the test, the producer loop acquired 200 samples from each channel in each loop iteration. The data was pushed into a queue and passed to the consumer loop. At the consumer loop, the data was removed from the queue, is "dequeued". The consumer loop procedure stopped if there were no elements present in the queue. The consumer loop contains two index arrays; their role was to return the voltage array and the current array. A "write to" measurement file function was used to save the voltage and the current waveforms in a TDMS file format. A new file was automatically created after 50 waveforms from each channel had been saved. The acquired signals through the daq card was compared with the signals shown on an oscilloscope connected with the daq card, identical signals for current and voltage were obtained. In addition the rms signal of the voltage shown on the computer screen was also checked in comparison with that shown on the LED of the control unit of the HV transformer.

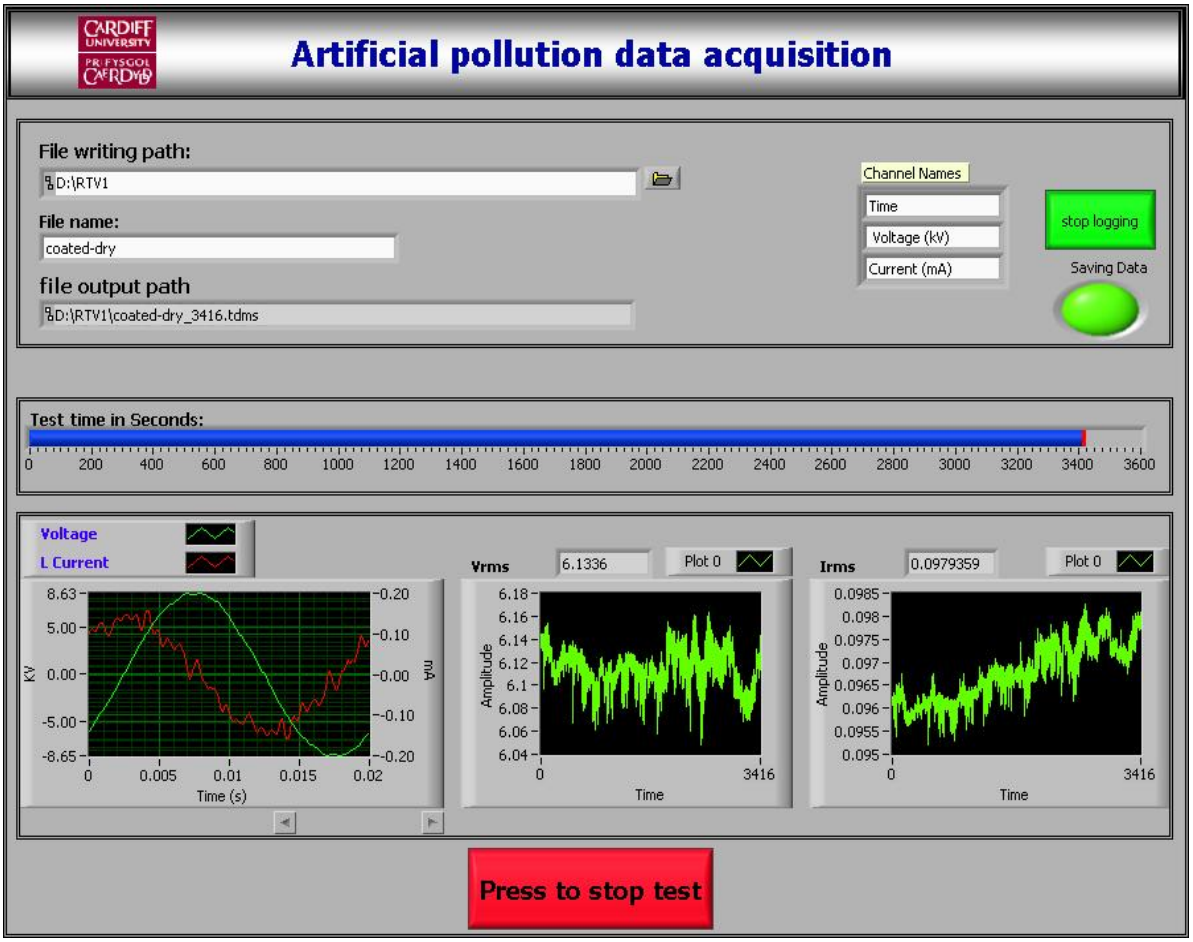

Figure 3.9: Front panel screen of data acquisition instrumentation

3.3. Inclined plane test and data acquisition system

3.3.1. Inclined plane test machine

The inclined plane test (IPT) machine was used to evaluate the performance of insulating materials used in severe ambient conditions at a power frequency of 50 Hz by measuring their resistance to tracking and erosion. The IPT unit was housed within an earthed, steel enclosure, and five samples can be tested at the same time. The unit is equipped with a back door to mount or remove the samples. A variac, used to adjust and control the test voltage, was mounted on the front panel of the enclosure. A Watson Marlow 205S/CA multi-channel pump was used to pump the contaminant from the reservoir of contaminant solution to the surface of the test samples. The pump was equipped with a digital display and a control unit was located at the bottom of the

enclosure together with the reservoir of contaminant solution. The pump speed was determined by a calibration test to determine contaminant flow rates according to the standard, and is given in Table 3.2.

Table 3.2: Values of the test voltage, series resistance and pump speed

Test voltage (kV)	Series resistor, resistance (kΩ)	Contaminant flow rate (ml/min)	Pump speed (rpm)
2.5	**10**	**0.15**	**9**
3.5	**22**	**0.30**	**16**
4.5	**33**	**0.60**	**32**

The samples to be tested were mounted at an inclined angle and exposed to a constant tracking voltage with liquid contaminants flowing over their surfaces. The criterion used for determining the end point of the test was criterion A of Method 1 of IEC60587 [3.6], which states: that when the current through the specimen exceeds 60 mA for 2 seconds an over current device should terminate the circuit. The sample was classified as having failed if it reached the end point criterion in less than 6 hours.

3.3.2. Electrical test circuit for the inclined plane test unit

The test circuit for the inclined plane test unit is shown in Figure 3.10. The test voltage was applied to the samples using HV vacuum relays controlled by a LabVIEW programme to control the data acquisition process, and to control the IPT unit by sending a 5 V DC signal through the digital output port to activate the relays. When the HV vacuum relays are active and the ON/OFF switch located on the front panel of the enclosure is ON, the test voltage is applied to the samples and can be raised to the voltage level of the test. The test voltage to each sample was connected in series through a number of HV resistors whose values depend on the test voltage level, and are specified in IEC60587, see Table 3.2. The appropriate resistance values could be selected by means of a plug-in connector.

A 240V/10kV, 10kVA HV transformer connected to the 220 V mains was used as supply for the inclined plane test unit through an isolation transformer and a filter for smoothing the applied voltage signals. The HV transformer was housed within a

separate earthed enclosure. The supply to the HV transformer was controlled using a key-operated interlock system. The voltage signal was measured with a high voltage (Ross Engineering VD120) probe with a ratio of 2000:1. The doors of the inclined plane test unit enclosure and the high voltage transformer enclosure were interlocked to prevent the application of a dangerous voltage while any part of the test arrangement was accessible.

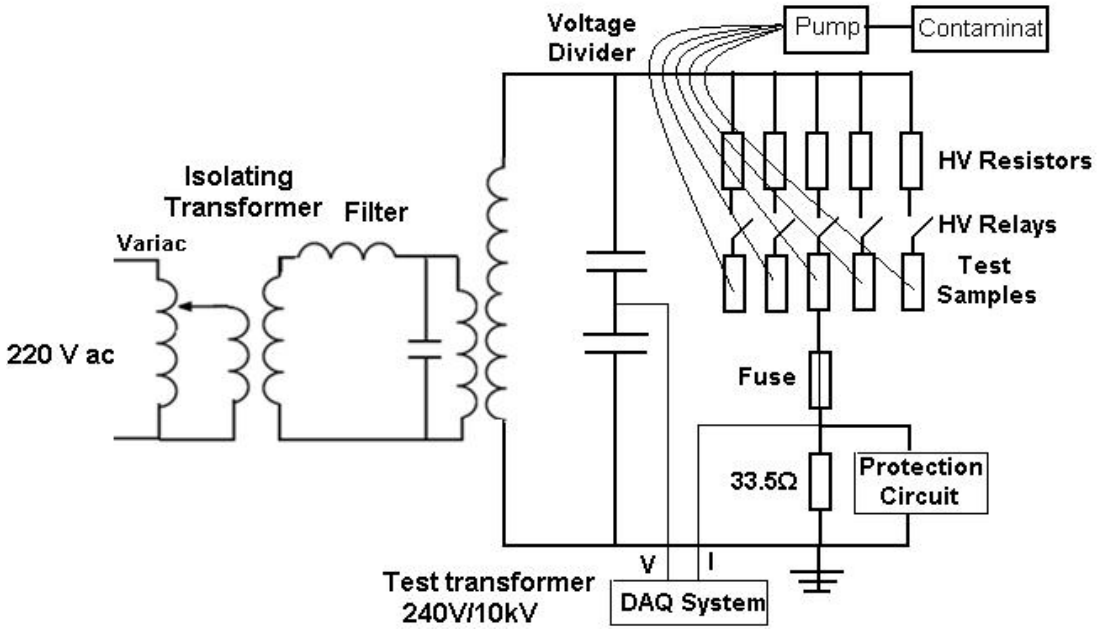

Figure 3.10: Test circuit for the inclined plane test unit

3.3.3. Data acquisition system for the inclined plane test

As a part of the DAQ system for the IPT, a 16-bit, 32 channel analog input National Instruments PCI-6254 card with a multichannel sampling speed of 1 MS/s, and single channel sampling speed of 1.25 MS/s was installed in a PC to control the IPT unit. A SCB-68 connector block was used as a physical connection for the input signals to the DAQ card and as an output for signals to control the HV relays through the digital output ports. A data flow diagram for the program is shown in Figure 3.11.

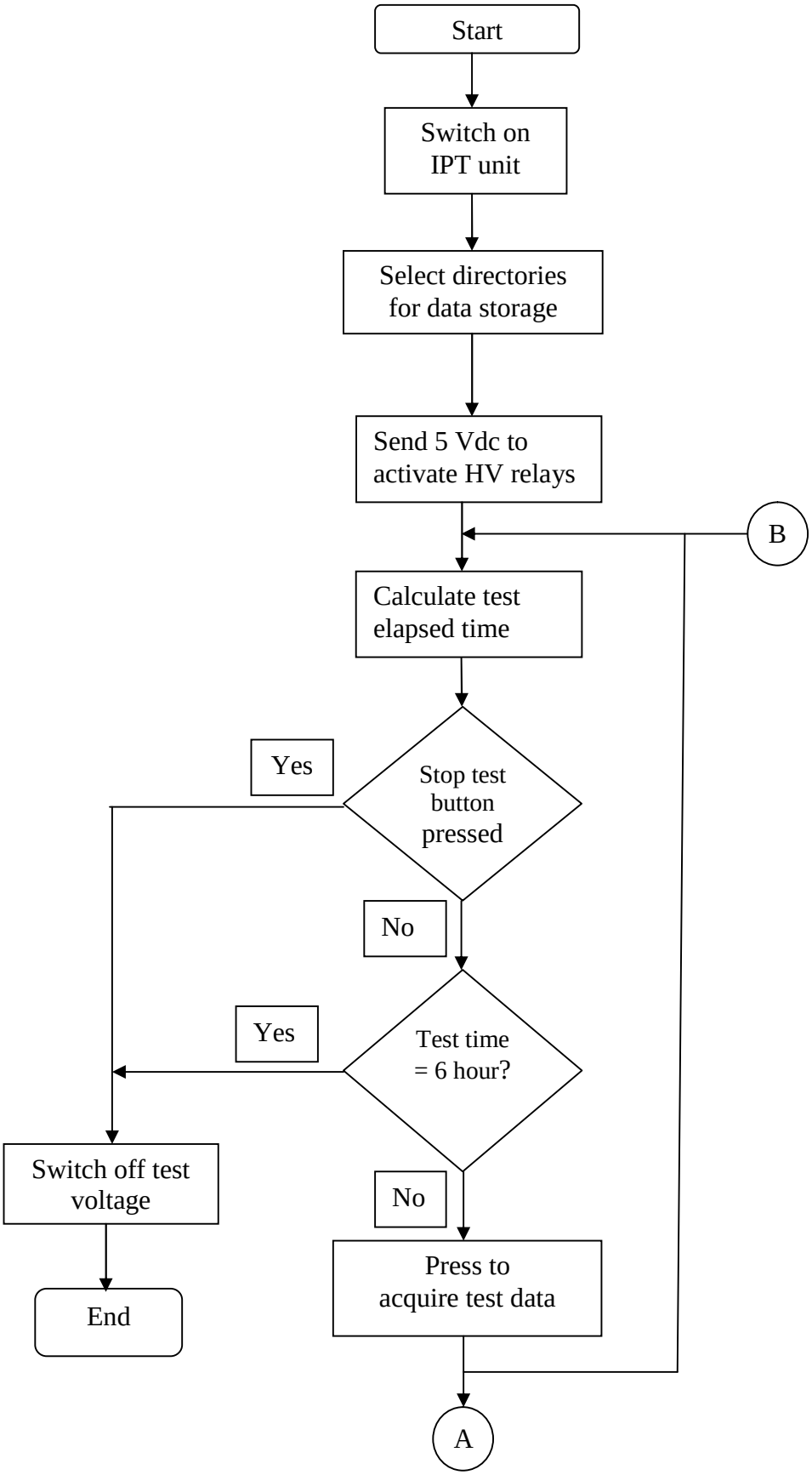

Figure 3.11: (a) Data flow diagram for the data acquisition program for the IPT

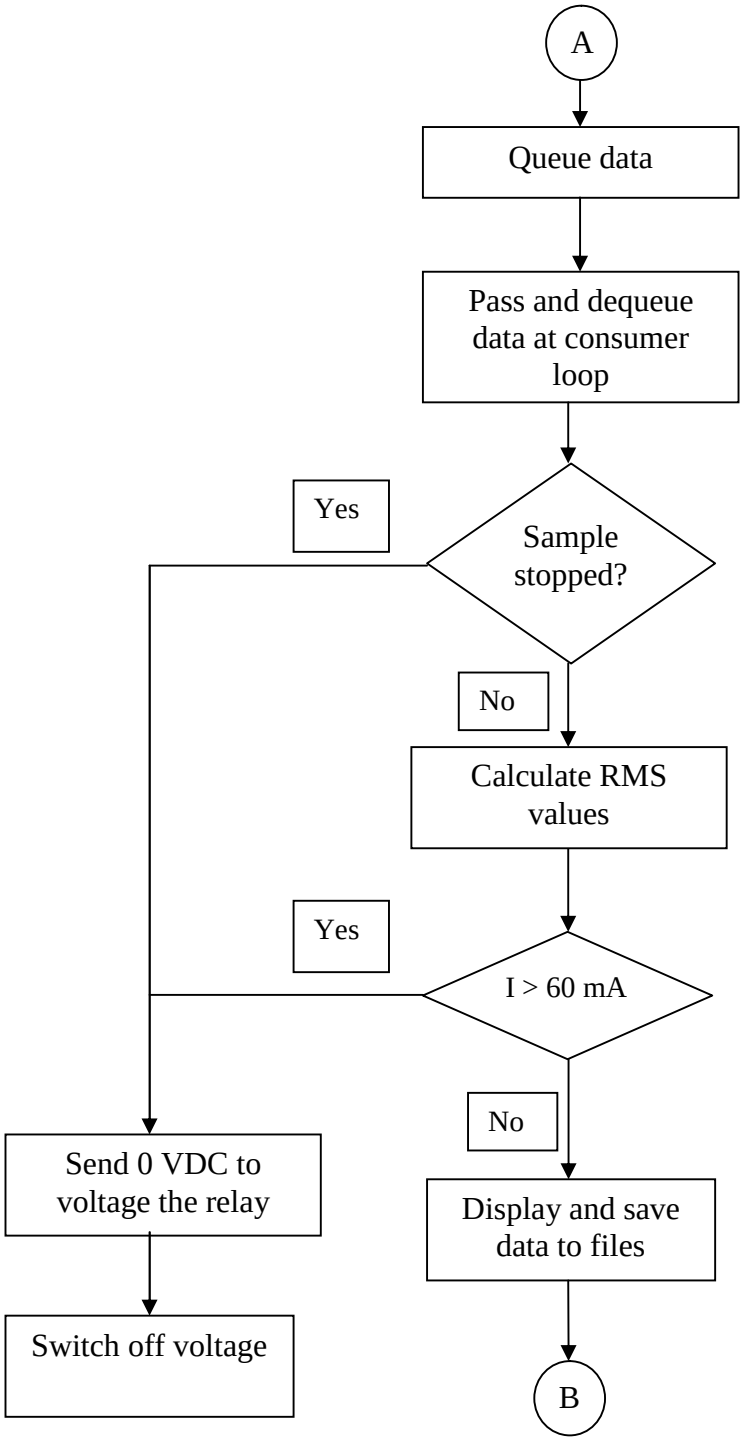

Figure 3.11: (b) Data flow diagram for the data acquisition program for the IPT (continued)

The software responsible for controlling the DAQ was also developed using NI LabVIEW by implementing Producer/Consumer and State Machines architectures [3.5]. In addition to the Producer and Consumer loop architecture shown in Figure 3.8, a third loop was implemented in the program to control the operation of the HV relays using a digital output function.

Six input channels were used in the tests, one for the applied voltage and the other five were used to acquire the leakage current signals. At the start of the test, the program prompts the user to select the directories where the data is to be stored. The ports of the data acquisition card are configured and a control signal is sent to the HV relays to permit the application of the test voltage. The data was acquired in the producer loop at a sampling rate of 10,000 samples per second, and 200 samples per cycle at the power supply frequency (50 Hz). The data was pushed into a queue and passed to the consumer loop. In the consumer loop, the data was dequeued and RMS calculations performed, and the values were displayed on the front panel screen. The data acquired from each of the six input channels were saved into TDMS files format. When 60,000 samples were saved, a new file was automatically created to save the next segment of the acquired data.

3.4. Data analysis program

A data analysis program was also developed using NI LabVIEW to read the files of the data which were stored during the tests and to calculate characteristics of the leakage current and the voltage waveforms for the purpose of describing the behaviour of the test objects. These results were displayed and stored for later analysis. The flow diagram for the data analysis program is shown in Figure 3.12. The front panel of the data analysis program is shown in Figure 3.13.

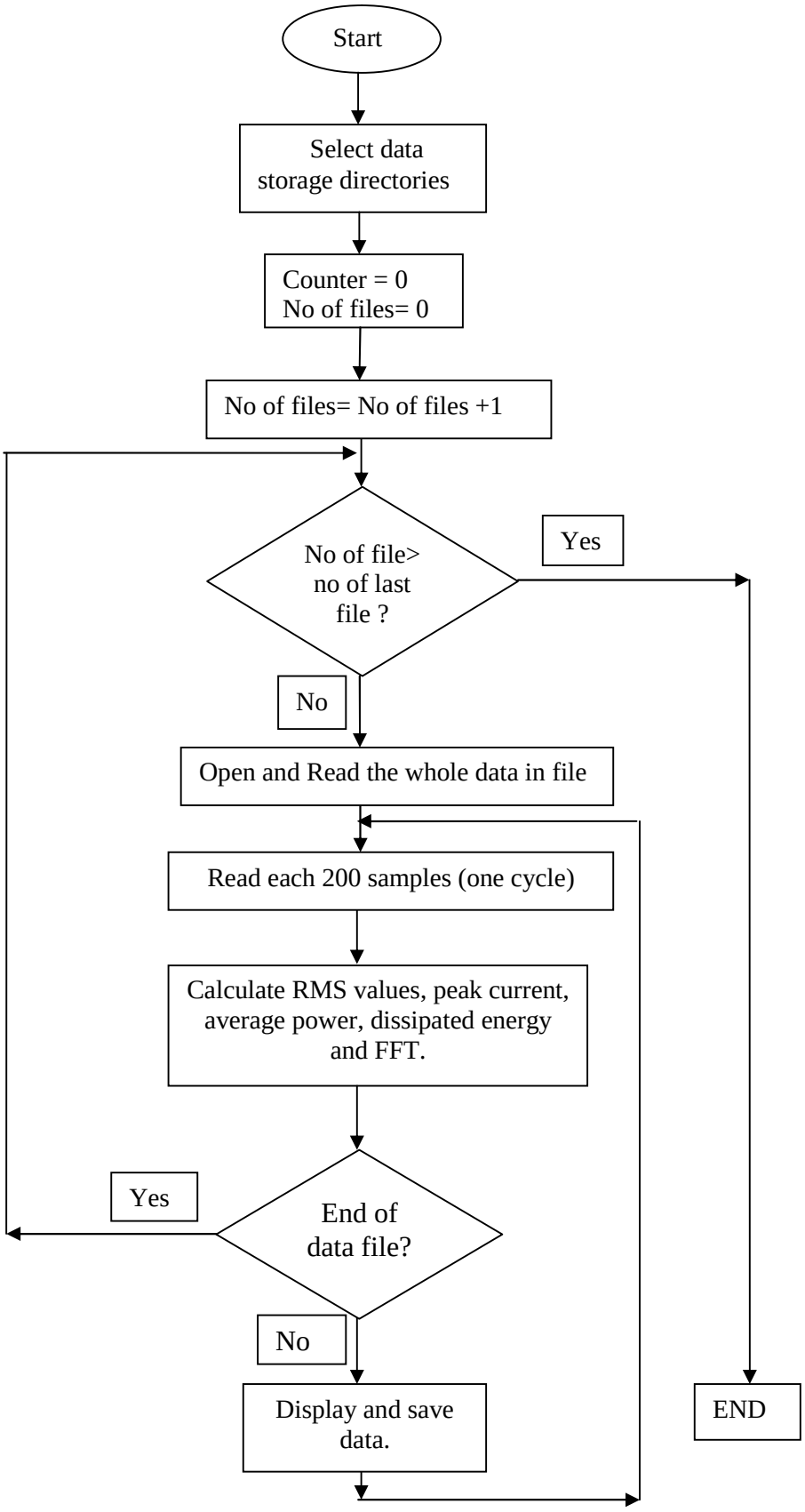

Figure 3.12: Data flow diagram for the data analysis program

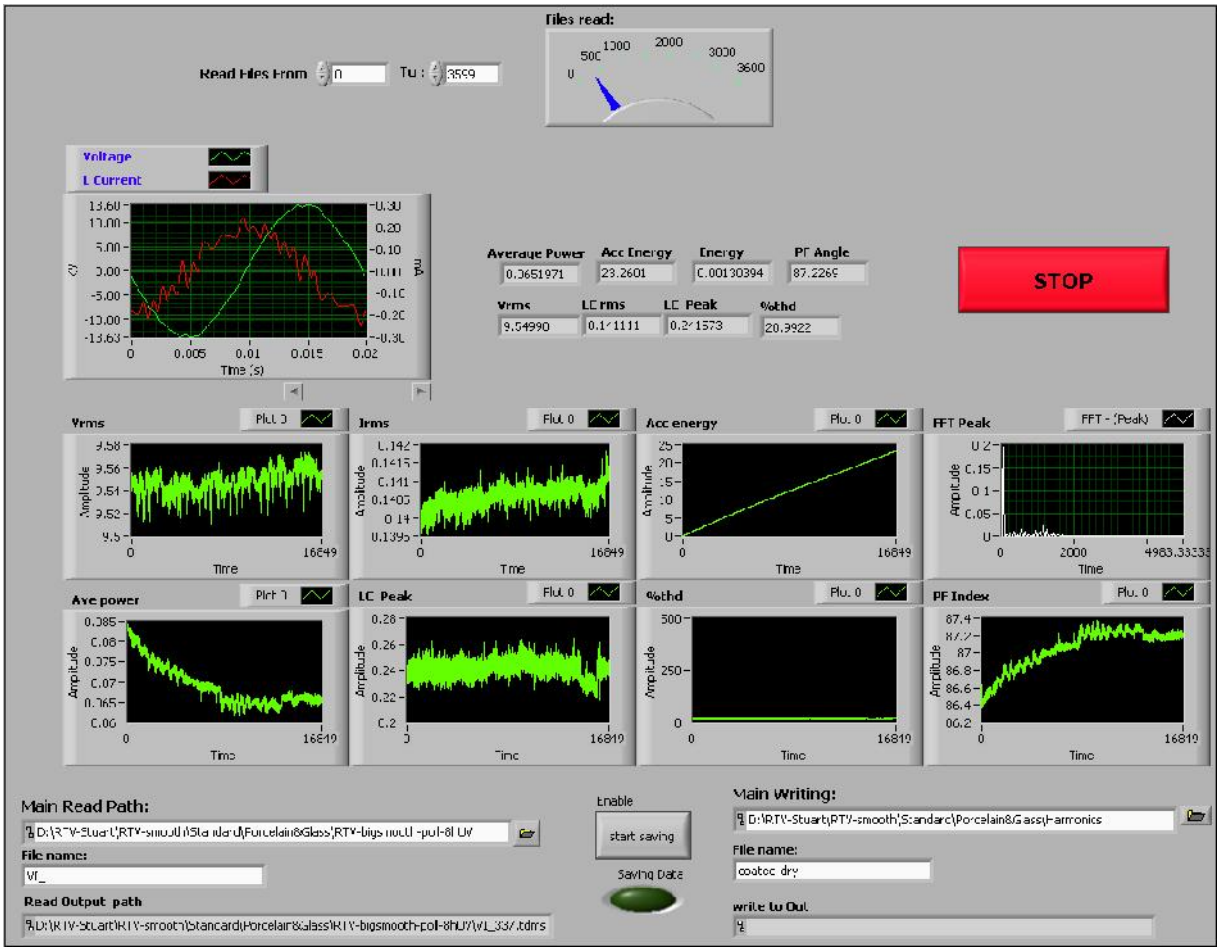

Figure 3.13: Data analysis program - front panel

The program comprises two nested loops for repetitive execution of commands. The directories and the numbers of the data files were selected. In the external loop, the Read from measurement file function reads the data contained in the first file and simultaneously incremented the pointer to point to the next file. The index array function returns the voltage and the current arrays. An array subset function was implemented in the inner loop. This function returns a portion of the data array starting at the first index and containing the length of the extracted portion. In this case, the array length represents a cycle length of 20 ms, which is the time for acquiring 200 samples, one cycle at 50 Hz. A series of derivatives characterising the leakage current waveform were calculated for each waveform read. The calculated characteristics of leakage current are RMS, average power, power factor index, accumulated energy, and leakage current peak magnitude.

3.5. UV radiation testing of coated insulators

The level of degradation of the polymeric material depends on both the intensity and the wave length of the UV light which can vary with season, elevation, latitude and the time of the day [3.7].

It has been reported that the contamination layer deposited on the surface of the coated insulator in field conditions protects the coating material from UV degradation by absorbing 40% to 60% of the radiated energy [3.8].

In this study, the effect of UV radiation on the coating materials was studied using an Atlas XXL+ artificial weathering test station which uses three air cooled Xenon arc lamps of 1700 W each. The lamps are capable of producing more than 90% of the natural sunlight spectrum. A daylight filter is used to produce different portions of the spectrum to match natural sunlight over a broad range of wavelengths. Figure 3.14 shows the Xenon lamp spectrum compared with sunlight [3.9].

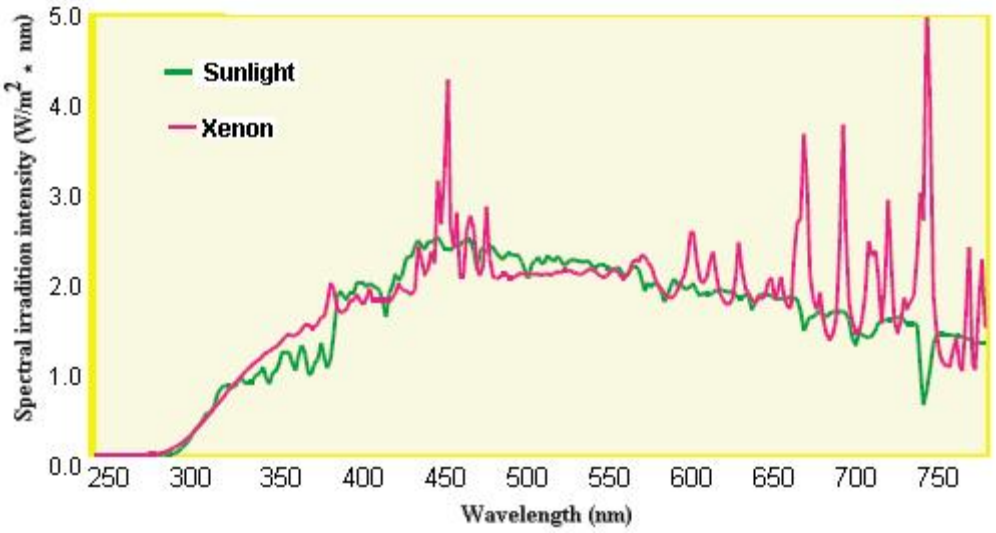

Figure 3.14: Xenon arc versus sunlight spectrum [3.9]

The Atlas XXL+ artificial weathering test machine can be programmed for the application of pre-defined standard UV cycles or user defined cycles under controlled temperature and humidity. Experiments have shown that HV outdoor insulators are most vulnerable when polluted and operating in wet conditions [3.10]. Based on this, the study of the effect of UV radiation on the RTV coating was performed in the fog chamber on insulators:

- A polluted RTV coated insulator, which is then exposed to UV radiation without water spray.
- A clean RTV coated insulator exposed to standard UV radiation and then polluted.

The duration of one standard UV cycle is 120 minutes and involves exposing the sample to 102 minutes dry followed by 18 minutes with water spray. The UV standard ISO 4892-2:2006 [3.11] was amended under the user defined option in the test machine so that the UV exposure period was completely dry. The reason behind this amendment was that the presence of the water spray for 18 minutes will wash the pollution layer of the insulator. The insulator will be tested in the fog chamber immediately after the UV exposure under the artificial solid layer method according to IEC 60507. In this case, the test results will be affected as the pollution layer will be washed by the water spray of the UV test machine. Figure 3.15 shows a typical Atlas XXL+ UV cycle for duration of 120 minutes during the tests curried out in these investigations. The relative humidity represented by the dotted line increased to 95% at the starting of the water spray at 108 minutes from the starting of the test. Figure 3.16 illustrates the two processes used in testing the coated insulators.

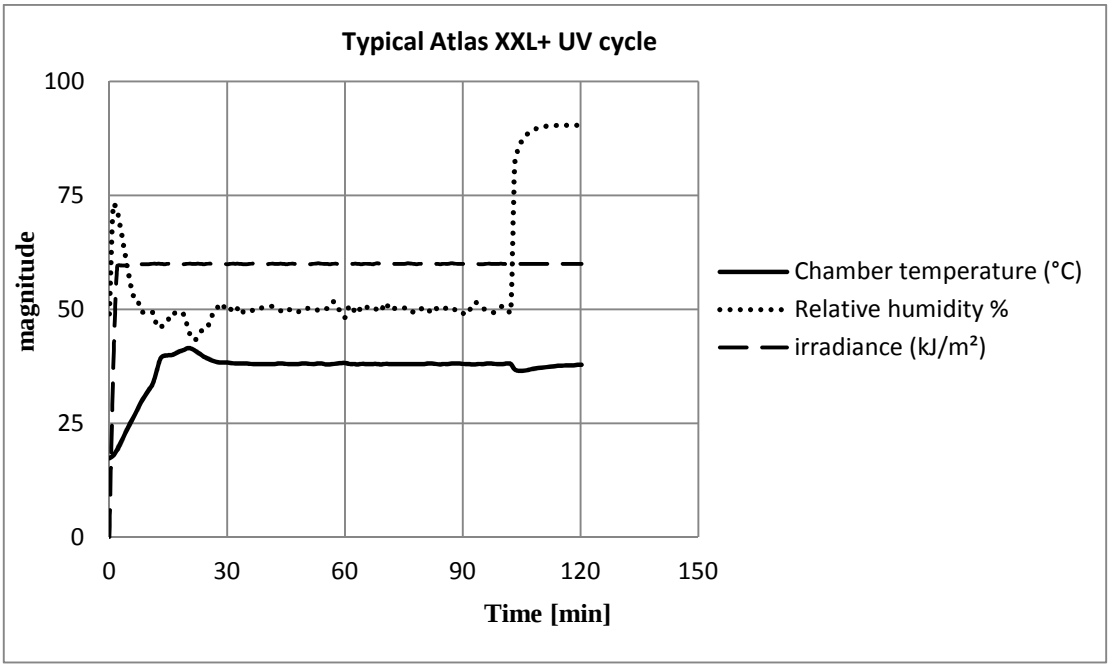

Figure 3.15: Typical Atlas XXL+ UV cycle

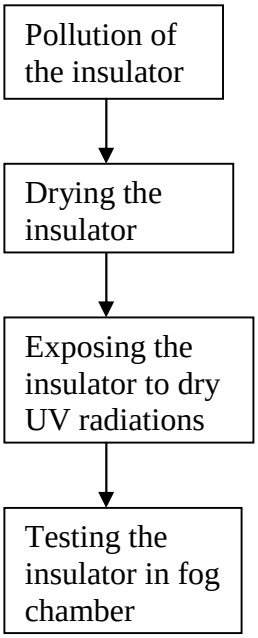

(a) Polluted insulator-exposed to UV radiation

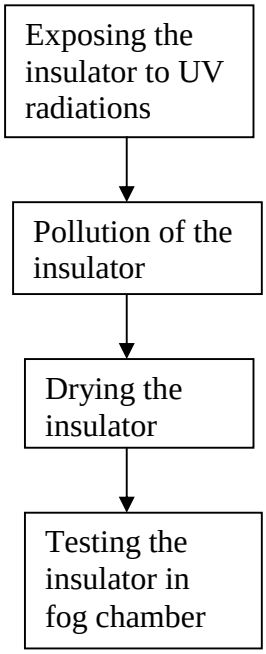

(b) Insulator exposed to UV radiation-then polluted

Figure 3.16: Flowchart of testing polluted insulator exposed to UV radiation

3.6. Conclusions

The chapter has described the methods used to evaluate the performance of the coating systems, and the test configurations and methodologies employed. The fog chamber test facility and the inclined plane test machine and their electrical circuits have been explained and discussed. The preparation of contaminant suspensions and the insulator pollution process have been explained. Computerised data acquisition systems were developed for the artificial pollution tests and the IPT to manage the capture of the leakage current waveforms and the voltage waveforms during the tests and to save these data in accessible file formats for later analysis.

The data acquisition system (DAQ) system software used for the artificial pollution tests acquired the voltage and current traces with a sampling rate of 10,000 samples per second (200 samples per cycle), performed root mean squares (RMS) calculations, displayed the waveforms on a PC screen, and saved the data for subsequent analysis.

The system also controls the ON/OFF application of voltage to the samples in the inclined plane tests and terminates the test for any sample when the end point condition was reached.

A data analysis programme has been developed to read the stored data and calculate quantities characterising the leakage current waveforms including r.m.s and peak values, average power, power factor angle index. The calculated quantities are stored in an easily accessible format to allow further analysis with the aim of evaluating the current suppression and erosion resistance performance of the coated insulators. The approach of acquiring and storing the acquired data using the producer consumer technique and using a separate programme for analysis minimises processing requirements during the test. It also allows analyses to be performed off-line as required to identify the characteristics of the leakage current giving the best indication of insulator performance and degradation.

Procedures for studying the effect of UV radiation of the coated insulators using an Atlas XXL+ machine were also explained.

Chapter 4 – Comparative performance of insulator coatings under artificial pollution test conditions

4.1. Introduction

Coatings for HV insulators have been used to enhance the performance of ceramic insulators under adverse weather conditions. The ability of various silicone elastomer coatings to suppress leakage current and prevent flashover of the insulators is different although the base material in all these coating systems is polydimethylsiloxane (PDMS). The RTV coating system consists of PDMS polymer, alumina tri-hydrate filler for increased tracking and erosion resistance, and a cross linking agent [4.1].

Another recently proposed solution for the problem of contamination of outdoor insulators consists of the application of a Nanocoating on the surface of the insulator. The nanocoating used in this work is a Voltshield coating. Voltshield is a chemically cross-linked polymeric resin with extremely good 'non-stick' properties used to improve the performance of porcelain insulators under wet polluted conditions [4.2]. Voltshield is applied to the surface of porcelain insulator as a liquid, it chemically bonds to the porcelain surface and it is polymerised. This results in a highly hydrophobic and uniform coat over the insulator surface. The new hydrophobic surface permits the rapid dispersal of water into small droplets and does not allow adherence of solid pollutants [4.3].

The coating systems used in this study are; Nanocoating, two RTV coatings from different manufacturers; RTV1, RTV2, and two types of Grease coatings. Many tests were performed on various insulators coated with these different hydrophobic coating systems to assess how well they optimized electrical performance. The performance of the coatings was investigated in the fog chamber under artificial pollution conditions using a procedure based on the solid layer method of IEC 60507. In this method, a uniform layer of a defined solid pollution is deposited on the surface of the insulator. The polluted insulator is exposed to a clean fog and energised by the

application of an AC voltage. Leakage current and test voltage waveforms were acquired throughout the tests.

This chapter presents results of tests performed on coated and uncoated insulators. The coated insulators were treated variously with Nanocoating, RTV1, RTV2 and grease coatings. The tests were performed in the laboratory fog chamber using the solid layer method of IEC60507. In this method the insulators were polluted and wetted by exposure to a clean fog. Leakage current and test voltage were acquired and saved for further analysis and discussion. RMS current, Average power and accumulated dissipated energy were calculated using the analysis program described in Chapter 3, and the results are presented and analysed with the aim of identifying trends related to the ability of coating systems to suppress the leakage current and reduce the dissipated energy on the insulator surface. The effect of different UV exposure with different dosages on the hydrophobicity of the coatings was also investigated under artificial pollution tests. Flashover voltage tests of all insulators in addition to sandblast tests for Nanocoated insulators are also investigated. An analysis of the results is presented in this chapter.

4.2. Test insulators

Cap and pin porcelain insulators, see Figure 4.1, with different creepage distances coated with four different coating systems were used in this study. Figure 4.1 shows a cap and pin type porcelain insulator with creepage length of 300 mm. This was coated in the laboratory with RTV1, RTV2 and grease coatings. A cap and pin type porcelain insulator with creepage length of 430 mm coated with Nanocoating was supplied by a utility. A bare porcelain insulator with creepage length of 470 mm was tested to compare its performance with that of the Nanocoating insulator. The Nanocoated insulator and a similar uncoated insulator are shown in Figure 4.2. Details of all the insulators used in these investigations are given in Table 4.1.

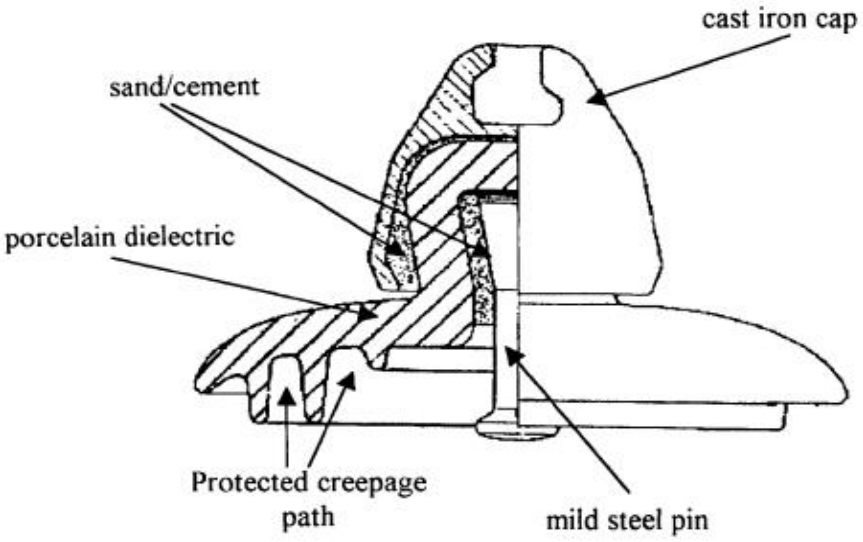

Figure 4.1: Cap and pin porcelain insulator with creepage distance of 300 mm [4.4]

Table 4.1: Types of porcelain insulators tested

Insulator type	Creepage length (mm)	Coating type	Test voltage(kV)	Number of sheds
A	430	Nanocoating	9.1	1
B	470	uncoated	9.6	1
C	300	RTV1	6.3	1
		RTV2	6.3	
		Silicone Grease	6.3	
		Hydrocarbon Grease	6.3	
		uncoated	6.3	
D	460	RTV1	8.8	1

(a) Nanocoated insulator

(b) Nanocoated and uncoated porcelain insulators

Figure 4.2: Nanocoated and uncoated insulators

4.3. Experimental procedure

4.3.1. Preparation and application of the pollution slurry

The contamination slurry consisted of 40g kaolin, 1 litre (1000 g) tap water, 1 g of wetting agent (Trixton-100) [4.5] and a suitable amount of NaCl of commercial purity to achieve a volume conductivity of 2.8 S/m, corresponding to a SDD of 0.07 mg/cm^2. The addition of the wetting agent to the pollution slurry was first introduced when testing highly hydrophobic polymeric insulators as it allows pollution to adhere to the surface. For insulators treated with hydrophobic coatings, a similar approach was adopted to obtain surface adherence with the pollution layer. The insulators were thoroughly cleaned with water, and were left to dry and then dipped in the contamination slurry and left to dry overnight. Appendix A shows the details of coatings used as supplied by the suppliers.

4.3.2. Application of the test voltage

A specific creepage distance of 20 mm/kV was used to determine the test voltage to be applied according to Appendix B of IEC 60507. The polluted insulator was installed in the chamber and fog generation started and maintained at a constant steady rate, as determined by the wetting rate measurement. Figure 4.3 shows an insulator hanging in the fog chamber.

The insulator was energised continuously at the specified test voltage. The test voltage for each of the tested insulators is as shown in Table 4.1. The test duration was 60 minutes. The voltage and leakage current waveforms were recorded throughout the test. Figure 4.4 shows the data acquisition system used for the artificial pollution tests.

Figure 4.3: Insulator placed in the fog chamber

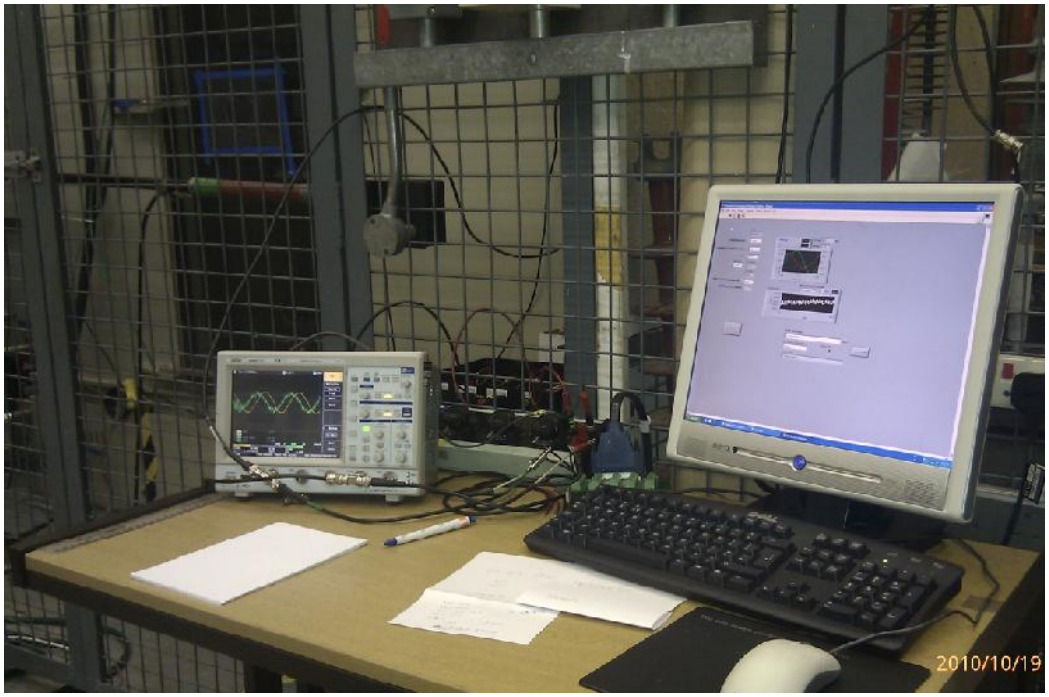

Figure 4.4: DAQ equipment: fog chamber test

4.4. Performance of Nanocoated insulators and uncoated insulators

In each test set, three cases representing clean dry, clean wet, and wet polluted conditions were performed on the insulators.

- Dry tests: in this case, the insulators were stressed with the test voltage without being exposed to fog.
- Wet tests: clean insulators were stressed with the test voltage as mentioned in table 4.1 while exposed to clean fog.
- Pollution tests: polluted insulators were stressed with the test voltage while exposed to clean fog.

4.4.1. Pollution performance test of Nanocoated and Uncoated insulators

(i) Leakage current

Leakage current variation with test time for the uncoated insulator can be clearly seen in Figure 4.5(a). The figure shows three curves representing the uncoated porcelain insulator under clean dry, clean wet and wet polluted operating conditions.

The r.m.s current for the unpolluted uncoated insulator under dry and wet conditions was 0.9 mA and 1.1 mA respectively. These remained more or less constant throughout the test due to the absence of a conductive pollution layer. However, the polluted uncoated insulator showed significant current variations. At the beginning of the test and with the commencement of fog generation, the r.m.s components of the surface leakage current increased as the conductivity of the pollution layer increased. When the conductivity of the pollution layer reached its maximum, the r.m.s value of the leakage current was at its maximum value of 2.4 mA. However, the r.m.s current had fallen to a stable value of 2.0 mA by the end of the test because of the washing effect of the fog. The leakage current was mainly resistive under pollution conditions with phase angle of 25° as in Figure 4.5(c, *ii*). The resistive current components lead to dry band arcing and power dissipation, which results in heating of the pollution layer. The surface of the Nanocoated insulator experienced a predominantly capacitive current as shown in Figure 4.5(c, *i*). The capacitive currents results in a lower dissipated power and less heating, which in turn leads to longer coating life. Figure 4.5(c) shows waveforms for the capacitive and resistive current components on the surface of coated and uncoated

insulators respectively. The r.m.s current for the Nanocoated insulator under clean dry, clean wet and wet polluted conditions was 0.18 mA, 0.21 mA and 0.25 mA respectively. These are all substantially lower than the current levels for the uncoated insulator and remained more or less constant throughout the test. Typically, the nanocoating reduced the r.m.s. current by about 80% as can be seen in Figure 4.5(b).

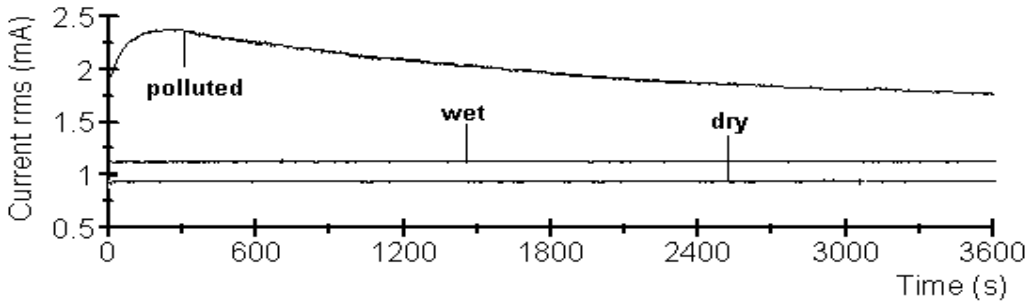

(a) Uncoated insulator

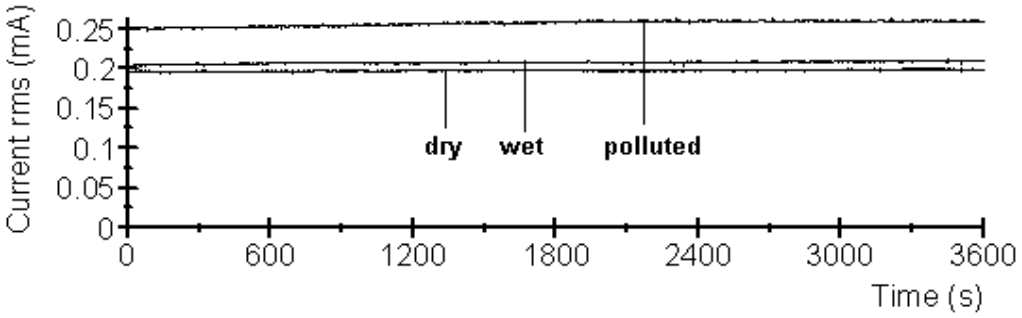

(b) Nanocoated insulator

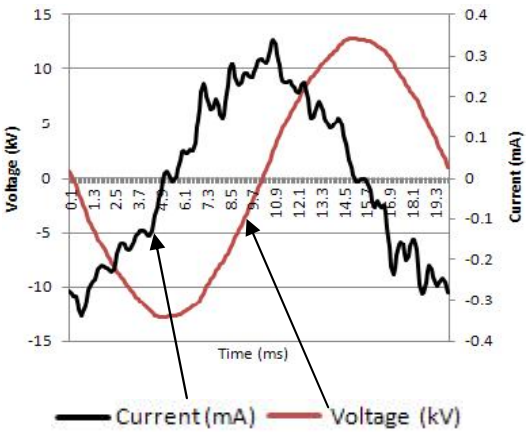

i) Capacitive current for nanocoated insulator

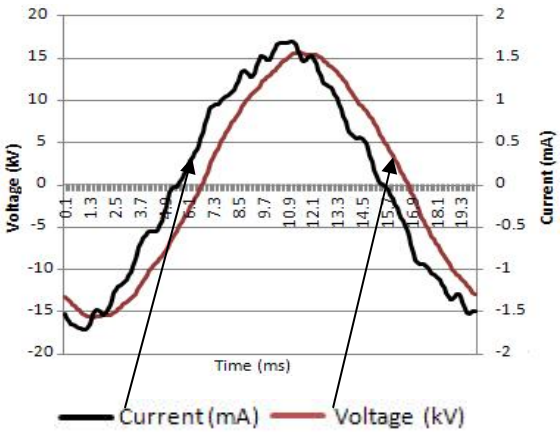

ii) Resistive current for uncoated insulator

(c) Leakage current waveforms for coated and uncoated insulators

Figure 4.5: Leakage current (a) uncoated insulator, (b) Nanocoated insulator (c) Leakage current waveforms for coated and uncoated insulators

The poor performance of the uncoated porcelain insulator is attributed to the fact that the ceramic surfaces have many “potholes”. These potholes can be covered with organic and inorganic contaminants. These contaminants deposit in the potholes and adhere tightly to the surface of the insulator. In contrast, Voltshield treated porcelain insulators overcome the problems of contaminant deposition on the surface with a highly non-stick surface property [4.6].

(ii) Average power

The average power of the uncoated insulator exhibited similar behaviour to that of the r.m.s leakage current. As in Fig 4.6 the polluted insulator showed the highest average power dissipation at the surface with 23 W when the conductance of the pollution layer was at its highest value as the surface was completely wet. This results in resistive current flow and an increase in dry band arcing on the surface. It then decreased to a constant value of about 17.5 W after about 1 hour due to the washing effect of the fog. The power dissipated under dry and wet operating conditions was generally much less than that under polluted conditions as the wet pollution layer is the reason for the creation of current activities that responsible for the surface heating and more power dissipation ; approximately 9 W and 11.5 W respectively as can be seen in Figure 4.6(a). As the Nanocoated insulator had shown considerably reduced current flows, it was expected that less power would be dissipated by this insulator. The Nanocoating decreased the average power dissipated on the surface of the insulator from 23 W to 0.33 W under polluted operating conditions. The capacitive components of the leakage current are a product of the surface hydrophobicity. Figure 4.6(b) shows that the presence of the Nanocoating reduced the average power dissipated from just over 11 W to less than 0.15 W for wet conditions and from just 9 W to less than 0.10 W for dry conditions. These represent very good results for the application of the Nanocoating.

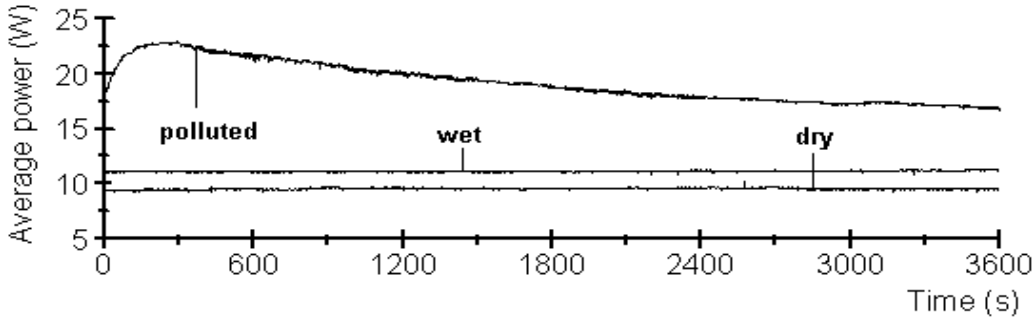

(a) Uncoated insulator

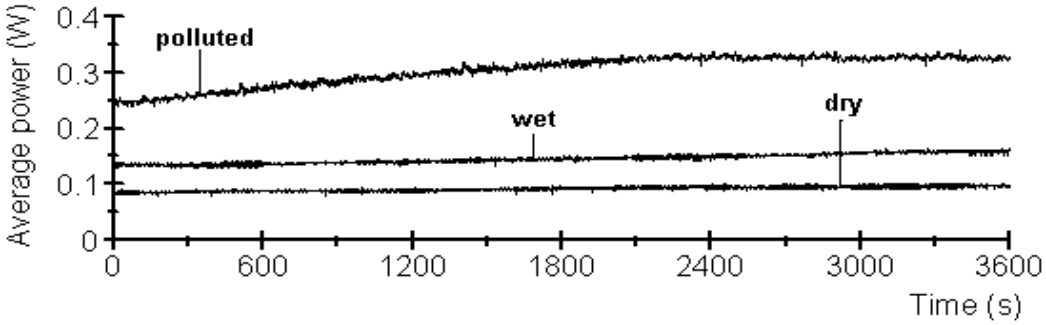

(b) Nanocoated insulator

Figure 4.6: Average power (a) uncoated, (b) Nanocoated insulators

(iii) Dissipated Energy

Figure 4.7(a) shows that the total dissipated energy as defined by Equation (3.12), on the surface of the uncoated insulator increased more or less uniformly (straight line graphs) for wet and dry conditions. The greatest rate of increase was for polluted conditions followed by wet conditions, and dry conditions showing least dissipated energy. At the start of the test and at the start of the fog, the accumulated energy dissipated on the surface increased at a high rate as the conductance of the pollution layer increased, and leakage current begins to flow. As the test progressed, the fog started to wash out the pollution layer, resulting in a reduction in current magnitude on the surface, which leads to a reduction in the rate by which the dissipated energy is increased on the surface as can be seen in Figure 4.7(a).

However, the accumulated energy on the surface of the Nanocoated insulator increased at a lower rate because of the lower current on its surface. The accumulated energy of the Nanocoated insulator can be seen in Figure 4.7(b). When applied to the porcelain insulator, the nanocoating minimised the cumulative dissipated energy under wet polluted conditions from 70 kJ to 1.2 kJ, a reduction of approximately 98%. With

millions of insulators installed and in service, the universal application of protective coatings shall greatly reduce losses in the power system.

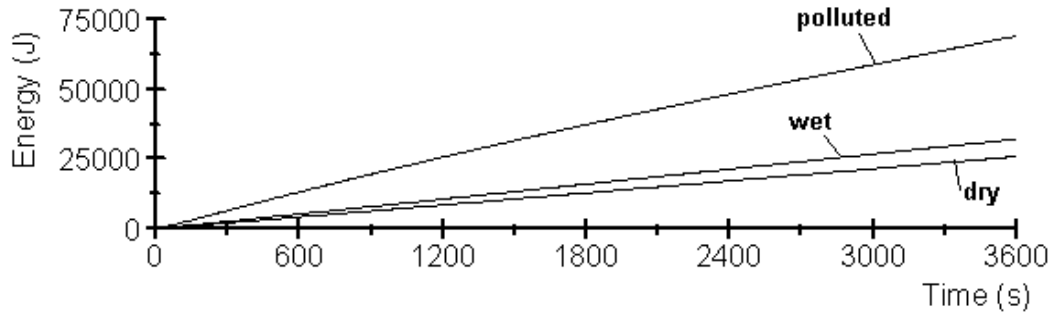

(a) Uncoated insulator

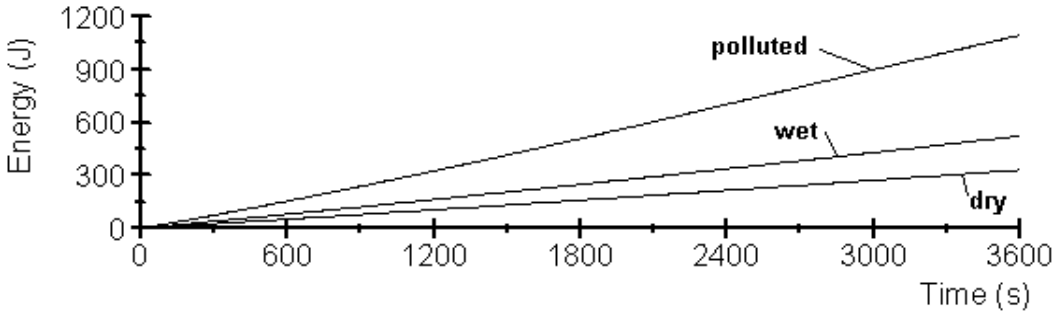

(b) Nanocoated insulator

Figure 4.7: Accumulated dissipated energy (a) uncoated, (b) Nanocoated insulator

4.5. Porcelain insulators coated with RTV Silicone Rubber

Three cap and pin type C porcelain insulators (creepage length 300 mm) were used in these experiments, the insulators are shown in Figure 4.8.

Two RTV coatings of commercial purity from two different manufacturers identified as RTV1 and RTV2, were applied to the insulators by brushing, and then left to vulcanize in room temperature for one week before the tests. The third insulator was left uncoated for comparison purposes. This section shows the results of the tests performed on RTV coated insulators, compared with results of uncoated insulators of similar geometry.

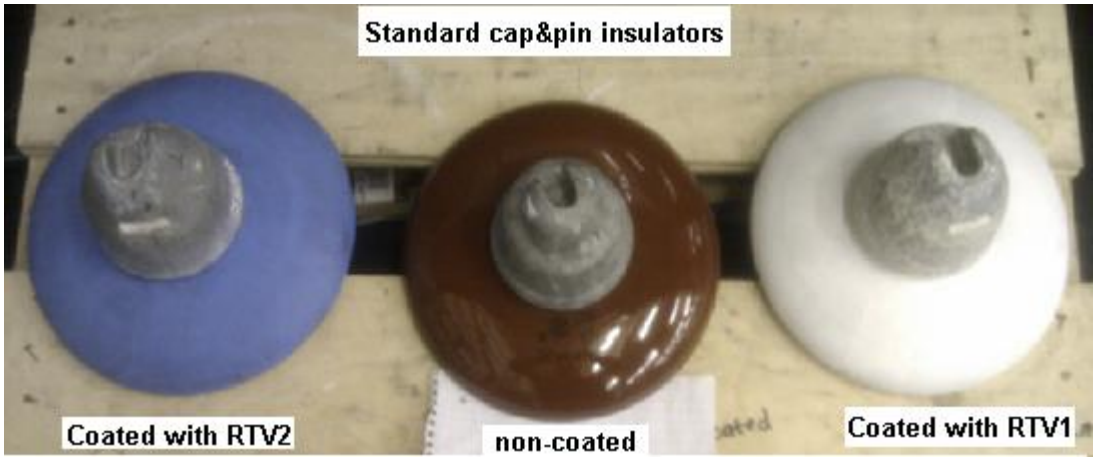

Figure 4.8: Standard porcelain insulators

4.5.1 Porcelain insulators without coatings

Figure 4.9 shows the experimental results for the uncoated insulator for the one hour test under dry, wet, and wet polluted conditions. Figure 4.9 (a) shows the r.m.s current for the uncoated porcelain insulator. The insulator operated best under dry conditions; the r.m.s. current was very low at 0.075 mA. Under clean wet conditions, it was 0.09 mA. However, the most dangerous working conditions are when the insulator operates under wet polluted conditions. At the start of the test and as the pollution layer becomes wet, the leakage current started to develop, and when the pollution layer reached its most conductive state, causing dry band arcing on the surface of the insulator with the highest r.m.s current being 1.20 mA, the current waveform became triangular in shape with a peak at the point where the pollution layer becomes most conductive with. This peak, and possible adjacent subsidiary peaks are caused by dry band discharges on the surface of the insulator indicating high resistive current as shown in Figure 4.5(a). As the test continued the current stayed at a high level; this may be attributed to the effect of the wetting agent which was used in the pollution slurry. The pollution stuck firmly to the surface of the porcelain insulator, and this makes it hard for the pollution to be washed away easily. However, as the test progressed, more salt dissolved on the surface of the insulator and this leads to increased leakage current and a greater number of current peaks in the last 20 minutes of the test. Due to the lower wetting rate of the fog at the pin electrode, these current activities continued for the whole test.

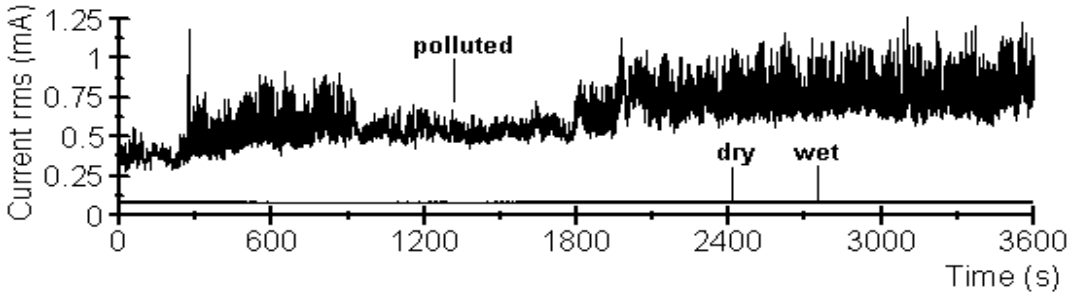

(a) R.M.S Current

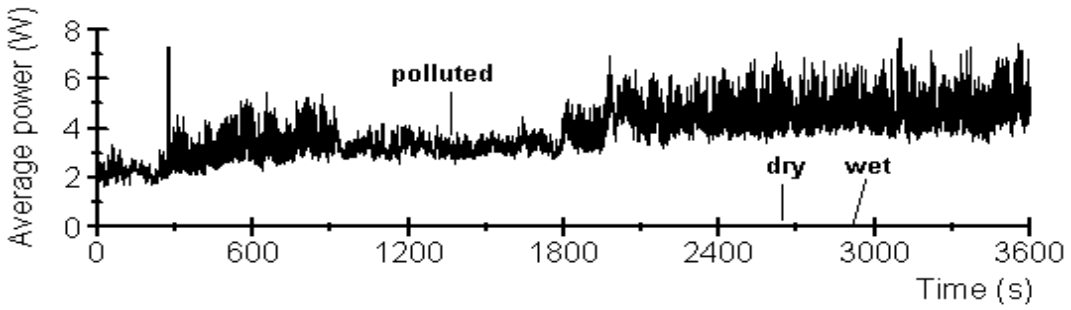

(b) Average power

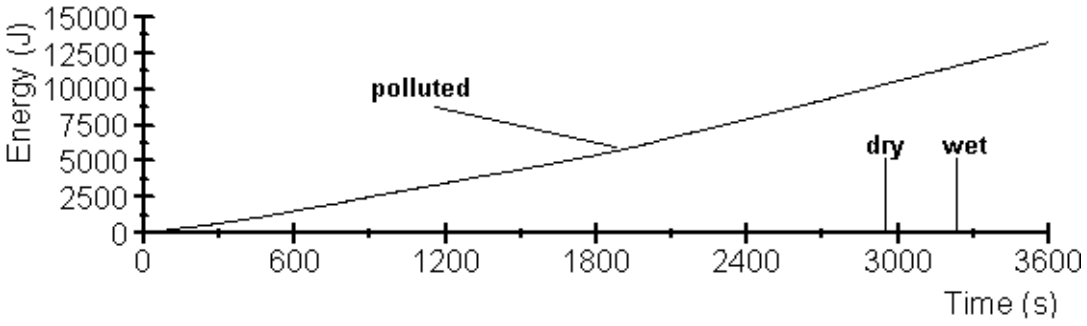

(c) Dissipated Energy

Figure 4.9: Leakage characteristics for uncoated porcelain insulator

The average power for the polluted insulator showed similar behaviour to that of the r.m.s. current. It increased from 2 W at the start of the test to a level between 4 to 6W in the last 20 minutes of the test. This resulted in more heating of the surface, which leads to drying of areas of the wet pollution layers and gives rise to dry band arcing, indicated by the spikes on the current trace for the polluted insulator. The average power levels for wet and dry conditions were very low compared to the polluted case, as can be seen in Figure 4.9(b).

The accumulated dissipated energy on the surface of the polluted insulator increased quite rapidly up to about half way through the test and then grew even more rapidly in the last half of the test to a value of 13.2 kJ. The dissipated energy for the wet and the dry insulators were at 177 J and 93 J respectively.

4.5.2. Porcelain insulators coated with RTV1

The results of the one hour test for the RTV1 coated insulator are shown in Figure 4.10. The surface current for the RTV1 coated insulator under dry and clean wet operating conditions was almost capacitive with almost identical r.m.s current values of 0.075 and 0.077 mA. The behaviour of the RTV1 coated porcelain insulator under wet polluted conditions was very much improved compared to that of the uncoated porcelain insulator under wet polluted conditions. At the start of the test as the pollution layer on the surface of the insulator becomes wet, the RTV1 coating suppressed the leakage current activity on the surface of the insulator to less than 0.08mA. Figure 4.10(a) shows that the performance of the insulator with RTV1 coated is similar for dry, wet clean and wet polluted operating conditions.

The trend for the average power on the surface of the coated insulator under wet polluted and clean wet conditions were very similar and increased gradually with time to a maximum of about 0.03 W, see Figure 4.10(b). The average power was reduced from 6 W for the uncoated polluted insulator to 0.03 W for the coated insulator under polluted conditions which results in less heating of the surface and thus longer coating life.

The dissipated energy on the surface of the RTV1 coated rose linearly for dry, wet, and wet polluted conditions but the maximum value attained was less than 100 J. When compared to the performance of the uncoated polluted insulator, there was a 99% reduction in the energy dissipated on the surface of the insulator for the total accumulated dissipated energy, see Figure 4.10(c). This behaviour can be utilised to drastically reduce losses in the outdoor insulators of power systems.

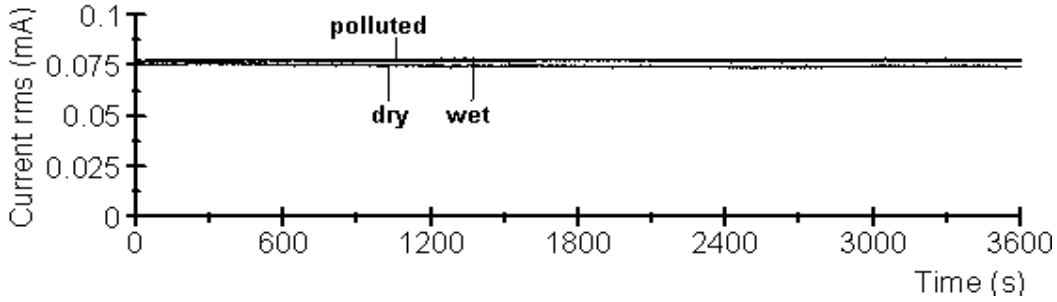

(a) R.M.S. current (mA)

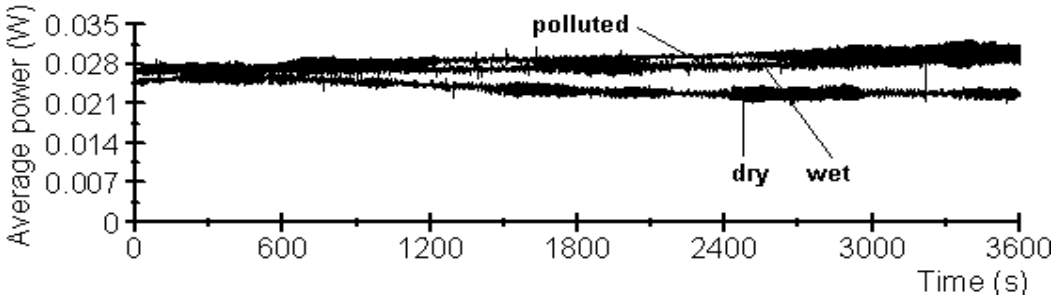

(b) Average power (W)

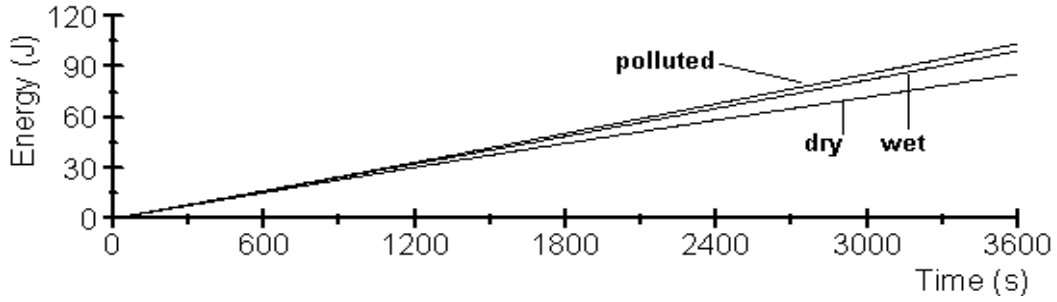

(c) Dissipated Energy (J)

Figure 4.10: Leakage current characteristics for RTV1 coated porcelain insulator

4.5.3. Porcelain insulators coated with RTV2

The performance of the insulator under the three operating conditions was almost identical to each other and similar to those obtained with the RTV1 coated insulator. The leakage currents for all three conditions were mainly capacitive with r.m.s values between 0.077 and 0.080 mA.

The one hour test results of the RTV2 coated insulator under clean dry clean wet, and wet polluted test conditions are shown in Figure 4.11. In Figure 4.11(a), the current axis scale was expanded to amplify the differences between the current trends because the currents are almost have the same r.m.s values and are at the same level for that of RTV1 coated insulator; the r.m.s current was 0.0775 mA across the surface under dry condition, 0.0780 mA for clean wet condition and 0.0785 mA for wet pollution conditions. The average power is almost identical for the insulator under the different operating conditions with approximately 0.021 W in average, see Figure 4.11(b). These low power levels resulted in less heat on the surface of the insulator and lead to reduced degradation of the coating. The dissipated energy trends for the insulator under all three conditions increased linearly with time and were at the same level with 80J; see

Figure 4.11(c). These low levels of dissipated power are attributed to the hydrophobic property of the coatings as they suppressed the leakage current, reducing it to low magnitudes even under wet polluted conditions. This is thought to be caused by the diffusion of the silicone fluid from the bulk to the surface of the coating to maintain the surface hydrophobicity and prevents the formation of large wet areas on the surface.

As with all the coatings tested in this investigation a reduction in the cumulative dissipated energy resulted from the application of the protective coatings on outdoors insulators will result in less energy loss and so more power system reliability.

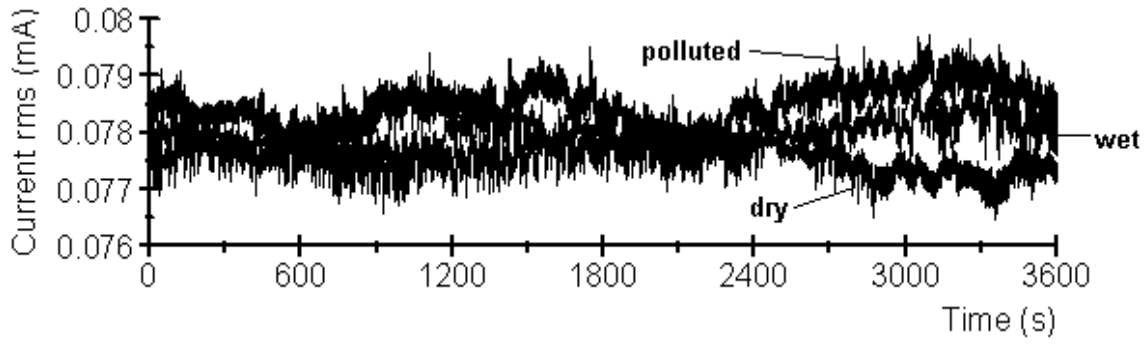

(a) R.M.S. current (mA)

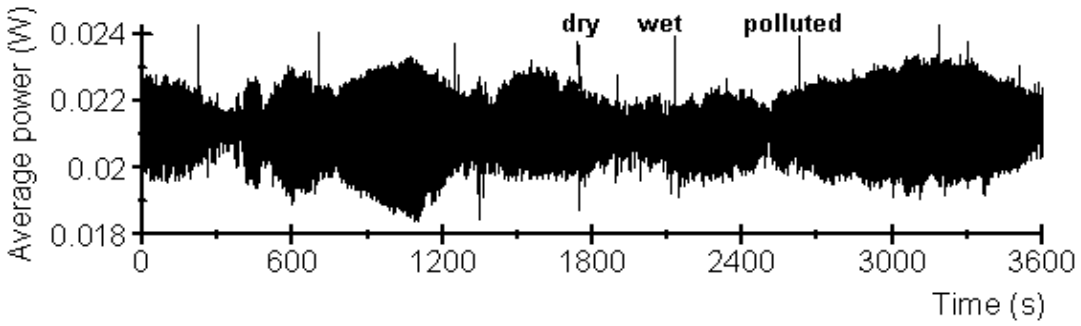

(b) Average power (W)

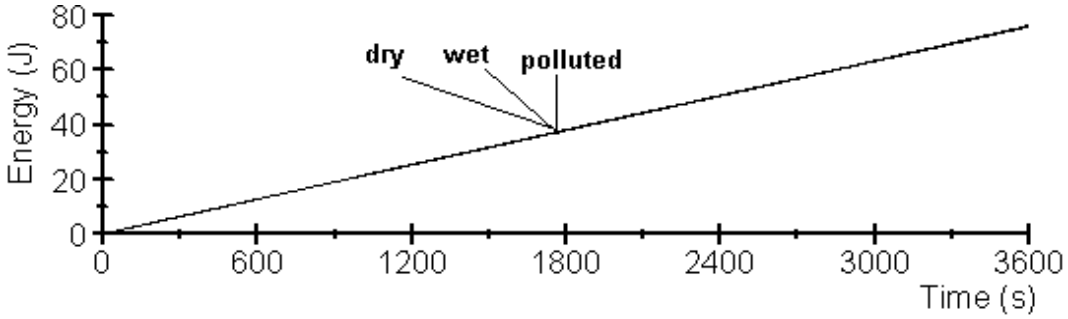

(c) Dissipated Energy (J)

Figure 4.11: Leakage characteristics for RTV2 coated porcelain insulator

4.5.4. Effect of RTV coating on top and bottom surfaces of porcelain insulators

Additional tests were performed in which two porcelain insulators of type C were coated with RTV1; one was coated from the top surface only while the bottom surface was left uncoated while the other insulator was coated from the bottom surface only while the top surface was left uncoated. Both insulators were tested under polluted conditions. The reason for these tests was to see the effect of coating the areas near the pin and the cap exchangeable. The area near the pin has lower wetting rate as it is not exposed to the fog directly. However, the area near the cap is directly exposed to fog application and has higher wetting rate.

The one hour test allowed a comparison of results between RTV1 top and bottom coated insulators under wet polluted conditions as shown in Figure 4.12. The r.m.s. current on the top coated insulator increased from 0.08 mA at the start of the test but after 30 min into the test the current jumped to 0.16 mA due to current activity near the pin as the pollution layer gets wet and the washing effect of the fog was weak because the under sheds near the pin slow the washing of the fog. This leads to dry band arcing in the area near the pin and cause the current activity shown on Figure 4.12 (a). The behaviour of the insulator is improved by coating the area surrounding the pin. This may be attributed to the high electric field region near the pin. Coating this area reduced the leakage current as the surface becomes hydrophobic. The r.m.s current was reduced to 0.075 mA for the duration of the test.

The average power trend followed the leakage current closely for both insulators. The maximum average power for the top coated insulator was at 1W. For the case where the insulator was coated at the area near the pin, the power dissipated was reduced to 95% of that of the top coated insulator, see Figure 4.12(b). The dissipated energy on the insulator surface is also significantly reduced by the presence of the coating on the bottom surface of the insulator, see Figure 4.12(c).

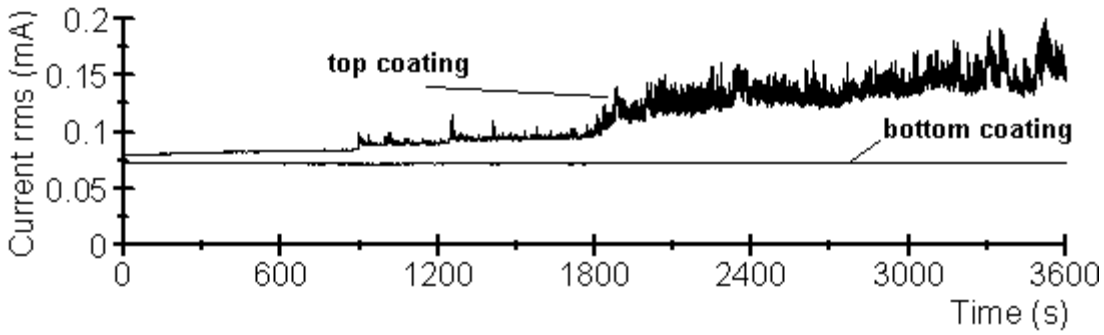

(a) R.M.S. current (mA)

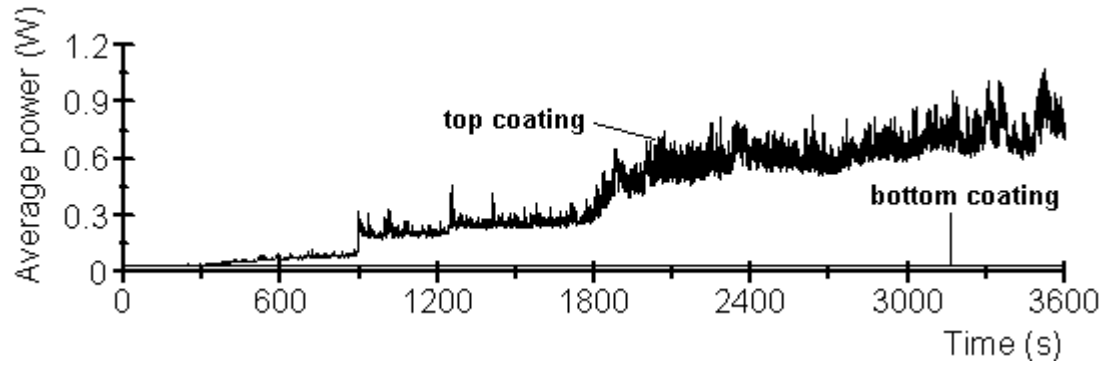

(b) Average power (W)

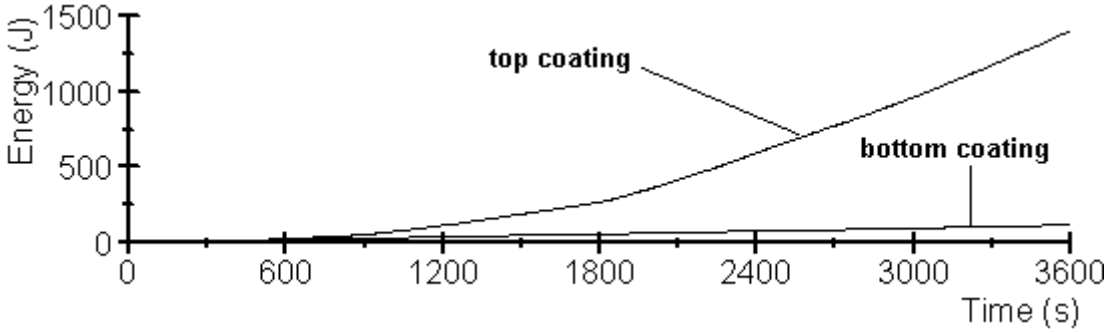

(c) Dissipated Energy (J)

Figure 4.12: Leakage current characteristics for RTV1 top and bottom coated porcelain insulators type C

4.6. Effect of UV radiations on the performance of the coatings

Ultraviolet (UV) radiation is a relatively short wavelength electromagnetic radiation and represents only 5% of the solar spectrum but is the most destructive rays for polymeric materials. This section presents test results on the effect of the UV on the coating performance under artificial pollution conditions, and its effects on the hydrophobicity of the coatings. The UV light is located between 280 and 315 nm [4.7, 4.8]. Corona discharges are a significant additional source of UV radiation [4.9]. Figure 4.13 shows

the whole solar spectrum and the location of the UVB radiations on the solar spectrum, which are considered the most aggressive part to the polymer. In this section the effect of UV radiation on the hydrophobicity and current suppression properties of the RTV1 coating is presented.

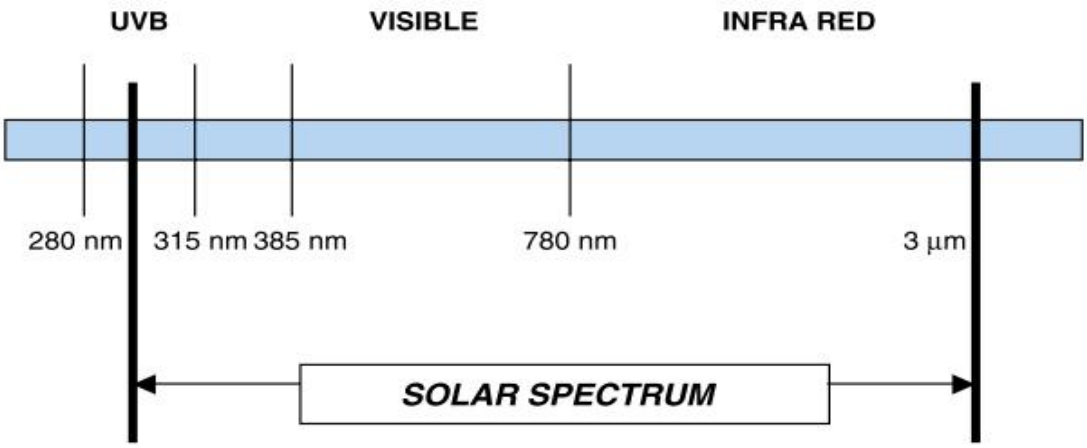

Figure 4.13: Solar radiation spectrum with ultraviolet light [4.8]

4.6.1. Effect of UV exposure after pollution application on RTV coating

The RTV1 coated insulator of type C was polluted as described in Section 4.3.1 and left to dry overnight. The insulators were put in the weathering machine and exposed to UV radiation. A flowchart of the test process was shown in Figure 3.16(a). Each UV cycle lasts for 2 hours and is equivalent to 87.5 hours of continuous exposure to real sunlight [4.7]. The insulator exposed to one cycle of UV radiation received 428 kJ/m^2 radiation energy, and for 4 cycles received 1712 kJ/m^2 radiation energy.

Figure 4.14 shows comparison results for a one hour test of two RTV1 coated insulators exposed to different UV cycles with a non UV exposed insulator. Further tests are required to investigate the effect of longer time periods of exposure to UV radiations on the performance of the RTV1. As can be seen from the figure, the sample exposed to 8 hours UV radiations experienced less r.m.s current than that exposed to 2 hours UV radiations. This maybe due to the UV radiation accelerating the diffusion of the silicone fluid from the bulk to the surface and also the contamination layer has protected the surface from the UV radiation. Another reason is that the UV stabiliser used in the coating formula also protects the coating from the damaging effects of the UV radiation.

Figure 4.14(b) shows that the dissipated energies on the surface of the tested insulators were of similar level for all three insulators, and in all cases, it was less than 120 J. In general, the RTV1 coating showed high stability against UV radiation.

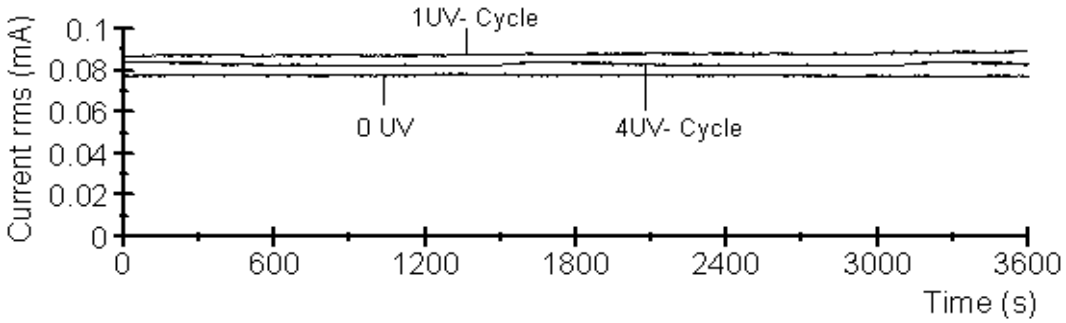

(a) rms current (mA)

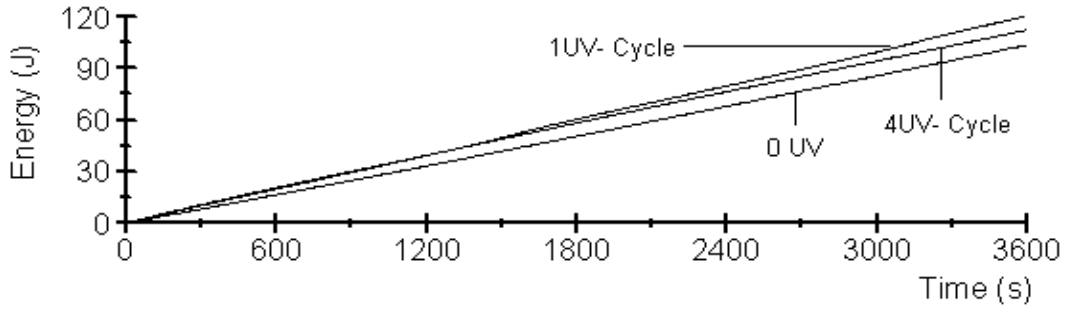

(b) Dissipated Energy (J)

Figure 4.14: characteristics for polluted RTV1 coated porcelain insulator type C exposed to UV radiation

4.6.2. Effect of UV exposure before pollution application on RTV coating

Tests were performed according to ISO 4892-2:2006 [4.10] on RTV1 coated insulators of type D, see Table 4.1. Figure 3.16(b) showed the flowchart of the test procedure. In this experiment, the RTV1 coated insulators were first exposed to 1, 2 and 4 UV cycles then polluted and left to dry for 8 hours at room temperature. They were then tested under clean fog conditions.

RTV1 coatings showed high resistance to UV radiation, and the results are shown in Figure 4.15. As can be seen in the Figure, the leakage current increased slightly when the sample was exposed to 1 and 2 UV cycles. But when the sample was exposed to more UV cycles, the leakage current decreased to a level equal to that of the unexposed insulator. This is thought to be caused by the UV radiation helping the diffusion of the

LMW silicone fluid on the surface, which improves surface hydrophobicity and results in the leakage being current suppressed.

The dissipated energy was higher for the sample exposed to 1 cycle UV light. The long UV exposure leads to reduced dissipated energy on the surface of the insulator from 520J for 1 cycle UV exposure to 240 J for 4 cycle UV exposure resulting in 60% reduction, see Figure 4.15 (b). However, it appears that the longer the exposure to the UV radiation, the less the dissipated energy on the surface of the insulator. These results demonstrate the stability of the RTV coatings when exposed to UV radiation.

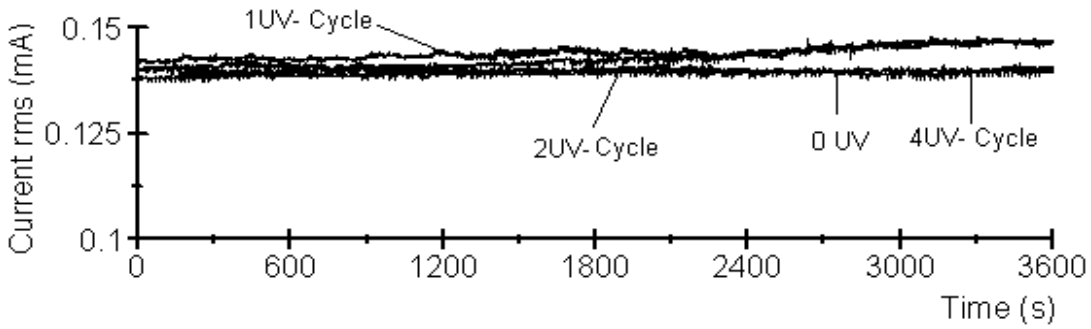

(a) R.M.S. current (mA)

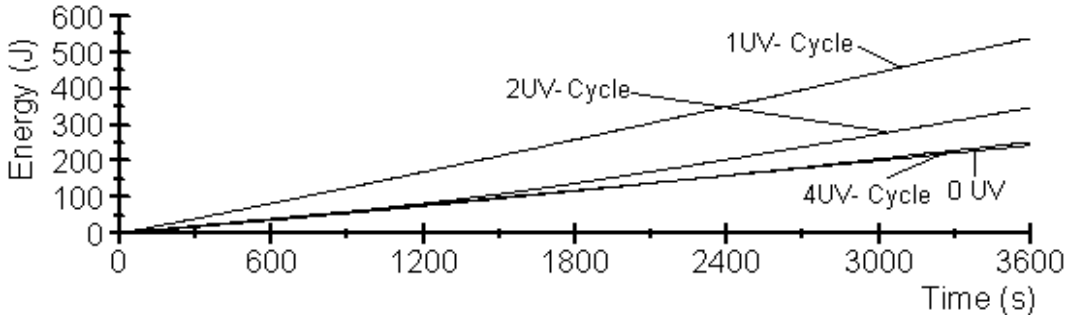

(b) Dissipated Energy (J)

Figure 4.15: Leakage characteristics for RTV1 coated porcelain insulator type D exposed to UV radiation

4.6.3. Effect of UV exposure on the performance of the Nanocoating

The Nanocoated insulator was exposed to 4 UV cycles and then polluted and left to dry then tested in the fog chamber under clean fog conditions. Figure 4.16 shows the r.m.s current on the surface of the Nanocoated insulator. In comparison with the un-exposed Nanocoated insulator of Figure 4.5 (b), the r.m.s current on the surface of the

Nanocoated insulator exposed to UV radiation was slightly increased from 0.25 mA up to 0.33mA. In contrast, the dissipated energy increased from 1200J for Figure 4.7 (b) to 1300J. This increase was not significant and did not reveal changes in the surface of the coating.

This result needs to be correlated with field data to judge the effects of UV radiation on the Nanocoating, where long exposure to direct sun light rays under different weather conditions of dry and wet pollution conditions may affect the performance of the Nanocoated insulator.

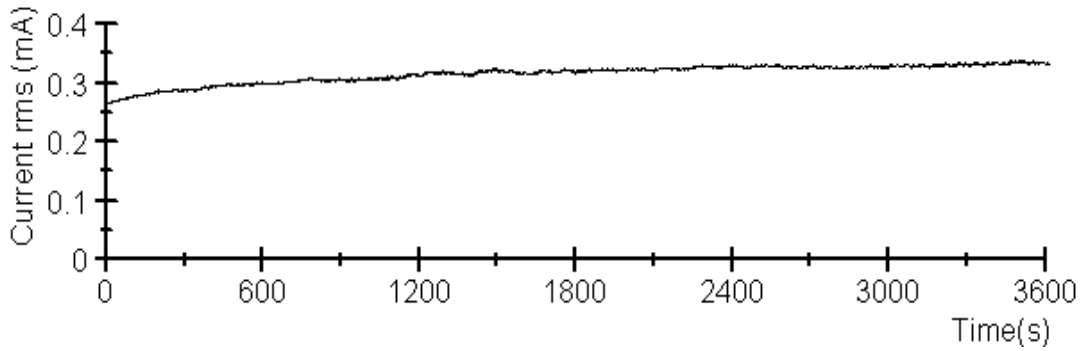

(a) R.M.S current

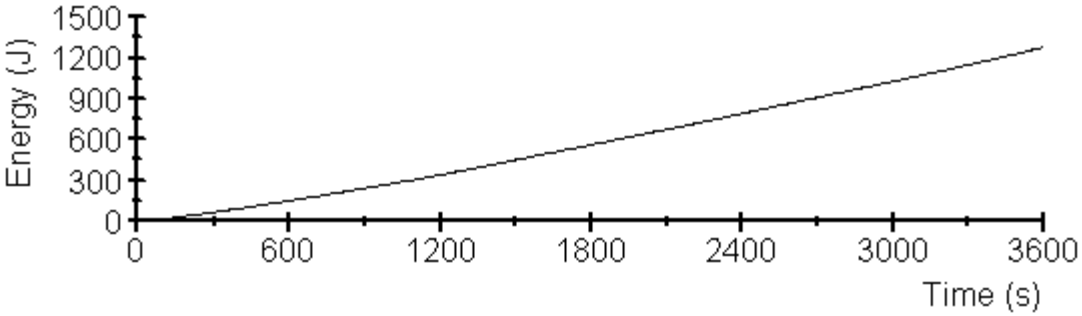

(b) Dissipated Energy (J)

Figure 4.16: Leakage current characteristics or Nanocoated insulator type B exposed to UV radiation

4.6.4. Effect of sandblast on the performance of Nanocoating

To simulate the effect of sand storms on the adhesion of the Nanocoating to the surface of the insulators, a Nanocoated insulator was exposed to particles of calcium silicate synthetic mineral abrasive with size range of 0.15 -0.2mm in a Blast Cabinet. Figure 4.17 shows the Nanocoated insulator after sandblast exposure. The Nanocoating showed good resilience to sand blasting; however, with long exposure to sand blasting, the surface began to exhibit pockmarks which are visible in the Figure 4.17.

After being exposed to sand blast, the insulator was polluted and tested in the fog chamber under clean fog conditions, and stressed with a test voltage as shown in Table 4.1. Figure 4.18(a) shows r.m.s leakage current on the surface of the Nanocoated insulator exposed to sandblast. Although, there was visible damage to the surface, the nanocoating reduced the r.m.s current on the surface of the insulator to 0.52 mA. Comparing this value with that of Figure 4.5 (b), there was a 50% increase in the current r.m.s value. However, this current value was less than the r.m.s current value on the uncoated insulator of Figure 4.5 (a) as the surface was not completely damaged by the sand blast, and there were small areas with Nanocoating. These areas remained as hydrophobic regions, which limits the creation of dry band arcs and so work on reducing the leakage current. The dissipated energy on the surface of the insulator rose linearly and the maximum value attained was 1500 J. There was a 20% increase in the energy dissipated on the surface of the insulator when compared to that of Figure 4.7 (b), see Figure 4.18(b).

Figure 4.17: Nanocoated insulator after sandblast exposure

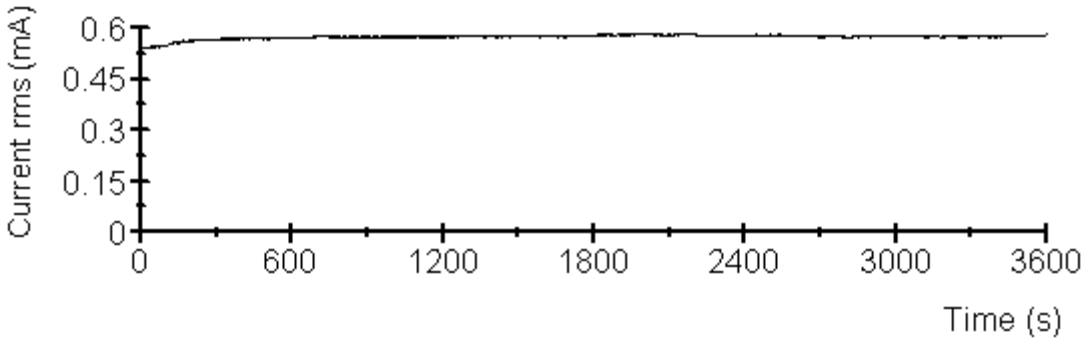

(a) R.M.S current

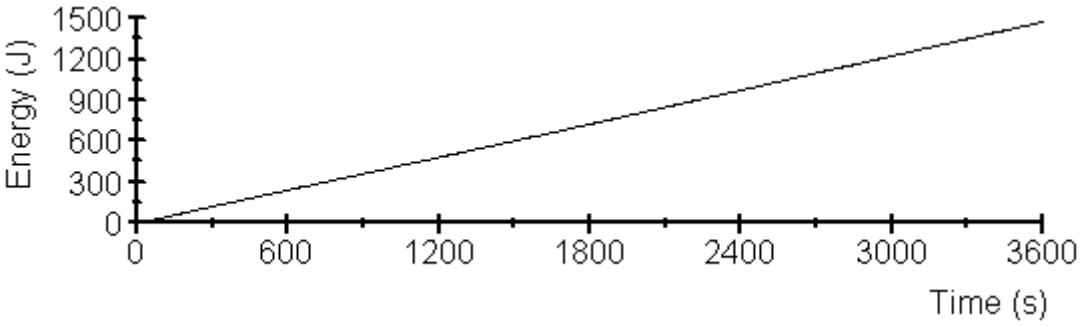

(b) Dissipated Energy (J)

Figure 4.18: Leakage current characteristics for Nanocoated insulator type B exposed to sandblast

4.7. Hydrophobicity tests

Hydrophobicity classification is the criterion used to classify the actual wetting appearance on the surface of the insulator as mentioned in section 2.4. Hydrophobicity classification ranges were defined from HC1 to HC6. A drop of water on an inclined surface shows two different contact angles see Figure 4.19, the advancing contact angle (θa) and the receding contact angle (θr).

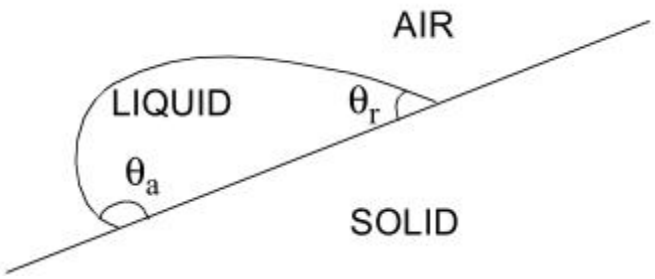

θ_a= advancing angle, θ_r = receding angle

Figure 4.19: Definition of contact angles [4.11]

4.7.1. Effect of pollution tests on the hydrophobicity of protective coatings.

Most hydrophobic coatings lose their hydrophobicity on exposure to fog. In this section, hydrophobicity tests were performed on the RTV1 coated insulator according to STRI Guide 92/1 [4.15] using a spray bottle filled with tap water capable of producing a fine mist. The results of the hydrophobicity tests are shown in Figure 4.20. Figure 4.20(a) shows a photo of an insulator newly coated with RTV1. As can be seen on the figure, the hydrophobicity of this surface can be classified as HC1 as the water droplets dispersed across the surface in scattered fashion with contact angles in excess of 90°, and thus conformed to the STRI guide.

(a) Surface newly coated with RTV1 (HC1)

The surface hydrophobicity was also checked after wet tests in the fog chamber. Figure 4.20(b) shows the insulator in the fog chamber immediately after the wet test. In this case, the surface may be classified as HC3 as the majority of droplets are no longer circular. Figure 4.20(c) shows a picture of an insulator newly Nanocoated. The surface can be classified as HC4 as both discrete droplets and wetted traces from on the surface.

(b) RTV1 coating after 1hour wet test in the fog chamber (HC3)

(c) Insulator surface newly Nanocoated (HC4)

Figure 4.20(d) shows the Nanocoated insulator in the fog chamber immediately after wet test, the insulator has completely lost its hydrophobicity, and was completely wet. The insulator can be classified as HC7 as continuous water film is formed over the whole observed area.

(d) Nanocoating after wet test in the fog chamber (HC6)

Figure 4.20: hydrophobicity classifications

The RTV coating showed good hydrophobicity surface properties after wet pollution tests and this agrees with the results of the leakage current measurements shown earlier in section 4.5.3. This is attributed to the hydrophobic surface property of the RTV1 coating as the silicone fluid diffused from the bulk to the surface of the RTV1 coating. On the other hand, although the Nanocoating has completely lost its surface hydrophobicity, it showed good performance in reducing the surface leakage current as shown earlier in the results of the leakage current measurements. The mechanism behind this still needs to be investigated as the Voltshield coating system is still new in the field of the operation of power systems.

4.7.2. Effect of UV radiation on the hydrophobicity of the RTV coatings

A porcelain sample of 50 mm width, 120 mm length was coated with RTV1. A blue dye was mixed with water in a syringe. As the size of the droplets was small, blue dyes were chosen to give good photos. The syringe was used to carefully apply a droplet of water onto the surface of the coated sample. The sample was exposed to two UV exposure cycles (2 hours and 8 hours UV exposure) [4.10].

Image J: is a public domain open source image processing software package. It can display, edit, analyze, process, save and print 8-bit, 16-bit and 32-bit images. It can read

many image formats including GIF, JPEG. The software was used to measure the advancing and receding angles of the droplets. It should be emphasised, however, that this is not a precise method as the accuracy of the measurement depends upon subjectivity and the judgement of the individual using the software. This means there are no significant differences between the angles measured. If they are accurate to ±5°, the angles are greater than 100 °, and this is a good indication for the hydrophobicity of the surface. Figure 4.21 (a) and (b) show the receding and advancing angles respectively, of a droplet on the surface of the RTV1 coated porcelain sample un-exposed to UV radiations. The coating showed high hydrophobicity with receding angle of 122.5° and advancing angle of 120.7°.

The sample with RTV1 coating was exposed to 1 and 4 cycles of UV radiation after which droplets of coloured water were placed on the surface. Figure 4.22 shows photos of droplets on the surfaces of the RTV1 coated samples. Table 4.2 shows the contact angles of a droplet on the RTV1 coating for exposed and non-exposed to UV radiation. Wankowicz et al. [4.12] have reported on measurements of contact angle with constant values of 125° on a virgin RTV specimen and after a period of 100 hours of UV exposure.

Table 4.2: Contact angles of a droplet on RTV coated exposed to UV radiations.

	θ_a advancing angle (°)	**θ_r receding angle (°)**
No UV	120	122
2 hours UV exposure	117	120
8 hours UV exposure	123	121

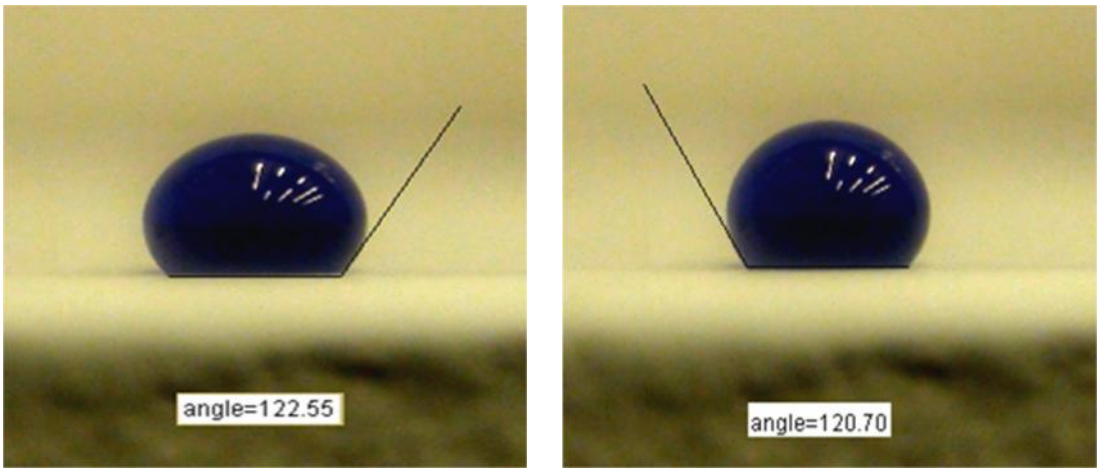

(a) θ_r receding angle **(b) θ_a advancing angle**

Figure 4.21: Contact angle measurement of a droplet without UV exposure

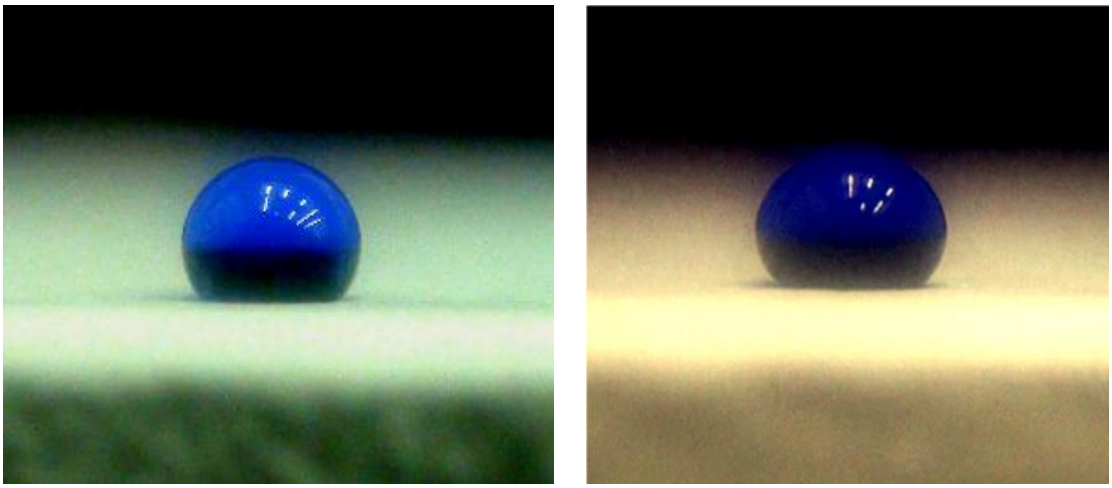

(a) After 2 hours UV exposure **(b) After 8 hours UV exposure**

Figure 4.22: Contact angle measurement of a droplet on coated samples

4.8. Grease as a surface coating

The basic constituents of greases are oil and fumed silica, and occur in two types, namely the petroleum jellies and silicone greases discussed in section 2.2.3 . Although greases do not reduce contaminant accumulation, the oil serves to encapsulate the contaminants, thereby retaining a water repellent surface [4.1].

4.8.1. Hydrocarbon grease (WT235 coldspray)

The hydrocarbon grease used in this experiment is WT 235 coldspray, which is a soft grease based on mineral hydrocarbons and synthetic polymers [4.13]. The grease was applied to a type C porcelain insulator by hand. The grease coated insulator was tested under clean dry, clean wet and wet polluted conditions based on the solid layer method of IEC 60507.

Figure 4.23 shows the performance of hydrocarbon grease coated porcelain insulators. It can be seen that the performance of the greased insulator under dry, wet, and polluted conditions are similar. The grease coating suppressed the surface leakage current on the insulator to less than 0.08 mA, see Figure 4.23(a). The dissipated energy increased linearly with time but did not exceed 110 J for the insulator under polluted conditions, see Figure 4.23(b).

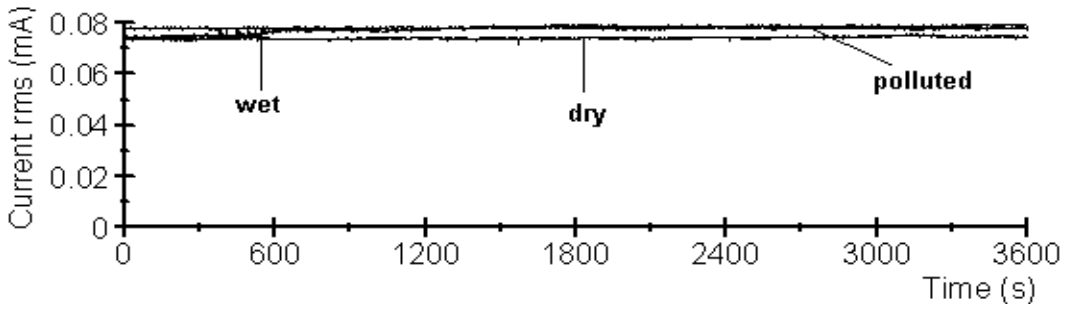

(a) R.M.S. current (mA)

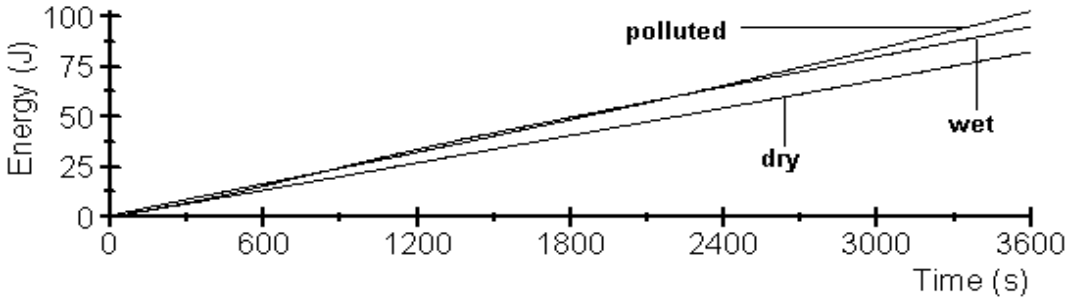

(b) dissipated Energy (J)

Figure 4.23: Leakage current characteristics for hydrocarbon grease coated porcelain insulators

4.8.2. Silicone grease (3099 HVIC)

The silicone grease used in this experiment is Dow Corning 3099 which has been formulated to give electrical insulators long-term resistance to water filming and flashover. It contains an arc track resistant filler that inhibits arc growth and extends working life whilst protecting the porcelain glazed surface [4.14].

The silicone grease was applied to a type C insulator by hand and tested in the fog chamber according to the solid layer method of IEC 60507. Tests were performed on the greased insulator under dry, wet, and polluted operating conditions and the results are shown in Figure 4.24. Silicone grease showed good performance in suppressing the leakage current to the similar level as the hydrocarbon grease, and reducing the energy loss on the surface of the insulator to values slightly less than the hydrocarbon grease..

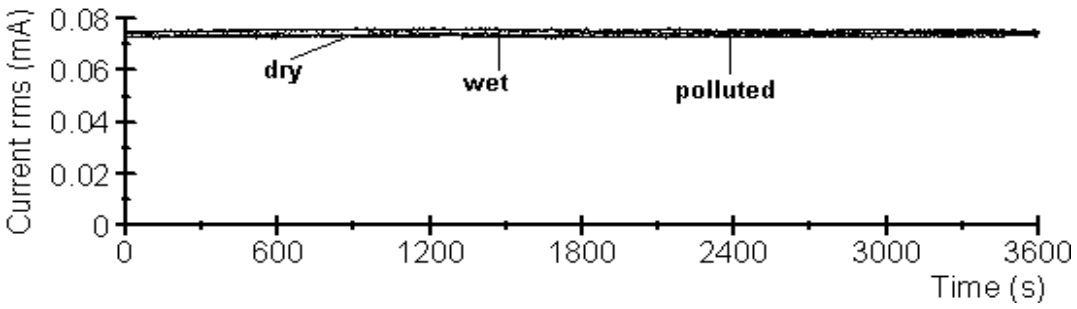

(a) R.M.S. current (mA)

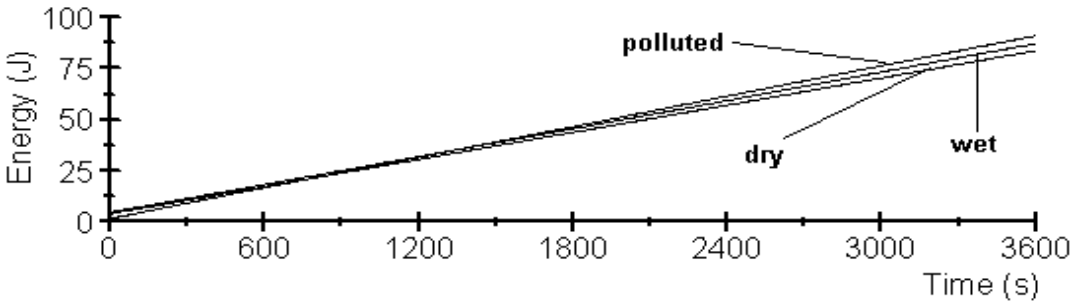

(b) Dissipated Energy (J)

Figure 4.24: Leakage characteristics for silicone grease coated type C porcelain insulator

4.9. Flashover voltage tests

In this study, flashover voltage tests were performed on coated and uncoated insulators to determine the flashover voltage levels of the insulators and to evaluate the performance of various HV insulator coatings in improving the flashover performance of porcelain insulators. These procedures were performed according to IEC60507, which stated that the insulator should withstand three consecutive tests without flashover. Two sets of tests were performed; the first set of tests carried out to measure the flashover voltage level of the insulators under clean wet and wet polluted conditions. In this case, the mode of operation of the control unit of the test transformer was set to automatic mode. Using the automatic mode, the voltage was increased automatically at a rate of 1.3 kV/min.

In the pollution flashover test, the polluted insulator was placed in the fog chamber and the fog generation started and maintained at a steady rate, and at the same time, a voltage was applied and increased automatically until flashover occurred. The same procedure was followed for the wet flashover tests.

Figure 4.25 shows the applied r.m.s voltage of flashover test for polluted insulator with automatic voltage increase. The insulator did flashover at 47kV under the automatic voltage increase method.

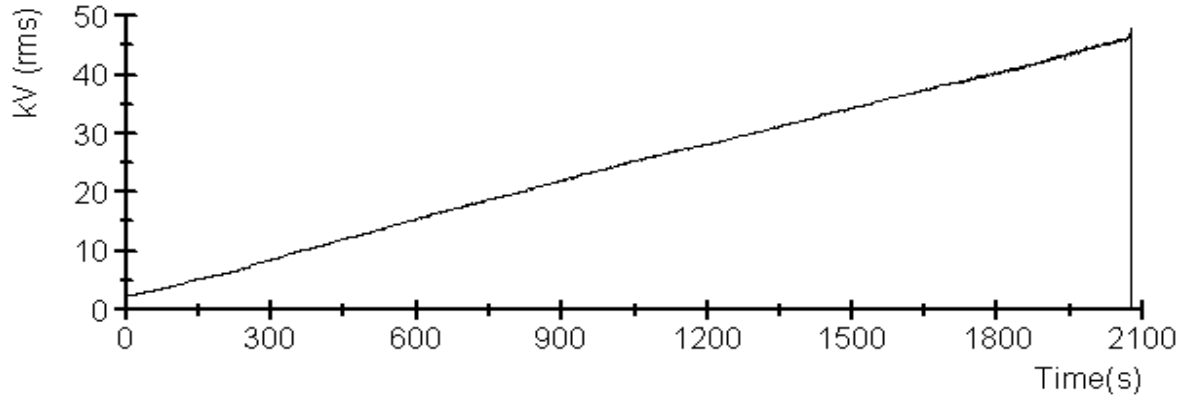

Figure 4.25: Polluted flashover voltage of porcelain insulator type B

i. Pollution flashover voltage tests

The second series of tests was performed according to procedure A of IEC 60507; wetting before and during energisation. In this method, the applied voltage was controlled manually. The insulators were subjected to clean fog for 25 min, which is the

time for the pollution layer to reach its maximum conductivity as determined by the wetting rate tests in Section 3.2.4. Then, the test voltage was applied and increased in a few seconds up to 5% less than the flashover voltage level determined in the previous tests and maintained until flashover or for 15 minutes if no flashover occurred.

ii. Test procedure

As an example of the test procedure, a polluted porcelain insulator of type C was subjected to clean fog for 25 minutes. At this time, a HV 20 kVr.m.s was applied to the insulator in a few seconds, the insulator did flash over in less than 3 minutes. The insulator was removed from the fog chamber and cleaned. The insulator was then polluted again and left to dry and then subjected to a voltage of 19 kVrms, a level 5% less than the previous flashover voltage. The insulator again flashed over. The same procedure was repeated, and at 18 kVrms, the insulator again flashed over. At an applied voltage of 17 kVr.m.s, no flashover occurred within 15 minutes. Three more confirmation tests were carried out at 17 kVr.m.s and again no flashover occurred.

This procedure was repeated with all the tested insulators. Figure 4.26 shows the polluted flashover test results. Table 4.3 shows the results of flashover voltage of the insulators.

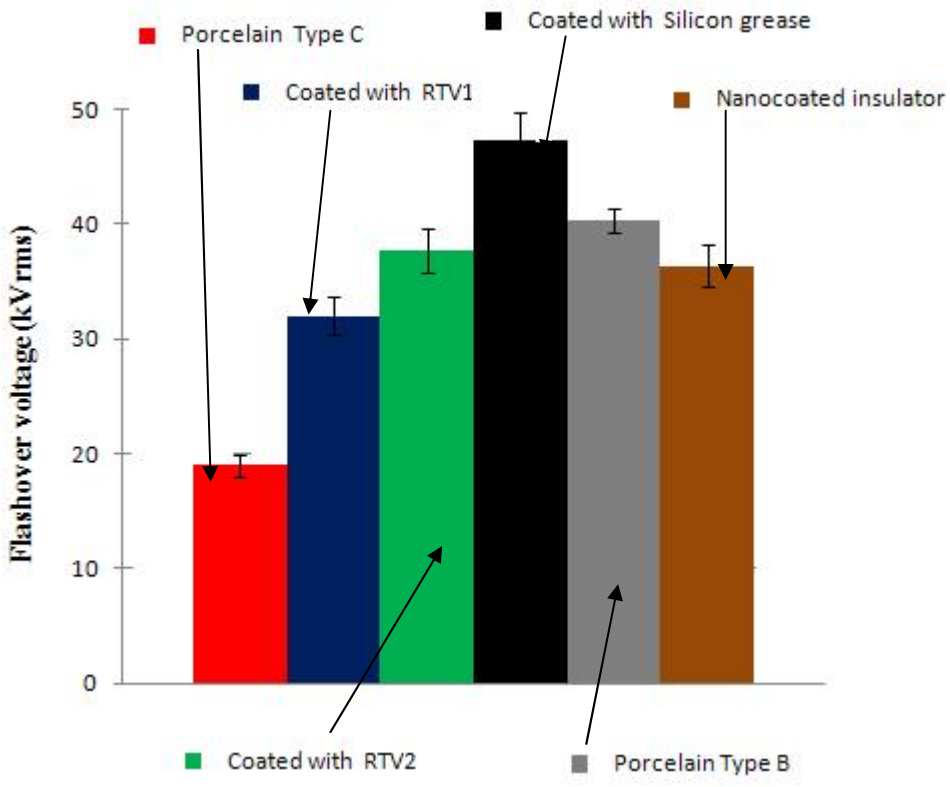

Figure 4.26: Polluted flashover voltage of coated and uncoated insulators

iii. Wet flashover voltage tests

In the wet flashover tests, a clean insulator was subjected to clean fog for 10 minutes, at which time the insulator was completely wet as confirmed by visual inspection. The voltage was then applied to the insulator and increased until flashover.

In the case of the porcelain insulator type C, the insulator did flash over at 33 kV. The test was repeated again and the insulator flashed over at 32 kV. The test was repeated again and the flashover of the insulator occurred at 31 kV. The test was repeated and the voltage level was reduced to 30kV and maintained for 15 min, no flashover was recorded. The same procedures were applied for the other insulators; the results are shown in Table 4.3.

Under dry test conditions, all insulators were stressed with 75kV which is the highest test voltage of the source, and no flashover was recorded even for the porcelain insulator with the lowest creepage distance of Type C.

The flashover voltages of the insulators were at different values. The grease coated insulator had the highest clean wet flashover voltage with 67 kVrms followed by the nanocoated insulator with 58 kVrms and the porcelain insulator of type B, which has the longest surface distance, had a flashover voltage of 55 kVrms then RTV2 with 50 kVrms and RTV1 with 44 kVrms. The porcelain insulator of Type C had the lowest flashover voltage with 30 kVrms. However, under polluted test conditions, the order had changed. The grease coated insulator showed the highest flashover voltage with 46 kVrms while the second highest flashover voltage was the porcelain insulator of type B with 40 kVrms, then the RTV2 coated insulator with 36 kVrms followed by the nanocoated insulator with 35 kVrms and the RTV1 coated insulator with 30 kVrms. The porcelain insulator of Type C had the lowest flashover voltage with 30 kVrms.

Table 4.3: Flashover voltages for dry, wet, and polluted insulators in kV

Types of insulators	DRY	WET	POLLUTED
Voltage unit	kV	kV	kV
Type C- Porcelain	>75	33	20
	>75	32	19
	>75	31	18
Type C- coated with RTV1	>75	45	34
	>75	45	32
	>75	43	30
Type C- coated with RTV2	>75	52	39
	>75	51	38
	>75	50	36
Type C- coated with Silicon grease	>75	68	49
	>75	67	47
	>75	67	46
type B- Porcelain	>75	56	41
	>75	55	40
	>75	55	40
type A -Nanocoated insulator	>75	61	36
	>75	60	38
	>75	58	35

Although the surface distances of the insulators are different, the hydrophobic surface property of the grease coated insulator prevents the formation of large wet areas on the surface of the insulator. This results in a high flashover voltage for the grease coated insulator even though it possesses the shortest surface distance among the insulators of 300mm. Although, the Nanocoated insulator has longer surface distance than the RTV2 coated insulator, the RTV2 coated insulator had higher flashover. This may be attributed to the properties of diffusion of low molecular weight silicone oil from the bulk to the surface which maintains the hydrophobic surface property and prevents the formation of large wet areas on the surface. This resulted in the higher flashover voltage for the RTV2 coated insulator. While the Nanocoated insulator lacks the property of silicone

diffusion from the bulk to the surface, and as the surface becomes wet, the arcs rooted at the high field regions lead to full flashover.

Although this investigation was carried out on insulators with different creepage surface distances, it showed that insulators treated with silicone coating systems have the highest flashover voltage. Figure 4.27 shows a picture of a Nanocoated insulator after a flashover test. This photo shows that the flashover peeled the coating of the surface of the insulator at certain spots. This poses a question on the adherence of the nanocoating to the surface of the insulator when the insulator experiences long periods of current arcing in service.

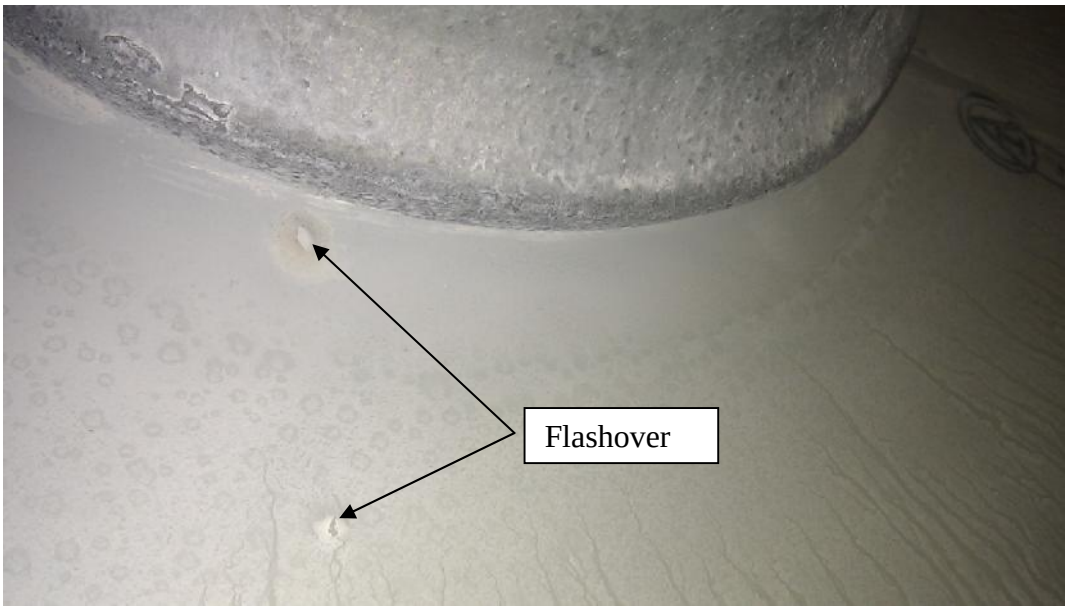

Figure 4.27: Flashover of polluted Nanocoated insulator

Table 4.4 shows a comparison of the coating results.

Table 4.4: Comparison of the coating systems characteristics

Insulator type	type- B	Nanocoated type- A	type- C	RTV1 coated type- C	RTV2 coated type- C	Silicone grease coated type- C
Surface distance (mm)	470	430	300	300	300	300
Current r.m.s (mA)	2.0	0.25	1.0	0.077	0.070	0.075
Dissipated Energy (J)	70,000	1,200	14,000	110	80	95
Polluted Flashover voltage (kV)	40	35	18	30	36	46
Surface distance at which polluted flashover occurs (mm/kV)	11.75	12.20	16.70	10	8.30	6.5
Surface status after wet test	HC 6	HC 5	HC 6	HC 4	HC 4	HC 4
Effect of UV on hydropicity (°)	-	-	-	>110°	>110°	-

4.10. Conclusions

In this chapter, extensive tests were carried out characterising the performance of different protective coatings in comparison with porcelain insulators. Insulators were coated with two different RTV coatings of commercial purity from two different suppliers. Another insulator was coated with Voltshield or Nanocoating. Two other insulators were coated with hydrocarbon and silicone grease coatings.

Tests were performed on coated and uncoated insulators under artificial pollution conditions based on the solid layer method of IEC 60507.

There were significant differences in the current waveforms for coated and uncoated insulators. In particular, the porcelain insulators showed clear resistive current components that were not present for the coated insulators, which behaved capacitively. The differences in performances were characterised by the r.m.s. values of leakage current, average power and the accumulated dissipated energy. The flashover voltage test results, in particular, indicate the improved performance of the coated insulators over the uncoated porcelain insulators.

The coated insulators showed superior performance over the non-coated insulators in the following:

- Suppressing leakage currents and dissipated energy; the leakage current on the surface of the uncoated insulator of type B with a surface distance of 470mm was 2 mA. However, Nanocoating when applied to porcelain insulator of type A with surface distance of 430mm reduced the leakage current to 0.25 mA resulting in 90% reduction. As a result of the current reduction, the dissipated energy had also reduced from 70 kJ for the porcelain insulator to 1.2 kJ resulting in more than 98% reduction.
- Surface hydrophobicity and flashover voltage; when new, the Nanocoated insulator exhibited hydrophobic surface property. However, under wet test condition the Nanocoated insulator wet easily and completely lost its hydrophobicity. This resulted in lower pollution flashover voltage performance than insulators treated with silicone materials having shorter surface distances. This may be attributed to Nanocoating which lacks the ability to generate the low molecular weight silicone fluid as it is a thin layer with nanometre width. This

layer became wet immediately when subjected to fog generation. Nanocoated insulator showed great stability under UV radiations, as it is a solid layer.

- Insulators treated with silicone materials like silicone grease and RTV silicone rubber minimized the leakage current by 92%. This reduction resulted in less dissipated energy. In addition, insulators coated with silicone materials had the highest pollution flashover. These attributed to the hydrophobic surface property of the silicone coatings that prevents the creation of water films on the surface and results in reducing insulator flashover. When compared to porcelain insulator, silicone grease coated insulator increased the flashover voltage by 60%. RTV2 coated insulator increased the flashover voltage by 50%. RTV1 coated insulator increased the flashover voltage by 40%. RTV1 and RTV2 coated insulators have different flashover values which are attributed to the different material compositions used in their formulations. RTV coatings showed high resistance to UV radiation in terms of retaining surface hydrophobicity and minimizing surface leakage current. The contact angle remained at the level of 120±3° even after 8 hours exposure to UV radiations, and the current levels stayed at levels less than 0.1mA. Nanocoated insulator showed good stability to UV radiations by reducing the leakage current to values similar to that of the un-exposed insulator to UV radiations, and showed good resilience to sand blasting; however, with long exposure to sand blast, the surface began to exhibit pockmarks. Nanocoated insulator lost its hydrophobicity when exposed to fog application in the wet tests of the fog chamber.

All the coating systems tested in these investigations proved their efficacy to be used as a remedy to the pollution problems under service operating conditions, as they suppressed the leakage current to low values which resulted in a reduction in the power dissipated. All coatings reduced the dissipated cumulative energy, which will lead to lower energy loss when applied in real operating service. Additionally, most of the coating systems increased the flashover voltage level, which is important for reliable operation of the power system. In the following chapter the ability of these coatings to resist tracking and erosion will be examined.

Chapter 5 – Comparative performance of RTV Coatings under Tracking and Erosion test conditions

5.1. Introduction

This chapter presents the results of the tests performed on RTV coating materials and how well the materials withstand the effect of tracking and erosion resulting from voltage stresses encountered in operating service. Rectangular standard size porcelain samples coated with RTV1&2 are subjected to high voltage stress at an inclined position. A salt contaminant solution is fed from the top of the sample and traverses the test surface as according to IEC 60587. The inclined-plane test is designed for assessing the ability of the materials used for HV applications to resist erosion and tracking. It is an international test designed to enhance the occurrence of dry-band discharges on the surface of the sample, resulting in material damage by these two processes.

Leakage current and test voltage were acquired and saved for further analysis and discussion. RMS current, average power and cumulative dissipated energy were calculated and analysed with the aim of identifying trends related to the tracking and erosion resistance of coatings. The chapter also demonstrates the effect of different UV exposure dosages on the resistance of RTV1 and RTV2 coatings against tracking and erosion. The data acquisition system used to control the inclined plane test unit and the data analysis program were described in Chapter 3.

5.2. Inclined plane tests on RTV coated samples

Porcelain samples with 50 mm width, 120 mm length and 5.5 mm thickness were used in these experiments. The samples were coated with RTV1 and RTV2, with coating thickness of approximately 1.0 – 2.0 mm. The samples were mounted at an angle of 45° to the vertical, and pair of stainless steel electrodes were connected to each sample. One electrode was connected to the upper end and the second electrode was connected to the lower end of the sample. Eight filter-papers were clamped between the top

electrode and the specimen to act as a flow control for the contaminant, see Figure 5.1(a).

The contaminant solution consisted of 0.1 ± 0.002 % by mass of ammonium chloride and 0.02 ± 0.002 % by mass of iso-octylphenoxypolyethoxyethanol (a non-ionic wetting agent) in water. This contaminant had a resistivity of 3.95 ± 0.05 Ωm at 23 ± 1 °C as in IEC 60587. Before the start of each test, the electrodes and the filter papers were attached to the samples and the samples were installed in the IPT unit. The upper electrode was connected to the HV source, while the lower electrode was connected to the DAQ system through current measuring resistor in parallel with protection elements. The tube for feeding the contaminant solution was installed and adjusted so that the contaminant solution would flow through the filter paper to the test samples and the conductivity of the contaminant solution was verified. A series resistor of value appropriate to the test, as was shown in Table 3.2, was selected. When all samples were installed, the pump started and the contaminant flow rate adjusted to the required level, as was shown in Table 3.2. When a uniform flow of the contaminant covered the surface of the tested sample, a 50 Hz high voltage was applied to the samples. Figure 5.1(b) shows RTV coated samples during a test in the inclined plane test machine.

The voltage supply to the HV transformer was switched on and adjusted to the voltage level of the test, as displayed on the computer screen. The applied voltage was measured using a capacitive divider having a ratio of 2000:1 and adjusted using a variac in the front panel of the test unit.

The data acquisition program was started and directories were selected for storing the acquired data. A voltage 5 Vdc was sent to activate the high voltage relays. At this time, the test voltage was applied to the samples using push button switches on the front panel of the IPT unit.

The leakage current was measured across a 33.5 Ω resistor which was connected in parallel with the protection elements. Both the resistor and the protection elements were connected to the lower electrode of the sample through a fuse.

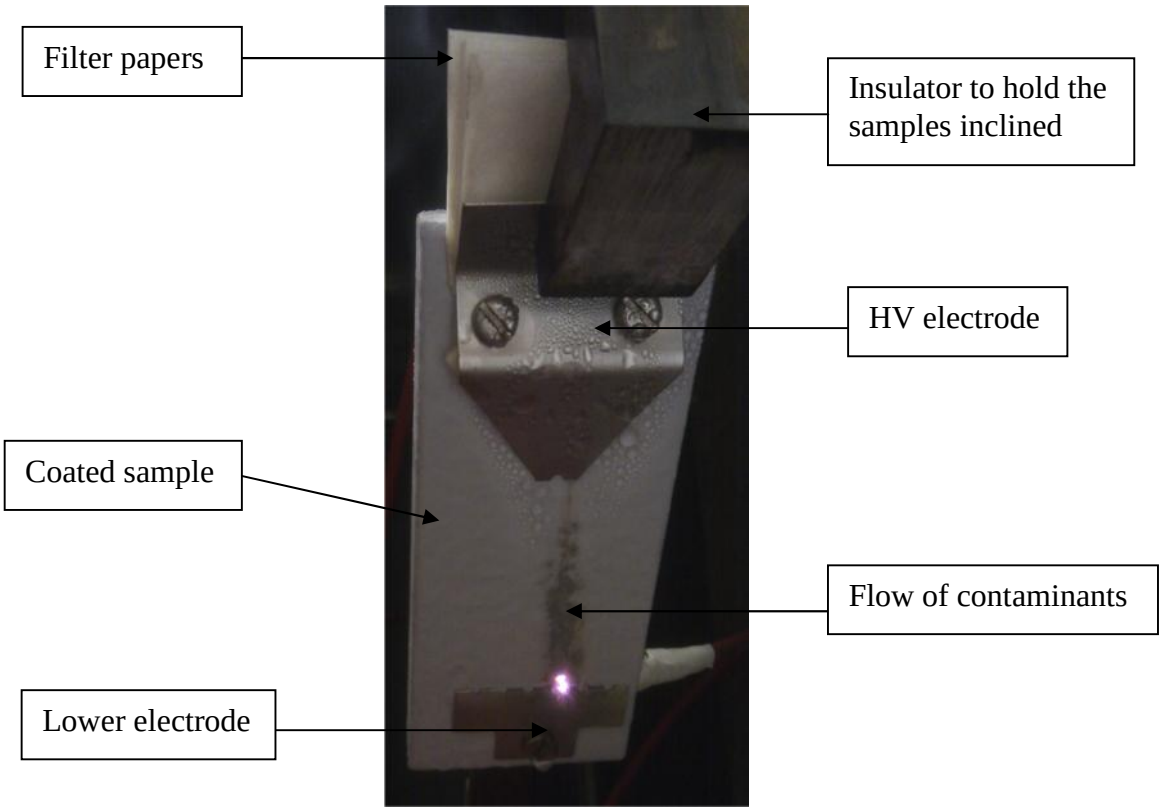

(a)

(b)

Figure 5.1: RTV coated sample under test: (a) Zoomed view showing electrodes and filter papers, (b) RTV coated samples under test

The samples were monitored and the data acquisition program continued to acquire and store the test data until one of the conditions for ending the test was met which are:

(a) If the current exceeds 60mA for 2 s or,

(b) If the 6 hours test time had elapsed.

Three series of tests were performed on the coated samples; the first tests were at a voltage of 2.5 kV, the second tests were at 3.5 kV, and the third series of tests were at 4.5 kV.

5.2. Inclined plane tests at 2.5 kV

The tests showed the development of the leakage current over the surface of the RTV coatings, which leads to the tracking and erosion of the materials and are hence used to judge the performance of the coatings in addition to the dissipated accumulated energy. Initially, when the voltage was applied, there were no discharges observed for either of the coatings, but as the test progressed, discharges began from the top electrode and moved down along the contaminant stream. These were observed as a blue light. With time, an intense bright yellow arc was observed, rooted at the lower electrode. As the test progressed, these current arcs started to cause erosion of the coating material. Figure 5.2 shows a comparison between the results of RTV1 with RTV2 coatings. As can be seen, the rms currents were at low levels between 10 and 20 mA for both of the coatings for the duration of the test, but some current spikes reached 45 mA on the RTV1 sample. The dissipated energy was almost identical for both of the coatings, however, RTV2 showed slightly more dissipated energy with a total of 300 kJ by the end of the test.

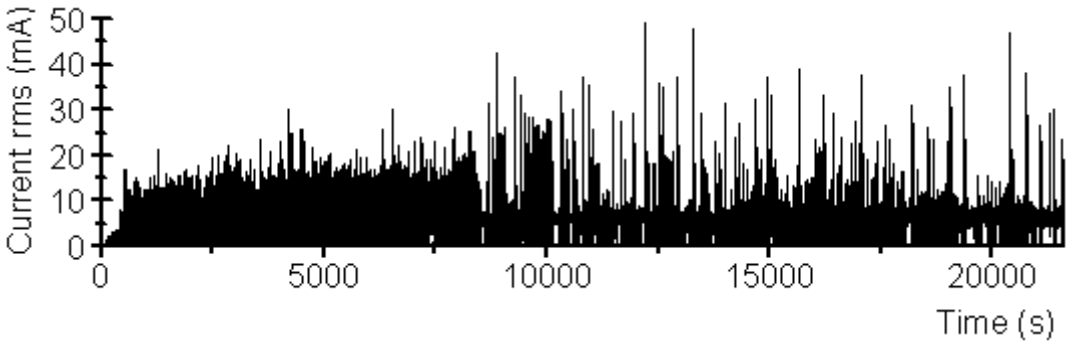

(a) R.M.S. current for RTV1

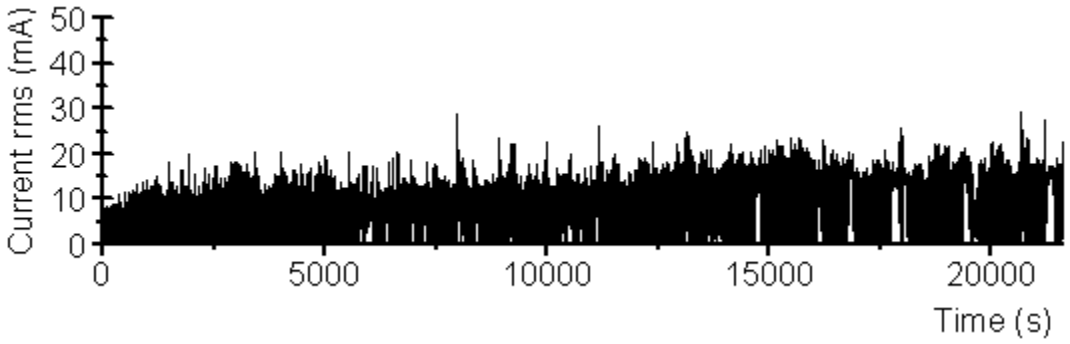

(b) R.M.S current for RTV2

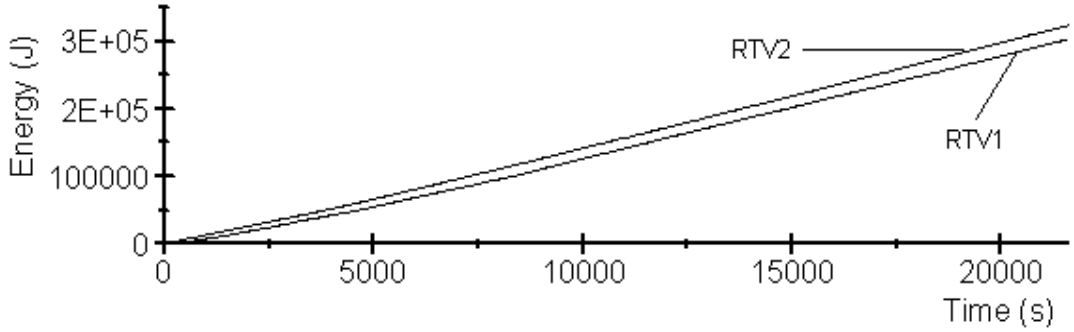

(c) Dissipated Energy (J) for RTV1 & RTV2

Figure 5.2: Leakage current and dissipated energy for RTV1 and RTV2 coated samples tested at 2.5 kV

Figure 5.3 shows photos of RTV1 and RTV2 samples after the inclined plane test. RTV1 performed better than RTV2 in terms of its resistance to tracking and erosion at 2.5kV. RTV1 showed almost no erosion as the filler which was incorporated into its formulation plays an important role when the surface becomes hot and, consequently, resists the degradative effect of high temperatures resulting from exposure of the coating to current arcing. However, RTV2 showed slightly more erosion than RTV1.

Figure 5.3: RTV1 and RTV2 samples after 6 hours at 2.5 kV in inclined plane test

5.3. Inclined plane tests at 3.5 kV

The following test was performed in order to investigate the ability of the RTV coating to resist tracking and erosion resulting from high voltage stresses. The test voltage was increased to 3.5 kV. In these tests, the rms current for the RTV1 coating was in the range between 15 to 25 mA with current spikes reaching 45 mA, as shown in Figure 5.4(a). The rms current for RTV2 coating was in the range of 15 to 25 mA for the first 3 hours of the test with a slight increase at the last hour of the test. Again, there were occasional current spikes reaching as high as 45 mA, as in Figure 5.4(b). Both coatings experienced similar r.m.s current values.

The energy dissipated on both of the coatings is almost at 600 kJ; see Figure 5.4(c).

Pictures of RTV1 and RTV2 after the 6 hours test can be seen in Figure 5.5.

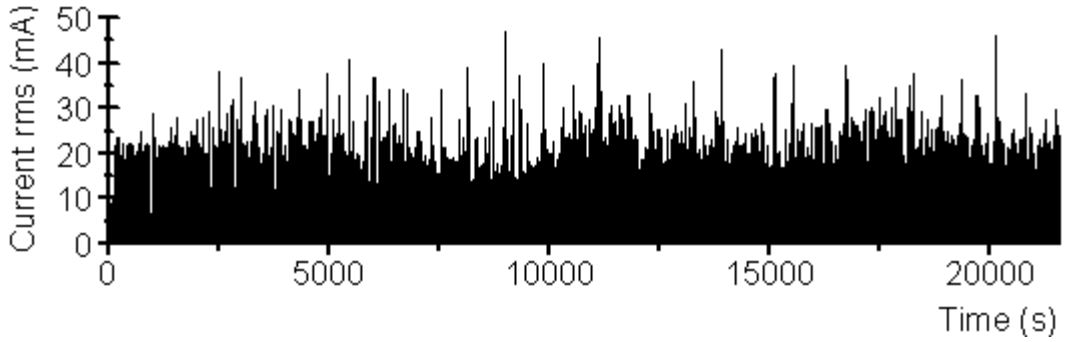

(a) R.M.S. current for RTV1 sample

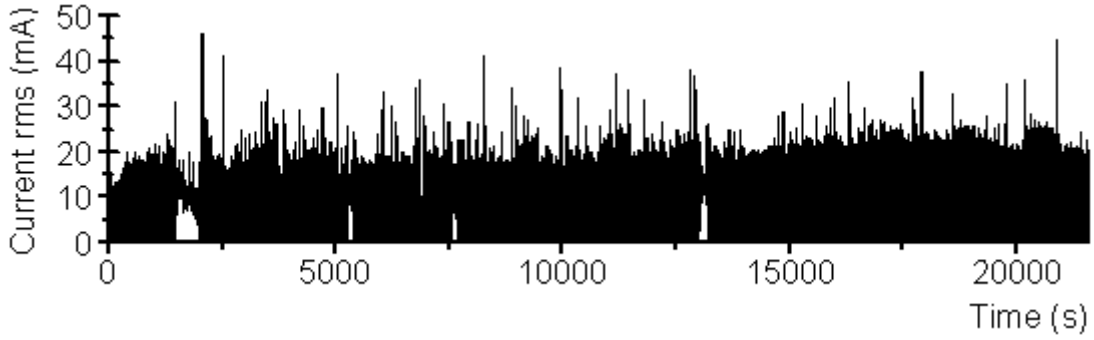

(b) R.M.S. current for RTV2 sample

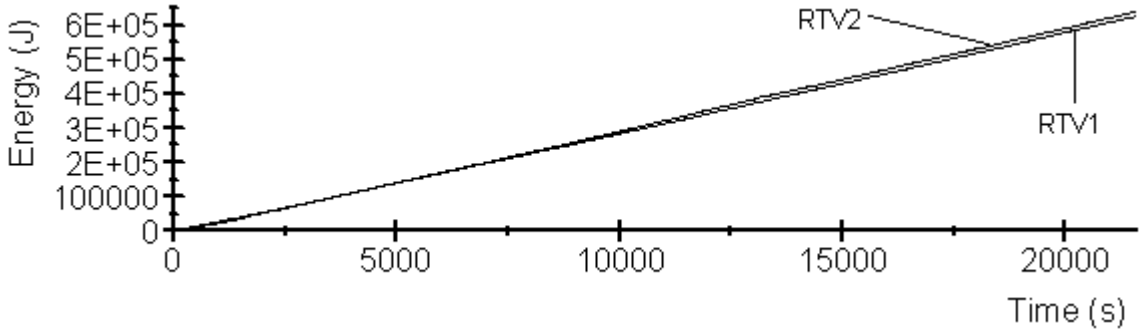

(c) Dissipated Energy (J) for RTV1 & RTV2 samples.

Figure 5.4: Leakage current and dissipated energy for RTV1 and RTV2 coated samples tested at 3.5 kV

In Figure 5.5, it can be observed that RTV2 had undergone more erosion than RTV1, although the dissipated energies on their surfaces are almost same, as both of the coatings experienced similar current magnitudes. This is attributed to the different in filler used in their formulations, as the tracking and erosion resistance is mainly dependant on the filler size and type.

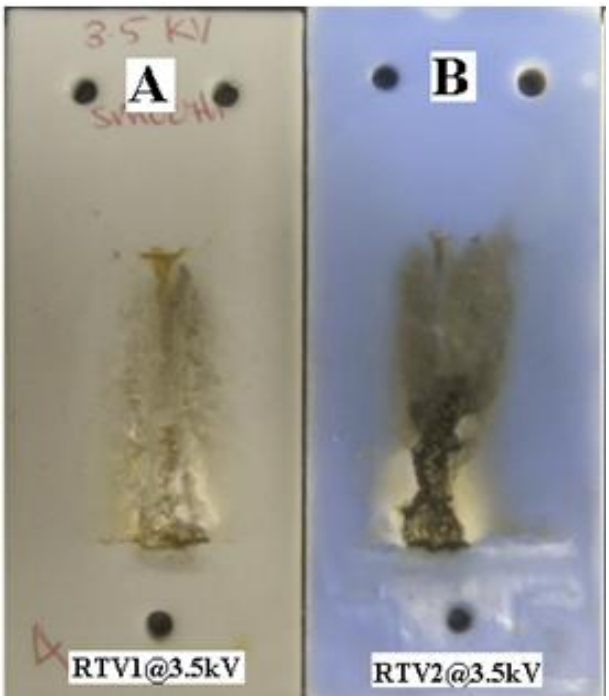

(A) **(B)**

Figure 5.5: Photos of samples tested at 3.5 kV: (A): RTV1, and (B): RTV2

5.4. Inclined plane tests at 4.5 kV

So far, RTV coatings had shown good resistance to tracking and erosion at 2.5 kV, and 3.5 kV. A third series of experiments was carried out at 4.5 kV voltage level.

The r.m.s current for both RTV1 and RTV2 coatings can be seen in Figure 5.6(a) and (b) respectively. The r.m.s current magnitudes on RTV1 appear to be consistently higher between about 20 and 30 mA, but with peaks, especially at the end of the test, rising to 40 mA. RTV2 showed less current intensity and the current range appears to be from 0 to about 30 mA with peaks between 40 and 50 mA.

The energy dissipated on the surface of RTV1 was 1.36 MJ while it was 1.2MJ over the surface of RTV2. The percentage of energy loss increased by up to 50% more than the dissipated energy over the samples tested at 3.5 kV. Figure 5.6(c) shows the energy dissipated on the coated surfaces.

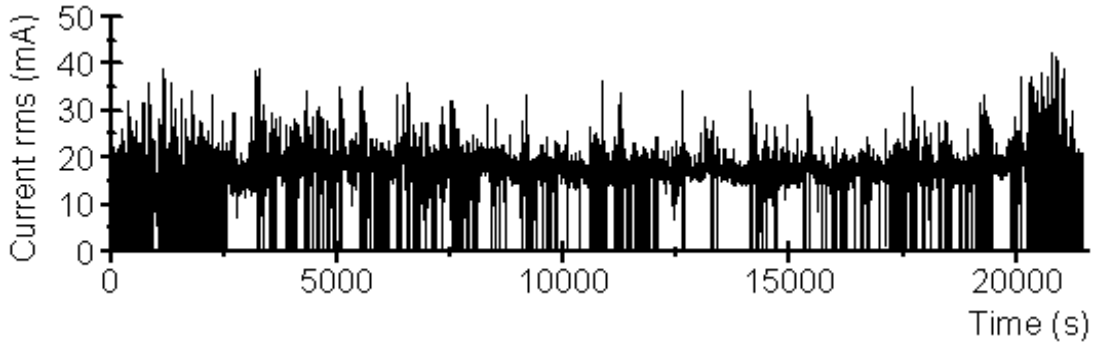

(a) R.M.S. current for RTV1

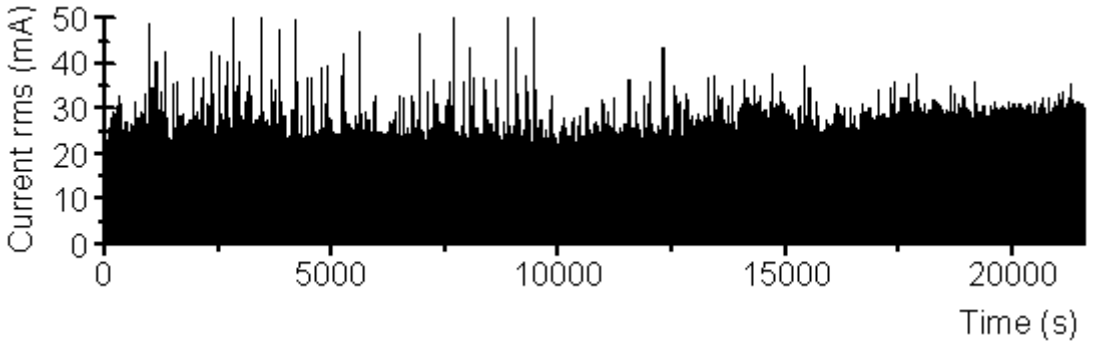

(b) R.M.S. current for RTV2

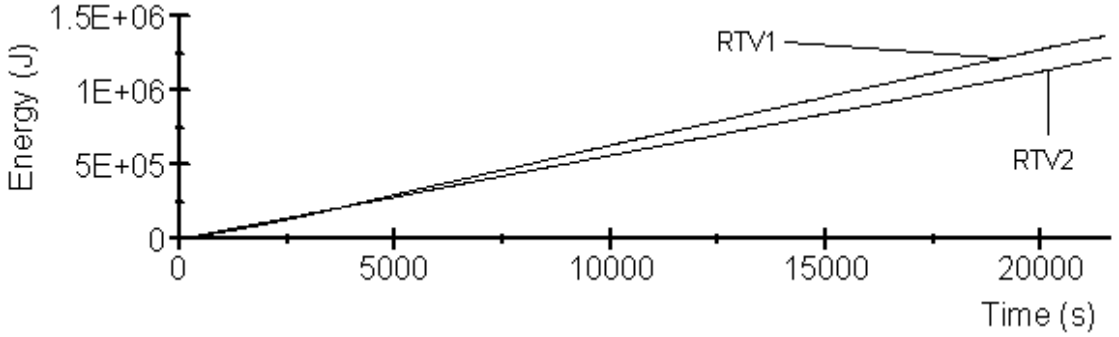

(c) Dissipated energy RTV1&2.

Figure 5.6: Leakage current and dissipated energy for RTV1&2 coated samples tested at 4.5kV

Figure 5.7 shows pictures of the tested samples after 6 hours. Both samples have eroded. Although the energy dissipated over RTV1 was higher than that over RTV2, RTV2 showed greater erosion. This is again attributed to the type of filler used in their formulation and the percentage of these in each of the coatings.

Figure 5.7: Photos of RTV1 and RTV2 tested at 4.5 kV for 6 hours

5.5. Effect of UV radiation on the performance of RTV coatings

5.5.1. Effect of 2 hours UV radiation

i. At 2.5 kV

RTV1 and RTV2 coatings were exposed to one cycle of UV radiation which is equivalent to 87.5 hours of natural sun light exposure and tested at 2.5kV.

Figure 5.8 (a)&(b) show comparative results for the samples exposed to 2 hours UV radiation. For the RTV1 sample, the r.m.s. current initially reached as high as 25 mA, and then for a period in the middle of the test (after about 90 minutes and until the end of the test) the current declined then settled down to a value less than 10 mA. Occasionally, there were current spikes as high as 45 mA, as can be seen in Figure 5.8(a). These spikes indicate current discharge activity on the surface which is associated with the formation of dry band arcing.

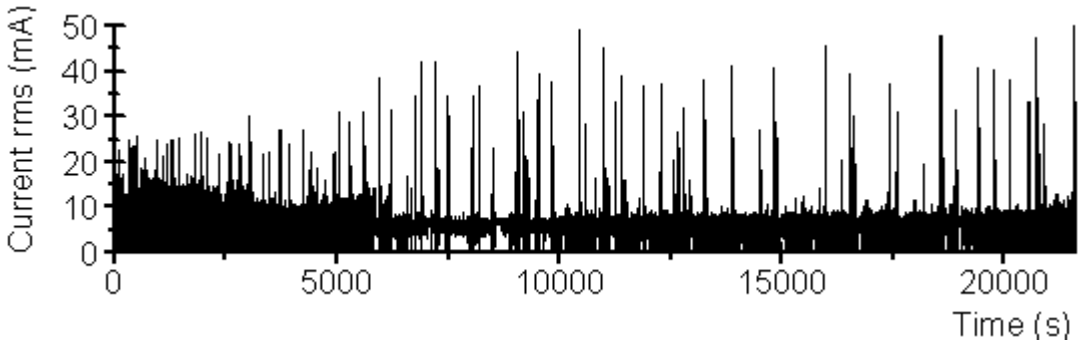

(b) R.M.S. current for RTV1 sample exposed to 2 hours UV

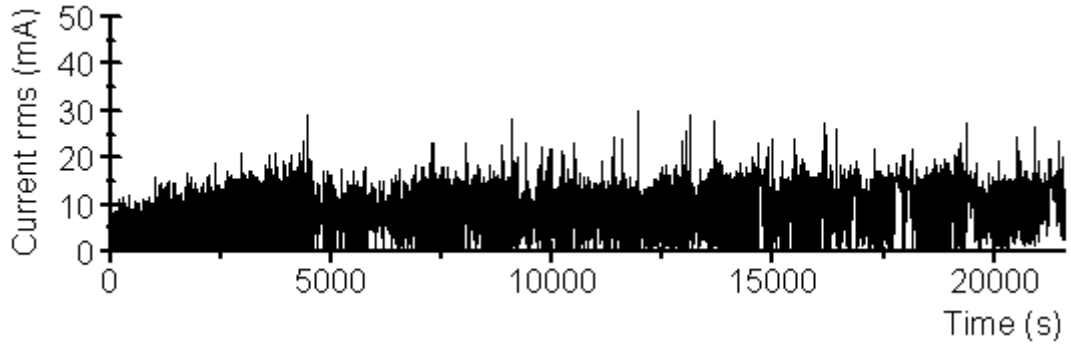

(b) R.M.S. current for RTV2 sample exposed to 2 hours UV

Figure 5.8: R.M.S current for RTV1 and RTV2 coated samples exposed to 2 hours UV radiation at 2.5kV

However, the rms current on the RTV2 coating sample at the start of the test was about 7 mA, and it soon increased to 15 mA. About one hour into the test, the current increased and reached 20 mA, and the coating started to track. The current remained at this level for the rest of the test; see Figure 5.8(b). Although RTV1 showed higher current spikes, both coatings had similar performance.

ii. At 3.5 kV

The good performance of RTV coatings after UV exposure at 2.5 kV triggers the need to perform more investigations on the resistance of the coatings to tracking and erosion after UV exposure under higher voltages. In these experiments, RTV1 and RTV2 samples were exposed to 2 hours UV radiation and tested using the inclined plane test for 6 hours. Figure 5.9, shows r.m.s currents for samples stressed with 3.5 kV.

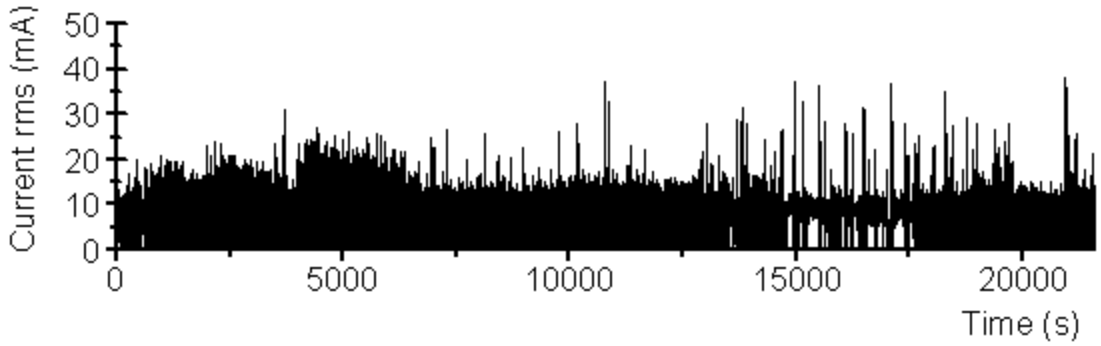

(a) R.M.S. current for RTV1 sample exposed to 2 hours UV radiation

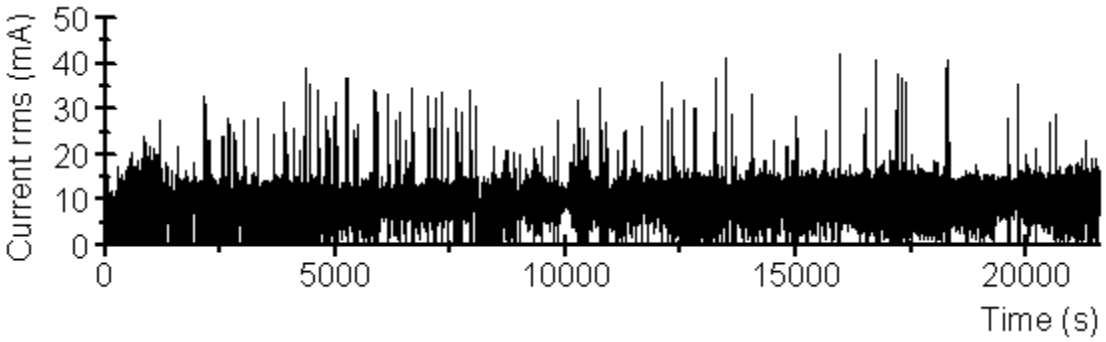

(b) R.M.S. current for RTV2 sample exposed to 2 hours UV radiation

Figure 5.9: R.M.S current of RTV1 and RTV2 coated samples exposed to 2 hours UV radiations at 3.5 kV

At the start of the test, and for the first 30 min, the rms currents for both of the samples were increased from 10 to 20 mA level. After 90 minutes of the start of the test, the rms current of the RTV1 sample declined to 15mA level and continued in the range between 0 mA to 15mA with some current peaks reaching 35 mA during the test; see Figure 5.9 (a). However, the rms current of the RTV2 sample declined and stayed consistently at 10mA level showing a consistent current arcing which resulted in more damage to the coating. At this test voltage, RTV1 showed better performance than RTV2, and this is attributed to the UV stabilizers used in the formulations of the coating. The types of UV stabilizers and inhibitors were previously mentioned in section 2.3.2.

iii. At 4.5 kV

RTV1 and RTV2 coatings were exposed to 2 hours UV radiation and tested for six hours in the inclined plane test unit at 4.5 kVrms.

For the first 15 minutes of the test, the r.m.s current for the RTV1 coating was relatively low at about 22 mA, but after 30 minutes, it increased to 30 mA and remained at this

level for about 40 minutes after which it decreased to 25 mA where it remained for the remainder of the test, dipping to about 20 mA for the final half hour, see Figure 5.10(a). For the RTV2 sample, the r.m.s current quickly reached 40 mA at the start of the test and continued in the range between 30 and 40 mA for the remainder of the test, though some current spikes did reach 50 mA, as can be seen in Figure 5.10(b).

These results show that RTV1 performed better than RTV2 by showing less current, less thermal degradation, fewer tracks and erosion and less material decompositions. These indicate that RTV1 showed more stability against UV radiation than RTV2, as it used different formulations. The RTV1 coating uses stabilizers to alleviate the effect of UV radiation. Also, the diffusion of silicone fluid from the bulk to the surface results in less heat which leads to potentially less damage of the RTV1 sample. The dependence of leakage current on the filler type was discussed in section 2.2.4.3.

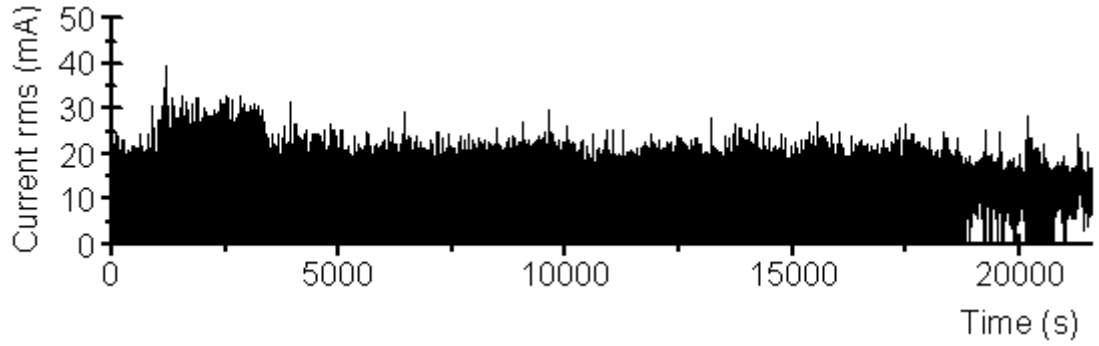

(a) R.M.S. current for RTV1 exposed to 2 hours UV radiation

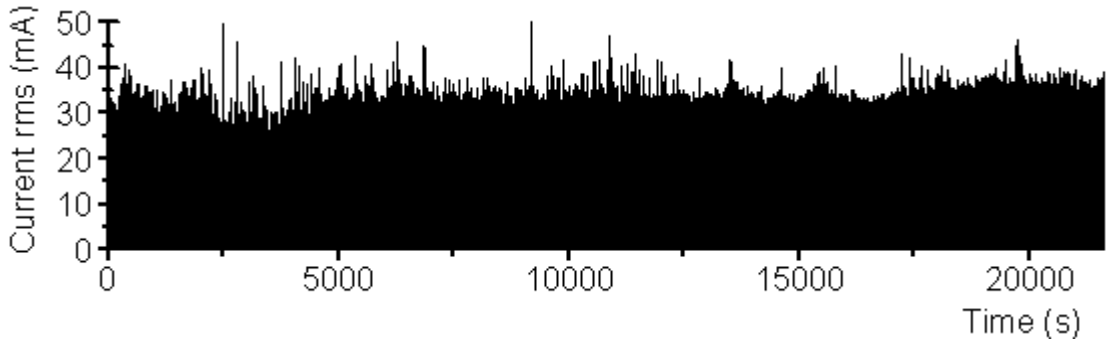

(b) R.M.S. current for RTV2 exposed to 2 hours UV radiation

Figure 5.10: R.M.S current for RTV1 and RTV2 coated samples exposed to 2 hours UV exposure and tested at 4.5 kV

Figure 5.11, shows the accumulated dissipated energy for RTV1 and RTV2 samples exposed to 2 hours UV radiation at test voltages of: 2.5 kV, 3.5 kV, and 4.5 kV.

RTV2 showed higher dissipated energy than RTV1 when exposed to UV radiation. At 2.5kVrms, the RTV2 coating showed slightly higher energy loss, but, at 3.5 kVrms, RTV2 showed more dissipated energy than RTV1. As the test voltage increased, the loss in the dissipated energy on the RTV2 sample increased, and this is clear at the 4.5 kVrms test voltage. This superior performance of RTV1 over RTV2 was attributed to the UV stabilizers used in its formulations such as, the UV absorbers, which reduces the amount of light absorbed by the coating.

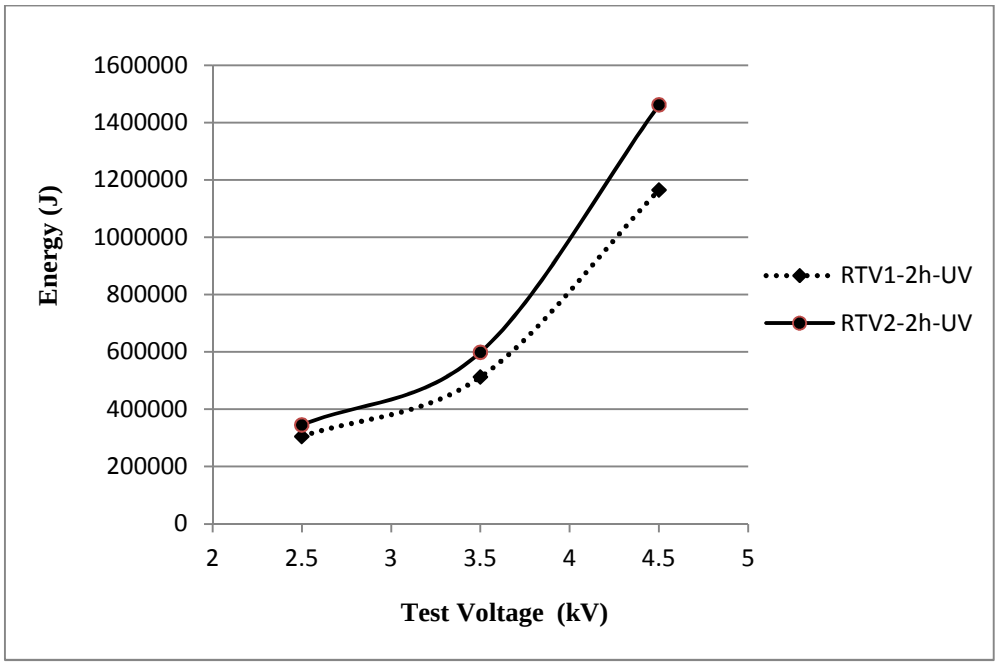

Figure 5.11: Maximum dissipated energy at different test voltages for RTV1&2 samples exposed to 2h-UV

Figure 5.12 shows a comparison between accumulated dissipated energy for RTV1 and RTV2 samples with and without UV exposure at test voltages; 2.5 kVrms, 3.5 kVrms, and 4.5 kVrms. The RTV1 sample showed less dissipated energy when exposed to UV radiation.

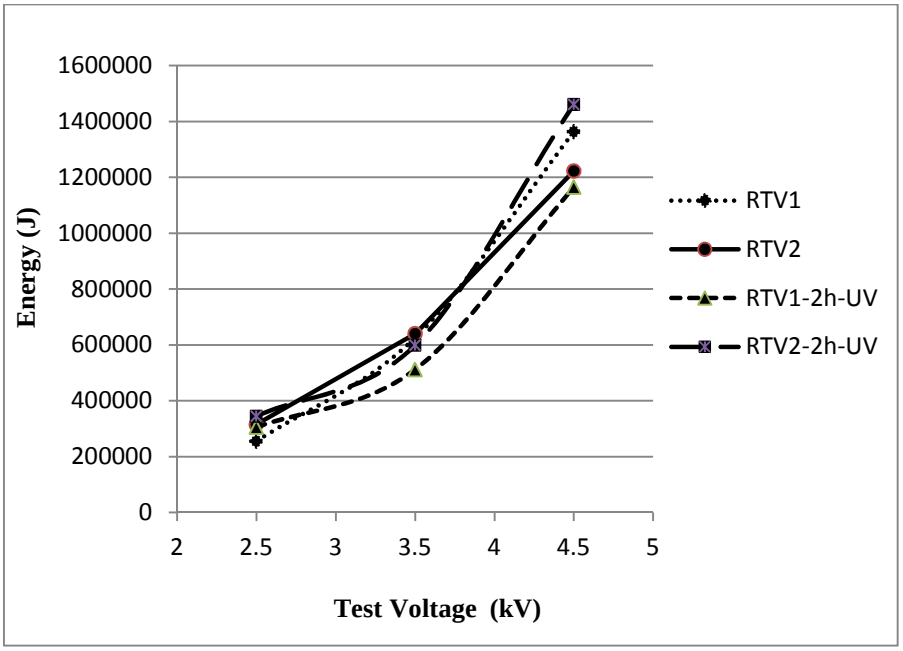

Figure 5.12: Maximum dissipated energy for RTV1&2 coated samples exposed and un-exposed to 2 hours UV and tested at 2.5,3.5, and 4.5 kVrms

Figure 5.13 shows pictures of the tested samples. RTV1 samples showed less damage at 2.5 kVrms. At 3.5kVrms, even though the energy loss on its surface was 0.5MJ, RTV1 showed very light erosion. However, at 4.5kVrms, both coatings had severe visible damaged, but the damage was worse for RTV2.

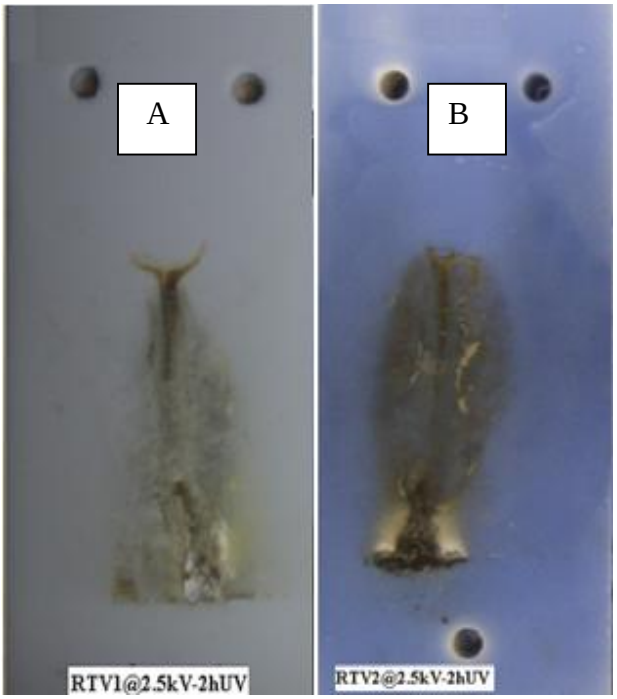

(a) RTV1 at 2.5kV (b) RTV2 at 2.5kV

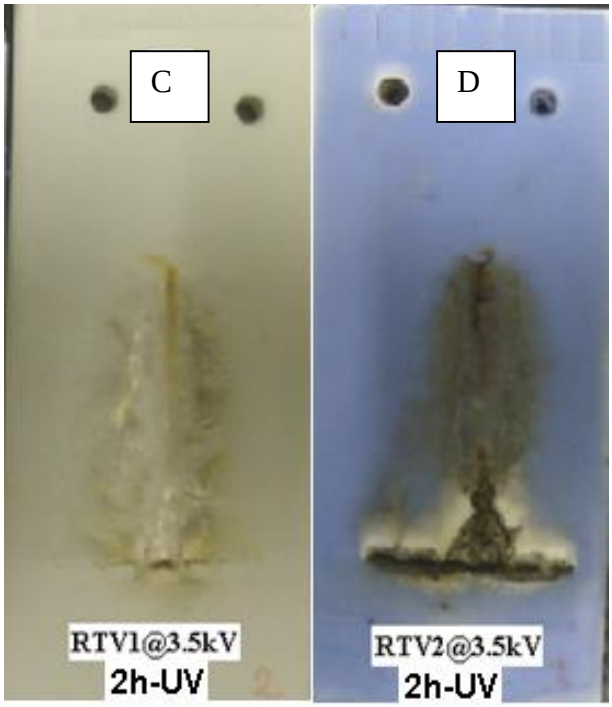

(c) RTV1 at 3.5kV (d) RTV2 at 3.5kV

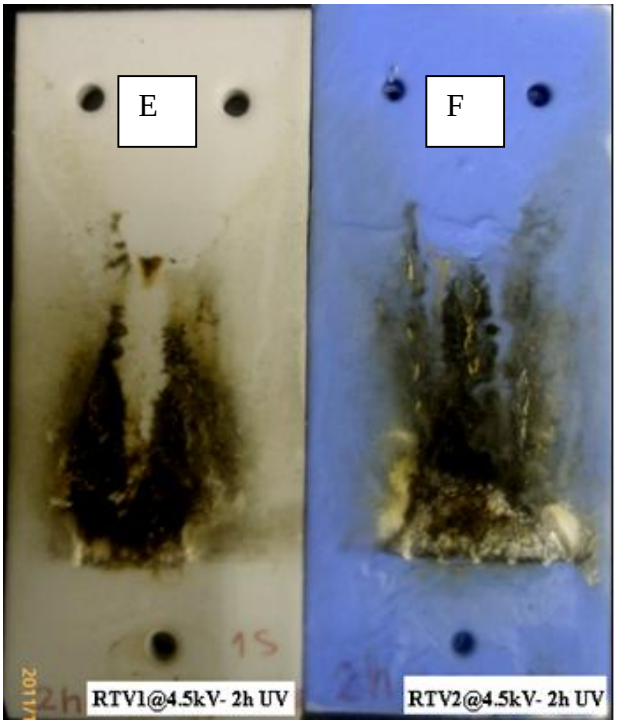

(e) RTV1 at 4.5kV (f) RTV2 at 4.5kV

Figure 5.13: RTV1and 2 samples exposed to 2h-UV radiations and tested at 2.5kV,3.5kV and 4.5kV

5.5.2. Effect of 8 hours UV Radiation

The RTV1 coating showed greater resistance to tracking and erosion than RTV2 when exposed to two hours UV radiation. A further experiment was performed in which RTV1 coatings was exposed to four UV cycles (8 hours) and its resistance to tracking and erosion was tested in the inclined plane test unit at 4.5 kVrms.

Figure 5.14 shows r.m.s. current for the RTV1 coating sample exposed to eight hours UV radiation and tested at 4.5 kV. At the start of the test, the current rose to 45mA level. However, after one hour of the test, the current declined to 20mA and continued at this level for the remainder of the test.

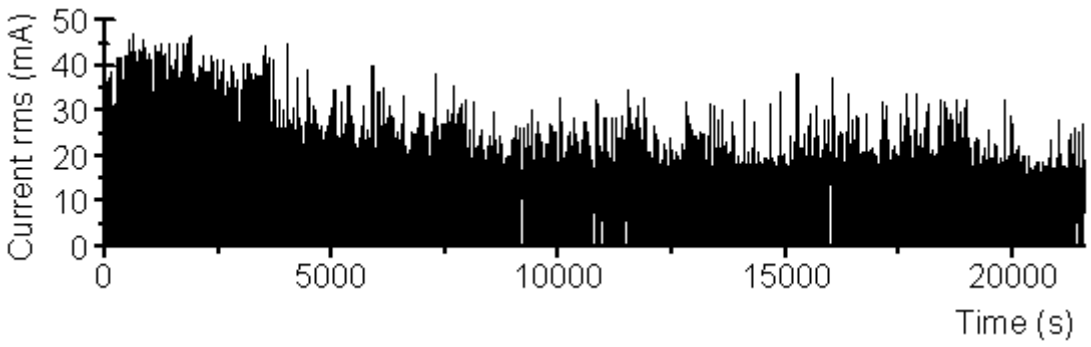

R.M.S. current for RTV1 with 8 hours UV exposure

Figure 5.14: R.M.S current for RTV1 coated samples exposed to 8 hours UV radiation and tested at 4.5kV

Figure 5.15, shows dissipated energy for the three samples tested at 4.5kV with and without UV exposure. The samples that were exposed to UV radiation showed less dissipated energy on their surfaces when compared to the non-exposed sample. This percentage reduction was around 14.5% for the sample exposed to 2 hour UV radiation, and 13% when exposed to 8 hour UV radiation. Figure 5.16 shows photos for RTV1 samples after the inclined plane test. The sample exposed to 8 hours UV radiation showed less damage compared to the other two samples, and this is attributed to the UV stabilizer used and also because the LMW has diffused to the surface of the sample by the heat effect of the arcing, which enhances the resistance of the coating to tracking and erosion.

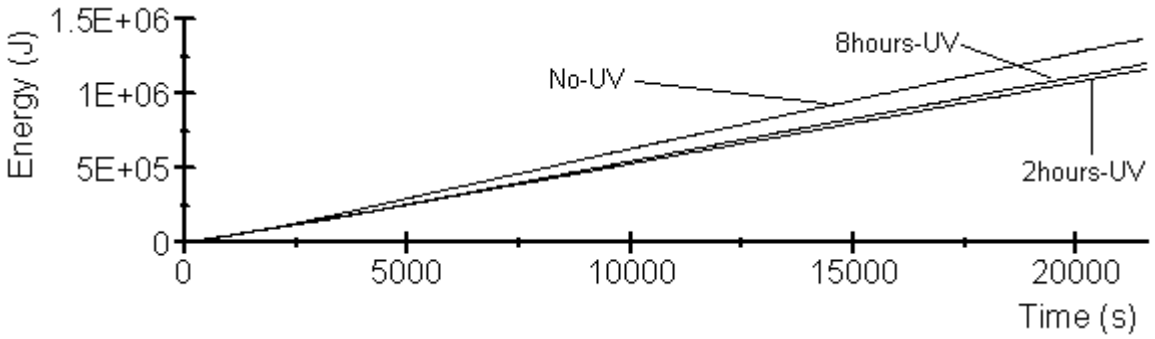

Dissipated energy RTV1 for zero, 2 and 8 hours UV exposure

Figure 5.15: Dissipated energy for RTV1 samples un-exposed and exposed to 2 and 8 hours UV radiation tested at 4.5kV

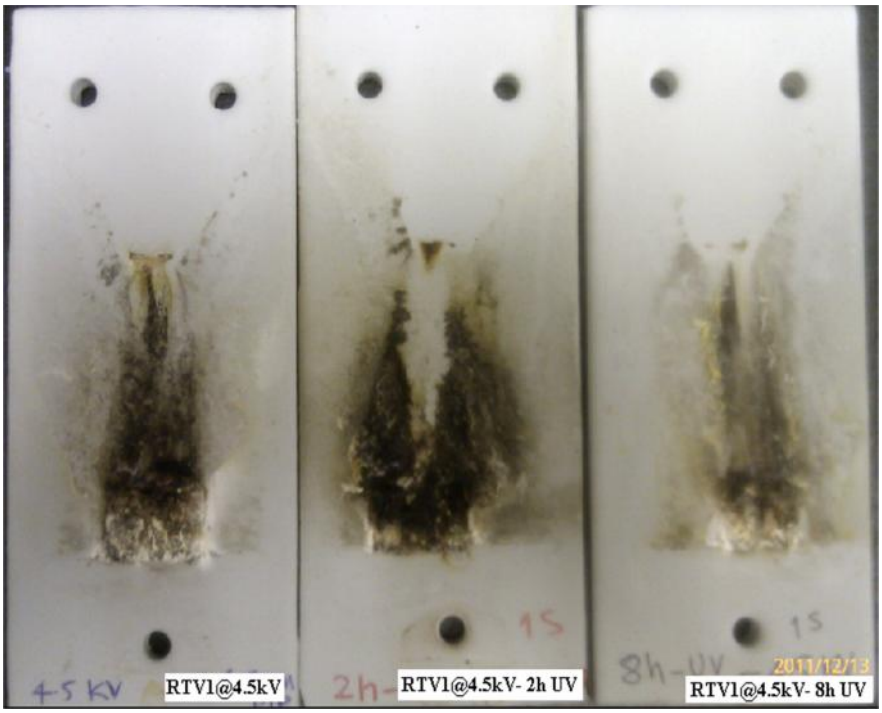

(A) No UV (B) 2hours UV (C) 8hours UV

Figure 5.16: Pictures of RTV1 samples exposed and un-exposed to UV radiations and tested at 4.5kV

5.6. Conclusions

Two sets of porcelain samples with standard size were coated with RTV coatings from two different suppliers, one set with RTV1 and the other set with RTV2 with thickness of approximately 1.0- 2.0 mm. The samples were tested at 2.5 kVrms, 3.5 kVrms and 4.5kVrms. The effects of UV radiation on the performance of the RTV coatings were also investigated.

At a lower voltage of 2.5kVrms, both coatings have shown resistance to tracking and erosion. RTV1 had shown fewer tracks and almost no erosion, while RTV2 showed signs of erosion and higher dissipated energy. At an increased voltage of 3.5kVrms, both coatings showed similar currents and identical loss of energy, however, RTV2 had shown more erosion than RTV1.

At higher test voltage of 4.5kVrms, both samples have shown large eroded areas. At lower test voltages of 2.5 kVrms and 3.5 kVrms both coatings had low r.m.s current and similar energy loss. However, RTV1 has shown better performance and less erosion than RTV2. This is attributed to the different recipes used in the formulation of each

coating, where the filler type, particles size and its percentage in the material play an important part in enhancing the tracking and erosion resistance of the material. At a higher test voltage, although both samples passed the IPT test as the current on their surfaces didn't exceed the criterion for terminating the test, both coatings are badly eroded. Moreover, the consistent arcing had depleted the silicone fluid and led to degrading of the coating.

The performance of these coatings was also investigated after 2 hours UV exposure. Again, at the lower test voltages of 2.5 kVrms and 3.5 kVrms, both coatings perform well. However, RTV2 showed higher energy loss and more damaged surface. RTV1 at 3.5 kVrms showed fewer signs of tracks and erosions. However, with increased voltage to 4.5 kVrms, both samples had eroded, but RTV1 showed less dissipated energy.

RTV1 was exposed to 8 hours of UV radiation, which is equivalent to 350 hours exposure to natural sunlight, the coating showed dissipated energy comparable to and almost identical to that after 2 hours exposure to UV radiation, and showed less damage to the surface than the sample exposed to 2 hours exposure to UV radiation and the sample with no UV exposure. This improved performance maybe attributed to the UV stabilizer used in the material and to the property of diffusion of silicone fluid from the bulk to the surface of the sample which help resisting the tracking of the materials. However, the time of exposure to UV radiation in these experiments is very short compared with the outdoor operating condition. RTV coatings showed resistance to tracking and erosion and exhibit higher resistance after exposure to UV radiation. More tests need to be performed in correlation to field service conditions as the insulators are exposed to longer periods of time to sunlight rays.

As the electric field is considered the drive of the electric current on the surface of the insulators which in turn responsible for surface damage, the following chapter investigating the distribution of the electric field on the surface of the insulators.

Chapter 6 - Computation of Electric field distribution on coated and uncoated insulators under polluted conditions

6.1. Introduction

A thorough understanding of problems such as dry bands and electric discharges can only be achieved through accurate determination of electric field distribution along the insulator surface under a range of atmospheric conditions. Simulations of the electric field over the surface of the insulators are intended to determine the high stress regions on the surface of the insulator. A commercial finite element package is employed for insulator modelling to determine the electric potential and the electric field distribution along the creepage distance of the insulator.

In this chapter, computer simulation based on the Finite Element Method [FEM] is used to compute the potential and the electric field distributions along the creepage distance of the insulators. The insulator model is developed for coated and uncoated insulators under dry-clean and wet-polluted conditions with linear and non-linear pollution model characterised by field-dependent conductivity to achieve a better and more realistic field simulation. The conductivity of the pollution layer was assigned with a value based on laboratory measurements.

It should be emphasised that, under normal conditions, polymeric surfaces would rarely be subjected to a uniform wetted surface situation, due to their excellent hydrophobic surface properties when new or undegraded. Nevertheless, the following simulation results help to identify the high field region that is vulnerable to dry band formations.

The study discusses the modelling procedures and simulation results rather than the mathematics of the modelling process as these are considered more beneficial. However, the mathematics of modelling can be explored in great detail in many textbooks, for example [6.1,6.2].

6.2. Essential features of Finite Element Method

FEM is a numerical technique for solving partial differential and integral equations met in many practical engineering problems. The region where the electric field intensities are to be found, including the surrounding region, is notionally divided into a large number of small non-separated, non-overlapping sub-regions, called finite elements. This process is called meshing. These finite elements can take a number of shapes, but generally triangular shapes are used for 2-D analysis. The potential, which is unknown throughout the region is approximated in each of these elements in terms of the potential at their vertices. For each node in the grid, the finite element method is used to set up an equation for the potential as a function of those elements for the surrounding nodes [6.3].

In this research, the insulator structure is cylindrical in shape so the modelling can be simplified into a 2-D axi-symmetric problem instead of a full three-dimensional (3D) model, which uses much of the computer memory and results in long computational delay. This simplification saves considerable memory and processing time without affecting the accuracy of the simulation, which makes the numerical computation much more efficient. Also, using symmetry, only half the insulator structure was used in the simulation.

A standard cap and pin porcelain insulator having a creepage distance of approximately 300 mm, see Figure 6.1.

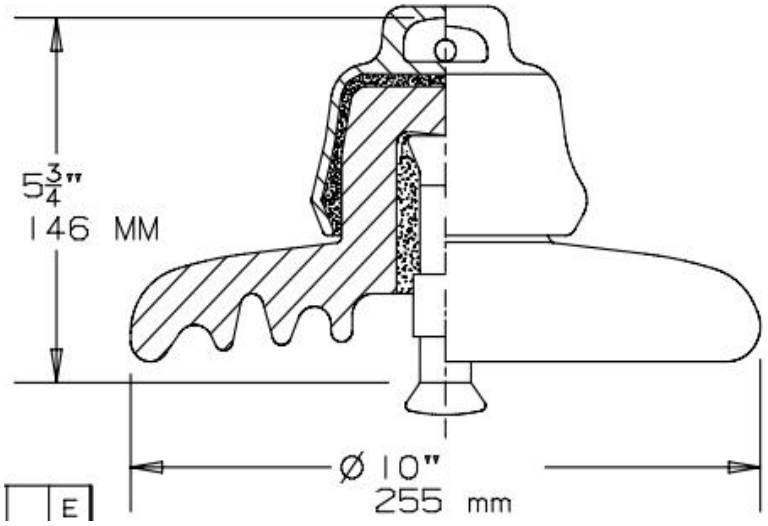

Figure 6.1: Cross-sectional profile and dimensions of the modelled insulator

Uncoated and coated with silicone material was modelled using COMSOL® Multiphysics. This software package is a finite element analysis and solver software package for physics and engineering applications. The software simulation environment facilitates all the steps necessary in the modelling process, defining the geometry, specifying the physics, meshing, solving and then post-processing the results. The software applications are based on partial differential equations (PDEs) [6.4].

Elements of the physical problem such as geometrical structure, material properties, boundary conditions and meshing criteria are presented as inputs in the pre-processing stage. The mathematical model, normally expressed as PDEs that describe the physical problem, is executed in the solving stage. Finally, in the post-processing stage, the package allows users to generate a suitable plot of the desired post-process variables or parameters. The flowchart in Figure 6.2 shows the general FEM procedures for the simulation work contained in this chapter.

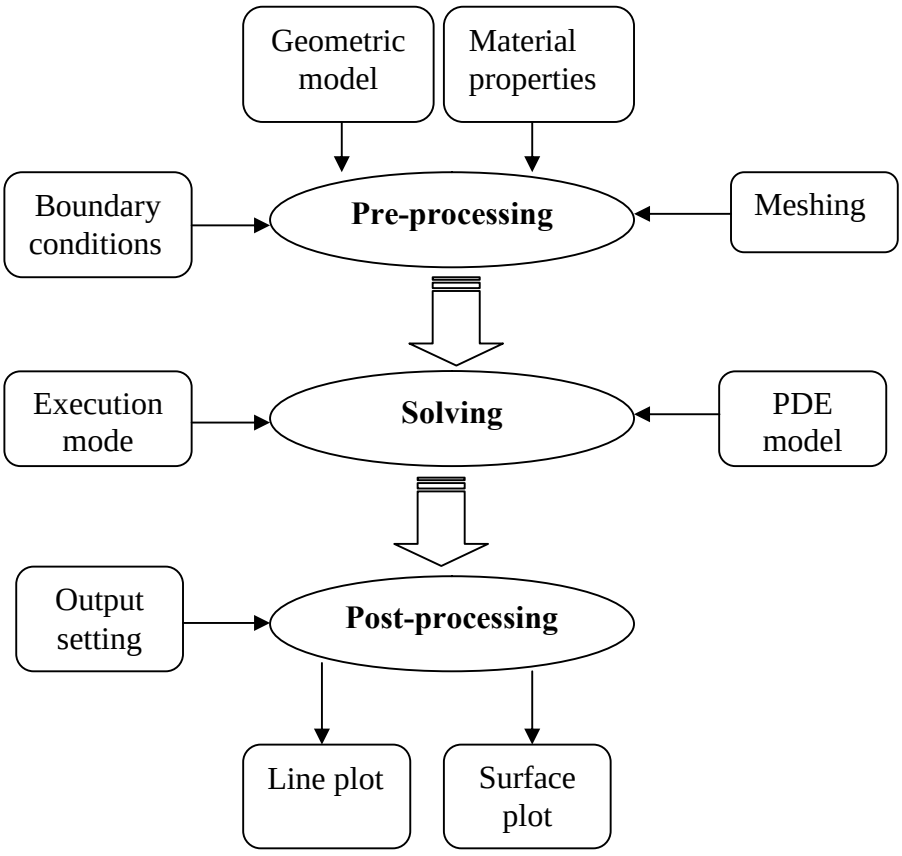

Figure 6.2: General procedures for FEM simulations

6.2.1. Water Droplet

On highly hydrophobic surfaces, water droplets tends to remain as droplets due to the strong hydrophobic properties of the surface. Many authors [6.5, 6.6, 6.7], have used hemispherical shapes to model water droplets, These droplets were modelled with diameter ranging between 1 and 3 mm and 90° contact angle. Field enhancement on the insulator surface due to water droplets may reach 50%, as reported in [6.5]. Other authors [6.7] have used water droplets for modelling insulator under rain and fog conditions. For the rain model, the droplets were created only on the upper surface while the underside was kept dry. The same model was adopted for the fog condition with the bottom shed surface being covered by a thin continuous water film. Therefore, Weigue et al. [6.8] have introduced a more practical droplet model, based on photographs captured during pollution tests in a fog chamber, shown in Figure 6.3. The droplets were categorised according to the hydrophobicity classification (HC) recommended (STRI). From the simulation results, it was verified that the size of water droplets and their distribution on the surface of the insulator are the main factors of the field enhancement.

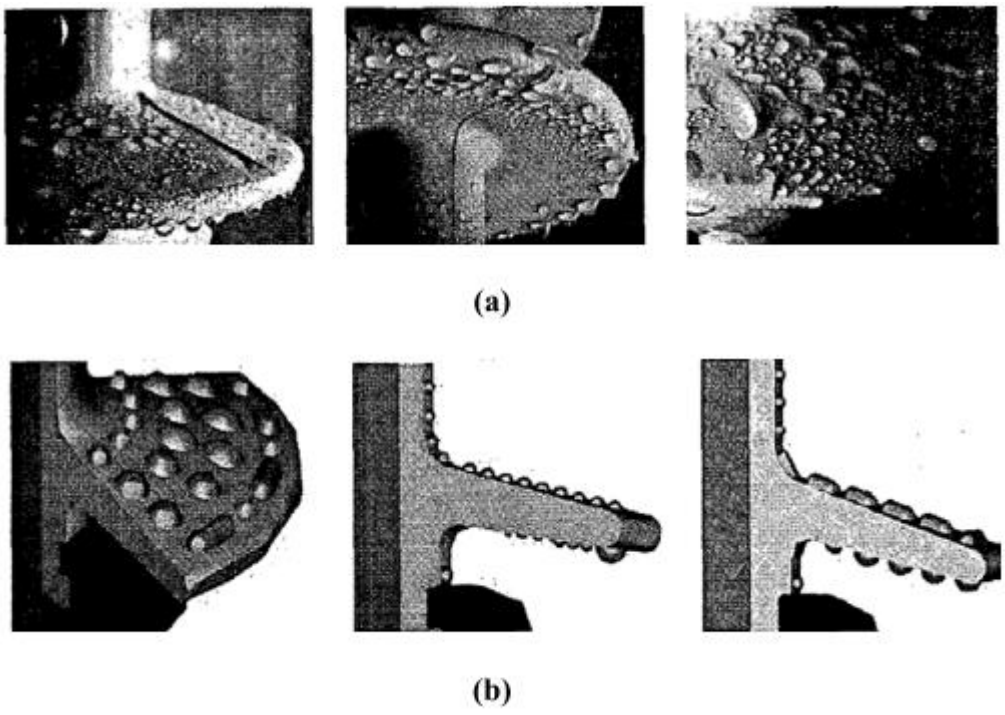

(a) Photographs of water droplets on the insulator surface,

(b) Droplet model used in the simulations [6.8]

Figure 6.3: Photographs of water droplets on the insulator surface

The insulator was drawn using AutoCAD® software and saved in a dfx file extension. The insulator was imported to COMSOL® Multiphysics software, and boundary conditions were set. The modelled insulator is shown in Figure 6.4. The pin of the insulator was modelled as a long rod as in the fog chamber test where the pin was directly connected to the earth electrode which is connected to the earth grid of the fog chamber.

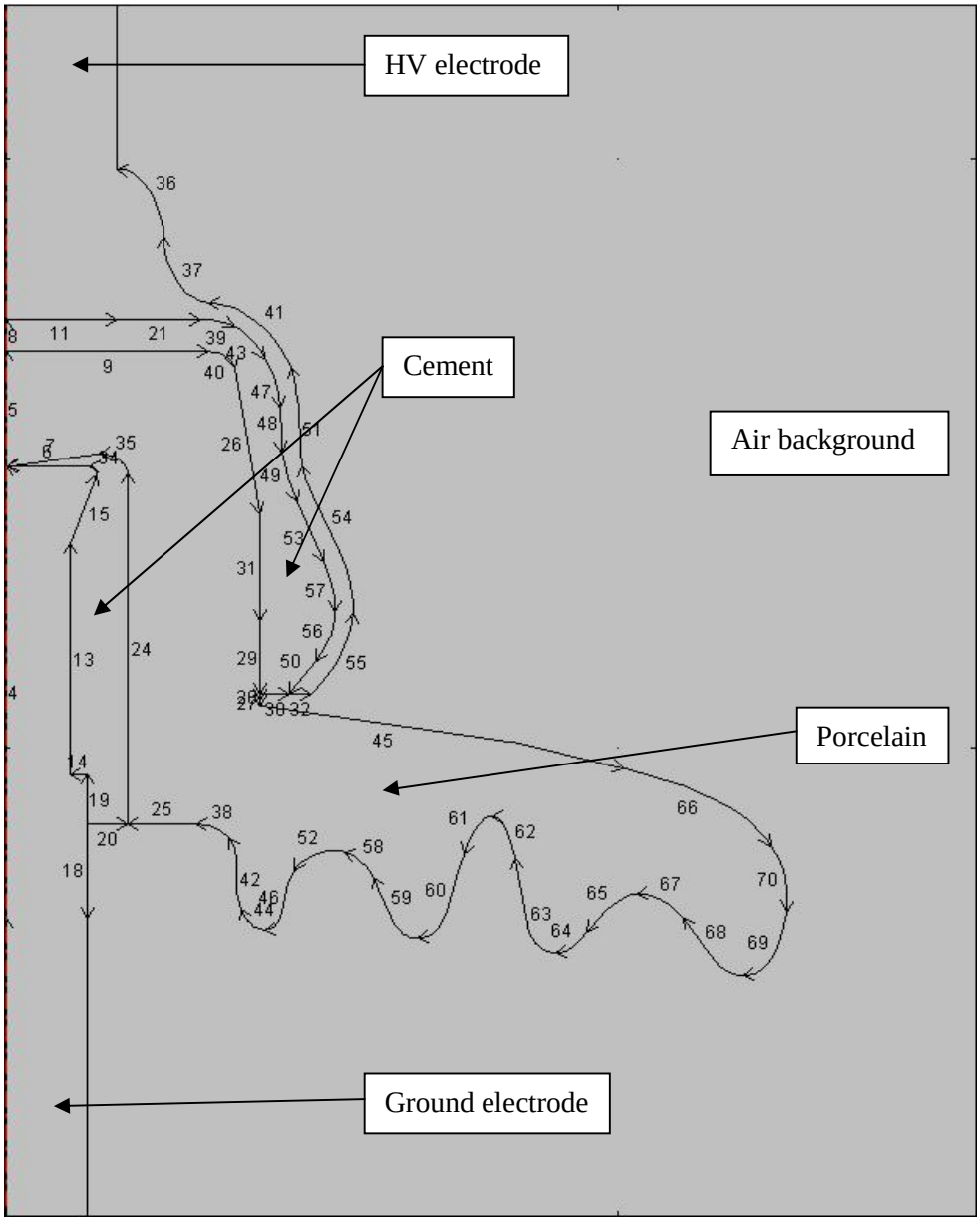

Figure 6.4: 2-D axi-symmetry model for a clean dry insulator

6.2.2. Material properties

The insulator consists of three main parts:

(*i*) The dielectric, which is porcelain material with silicone coating;

(*ii*) The terminations, which are iron for the cap and steel for the pin; their role is to couple the dielectric to the mechanical structure.

(*iii*) The intermediaries like cement which are used to fix the metal fittings to the porcelain insulator [6.9].

Each region of the model was specified with appropriate material properties. The dielectric materials, the silicone coatings and the porcelain were assigned a low conductivity as in Table 6.1. The surface water was considered the dominant substance when the pollution layer is completely wet and saturated with moisture, thus the pollution layer was assigned with a relative permittivity of 80 as, it is fairly good conducting medium with pollution, it is equivalent to a higher permittivity and the conductivity was assigned a value 6.0×10^{-7} S/m found by laboratory measurements as reported in [6.10] and was identical to the built-in values found in the COMSOL software. The air region surrounding the insulator was specified with a very low conductivity, $\sigma = 1.0\times10^{-15}$ S/m. The silicone coating layer was assumed homogenous and uniformly distributed along the creepage path of the insulator surface, and using AutoCAD software, the thickness of the layer was precisely assigned with a thickness of 0.5mm. The same value was initially assigned to the pollution layer. In this case, it is assumed that it is uniformly distributed along the creepage path of the insulator surface. However, it was also non-uniformly distributed as patches of pollution layer with thicknesses ranging from 0.5 to 1.5 mm near the electrode regions and along the top surface. Therefore, based on photographs captured during the wetting of the insulators in the fog chamber. The droplets were simulated and categorised according to the hydrophobicity classification (HC) by STRI Guide introduced in chapter 2.

The properties of material used in the simulations are summarised in Table 6.1.

These material properties are Comsol built-in materials.

TABLE 6.1: Material properties used for insulator modelling

Material	Relative Permittivity, ε_r	Conductivity, σ (S/m)
Air background	1.0	1.0×10^{-15}
Porcelain	4.2	1.0×10^{-14}
Silicone Rubber	12.1	1.0×10^{-12}
Pollution layer	80	6.0×10^{-7}
Iron	1.0	1.0×10^{7}
Cement	2.09	1.0×10^{-14}

6.2.3. Boundary Conditions

The cap which represents the HV electrode was energised with an AC voltage of 6.3 kV at 50 Hz. This was the rms potential to which the insulator was subjected to under heavy pollution conditions, according to the IEC 60507 standard. The bottom electrode was connected to ground at 0 V. The air space surrounding the insulator in the fog chamber was simulated large enough to minimise its effect on the distribution of potential near the electrodes and along the insulator profile, and also to simulate the air surrounding the insulator in the fog chamber. The outer edges of the air background region are assigned with a boundary that assumed zero external current and electromagnetic sources, hence representing a physical system that is in an isolated open space. The symmetry line of the insulator was set to be the axi-symmetric along the axis on the r-z plane. The electric field profiles along the insulator surface for clean and polluted insulators were calculated at different surface distances. For the polluted insulators, the tangential electric field is calculated for a surface distance beginning from the HV cap to the ground electrode. It is assumed that the pollution layer covered the entire surface of the insulator. For clean insulators, the tangential electric field was calculated for a surface distance commencing from the start of the porcelain surface at the cap to the end of the porcelain surface near the pin, and this applies for the coated insulator, as can be seen in Figure 6.5.

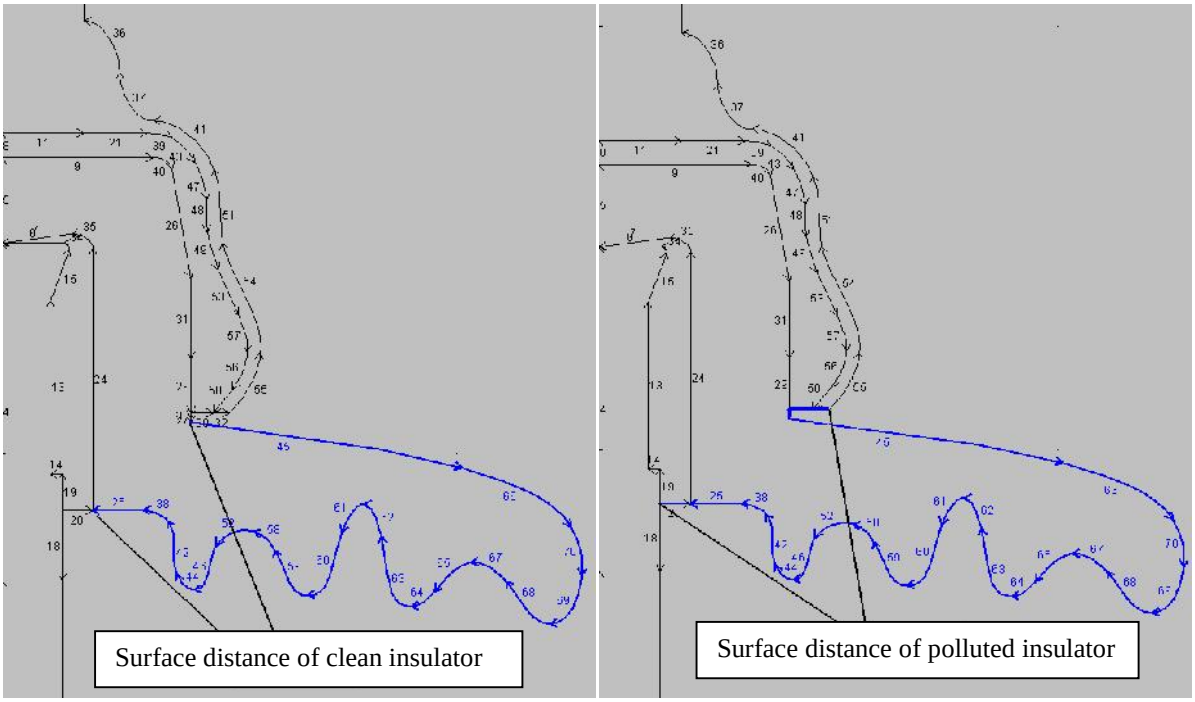

(a) (b)

Figure 6.5: surface distances of clean and polluted insulator

6.2.4. Meshing

As part of the FEM procedure the entire domain is divided into non-overlapping triangular mesh elements. The size of the mesh elements can be varied manually on any chosen part of the insulator's surface to enhance the accuracy of the simulation. Fewer mesh elements may reduce the accuracy of the simulation results, while too many elements can lead to high memory consumption and longer processing time. Determining an optimised mesh will facilitate a faster computation time without reducing the accuracy of the result. Mesh discretisation of the insulator domain problem can be seen in Figure 6.6. The insulator model was simulated in the FEM analysis using an AC/DC module (Static Electric mode), which assumes that currents and electromagnetic fields vary slowly. This mode is valid for many HV applications including outdoor insulators that operate at power frequencies of 50-60 Hz [6.4].

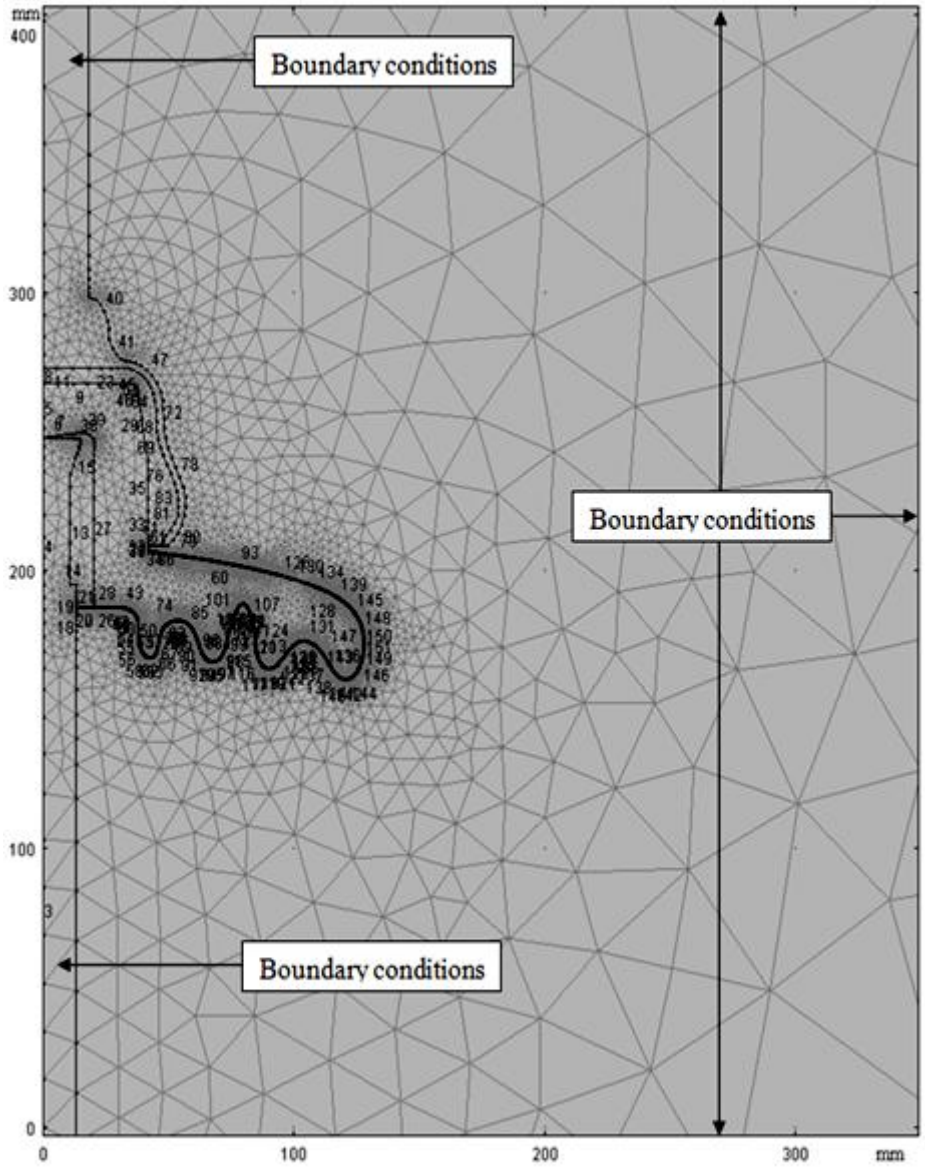

Figure 6.6: Mesh discretisation of insulator domain

6.3. Simulation results

6.3.1. Electric potential distribution along surface of insulators

The resistive component of the leakage current along the pollution layer on the surface of the insulator is driven by the electric field, particularly the tangential component. The flow of leakage current causes surface heating, leading to the formation of dry bands and non-uniform distribution of the pollution on the surface of the insulator [6.4].
Water on the polymeric surface tended to remain as separated droplets due to the strong hydrophobic properties of the surface. Water drops were modelled as having circular shape with different contact angles and diameters ranging between 1 and 3 mm, as can be seen in Figure 6.7. A hemispherical shape with 90° contact angle can be too ideal to represent a water droplet on a practical insulator as reported by Weigue et al. [6.8] who introduced a realistic droplet model, based on photographs captured during the wetting of a polymeric insulator in a fog chamber.

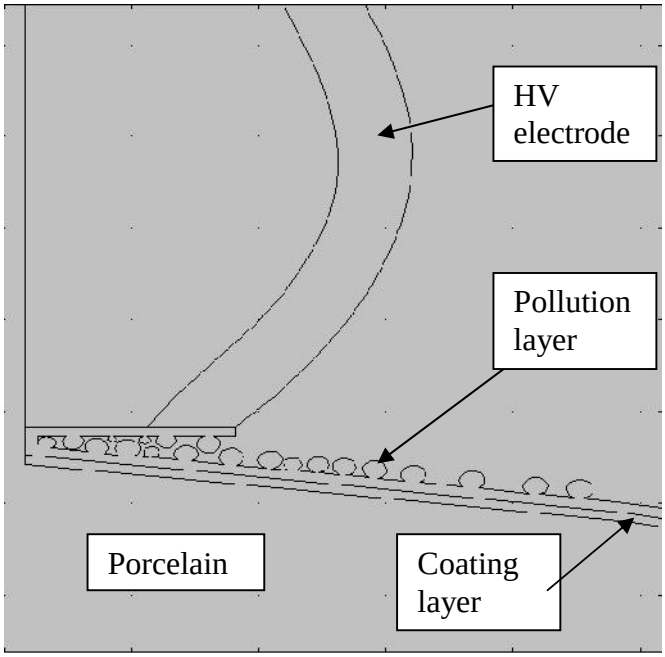

Figure 6.7: Simulation of droplets near the HV electrode on coated insulator

The voltage distribution was computed along different surface distances for clean, uniformly polluted and non-uniformly polluted insulators. A voltage of 6.3 kV at 50 Hz was applied to the cap while the pin was set at zero potential, the resulting voltage

distribution for coated and uncoated insulators can be seen in Figure 6.7(a) and (b) respectively.

For the coated clean and coated uniformly polluted surfaces, the potentials followed very similar trends: a steep rise up to about 3700 V at a surface distance of about 25 mm near the ground electrode which smoothed into a plateau of 4000 V between 50 mm and 225 mm along the surface distance of the insulator with a final increase in voltage to just under 5000 V at 280 mm near the HV electrode. The major difference between clean and uniformly polluted surfaces was that the potentials were calculated at different surface distances, as the longer path was due to the presence of water droplets on the surface, and the voltage was calculated along the droplets and their profiles.

When water droplets were added to the polluted surface near the electrode regions as was shown in Figure 6.6. The shape of the plot was significantly changed, being stretched along the surface distance axis; see Figure 6.8(a). Now the initial sharp increase was to about 3700 V at 50 mm, followed by a transition to a plateau that extended to 300 mm and then a relatively steep rise in voltage to about 5500 V at 380 mm where the region is close to the HV electrode. The extension in the surface distance seen on Figure 6.8(a) and (b) was due to the fact that the surface distance path was considered along the edge profile and the droplets profiles. Water droplets on top of the uniformly polluted surface disturbed the voltage distribution along the insulator surface as it can be seen as ripples or undulations especially at the HV electrode, and produced local variations in the resistive leakage current on the insulator and redistributed the voltage producing undulations seen on the voltage profiles in Figure 6.8(a) and (b). This non-uniform voltage distribution could cause extremely high electric field magnitudes locally, especially around the cap and pin regions. The magnitude of the resulting voltage variations could be sufficient for the formation of dry bands.

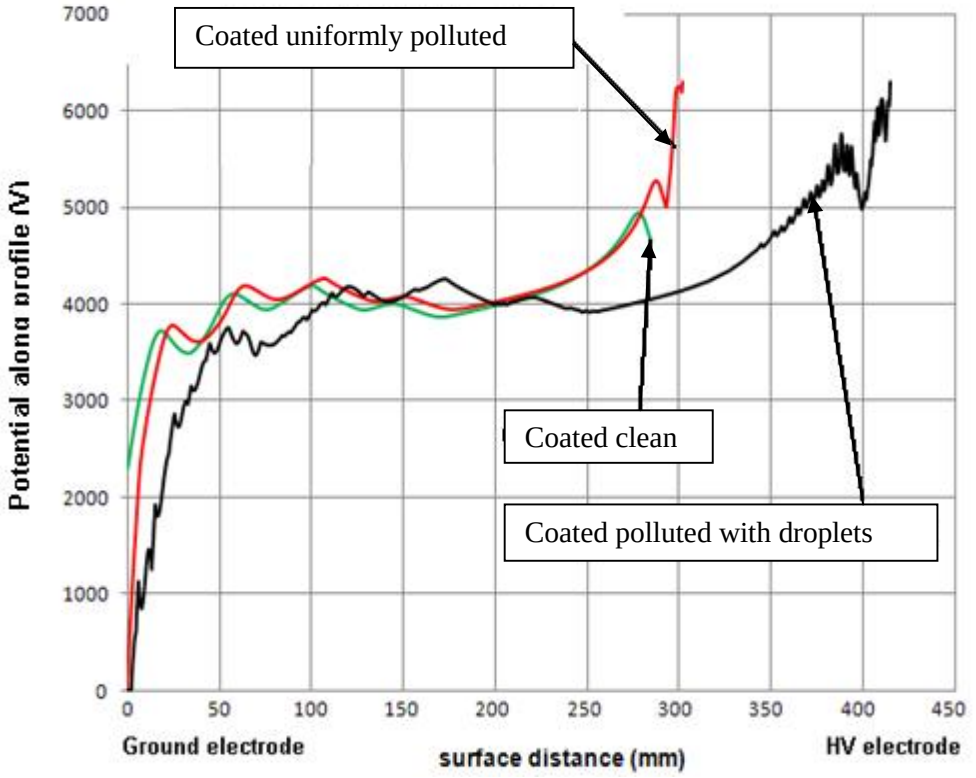

(a) Coated insulator

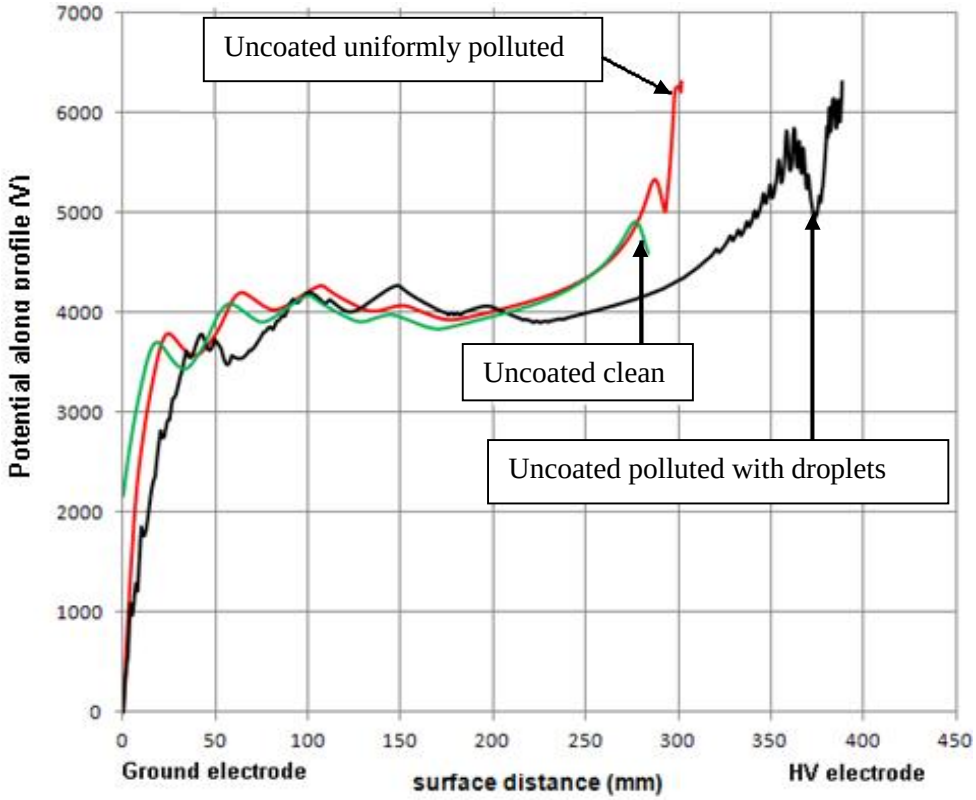

(b) Uncoated insulator

Figure 6.8: Electric potential distribution along surface distance of: (a) coated insulator, (b) uncoated insulator

Figure 6.9 shows the equipotential lines along the surface distance of a coated insulator with a clean dry surface. The individual equipotential lines that cross the insulator profile cause the undulations seen on the voltage profile. These undulations are accompanied by electric field reversal along the surface at the insulator skirts, i.e. lines can be directed either from air into porcelain or from porcelain out to air. Generally, the equipotential contours are concentrated near the metal fittings, indicating high field regions with less field intensity along the insulator surface.

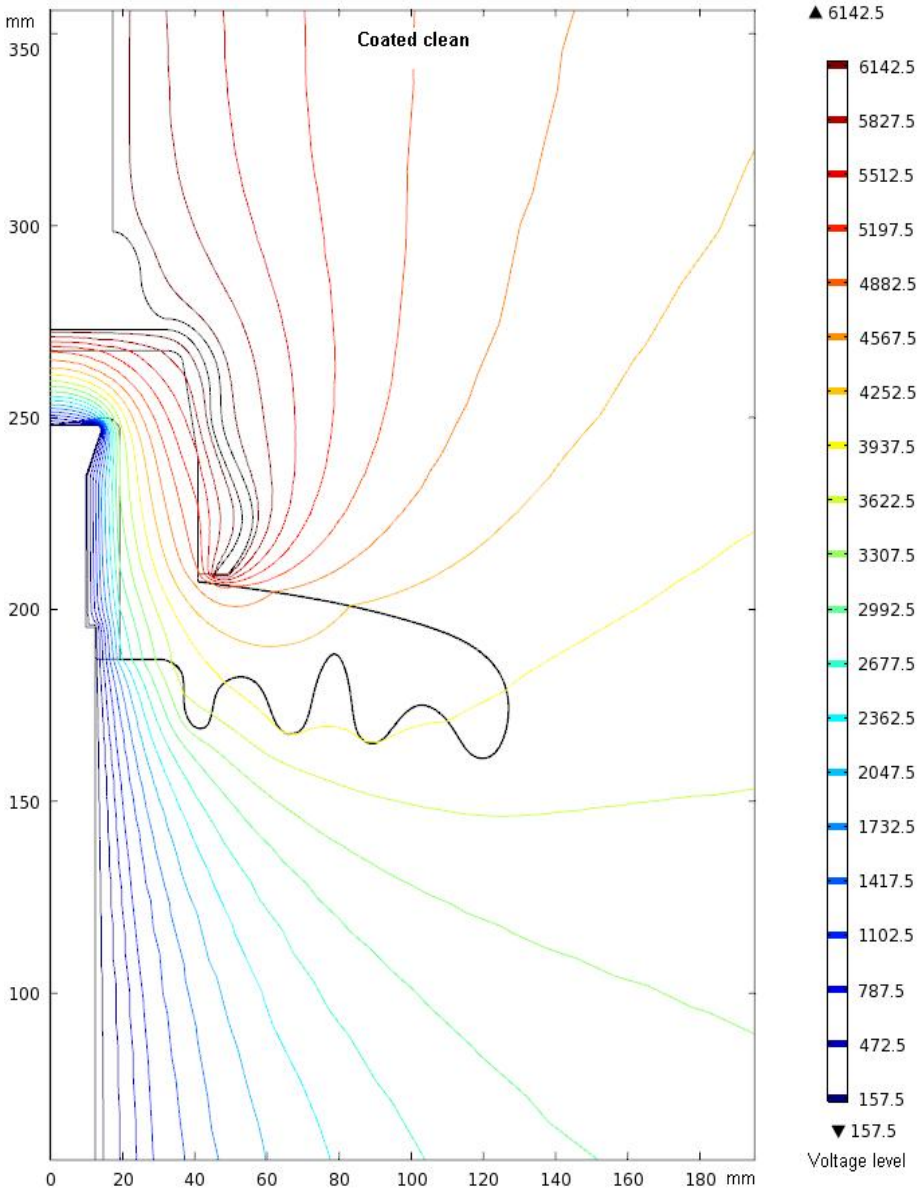

Figure 6.9: Equipotential lines along the surface distance of the coated dry clean insulator

6.3.2. Electric field distribution along uncoated insulators

Figure 6.10 shows four plots of the tangential electric field strength with different surface distances depending on the insulator pollution condition: clean dry, uniformly polluted, non-uniformly polluted with pollution patches, and non-uniformly polluted with scattered droplets of pollution near the electrodes. The surface distance is longer in the case of droplets, again, this is because the path along the edge profile of the insulator includes the edge profile along the water droplets circumferences. Figure 6.10 shows wetting patterns of insulators coated with silicone rubber; polluted with water patches, and polluted with water droplets.

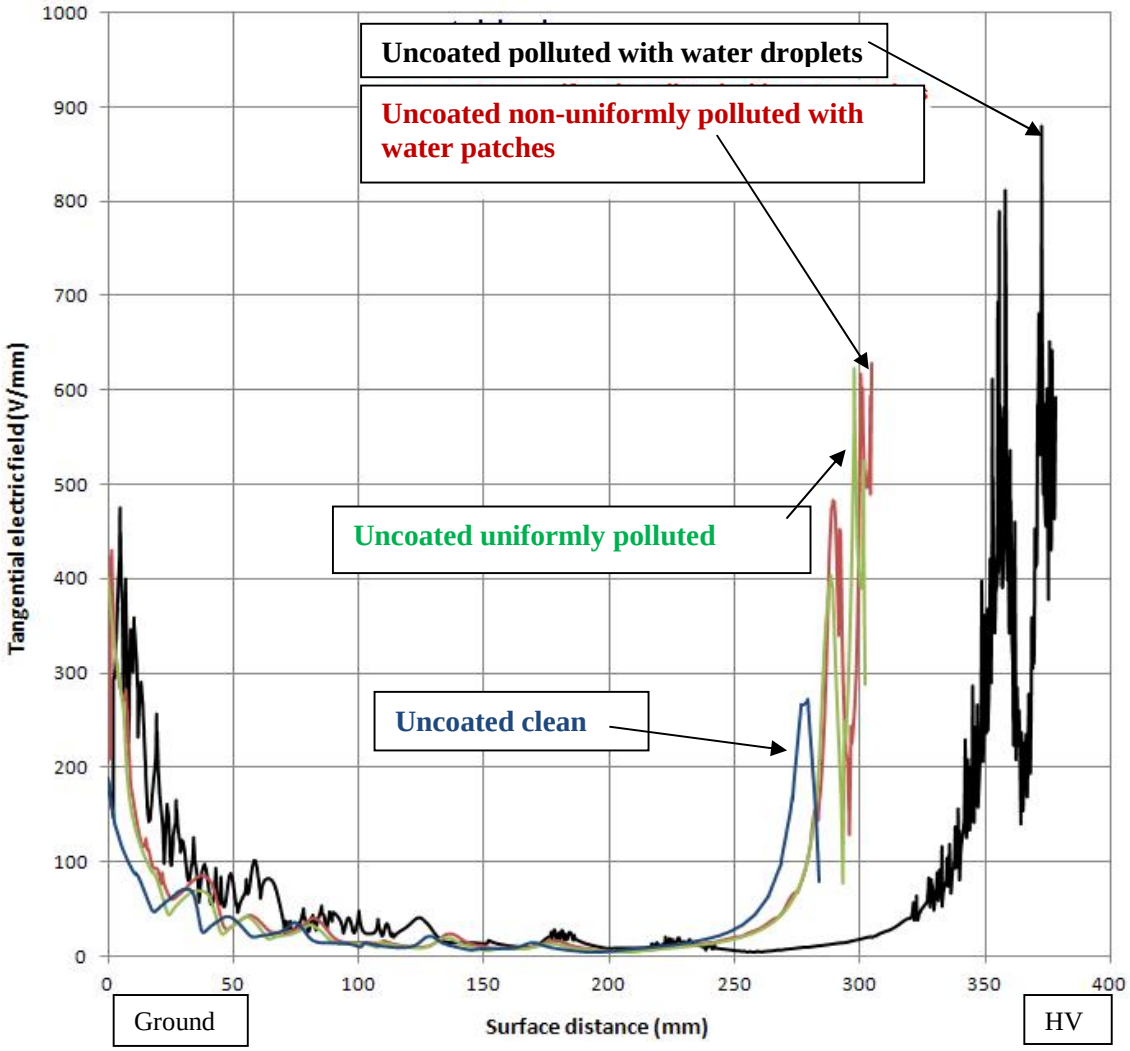

Figure 6.10: Tangential field with leakage distance of uncoated insulator: dry clean, uniformly polluted, non-uniformly polluted with water patches, polluted with scattered small water drops

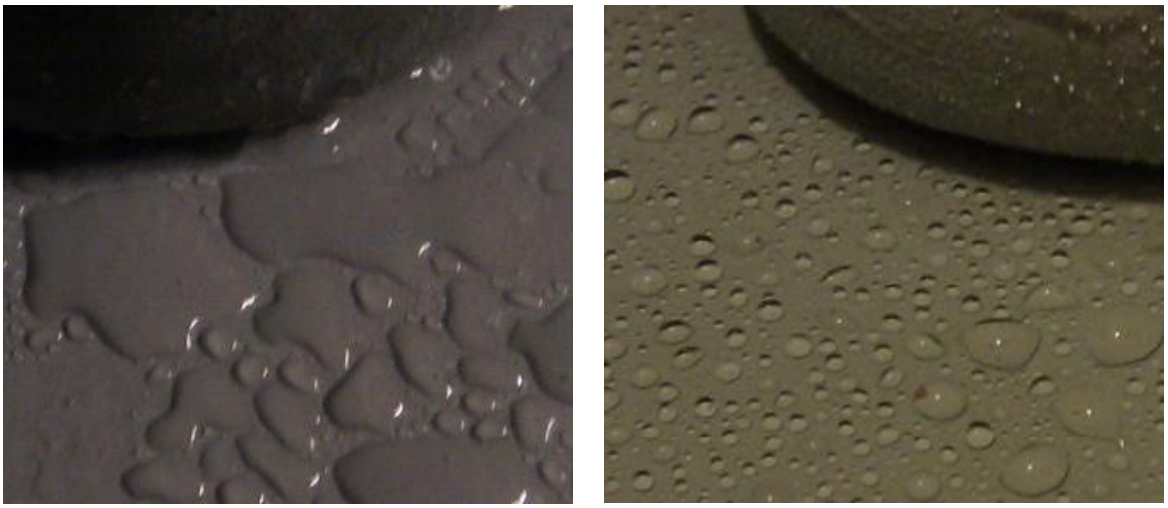

(a) Coated insulator with water patches (b) Coated insulator with water droplets

Figure 6.11: Real life wetting patterns of coated ceramic insulators

Peaks can be seen in the rate of change of the tangential electric field at both the HV electrode and the ground electrode. These peaks confirmed the equipotential results concerning the high field regions as in Figure 6.9. However, away from the metal fittings along the surface distance of the insulator, the gradient of the tangential electric field for all four test conditions was reduced to a lower, more or less constant value with undulations on the tangential electric field profile caused by the equipotential lines crossing the surface of the insulator.

In the case of the uncoated dry clean insulator, the plot showed the highest electric field strength was at the end fittings with a value of 260 V/mm at a surface distance of 280 mm, which is very close to the HV electrode.

For the uncoated uniformly polluted insulator, the surface distance was increased, and the field calculations were over a greater surface distance and the field calculations were from the cap to the pin of the insulator. Once again, the rate of change of voltage was greatest at the electrodes, but particularly at the HV electrode. The maximum calculated value was 620 V/mm at the HV electrode, more than double the value for the dry clean insulator.

In the case of the uncoated insulator, non-uniformly polluted with water patches the overall plot was very similar to that for the uncoated uniformly polluted insulator rising to the same peak value of 620 V/mm at the HV electrode. However, there were some

disturbances in the high field region near the HV electrode as a result of the water patches.

The effect of adding water droplets to the uniformly polluted uncoated insulator near the electrodes was clearly seen in Figure 6.10. The electric field strength was highly disturbed especially near the HV electrode where the highest peak value was 880 V/mm, showing a substantial increase of more than 30% compared to the uncoated uniformly polluted insulator and uncoated non-uniformly polluted insulator with water patches.

6.3.3. Electric field distribution along coated insulators

For comparison, the coated insulator was simulated under identical conditions to the uncoated insulator. Figure 6.12 shows the tangential electric field results along surface distance of the coated insulator. The rate of change of the magnitude of the tangential electric field of the coated insulator under dry clean conditions was generally low, with highest values of 260 V/mm at the HV electrode and 340 V/mm at the ground electrode. The peak magnitude of the tangential electric field for the coated insulator with uniform pollution was higher; 640 V/mm at the HV electrode and 410 V/mm at the ground electrode. These represented more than a doubling at the HV electrode with a 20% increase at the ground electrode. The increase in tangential electric field strength was correlated to the calculations that were considered over a greater surface distance along the cap and pin insulator profile.

The high field intensity leads to the initiation of dry band arcs. These arcs disturb the applied voltage and so the tangential electric field components are also affected. The partial arc activities cause further drying to the surrounding pollution layer and stop as the dry region increases [6.11].

6.3.3.1. Effect of water droplets on electric field distribution along coated insulators

The effect of water droplets of diameter of 0.5 mm and a density of 1g/cm^3 scattered around the HV electrode and the ground electrode on the electric field distribution is shown in Figure 6.11. It is clearly seen that, the tangential electric field increased sharply to high values with peaks of 1800 V/mm at the HV electrode and 780 V/mm at the ground electrode.

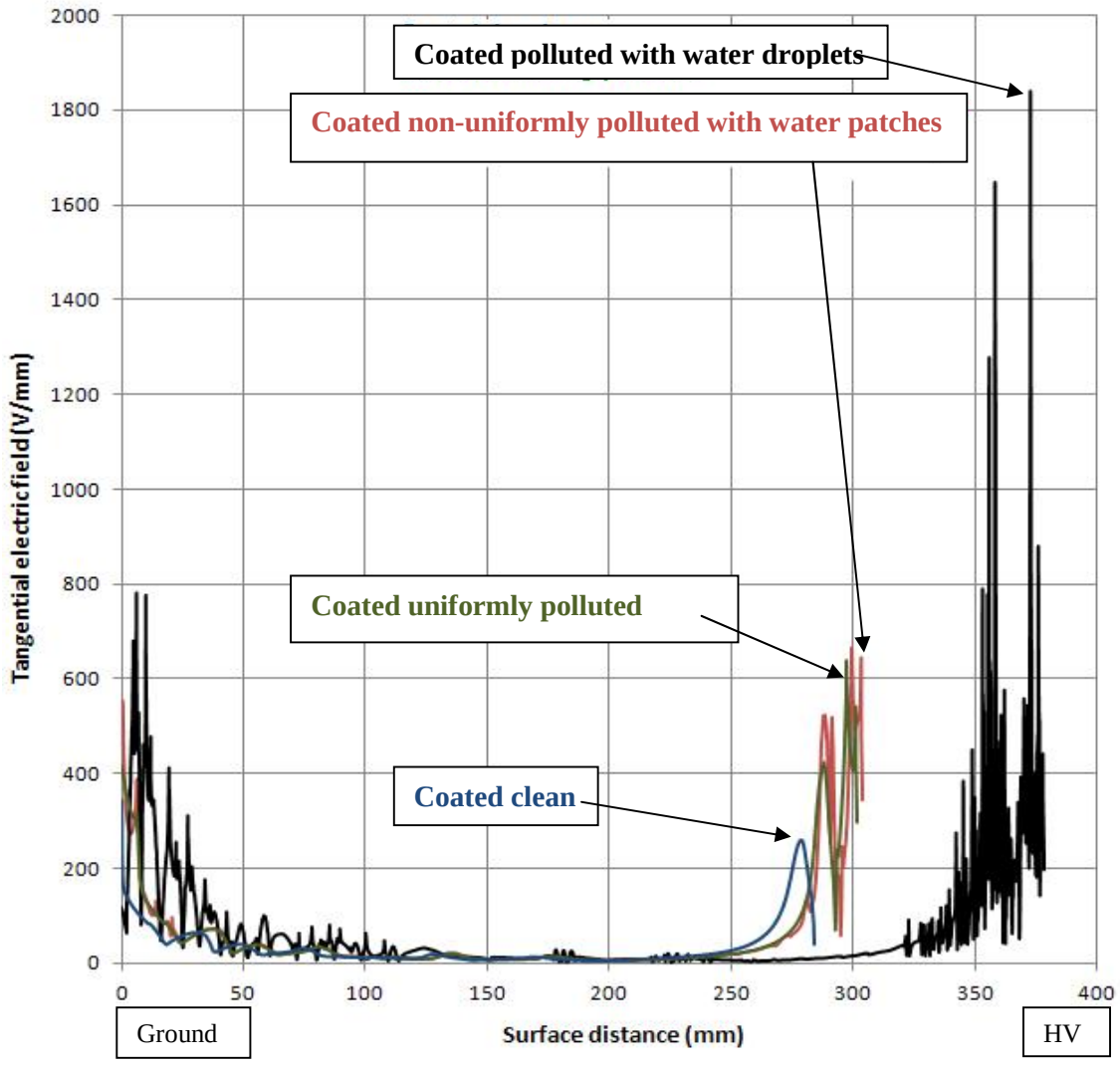

Figure 6.12: Tangential field with leakage distance along coated insulator: dry clean, uniformly polluted, non-uniformly polluted with water patches, uniformly polluted with scattered small water drops

The reason for this is that water droplets deform the electric field and give a field enhancement at the edge of the droplet, which eventually results in a loss of surface hydrophobicity. As a result, the water droplets come together to form larger water drops and then water patches before developing into water filaments.
The effect of droplets on maximum tangential electric field values when compared to the case of coated clean dry surface was a huge increase from 260 V/mm to 1800V/mm at the HV electrode, resulting in an increase in the maximum tangential electric field by 180% at the HV electrode.

6.3.3.2. Effect of larger water drops on electric field distribution along coated insulators

When small droplets in the range of 0.5mm to 1.0mm were present near the electrode areas on the insulator surface, the electric field strength reached its highest values. Such high field magnitudes if increased to higher magnitudes will lead to the formation of dry band arcs. The heat generated from these arcs consumes the silicone fluid and results in loss of hydrophobicity in the high field regions. As hydrophobicity is lost, small droplets of water come together to form bigger drops at the electrodes before forming patches of water which grow to form a film on the surface of the coated insulator.
The same coated insulator was modelled with bigger droplets having diameters ranges from 1.0 mm to 3.0 mm at the HV electrode and the ground electrode. A decrease in the maximum electric field was observed with increase in droplet size, see Figure 6.13.

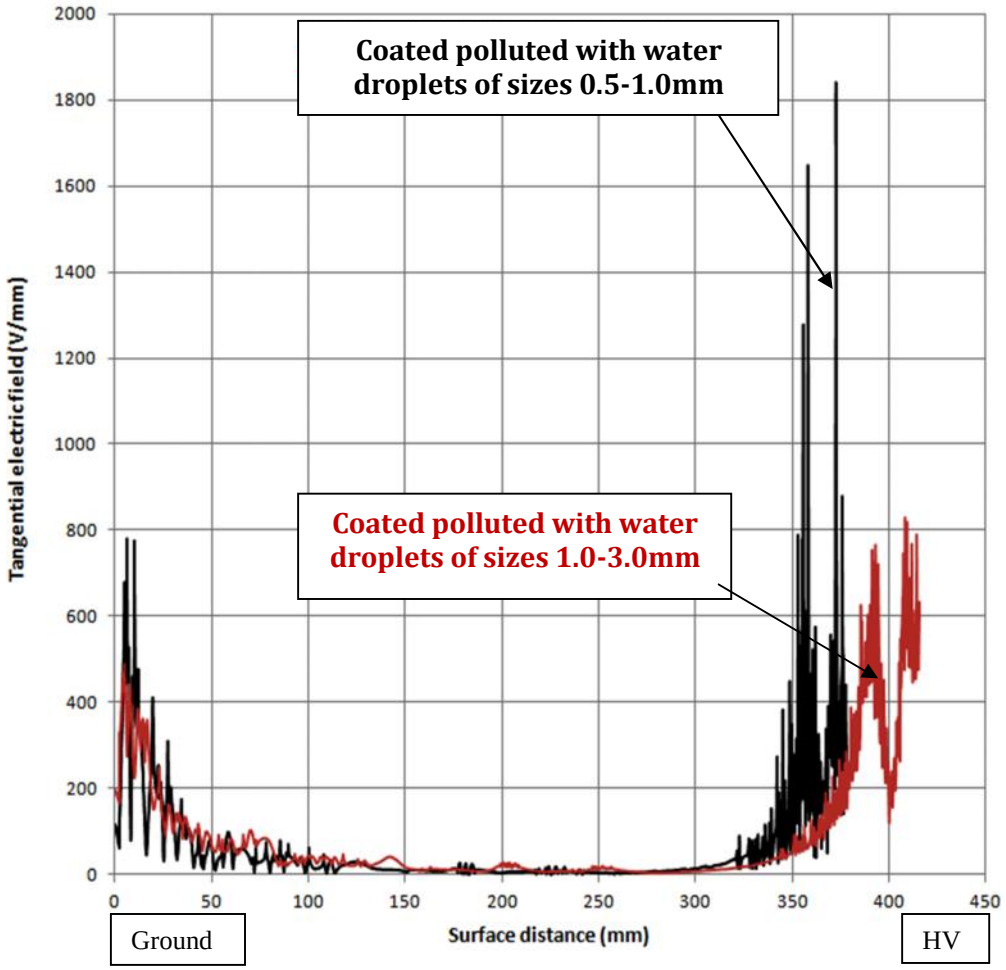

Figure 6.13: Tangential field with leakage distance of coated insulator; coated insulator non-uniformly polluted with small water drops on surface, coated insulator non-uniformly polluted with large water drops on surface

The presence of the larger droplets reduced the maximum electric field strength by 55% at the HV electrode and by 38% at the ground electrode compared with the small water droplets. This result confirms the work of El-Kishky et al. [6.11] which showed that, the maximum electric field strength is related to the increase in size of water droplet.

Droplets, irrespective of their sizes, are subjected to severe field intensification near the HV electrode. With an increase in the droplet size the electrostatic energy increases, and for the same size of the droplet, the energy is higher if it is closer to the HV electrode. Thus, larger size droplets can lead to more intensive discharges than smaller droplets, especially if they are close to the HV electrode. The fact that droplets near the HV electrode quickly lead to discharges is again confirmed by the findings of El-Kishky et al [6.11].

6.3.3.3. Effect of single water droplets on electric field distribution along clean coated insulator.

In the previous sections, the effect of water droplets near the electrode regions on the tangential electric field distribution was presented. This section, studies the effect of a single droplet near the HV electrode region on the tangential electric field distribution. The electric field is calculated as in Figure 6.14; (a) along the edge profile including the water droplet, and (b) Along the edge and the droplet profile.

The tangential electric field for the coated clean insulator peaked at the HV electrode with 260 V/mm as was shown in Figure 6.11. However, the strength of the tangential electric field along the edge profile including the water droplet almost reached the same peak, but with field disturbance as can be seen in Figure 6.14 (a). While the tangential electric field strength along edge and droplet profiles reaches a peak with a value of 500 V/mm as can be seen in Figure 6.14 (b). This increase is attributed to the electric field inside the water droplet is higher than its value outside the droplet as the permittivity and electrical conductivity of the droplet is higher than those for the air surrounding the droplet, and the current density is directly proportional to the electrical conductivity of the medium.

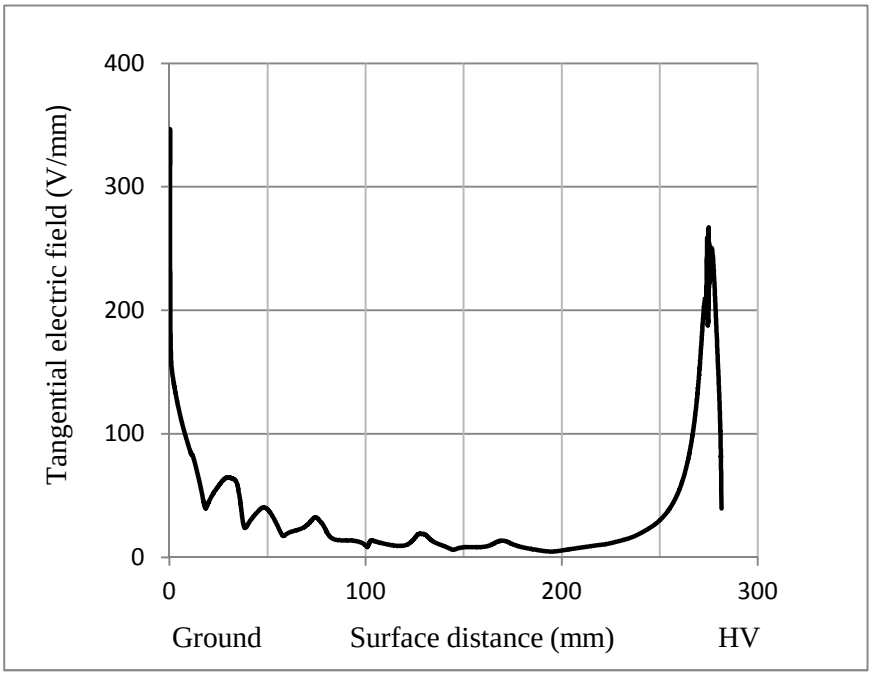

(a) Along edge profile including water droplet

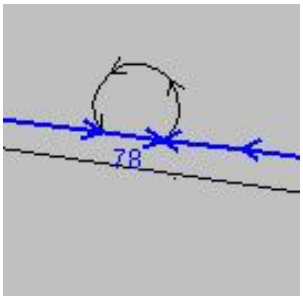

Simulation in Comsol

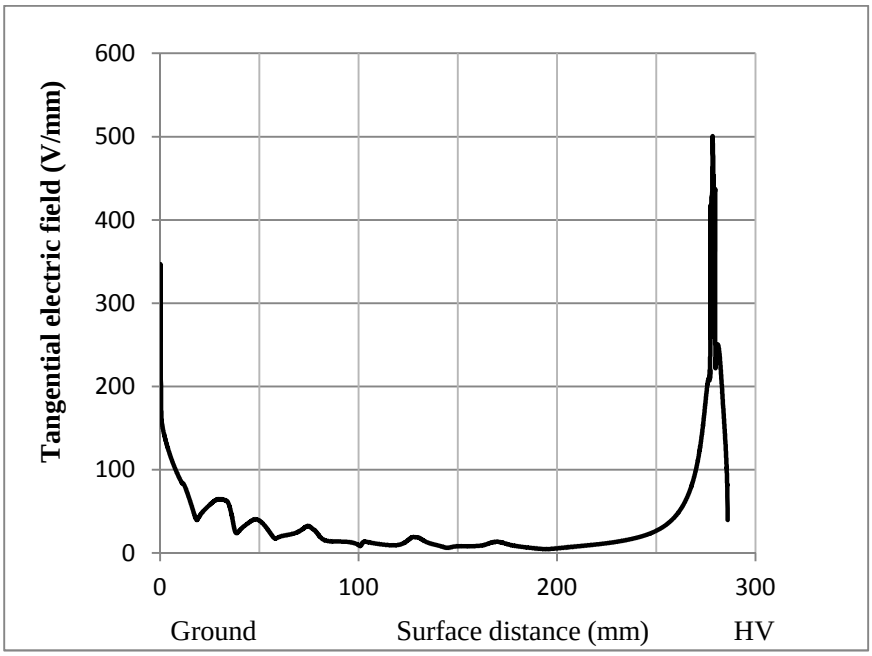

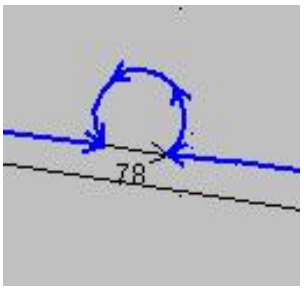

Simulation in Comsol

(b) Along edge and droplet profile

Figure 6.14: Tangential field along clean coated insulator

6.3.4. Power dissipation in the pollution layer of coated insulator

The tangential components of the electric field are the main reason in developing the surface leakage current in the wetted pollution layer. These currents will cause power dissipation leading to resistive heating in the pollution layer which, as a result, will lead to the formation of dry band arcs. The power dissipation in a thin pollution layer of thickness, t_{poll}, per unit surface area along the insulator surface was derived in [6.12]:

$$P_{\Omega} = \sigma \ E_t^2 \times t_{poll} \qquad 6.1$$

where

E_t : is the tangential electric field (V/mm).

t_{poll} : thickness of the pollution layer as it is assumed to be uniform along the surface path (mm).

σ : the conductivity of the pollution layer as it is assumed to have the same value along the surface path (S/m).

The power dissipated in the pollution layer along the surface distance of the coated polluted insulator is shown in Figure 6.14 and calculated using Equation (6.1) and the tangential electric field values of the uniformly polluted coated insulator of Figure 6.12.

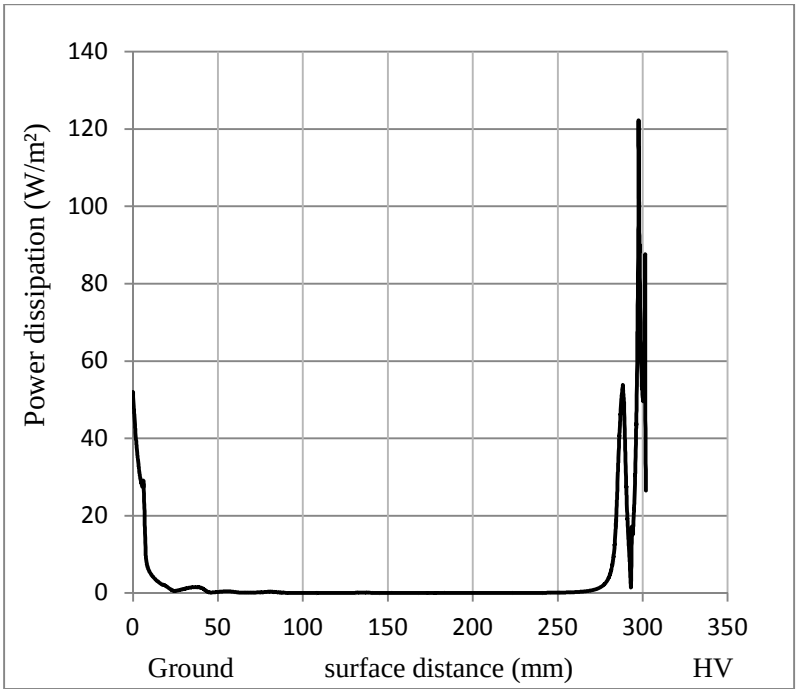

Figure 6.15: Surface power dissipation in the pollution layer along the coated insulator surface

Figure 6.15 shows two dissipated power peaks near the metal electrodes in the same locations where the highest tangential electric field peaks occurred. In these high power dissipated areas and during the lower wetting rate, the formation of dry bands is unavoidable due to the long-lasting heating effect. This continuous heat destroys the hydrophobicity of the coated insulator, and leads to degradation of the coating on the long term.

6.4. Conclusions

The electric field and the voltage distribution along the surface of coated and uncoated ceramic insulators, clean and polluted have been studied using the COMSOL® Multiphysics finite element analysis and solver package.

The coating layer was simulated as 0.5 mm thick, and the uniform pollution layer was assumed 0.5 mm thick. A non-uniform pollution layer was simulated in the form of pollution patches and as water droplets having diameters ranging from 0.5 mm to 3.0 mm. The surface water on a pollution layer was simulated as having the properties of the pollution itself; this is because in the laboratory tests, the pollution layer was thoroughly wetted with fog.

The electric field along the surface distance of dry clean insulators was generally very low but significantly increased near the electrode regions. The same observations applied to uniformly polluted insulators.

The electric field at the HV electrode of the coated insulator in the presence of small droplets of water increased to high values which can lead to discharges in this region. These discharges may lead to loss in hydrophobicity and eventually to water filming on the surface of the insulator, and may result in flashover.

The electric field is a function of droplets size, and their location with respect to the HV electrode. As the droplet size increased, the electric field decreased to values comparable to that of the uniformly polluted insulator.

The dissipated power on the surface of the wet polluted insulator is directly proportional to the strength of the electric field, particularly, the tangential electric field. This field component is responsible for the developments of the surface leakage current leading to resistive heating in the pollution layer which, in turn, is responsible for the formation of dry band arcs.

These calculations showed that the coated insulator experiences higher electric field strength near the HV electrode than that of the uncoated insulator, especially, in the presence of water droplets near the electrode regions. This provides useful information about surface heating that can be used to predict dry band formation along the leakage path. The coated insulator showed superior performance in comparison with the uncoated insulator under the artificial pollution tests in the fog chamber, under the same wetting and pollution conditions. However, under long lasting dry band arcs,

particularly, at the high field regions, the coating material will lose its hydrophobicity which lessens the performance of coated insulators, but not lower than the performance of the un-coated insulators.

These results showed that, the coated insulators are subject to higher electric field magnitudes than the porcelain insulators. The tangential component of the electric field in particular is responsible for the current leakage on the surface of the insulator. These currents in the long term lead to loss of hydrophobicity of the surface. The loss of hydrophobicity puts the insulator at risk of flashover under polluted environmental conditions.

Chapter 7 - General Discussion and Conclusions

The main objectives of the work reported in this thesis were to determine a better understanding of the evaluation criteria for the performance of coatings used for the outdoor HV insulators, and the development of an effective approach for controlling electric field stress on the surface of the HV outdoor insulators.

The performance of the coatings used in this thesis was evaluated through extensive experimental investigation, alongside electric field computational modelling. An overview of the research work findings and major conclusions drawn from the studies undertaken, and recommendations for future research work are presented in this chapter.

Many hydrophobic coatings have been applied to conventional high voltage outdoor insulators to improve their surface hydrophobicity and, therefore, their electrical performance under wet and polluted weather conditions. Some hydrophobic coatings had been investigated in the laboratory and the conclusions are presented in this chapter.

The laboratory tests throughout this work involved challenges that needed to be overcome. These difficulties are including preparing and understanding the test setup of the fog chamber and the inclined plane test facility, and in designing a computer program as part of the data acquisition system (DAQ) that is responsible for the data acquisition during the tests in a way that no data loss had occurred, and in controlling the voltage application to the tested samples and terminating the test for certain criteria.

The coating systems were investigated under the artificial pollution tests using the solid layer method of IEC60507, and the material's tracking and erosion resistance was examined using the inclined plane test according to IEC60587.

A symmetrical 2D model of a standard cap and pin porcelain insulator using COMSOL® Multiphysics software package was developed for computational modelling. Simulations for coated and uncoated insulators with dry clean and wet-polluted surfaces were also performed.

7.1. Clean-fog tests

In the artificial pollution test method, polluted insulators were exposed to clean fog. This method was internationally used with ceramic insulators and is not intended to be used with insulators having hydrophobic surface properties, particularly, insulators coated with room temperature vulcanising (RTV) silicone rubber, and with Nanocoating. This property does not allow the adherence of the pollution to the surface of the coated insulators. However, a proposed test procedure for clean-fog tests of ceramic insulators coated with polymeric materials was used based on the solid layer method for ceramic insulators. It includes the addition of non-ionic wetting agent in the kaolin pollution suspension. This has been introduced and used in dealing with insulators having hydrophobic surface property.

The test insulators were cap and pin porcelain insulators with different creepage distances. The Nanocoated insulator has a creepage distance of 430 mm while the uncoated insulator has a creepage distance of 470 mm. Standard porcelain insulators with a creepage distance of 300 mm were coated with two different types of RTV silicone rubber coatings from two different suppliers, while two other porcelain insulators were coated with silicone grease and hydrocarbon grease with an identical set of porcelain insulators left uncoated. These porcelain insulators were tested along with the coated insulators in the fog chamber for comparison reasons. Flashover voltage of insulators under dry, clean wet and pollution conditions were investigated. In addition, the effect of Ultra Violet (UV) radiation on the coated insulators was also investigated under the artificial pollution test conditions. The hydrophobicity of the coated insulators was checked after the artificial pollution tests and after UV exposure.

The experimental work was enhanced by developing computerised procedures for monitoring different insulators under test. A data acquisition system was developed and used with the fog chamber facility. LabVIEW software from National Instruments was used to control the data acquisition, and Producer/Consumer architecture was implemented to manage the capture of the leakage current and voltage waveforms during the tests and to save these data in accessible file formats. A data analysis program was developed using LabVIEW to read the saved data and to find measurable quantities as derivatives of leakage current and test voltage that may be used as diagnostic indicators for the performance of the coating systems.

7.1.1. Clean-fog tests conclusions and discussions

All the coating systems applied to the porcelain insulators were found to reduce the leakage current significantly. The Nanocoated insulator, when applied on the surface of an uncoated insulator reduced the leakage current by 90%. As a result of this current reduction, the dissipated energy was also reduced 98%.

Newly applied Nanocoating showed good hydrophobic surface property. However, under wet tests, Nanocoated insulator wet readily and exhibited hydrophilic surface property. This leads to poor pollution flashover voltage performance and resulted in a lower flashover voltage than that of the uncoated insulator of similar creepage distance and those treated with silicone materials with shorter creepage distances. The poor pollution flashover performance of the Nanocoated insulator maybe attributed to the property of generation and diffusion of low molecular weight silicone fluid from the bulk of the coating to the surface which is responsible for maintaining the surface hydrophobicity. The Nanocoating lacks this property as it is a solid nano scale layer, which becomes wet when exposed to fog application. When exposed to 8 hours UV radiation in the Suntest machine, which is equivalent to 350 hours exposure to natural sun light, the Nanocoated insulator showed good stability in terms of minimizing leakage current on its surface. Furthermore, after sand blast exposure, the Nanocoated insulator showed good resilience to sand blasting. However, with long exposure to sand blast, the surface began to show evidence of visible pockmarks on its surface. These pockmarks were found to lower the performance of the Nanocoated insulator under polluted test conditions by 50% compared with new Nanocoated insulator.

The insulators coated with silicone coatings like RTV1, RTV2, and silicone grease reduced the leakage current by 92%. This reduction resulted in less dissipated energy on the surface of the coated insulator by 99%. Moreover, the silicone grease increased the pollution flashover voltage by 60% when compared to uncoated insulator. RTV1 and RTV2 coated insulators also increased the pollution flashover voltage by 40% and 50%, respectively. The difference in the flashover voltage levels of the insulators coated with silicone materials is attributed to the differences in the material compositions of each coating. RTV coatings were also exposed to 8 hours UV radiation in the Suntest machine. RTV coatings showed resistance to UV radiation and performed as good as the situation where the coating had not been exposed to UV radiation, namely in reducing the leakage

current under the artificial pollution tests, and in showing high surface hydrophobicity with contact angles greater than 110°. This improved performance may be attributed to the type of stabilizers used in the coating formula which act to inhibit degradation of the polymer. Moreover, the heat generated from the UV light increases the diffusion process of the silicone fluid from the bulk of the coating to the surface which improves the hydrophobic surface property.

7.2. Inclined plane tests

The inclined plane test method, described in IEC60587 is a method for evaluating the performance of the insulating materials against tracking and erosion induced by surface discharges. Porcelain tiles were cut into a rectangular shape with dimensions 120 mm × 50 mm, and coated with the two RTV materials used in the fog chamber tests. The samples were mounted in the inclined plane machine at an inclined angle with contaminant solution of water and ammonium chloride and a non-ionic wetting agent flowing on their surfaces while stressed with the specified test voltage level. The samples were tested under three test voltage levels 2.5kVrms, 3.5kVrms and 4.5kVrms. The performance of the RTV coatings were also investigated at the same voltage levels after exposure to 2 and 8 hours of UV radiation.

At a test voltage of 2.5kVrms, both coatings have shown resistance to tracking and erosion, RTV2 showed signs of tracking and some erosion while RTV1 showed fewer tracks and almost no erosion. Both coatings showed similar rms current levels, however, RTV2 showed slightly more dissipated energy. At a test voltage of 3.5kVrms, both coatings showed similar r.m.s current levels and identical loss energy. However, RTV2 showed more erosion than RTV1. While at a higher test voltage of 4.5kVrms, both samples had severely eroded. Although, RTV1 showed higher loss energy, RTV2 underwent more erosion. The criterion used to terminate the test was based on the current level flowing across the samples: the current should not exceed 60 mA for 2 s. Both samples have passed the test since the current on their surfaces did not reach the threshold value of ending the test.

The performance of these coatings was also investigated after 2 hours UV exposure. At test voltages of 2.5 kVrms, both coatings have shown good performance with similar r.m.s current magnitudes. However, RTV2 showed higher energy loss and more

damaged surface. At 3.5 kVrms, both coatings experienced the same level of currents. RTV1 showed almost no signs of tracking or erosion, whilst, RTV2 was eroded. This may be attributed to the different UV stabilizer and to the type of filler used in their formulations. Specific information of the properties of coatings used in the thesis was not made available by the suppliers due to commercial sensitivity. With increased test voltage to 4.5 kVrms, although both samples passed the test, the both were eroded. However, RTV1 showed less dissipated energy.

After 8 hours UV exposure and test voltage of 4.5 kVrms, RTV1 coating showed dissipated energy comparable and almost identical to that of the sample exposed to 2 hours UV radiation, and showed less damage to the surface than the samples exposed to 2 hours UV and the sample with no UV exposure.

7.3. Computation of electric field along insulator surface

The finite element analysis and solver software package, COMSOL Multiphysics®, was used to calculate the tangential electric field strength and voltage distribution along the surface of coated insulators under different operational conditions.

The coating layer was simulated as 0.5 mm thickness and the pollution layer was simulated as a uniform pollution layer of 0.5 mm thickness and as patches of 0.5 mm thickness distributed on the surface of the coated and uncoated insulators. Water droplets with different diameters ranging from 0.5 mm to 3 mm as non-uniform pollution layer distributed along the surface and around the metal fittings were also simulated.

Invariably, the electric field was at a maximum peak at the HV electrode with a secondary peak at the ground electrode. Furthermore, it was found that the electric field strength was a function of the size of the droplets and their location with respect to the HV electrode. The presence of droplets around the HV electrode increased the electric field of the coated insulator by 180% when compared to the case when the insulator was uniformly polluted. These high field strength values lead to the formation of discharges in the electrode regions. These discharges are responsible for the loss of hydrophobicity of the coating. However, in the HV electrode region as the droplet size increased the electric field strength decreased. The maximum electric field strength is related to the increase in size of water droplets. The results showed also that the electric field strength on the uncoated insulator was lower than that of the coated

insulator. However, under the pollution tests, the performance of the coated insulator was superior to that of the uncoated insulator.

Water-drop discharges may lead directly to complete flashover. Even if this does not occur, however, it may lead to loss of hydrophobicity. As hydrophobicity is lost droplets join together to form a water film on the surface of the insulator, and the consequent leakage current will cause localized drying of the surface which leads to the initiation of dry band arcing. Flashover of the coated insulator becomes inevitable in this case.

Intense and continuous water-drop discharges can destroy the hydrophobicity and gradually consume the insulation surface through tracking and erosion. In practice, signs of material degradation due to electric discharges were manifested as surface crazing, cracking and discoloration. In some cases, the insulator may show the appearance of chalky white traces, attributed to the ATH fillers diffusing to the surface.

In this study, protective coatings were applied to the porcelain insulators as to minimise flashover under pollution conditions. The coatings reduced the current magnitudes and eliminate the dry band arcing activities. The coatings showed good resistance to tracking and erosion resulting from the current discharges and their accompanied generated heat.

As a result of these outcomes, if applied to the HV outdoor insulators in severe weather conditions, these protective coatings will minimise the current activities and reduce the power dissipation which results in less heat on the surface of the coated insulator. This in turn leads to less dry band arcing and leads to longer coating life. The ability of the coatings to resist tracking and erosion will be significantly improved because of the migration of the silicone fluid from the bulk to surface of the coatings which help in maintaining the surface hydrophobicity and reducing the heat generated from the current discharges.

In general, the coating systems will improve the performance of the outdoors HV insulators by (a) reducing the flashover incidence, and (b) minimising the total energy loss which improves the efficiency of the power system as a whole.

7.4. Recommendations for future work

In this study, different coatings like Nanocoating, RTV and grease which are used as protective coatings for high voltage insulators, were investigated in the laboratory. However, there are still aspects which may affect the performance of these coatings, and more research is suggested to optimize the performance of the protective coatings.

1. More test methods like salt fog tests would provide supplementary results to the clean fog test results. The tracking wheel facility can also be used to assess the ability of different coating systems to resist erosion and tracking in addition to the IPT tests performed in this study
2. Simulations of natural outdoor conditions, for instance, when coatings are exposed to very low temperature due to snow and ice. Coatings are also used in areas where the temperature fluctuates between day and night, and in areas where coatings are exposed to dust accumulation and sand storms in desert environments.
3. Since HVDC transmission systems are used in service, and due to its unidirectional electric field on the surface, insulators can accumulate contaminants more than those accumulated when working under AC systems. The performance of the insulators under pollution conditions, the flashover voltage, the surface erosion under DC electric stress are possibly different compared to insulators working under AC energisation.
4. Coatings could offer considerable saving over other existing maintenance methods used for insulators maintenance. In the literature, 0.5 mm thickness for RTV coating was reported as the optimum thickness for better performance. If the coatings could be investigated under less coating thicknesses, it would be beneficial to reduce the amount of coating used and the associated labour costs.

   The variables that determine what method is best for a given coating measurement include the type of coating, the substrate material, and the thickness range of the coating. Commonly used measuring techniques include non-destructive dry film methods such as magnetic, eddy current, ultrasonic, or micrometer measurement and also destructive dry film methods such as cross-

sectioning or gravimetric measurement. One of these methods could be used to determine the optimum coating thickness.

5. Developing a 3D FEM modelling is necessary to understand the effect of the practical configurations and the metal attachments of the towers for a better and more realistic electric field computation and analysis. The effect of water droplet shape on the distortion of the electric field along coated and uncoated insulators can also be achieved with 3D modelling.
6. Study of degradation and ageing of outdoor protective coatings resulting from UV exposure is a potential research area which could help to assess long-term coating performance under normal weather conditions. The time of exposure to UV radiation in these experiments is very short compared with the outdoor operating condition. More tests need to be performed in correlation with field service conditions as the insulators are exposed for longer periods of time to direct sunlight.
7. The tracking wheel facilities in Cardiff University could also be used to assess the ability of coated insulators to resist erosion and tracking. Such tests will provide complimentary data on the anti-erosion and anti-tracking performance of RTV coatings.
8. Artificial test procedures in the laboratory are based on theoretical approaches and assumptions and cannot really reflect the actual field operating conditions unless continuously correlated with field operating experiences. In this way, the actual field operating condition is said to be fulfilled.
9. Dry band arcing produces high temperature hot spots which may directly dissociate the chemical bonds at the surface of the coating. The heat produced from dry band arcing causes hydrolysis, scission and interchange of the siloxane bonds. The significant changes of the surface resulted in increased oxygen in the Si-O bonding of the silicone chain. Increased oxygen is responsible for forming hydrogen bonding between RTV and water resulting in a rabid loss of hydrophobicity. Few studies report the life time of RTV coatings based on thermal degradation, and thermal degradation is not suitable to estimate the life time of RTV coatings because of the diffusion of LMW silicone fluid. Therefore it is suggested to develop a new technique to estimate the life time of RTV coatings.

References

[1.1] Looms, J. S. T., Insulators for High Voltages, London: The Institution of Electrical Engineers, 1988.

[1.2] Mishra, A. P., Gorur R. S., and Venkataraman S., "Evaluation of Porcelain and Toughened Glass Suspension Insulators Removed from Service," *IEEE Transaction on Dielectrics and Electrical Insulation, Vol. 15, pp. 467-475, 2008.*

[1.3] Hackam, R., "Outdoor HV composite polymeric insulators," *IEEE Transactions on Dielectrics and Electrical Insulation*, vol. 6, pp. 557-585, 1999.

[1.4] Gorur, R. S., Cherney, E. A., Hackam, R., and Orbeck, T.,"The electrical performance of polymeric insulating materials under accelerated aging in a fog chamber," *IEEE Transactions on Power Delivery, vol. 3, pp. 1157-1164, 1988.*

[1.5] Mackevich, J., and Simmons, S.,"Polymer outdoor insulating materials. II. Material considerations," *IEEE Magazine on Electrical Insulation*, vol. 13, pp. 10-16, 1997.

[1.6] Gorur, R. S., Cherney, E. A., de Tourrcil, C., Dumora D., Harmon R., and Hervig H., "Protective coatings for improving contamination performance of outdoor high voltage ceramic insulators," *IEEE Transactions on Power Delivery*, Vol. 10, No. 2, April 1995.

[1.7] Crespo-Sandoval, J., "Condition Monitoring of Outdoor Insulation using Artificial Intelligence Techniques," PhD Thesis, University of Wales Cardiff, 2005.

[1.8] Gorur, R. S., and Olsen, R.,"Prediction of Flashover Voltage of Insulators Using Low Voltage Surface Resistance Measurement," PSERC Publication 06-42, Nov. 2006. http://www.pserc.wisc.edu/documents/publications/reports/2006_reports/ (Accessed on 2011).

[1.9]Kim, S. H., Cherney, E. A., and Hackam, R.,"The Loss and Recovery of Hydrophobicity of RTV Silicone Rubber Insulator Coatings," *IEEE Trans. PD*, Vol. 5, pp. 1491-1499, 1990.

[1.10] Gorur, R. S., Sundhara, S., and Amburgey, O. G.,"Contamination performance of polymeric insulating materials used for outdoor insulation applications," *IEEE Trans. Electrical Insulation,* Vol. 24, No. 4, pp. 713-716, Aug. 1989.

[1.11] Kimoto, I., Kito, K., and Takatori, T., "Anti-pollution design criteria for line and station insulators," IEEE paper 71 TP649-PWR, pp.317-327,1971.

[1.12] Gorur, R. S., Cherney, E. A., de Tourrcil, C., Dumora D., Harmon R., and Hervig H., "Protective coatings for improving contamination performance of outdoor high voltage ceramic insulators," *IEEE Transactions on Power Delivery*, Vol. 10, No. 2, April 1995.

[1.13] Kim, S. H., Cherney, E. A., and Hackam, R.,"Suppression mechanism of leakage current on RTV coated porcelain and silicon rubber insulators," *IEEE Transactions on Power Delivery*, Vol. 6, No. 4, October 1991.

[1.14] Ratner M. and Ratner D, "Nanotechnology: A Gentle Introduction to the next Big Idea", Pearson Education, 2003.

[1.15] Akhilesh, K., Watve, N." Assessment of nanoscience and nanotechnology initiatives in India," Portland International Conference on Management of Engineering & Technology, 2009.

[1.16] Lewis, T. J., "Nanometric Dielectrics," IEEE Trans. Dielectr. Electr. Insul., Vol. 1, pp. 812–825, 1994.

[1.17] Yasuhiro Tanaka, Yuji Hayase, Hiroyuki Aoyama, Tatsuo Takada," Space Charge Formation in LDPE/MgO Nano-composite Thin Film under Ultra-high DC Electric Stress," International Conference on properties and applications of Dielectric Materials 8th, 2006.

[1.18] El-Hag, A. H., Simon, L. C., Jayaram, S. H., and Cherney, E. A.,"Erosion resistance of nano-filled silicone rubber," *IEEE Transactions on Dielectrics and Electrical Insulation,* Page(s):122-128, 2006.

[1.19] Montanari, G. C., Fabiani, D., Palmieri, F., Kaempfer, D.," Modification of electrical properties and performance of EVA and PP insulation through nanostructure by organophilic silicates," IEEE Transactions on Dielectrics and Electrical Insulation 2004 , Page(s): 754 - 762

[1.20] SUMEREDER, C., MUHR, M.," The prospects of nanotechnology in electrical power Engineering," 19th International Conference on Electricity Distribution. Vienna, 21-24 May 2007. Paper 0594. CIRED2007.

[1.21] IEC 60507, 1993, "Artificial pollution tests on high-voltage Insulators to be used on A.C. systems," May 1993.

[1.22] IEC 60587:2007, "Electrical insulating materials used under severe ambient conditions. Test methods for evaluating resistance to tracking and erosion," 2007.

[2.1] Conner, J. E., and Lantz, A. D., "The Insulator Contamination Problem as Influenced by Silicone Surface Coatings," *Trans. on Power Apparatus and Systems, Part III. American Institute of Electrical Engineers*, 1958.

[2.2] CIGRE Committee 22, Subworking Group 03-01, "Worldwide Service Experience with HV Composite Insulators, Electra No. 130, 1989.

[2.3] Starr, W. T., "Polymeric Outdoor Insulation," *IEEE Trans. Electrical Insulation,* Vol. 25, pp. 125-136,1990.

[2.4] Cherney, E. A., and Stonkus, D. J., "Non-Ceramic Insulators for Contaminated Environments," *IEEE Trans. Electrical Insulation*, Vol. 100, pp. 131-142, 1981.

[2.5] de Oliveira, S.M, and de Tourreil, C H. "Aging of distribution composite insulators under environmental and electrical stresses," *IEEE Transactions on Power Delivery*,1990.

[2.6] Hackam, R.,"Outdoor HV composite polymeric insulators," *IEEE Trans. Dielectr.Electr.Insul.*, vol.6, no.5, pp.557–585, Oct.1999.

[2.7] Gorur, R. S., Cherney, E. A., de Tourrcil, C., Dumora D., Harmon R., and Hervig H., "Protective coatings for improving contamination performance of outdoor high voltage ceramic insulators," *IEEE Transactions on Power Delivery*, Vol. 10, No. 2, April 1995.

[2. 8] CIGRE Task Force 33.04.01, 'Polluted Insulators: A review of current knowledge', 2000.

[2.9] Hampton, B.F., 'Flashover mechanism of polluted insulation', Electrical Engineers, Proceedings of the Institution of, Vol. 111, (5): pp. 985-990, 1964.

[2.10] Gonos, I.F., Topalis, F.V., Stathopolos, I., "Genetic algorithm approach to the modelling of polluted insulators," IEE Proceedings on Generation, Transmission and Distribution, Page(s): 373 – 376, Year: 2002.

[2. 11] Gorur, R. S., Chang, J., and Amburgy, O. G., "Surface hydrophobicity of polymers used for outdoor insulation," *IEEE Transactions on Power Delivery,* Vol. 5, No. 4, pp 1923 - 1933. October 1990.

[2.12] Siderakis, K., Agoris, D., and Gubanski, S., "Influence of heat conductivity on the performance of RTV SiR coatings with different fillers," J. Phys. D: Appl. Phys. 38 (2005).

[2.13] Cherney, E. A., and Gorur, R. S., "RTV silicone rubber coatings for outdoor

insulators," *IEEE Transactions on Dielectrics and Electrical Insulation*, Page(s): 605 – 611, 1999.

[2.14] IEEE Std 1523, "IEEE Guide for the Application, Maintenance, and Evaluation of Room Temperature Vulcanizing (RTV) Silicone Rubber Coatings for Outdoor Ceramic Insulators," 2002.

[2.15] Gorur, R. S., and Orbeck, T., " Surface dielectric behavior of polymeric insulation under HV outdoor conditions," *IEEE Transactions on Electrical Insulation*, pp 1064 – 1072, 1991.

[2.16] Forrest, J. S., Lambeth, P. J., and Oakeshott, D. F., "Research on the performance of high-voltage insulators in polluted atmospheres," *IEE Proc.,* pp. 172-187,1960.

[2.17] Lambeth P. J., "Effect of pollution on outdoor high voltage insulators," *Proceedings of the Institution of Electrical Engineers*, 1971.

[2.18] Forrest, J. S., "Electrical Properties of Semi-Conducting Ceramic Glazes," Journal of Scientific Instruments, 1947, p. 211.

[2.19] Moran, J. H., and Powell, D. G., "Resistance Graded Insulators - The Ultimate Solution to the Contamination Problem," *IEEE Transactions on Power Apparatus and Systems,* Page(s): 2452 – 2458, 1972.

[2.20] Matsui, S., Suzuki, Y., Nakashima, N., Kasaki, F., Fujii, O., and Matsuda, E., "State of the Art of Semiconducting Glazed Insulators for Transmission Lines in Heavily Contaminated Area," *Proc.5th Intern. Conf. Properties and Applicalions of Dielectric Materials, Seoul, South Korea*, pp. 726-729, 1997.

[2.21] Shinoda, A., Okada, H., Nakagami, M., Suzuki, Y., and Akizuki, M., **"**Development of High-Resistance Semi- Conducting Glaze Insulators," *IEEE Power Engineering Society General Meeting,* 2005.

[2.22] Lucas, D. H., "The Properties of Semi-Conducting Ceramic Glaze", *British Journal of Applied Physics*, 1952.

[2.23] Lambeth, P J, Looms, J S T, Stalewski, A, and Todd, W G. "Surface coatings for H.V. insulators in polluted areas," *Proceedings of the IEEE, 113,* (5), pp. 861-869, 1966.

[2.24] CIGRE Brochure 158, "Polluted insulators: A review of current Knowledge," Task Force 33.04.01, June 2000.

[2.25] Krasa, R., and Orbeck, T., "Development of Arc Resistant Silicone Greases," Proc. Doble Conference,Sec 9-701, 1975.

[2.26] Kim, S. H., Cherney, E. A., Hackam, R., and Rutherford, K. G., "Chemical changes at the surface of RTV silicone rubber coatings on insulators during dry band arcing," *IEEE Trans. Dielectrics and Electrical Insulation*, Vol. 1, pp. 106-123, 1994.

[2.27] Kim, S. H., Cherney, E. A., and Hackam, R., "Effects of Filler Level in RTV Silicone Rubber Coatings Used in HV Insulators," *IEEE Trans. El*, Vol. 27, pp. 1065-1072, 1992.

[2.28] Cherney, E. A., Hackam, R., and Kim, S. H., "Porcelain Insulator Maintenance with RTV Silicone Rubber Coating," *IEEE Trans. PD*, Vol. 6, pp, 1177- 1181,1991.

[2.29]CIGRE, Taskforce D1.14, Important Material Properties of RTV Silicone Rubber Insulator Coatings. 478, October 2011.

[2.30] Meyer, L. H., Cherney, E. A., and Jayaram, S. H., "The Role of Inorganic Fillers in Silicone Rubber for Outdoor Insulation—Alumina Tri-Hydrate or Silica," Electrical Insulation Magazine IEEE, Vol: 20, Issue 4, page(s): 13-21, July-Aug 2004.

[2.31] Deng, H., Hackam, R., and Cherney, E. A., "Influence of Thickness, Substrate type, Amount of Silicone Fluid and Solvent Type on the Electrical Performance of RTV Silicone Rubber Coatings," *IEEE Trans. PD*, Vol. 11, pp. 431-443,1996.

[2.32] Deng, H., Hackam, R., and Cherney, E. A., "Effects of coating thickness of RTV silicone rubber on its electrical performance," *IEEE Trans. On Dielectric and Electrical Insulation,* 1994.

[2.33] Deng, H., Hackam, R., and Cherney, E. A., "Factors influencing the electrical performance of RTV silicone rubber coatings", *IEEE Trans. Dielectric and Electrical Insulation,* 1994.

[2.34] Deng, H., and Hackam, R., "Electrical Performance of RTV Silicone Rubber Coating of Different Thicknesses on Porcelain," *IEEE Trans. PD*, Vol. 12, pp. 857-866. 1991.

[2.35] Abd-Elhady, A. M., Mohammed, A., and Izzularab, M. A., "Clean Fog Evaluation of RTV Silicone Rubber Coatings with Different Thicknesses and Pollution Levels," *IEEE Trans. On Dielectric and Electrical Insulation*, 2009.

[2.36] Deng, H., Hackam, R., and Cherney, E. A., "Role of the Size of Particles of Alumina Trihydrate Filler on the Life of RTV Silicone Rubber Coating," *IEEE Trans. PD,* Vol. 10, pp. 1012-1024,1995.

[2.37] Kim, S. H., Cherney, E. A., and Hackam, R., " The Loss and Recovery of Hydrophobicity of RTV Silicone Rubber Insulator Coatings," *IEEE Trans. PD,* Vol. 5, pp. 1491-1499, 1990.

[2.38] Kim, S. H., and Hackam, R., "Formation of silicone fluid at the surface of RTV silicone rubber coating due to heat," *IEEE-CEIDP*, pp.605-611, 1993.

[2.39] Pasand, M. S., Jahromi, A. N., El-Hag, A., and Jayaram, S. H., "Comparison of Available Silicone Rubber Coatings for High Voltage Applications," Int. Journal of Emerging Electric Power Systems, Volume 9, Issue 1, 2008.

[2.40] Omranipour, R, Meyer, L, Jayaram, S, and Chemey, E. "Tracking and Erosion Resistance of RTV Silicone Rubber: Effect of Filler Particle Size and Loading," *Annual Report Conference on Electrical Insulation and Dielectric*, 2002.

[2.41] Meyer, L. H.,"Tracking and erosion resistance of RTV silicone rubber: effect of filler particle size and loading," *IEEE/PES, Transmission and Distribution Conference and Exposition,* 2004.

[2.42] Deng, H., Cherney, E. A., and Hackam, R., "Effects of particles size of ATH fillers on the performance of RTV rubber coatings," *IEEE CEIDP*, pp. 598 – 604, 1993.

[2.43] Kim, S. H., Cherney, E. A., and Hackam, R.,"Thermal characteristics of RTV silicone rubber coatings as a function of filler level," *IEEE CEIDP*, pp. 713-718, 1992.

[2.44] El-Hag, A H., Simon, L C., Jayaram, S. H., and Cherney, E. A.,"Erosion resistance of nano-filled silicone rubber," *IEEE Transactions on Dielectrics and Electrical Insulation,* Page(s):122-128, 2006.

[2.45] Venkatesulu, B., and Thomas, M. J., "Studies on the Tracking and Erosion Resistance of RTV Silicone Rubber Nanocomposite," *IEEE CEIDP* , pp204-207, 2008.

[2.46] Kim, S. H., Cherney, E. A., and Hackam, R., "Effect of Dry Band Arcing on the Surface of RTV Silicone rubber Coatings," *IEEE Inter. Symps. On Electr. & Insul.,* Baltimore, pp.237-240, 1992.

[2.47] Iida, K., and Hackam, R.," Effects of heating on the generation of fluid in an alloy of EPDM/ SiR," Properties and Applications of Dielectric Materials, Page(s): 603 – 606,2003.

[2.48] Heping Liu., Cash, G. A., Sovar, R. D., George, G. A., and Birtwhistle, D., "Studies of the diffusion of low molecular weight silicone fluids on polluted HV silicone

insulators. I. use of diffuse reflectance FTIR," *IEEE Trans. on Dielectrics and Electrical Insulation,* Page(s): 877 – 884, 2006 .

[2.49] Gubanski, S. M., and Vlastos, A. E., "Wettability of naturally aged silicone and EPDM composite insulators," *IEEE Trans. on Power Delivery*, Vo1.5, pp. 1527- 153 5, 1990.

[2.50] Deng, H., and Hackam, R., "Low Molecular Weight Silicone Fluid in RTV Silicone Rubber Coatings," *IEEE Trans. DEI*, Vol. 6, pp. 84-94.1499.

[2.51] Moreno, V. M., and Gorur, R. S., "AC and DC Performance of Polymeric Housing Materials for HV Outdoor Insulators," *IEEE Trans. Dielectr. Electr. Insul*, Vol. 6, pp. 342-350, 1999.

[2.52] Gorur, R. S., Cherney, E. A., and Hackam, R., "The AC and DC Performance of Polymeric Insulating Materials under Accelerated Aging in a Fog Chamber," *IEEE Trans. Power Delivery,* Vol. 3, pp.1892 – 1902, 1988.

[2.53] Gustavson, T. G., Gubanski, S. M., Hillborg, H., Karlson, S., and Gedde, U. W., "Aging of Silicone Rubber under AC or DC Voltages in a Coastal Environment," *IEEE Trans. Dielectr. Electr. Insul,* Vol. 8,pp. 1029–1039, 2001.

[2.54] Heger, G., Vermeulen,H. J., Holtzhausen, J. P., and Vosloo, W. L., "A comparative study of insulator materials exposed to high voltage AC and DC surface discharges," *IEEE Trans. Dielec. and Electrical Insulation*,Page(s): 513 – 520, 2010.

[2.55] El-Hag, A. H., Jahromi, A., and Shesha, J., "Aging Performance of ATH based RTV Insulator Coatings," *IEEE International Conference on Solid Dielectrics*, pp 172 – 175, 2007.

[2.56] Naderian, J. A., Cherney, E. A., El-Hag, A., and Shesha, J., "Effect of Acid on Different RTV Silicone Rubber Coatings in Inclined Plane Test," CEIDP, Nashville, USA, pp. 313-316, 2005.

[2.57] Wang, X., Kumagai, S, and Yoshimura, N., "Contamination Performances of Silicone Rubber Insulator Subjected to Acid Rain, " *IEEE Transaction on Dielectrics and Electrical Insulation,* Vol. 5, No. 6, pp. 909-916, 1998.

[2.58] Homma, H., Mirley, C. L., Ronzello, J., and Boggs, S. A., "Field and Laboratory Ageing of RTV Silicone Insulator Coatings," *IEEE Trans.on Power Delivery*, pp. 1298-1303, 2000.

[2.59]Mukherjee P K, Ahmed A, and Singer H., "Electric field distortion caused by asymmetric pollution on insulator surfaces," *IEEE Transactions on Dielectrics and*

Electrical Insulation, vol. 6, pp. 175-180, 1999.

[2.60] Sima W., Espino-Cortes, F. P., Cherney, E. A., and Jayaram, S. H., "Optimization of corona ring design for long-rod insulators using FEM based Computational analysis," *in Conference Record of IEEE International Symposium on Electrical Insulation,* pp. 480-483,2004.

[2.61] El-Kishky, H., and Gorur, R. S., "Electric Field and Energy Computation on Wet Insulating Surfaces," *IEEE Transactions on Dielectrics and Electrical Insulation,* Vol. 3, August 1996.

[2.62] Katada, K., Takada, Y., Takano, M., Nakanishi, T., Hayashi Y., and Matsuoka, R., "Corona discharge characteristics of water droplets on hydrophobic polymer insulator surface," *in proceedings of the sixth international conference on properties and applications of dielectric Materials,* pp. 781-784, 2000.

[2.63] Haddad, A., Griffiths, H., and Waters, R. T., "Principles of anti-fog design for polymeric insulators," Piscataway, NJ 08855-1331, United States, 2007, pp. 302-305.

[2.64] Karady, G G. "Flashover mechanism of non-ceramic insulators," *IEEE Trans. Dielectrics and Electrical Insulation,* pp. 718-723, 1999.

[2.65] http://en.wikipedia.org/wiki/Photo-oxidation_of_polymers. (accessed on 3013).

[2.66] Jun, L.I., Lianhug Fan., Ching-ping wong., Franklin Cook., "Insulator coating and methods for forming same ," US Patent US2010/0189925, Jul 2010.

[2.67] CIGRE Committee 22, Subworking Group 03-01, "Worldwide Service Experience with HV Composite Insulators,"Electra No. 130, 1989.

[2.68] Crespo-Sandoval, J., "Condition Monitoring of Outdoor Insulation using Artificial Intelligence Techniques," PhD Thesis, University of Wales Cardiff, 2005.

[2.69] STRI GUIDE: "Hydrophobicity Classification Guide," Guide 1, 92/1, 1992.

[3.1] Williams D. L., "Insulation failure mechanisms in artificial pollution tests," PhD Thesis, University of Wales Cardiff, 1997.

[3.2] IEC 60507, "Artificial pollution tests on high-voltage Insulators to be used on a.c. systems," May 1993.

[3.3] Reading and Writing TDM/TDMS Files in LabVIEW, http://zone.ni.com/devzone/cda/tut/p/id/9334, (accessed on 2010).

[3.4] National Instruments, LabView user manual, 2003 Edition.

[3.5] Application Design Patterns: Producer/Consumer,

http://zone.ni.com/devzone/cda/tut/p/id/3023, (accessed on 2010)

[3.6] IEC 60587, "Methods for evaluating resistance to tracking and erosion of electrical insulating materials used under severe ambient conditions," 1986.

[3.7] Amin, M., and Ahmed, M. , "Effect of UV radiation on HTV silicon rubber insulators with moisture," IEEE International, Lahore, Pakistan, pp. 1-5, 28-30 Dec. 2007.

[3.8] CIGRE Brochure 478. "Important Material Properties of RTV Silicone Rubber Insulator Coatings", Working Group D1.14 2011.

[3.9] http://www.upc.edu/pct/documents_equipament/d_149_id-633.pdf (accessed on 2011).

[3.10] Gorur, R. S., Cherney, E. A., de Tourrcil, C., Dumora D., Harmon R., and Hervig H., "Protective coatings for improving contamination performance of outdoor high voltage ceramic insulators," *IEEE Transactions on Power Delivery*, Vol. 10, No. 2, April 1995.

[3.11] ISO 4892-2:2006. "Plastics -- Methods of exposure to laboratory light sources," Part 2: Xenon-arc lamps.

[4.1] Gorur, R. S., Cherney, E. A., de Tourrcil, C., Dumora D., Harmon R., and Hervig H., "Protective coatings for improving contamination performance of outdoor high voltage ceramic insulators," *IEEE Transactions on Power Delivery*, Vol. 10, No. 2, April 1995.

[4.2] Blackett, J. "VoltShield - Anti-pollutant treatment for glass and glazed porcelain insulators", 20th International Conference on Electricity Distribution, 8-11 June, pp 1 – 4, 2009.

[4.3] HVL Test Report: Ref HV381: "Evaluation of VoltShield Insulator Treatment on Third Rail Insulators," 2003.

[4.4] Crespo-Sandoval, J. "Condition Monitoring of Outdoor Insulation using Artificial Intelligence Techniques", PhD Thesis, University of Wales Cardiff, 2005.

[4.5] CIGRE Brochure 361, "Outdoor insulation in polluted conditions: Guidelines for selection and dimensioning", working Group C4.303, June 2008.

[4.6] http://www.ritec.co.uk/voltshield-system/how_it_works, (accessed on 2010).

[4.7] Nekeb, A., Harid, N., Haddad, A., "Effect of UV Irradiation on the Leakage Current of Polymeric Insulators," UPEC, Page(s): 1 – 4, 2011.

[4.8] http://www.cabot-com/wcm/download/en%20us/sb/UV%20WEATHERING.pdf

(accessed on 2011)

[4.9] CIGRE, Working Group D1.14,"Important Material Properties of RTV Silicone Rubber Insulator Coatings," 2011.

[4.10] ISO 4892-2:2006. "Plastics -- Methods of exposure to laboratory light sources," Part 2: Xenon-arc lamps.

[4.11] Kim, S. H., Cherney, E. A., and Hackman, R., "Hydrophobic Behavior of lnsulators coated with RTV Silicone Rubber," *IEEE Transactions an Electrical Insulation*, vol.27 No. 3,June 1992, pp. 610-622.

[4.12]Wankowicz, J. G., Gubanski, S. M., Lampe, W. D., "Loss and recovery of hydrophobicity on RTV coating surfaces," *IEEE Transactions on Dielectrics and Electrical Insulation,* Vol. 1 NO. 4, August 1994.

[4.13] http://ccs-network.com/page26.html (accessed on 2012).

[4.14] http://www.ccs-network.com/3099%20PDS.pdf (accessed April 2012).

[4.15] STRI GUIDE: "Hydrophobicity Classification Guide," Guide 1, 92/1, 1992.

[6.1] Zhou, P. B., "Numerical Analysis of Electromagnetic Fields," Berlin: Spinger-Verlag, 1993.

[6.2] Klaus-Jurgen, B., "Finite Element Procedures". New Jersey: Prentice Hall, 1996.

[6.3] COMSOL Multiphysics, "User's Manual", Version 4.1, 2011.

[6.4] Abd Rahman, R., Harid, N., and Haddad, A., "Stress Control on Polymeric Outdoor Insulators," UPEC2010, Sept 2010.

[6.5] Doshi T., Gorur R. S., and Hunt J., "Electric field computation of composite line insulators up to 1200 kV AC," IEEE Transactions on Dielectrics and Electrical Insulation, vol. 18, pp. 861-867, 2011.

[6.6] Souza A. L. and Lopes I. J. S., "Electric field distribution along the surface of high voltage polymer insulators and its changes under service conditions," in Conference Record of the 2006 IEEE International Symposium on Electrical Insulation, 2006, pp. 56-59.

[6.7] Weiguo Q. and Sebo S. A., "Electric field and potential distributions along non-ceramic insulators with water droplets," in Proceedings of 2001 Conference on Electrical Insulation and Electrical Manufacturing & Coil Winding 2001, pp. 441-444.

[6.8] Weiguo Q. and Sebo S. A., "Typical cases of electric field and voltage distribution calculations along polymer insulators under various wet surface

conditions," in Annual Report Conference on Electrical Insulation and Dielectric Phenomena, 2002, pp. 840-843.

[6.9] Looms, T. J., 'Insulators for High Voltage', Peter Peregrinus Ltd., London, United Kingdom, 1988.

[6.10] Williams, D L, Haddad, A, Rowlands, A R, Young, H M, and Waters, J. "Formation and characterisation of dry bands in clean fog on polluted Insulators," *IEEE Transactions on Dielectrics and Electrical Insulation*, Vol. 6, No.5, Oct 1999, pp 724 – 731.

[6.11] El-Kishky, H, and Gorur, R S. "Electric Field and Energy Computation on Wet Insulating Surfaces", IEEE Trans. Dielectrics and Electrical Insulation Vol. 3, Aug. 1996.

[6.12] Rahisham A., "investigations of zno microvaristor for stress control on polymeric outdoor insulators," PhD Thesis, Cardiff University, 2012.

Appendix A

Data sheets for materials used in this investigation

Appendix B

Test methods for evaluating electrical performance of different coating systems

Several test methods have been standardised and used by manufacturers and researchers to assess and evaluate the pollution performance of ceramic insulators. Until now, there are no standard pollution test procedures for testing polymeric insulators or ceramic insulators treated with protective coatings. However, a test technique has been proposed and adapted to test insulator with hydrophobic surfaces in which the solid layer method of IEC60507 (Artificial pollution tests on high-voltage insulators to be used on a.c. systems) is used. The salt fog test method of IEC60507 has also been adopted and used to test such surfaces.

On the other hand, procedures for evaluating the resistance to tracking and erosion of materials used for outdoor high voltage applications are specified in IEC60587 (Electrical insulating materials used under severe ambient conditions).

1. Salt fog method

In the salt fog method, a salt solution made of sodium chloride of commercial purity and tap water is used. The conductivity of the solution shall be one of specified values between 0.43 and 20 S/m at 20°C. The value chosen for the test is called the reference salinity. Sprays were used to atomise the solution with a stream of compressed air to produce fog in the test chamber. The flow rate of the solution of each nozzle is specified to be 0.5 dm^3/min for the period of the test. The sprays shall be in two columns parallel to the tested insulator and on opposite sides of the insulator.

The insulator is subjected to a preconditioning process after which the insulator is tested at the test voltage level and the reference salinity for a period of 20 minutes or until flashover occurs. If the insulator does not flashover, the voltage is raised in steps of 10% of test voltage every 5 min until flashover occurs. The voltage is then re-applied and raised to 90% of the flashover voltage obtained earlier, and then increased in steps

until a further flashover occurs. This last procedure is repeated until a total of eight flashovers have occurred. The insulator is then washed with tap water, and the withstand test can be started. The insulator is subjected to a series of tests of one hour duration at the specified test voltage and salinity. The insulator is said to comply with specification if it withstands three consecutive tests without flashover. If one flashover occurs, the insulator should pass a fourth test.

2. Solid layer method

In the solid layer method, a solid pollution layer is applied to the insulator surface and the insulator is exposed to clean fog. The pollution layer is a suspension of defined composition based on either Kieselguhr or kaolin and a specified weight of sodium chloride mixed in 1000 g tap water. The composition is modified by adding a small amount of wetting agent 'Triton X-100' to the contaminating suspension [2.62]. The use of wetting agent is first introduced when dealing with hydrophobic surfaces. It allows a uniform pollution layer to adhere to the insulator surface. The required volume conductivity is achieved by adjusting the quantity of salt. The pollution layer is applied by spraying or flowing the contaminating suspension onto the surface of the cleaned insulator or by dipping the insulator in the suspension. The insulator cannot be tested until the pollution layer is entirely dry.

The two alternative test procedures proposed in the standard;

- Procedure A, "wetting before and after energisation", the polluted and dried insulator is placed in position in the test chamber and the fog generation is started. The fog shall produce the maximum conductivity of the pollution layer in 20 to 40 min from the start of the fog. The test voltage is then applied and maintained for 15 minutes or until flashover.
- Procedure B, "wetting after energisation", the polluted and dried insulator is placed in the test chamber. The test voltage is applied and the fog generation is started. The test voltage is maintained until flashover occurs, or for 100 minutes, or until the current peaks have decreased to less than 70% of the maximum peak recorded. The insulator complies with the specification if it withstands three consecutive tests without flashover. The insulator must withstand a fourth test if a single flashover occurred.

3. Inclined plane test

IEC60587 standard describes a test technique for measuring the resistance of electrical insulating materials to tracking and erosion using inclined plane insulator samples and a conductive liquid film on the material surface. Artificial polluting and wetting agents are used.

A pair of stainless steel electrodes is attached to the surface of a flat, rectangular insulator sample. The sample is mounted at an angle of 45° to the horizontal with the test surface on the underside. A filter paper pad is clamped beneath the top electrode such that a steady flow is established down the face of the sample between the electrodes. The test is carried out on a set of five samples.

Materials are classified according to the time and voltage required to track or erode.

- constant tracking voltage; the voltage is increased to one of the test voltages specified in the standard and maintained constant for 6 hours. The material is classified according to the highest voltage withstood by all five samples for 6 hours without failure.
- stepwise tracking voltage; the voltage is raised in steps of 250 V at intervals of 1 hour. The material is classified according to the highest voltage withstood by all five samples for 1 hour.

The test is terminated either when the current across a sample exceeds 60 mA (preferred criterion), or when tracking on the sample surface reached a mark 25 mm from the lower electrode.